THE UNIVERSITY OF ADELAIDE
Department of Mechanical Engineering

THE VIBRATIONAL RESPONSE OF AND THE ACOUSTIC RADIATION FROM THIN-WALLED PIPES, EXCITED BY RANDOM FLUCTUATING PRESSURE FIELDS

by

D.C. Rennison, B.E.

Thesis for the Degree of Doctor of Philosopy

September 1976

SUMMARY

The results of an experimental and theoretical investigation of the vibrational response of and the acoustic radiation from thin-walled pipes, excited by random pressure fields, are presented: a wide range of structural parameters and both fully-developed turbulent flow and propagating acoustic plane waves have been considered.

For flow excitation, steel, brass and P.V.C. pipes were tested in the experimental work. The measured non-dimensional spectral densities of the acceleration response of the various pipes are proportional to the non-dimensional spectral density of the turbulence wall-pressure field; to the average quality factors of the particular pipes; and to the fifth or higher power of the flow speed. For steel pipes, the acceleration response depends on the cube of the pipe wall thickness. These characteristics are in substantial agreement with theoretical predictions made using a statistical analytical approach.

Likewise, the measured non-dimensional spectral density of the acoustic power radiated is proportional to the non-dimensional spectral density of the turbulence wall-pressure field; to an average quality factor of radiating pipe modes; and to the fifth or higher power of the flow speed. For steel pipes, the power radiation depends on the square or cube of the pipe wall thickness. For frequencies below the acoustic coincidence frequency, the radiation is controlled by low circumferential-order subsonic modes, which are usually more lightly-damped than supersonic modes at the same frequency: in fact, subsonic modes will radiate up to 10dB more acoustic power than supersonic modes at frequencies where both subsonic and supersonic modes occur.

The degree of agreement between theoretical predictions of the vibrational response and acoustic radiation and the data measured during the experimental programme depends on the closeness of conditions to hydrodynamic coincidence. For the brass pipe used, hydrodynamic coincidence occurred and there is close agreement. For the steel pipes and, to a lesser extent, for the P.V.C. pipe, conditions were far removed from hydrodynamic coincidence and theoretical overestimates of the response and radiation of from 10 to 25 dB are found. These discrepancies between experiment and predictions can be attributed to the inappropriate use of the empirical model for the cross-spectral density of the turbulence wall-pressure field.

Large broad-band reductions in the vibrational response of and the acoustic radiation from lightly-damped steel pipes can be produced by the application of simple damping treatments to the pipe surface, except at those low frequencies where n = 1 modes influence the radiation from the undamped pipe, in which case much smaller reductions in acoustic radiation occur.

For acoustic excitation, the concept of a lower bound to the acoustic radiation from pipes excited by acoustic plane waves propagating internally (corresponding to the radiation from the forced vibrational response) is verified for a highly-damped pipe: this serves as a reference with which to compare the results of experiments with lightly-damped pipes.

The resonant contribution to both the vibrational response and the acoustic radiation increases as the structural damping decreases. The maximum increases in both acceleration response and acoustic power radiation occur at low frequencies and in those frequency bands where the modal quality factors and the density of resonant modes are highest. While the near-field of an acoustic source can be most important in

determining the power radiation in practical systems where the source is directly connected to the radiating pipe, it is not responsible for the large discrepancies between the theoretical and measured power radiation results in the present experiments with lightly-damped pipes. It appears, from experiments and supporting theoretical analysis, that the resonant response and the associated acoustic radiation result primarily from intrinsic inhomogeneities in the pipe, and in particular from variations in pipe wall thickness.

The power radiation from resonant modes can be reduced to the lower-bound prediction by the application of surface damping treatments only when the quality factors of $n = 1$ modes are reduced to values of approximately 20. As it is most difficult to damp these $n = 1$ modes, the lower-bound prediction of the power radiation will be exceeded in the general case.

STATEMENT OF ORIGINALITY

This thesis contains no material which has been accepted for the award of any other degree or diploma in any University. To the best of the author's knowledge and belief, this thesis contains no material previously published or written by another person, except where due reference is made in the text.

D.C. Rennison

September 1976

ACKNOWLEDGEMENTS

The work described in this thesis has been carried out in the Department of Mechanical Engineering of the University of Adelaide under the aegis initially, of Professor H.H. Davis and finally, of Professor R.E. Luxton, to whom the author is indebted for the opportunity to conduct this research.

The author wishes to express his sincere appreciation to his supervisor Dr. M.K. Bull, for the stimulating help and constant encouragement he has generously given throughout the duration of this research and for his critical advice with this thesis.

Similarly, the author acknowledges the keen interest taken by Dr. G.L. Brown in part of this work and the perceptive suggestions he has made.

The assistance of the workshop staff, under Mr. D. Kerr, is greatfully acknowledged, particularly the invaluable help provided by Mr. D. Morrison in the construction of the experimental pipe flow equipment.

Acknowledgement is made of the financial support provided by the Australian Research Grants Committee, without which this work would not have been possible.

CONTENTS

FIGURES

SYMBOLS

a	Mean pipe radius
a_x, a_y	$= c_x k_c$, $c_y k_c$ - see equations (1.1) and (4.15)
c	Speed of sound in acoustic medium surrounding pipe
c_B	Speed of sound inside pipe
c_{Lp}	Compressional wavespeed in plate = $(E/\rho_s \gamma^2)^{\frac{1}{2}}$
c_x, c_y	Empirical decay constants for the axial and circumferential narrow-band correlation coefficients of the turbulence pressure field
E	Modulus of elasticity
$f(\nu)$	Non-dimensional modal density function - equation (2.29)
h	Pipe wall thickness
H_α	Modal filtering function - equation (4.10)
$j^2_{\alpha\alpha}(\omega)$	Joint acceptance of the αth structural mode - equation (2.3)
$j^2(\nu,\theta)$	Joint acceptance, as function of frequency ν and waveangle θ
$J(\nu)$	Pipe joint acceptance, integrated over all pipe modes at frequency ν, per unit frequency, defined by equation (2.16)
$J_s(\nu)$	Pipe joint acceptance, integrated over supersonic modes - equation (2.23)
k_a	Acoustic wavenumber = (ω/c)
k_c	Convection wavenumber = (ω/U_c)
k_m	Axial component of structural wavenumber = $(m\pi/\ell)$
k_n	Circumferential component of structural wavenumber = (n/a)
k_x	Axial wavenumber component
k	Structural wavenumber of (m,n)th mode = $(k_m^2 + k_n^2)^{\frac{1}{2}}$
K_a	$= k_a a$
K_B	$= \omega a/c_B$
K_c	$= k_c a = \omega a/U_c$
K_m	$= k_m a = m\pi/\Lambda$
K_n	$= k_n a = n$
K	$= (K_m^2 + K_n^2)^{\frac{1}{2}}$
$\bar{K}_a$	$= \sqrt{\beta/\gamma}\, K_a$

Non-dimensional wavenumbers

(continued over page)

$\bar{K}_c = \sqrt{\beta/\gamma}\, K_c$

$\bar{K}_m = \sqrt{\beta/\gamma}\, K_m$

$\bar{K}_n = \sqrt{\beta/\gamma}\, K_n$

$\bar{K} = \sqrt{\beta/\gamma}\, K$

ℓ Pipe length

m Axial mode order

m' Surface density of pipe = $\rho_s h$

M_α Generalised mass of αth vibrational mode

M_c Non-dimensional convection speed of pressure field = U_c/c

M_o Non-dimensional flow speed of pipe flow = U_o/c

$M_{Lp} = c_{Lp}/c$

n Circumferential mode order

$n(\omega,\theta)$ Modal density of pipe, per unit waveangle θ and frequency ω

$n(\nu,\theta)$ Modal density of pipe, per unit θ and ν - equation (2.9)

$N(\nu)$ Pipe modal density - equation (2.10)

$N_s(\nu)$ Modal density of supersonic modes

p Radial order of acoustic mode inside pipe

p' Root-mean-square pressure of turbulence pressure field

q_o Flow dynamic pressure

Q Average quality factor for all modes in narrow frequency band

Q_s Quality factor of supersonic modes in narrow frequency band

Q_α Quality factor of αth mode

$Q(\nu,\theta)$ Quality factor, as function of θ and ν

$\underset{\sim}{r}$ Co-ordinate on pipe surface

$R_p(\underset{\sim}{\xi},0;\omega)$ Narrow-band correlation coefficient of pressure field

S Pipe area ($= 2\pi a\ell$)

$T(k_x)$ Defined by equation (4.16)

u	$= U_c/U_o$
U_c	Convection velocity of turbulence pressure field
U_o	Centreline velocity of turbulent flow
(u_l, v, w)	Pipe displacements in axial, tangential and radial directions
$\dot{w}$	Radial pipe velocity
$\ddot{w}$	Radial pipe acceleration
(x, y, z)	Co-ordinate axes: axial, circumferential and radial vectors
Z_α	Impedance of αth pipe vibration mode - equation (2.2)
Z_τ	Transmission impedance of infinite pipe - equation (8.1)
α	Mode order
β	Pipe wall-thickness parameter $= h/\sqrt{12}a$
δ^*	Displacement thickness of boundary layer $\simeq a/8$
γ	$= (1 - \mu^2)^{\frac{1}{2}}$
η	Circumferential spatial separation
θ_1	Waveangle for the n = 1 structural mode at frequency ν
θ_2	Minimum waveangle for supersonic modes at frequency ν
Λ	$= \ell/a$
μ	Poisson's ratio
ν	Non-dimensional frequency $= \omega/\omega_r$
ν_A, ν_B	Upper and lower frequencies defining the region of frequency where no supersonic modes occur
ν_{ac}	Non-dimensional acoustic coincidence frequency $= \omega_{ac}/\omega_r$
ν_{hc}	Non-dimensional hydrodynamic coincidence frequency $= \omega_{hc}/\omega_r$
ν_{mn}	Non-dimensional frequency of (m,n)th pipe mode $= \omega_{mn}/\omega_r$

$\bar{\nu}$	$= \nu/\gamma$	Non-dimensional frequencies
$\bar{\nu}_A, \bar{\nu}_B$	$= \nu_A/\gamma, \quad \nu_B/\gamma$	
$\bar{\nu}_{ac}$	$= \nu_{ac}/\gamma$	
$\bar{\nu}_{hc}$	$= \nu_{hc}/\gamma$	
ξ	Axial spatial separation	
ρ	Density of acoustic medium outside pipe	
ρ_f	Density of pipe fluid	
ρ_s	Density of pipe material	
ρ_{fs}	$= \rho_f/\rho_s$	
σ	Radiation ratio = $(R_{rad}/S\rho c)$	
σ_α	Radiation ratio of αth pipe vibration mode	
$\phi_p(\omega)$	Power spectral density of excitation pressure field	
$\Phi_p(\omega)$	$= \phi_p \, U_o/q_o^2 \, a$	
$\phi_p(\xi,\eta,\omega)$	Cross-spectral density of excitation pressure field	
$\Phi_p(\underset{\sim}{k},\omega)$	Wavenumber-frequency spectral density of excitation pressure field	
$\Phi'_p(\underset{\sim}{k},\omega)$	$= \Phi_p(\underset{\sim}{k},\omega)/\phi_p(\omega)$	
$\phi_\pi(\omega)$	Spectral density of the radiated acoustic power	
$\Phi_\pi(\omega)$	Non-dimensional spectral density of radiated power = $\phi_\pi/S\rho c^2 a$	
$[\![\phi_w(\omega)]\!]$	Spectral density of pipe displacement response (surface averaged)	
$\Phi_w(\omega)$	$= [\![\phi_w(\omega)]\!] \omega_r/a^2$	
$[\![\phi_{\dot{w}}(\omega)]\!]$	Spectral density of pipe velocity response (surface averaged)	
$\Phi_{\dot{w}}(\omega)$	$= [\![\phi_{\dot{w}}(\omega)]\!]/\omega_r a^2$	
$[\![\phi_{\ddot{w}}(\omega)]\!]$	Spectral density of pipe acceleration response (surface averaged)	
$\Phi_{\ddot{w}}(\omega)$	$= [\![\phi_{\ddot{w}}(\omega)]\!]/\omega_r^3 a^2$	

$\psi_\alpha(x,y)$	Function describing αth mode shape - equation [2.6]
ω	Radian frequency
$\Delta\omega$	Frequency bandwidth
ω_{ac}	Acoustic coincidence frequency = $2\sqrt{3}\ c^2/hc_{Lp}$
ω_{hc}	Hydrodynamic coincidence frequency = $2\sqrt{3}\ U_c^2/hc_{Lp}$
ω_{np}	Cut-off frequency of the (n,p)th acoustic mode inside pipe = $K_{np}c_B/a$
ω_o	Centre frequency of frequency band
ω_r	Pipe ring frequency = c_{Lp}/a
ω_α	Resonance frequency of αth mode
$X(\nu)$	Relative joint acceptance between flow and acoustic excitations.

GENERAL INTRODUCTION

Frequently in the petro-chemical and process industries, plant and surrounding community noise levels are determined by the acoustic radiation from piping networks. Noise sources exist throughout such networks, so that the resulting radiated power tends to produce a diffuse acoustic environment within the plant, making the precise location of the dominant sources difficult. Consequently, noise control treatments tend to be applied to vast areas of pipe and at considerable cost. On the other hand, adequate plant design is hampered by the lack of suitable methods for predicting the importance of potential noise sources. Trends to larger-sized plants with their higher flow speeds and gas pressures suggest that the acoustic radiation from pipes will assume an even greater industrial significance in the future.

The sources of this piping noise may be broadly categorised, in relation to the length of the radiating pipe, as either localised or distributed. Localised sources would include flow control devices, such as valves, mitred bends and compressors, which, as a by-product of their primary function, generate locally intense levels of rapidly decaying turbulence or which themselves vibrate and feed high levels of energy directly to the pipe wall. Generally, these localised effects can be isolated from connected piping with mechanical filters, although high radiation levels may occur in the region of the source. In contrast, the effects of a distributed noise source may exist for many hundreds of pipe diameters. For example, the random wall-pressure field which is associated with turbulent fluid flow, extends over complete piping lengths and cannot be removed from the flow: it represents a lower bound excitation always present within the pipe. Pipe internal surface roughness and, for gases, increased internal pressures will increase the intensity of the turbulence

wall-pressure field. Moreover, the intense pressure fields generated at flow control equipment will radiate strong acoustic fields, which will propagate essentially unattenuated for considerable distances.

In view of this source complexity and the fact that this is, in many ways, an introductory investigation, the present work is directed towards some of the simpler aspects of the problem, aspects which previously have received little attention. Rather than attempting to quantify the effects of the broad range of operating sources, we are concerned to understand the nature of the coupling of an excitation, whose properties are known, to the bounding pipe. We then examine the coupling of the resulting vibrational response of the pipe with the surrounding acoustic medium. In fact, two different excitations have been considered.

Firstly, the random wall-pressure field associated with fully-developed turbulent pipe flow was chosen. Fully-developed turbulent flow is the least complex flow excitation existing within pipes. Previous investigations have produced an adequate description of the dominant statistical properties of the random wall-pressure field acting inside pipes carrying fully-developed turbulent flow. Such an excitation is consequently a useful tool for the testing of chosen analytical methods.

The major emphasis of the work has been on making an assessment of turbulent pipe flow as a source of external acoustic noise. Theoretical predictions concerning the dependence of the pipe vibrational response and the acoustic radiation on various fluid and structural parameters will be summarised. The results from a detailed set of experimental measurements to examine these conclusions will be presented for comparison with the main conclusions of the analysis.

Secondly, acoustic plane waves propagating inside the pipe have been used to model the far-field pressures produced by a valve. It is known that, in general, the important piping noise sources radiate high intensity acoustic waves inside the pipe. There are considerable discrepancies, however, between existing experimental results and theoretical

predictions, even for the elementary case of a plane acoustic wave propagating inside the pipe. This latter situation has been investigated experimentally in some detail in order to determine the reasons for the observed discrepancies.

For convenience, this thesis is divided into two parts, each concerned with one of the excitations. Part I describes the investigation involving the use of fully-developed turbulent flow, while Part II reports the work done using plane wave acoustic excitation. Much of the detail described in Part I is common to both Part I and Part II, although the two aspects have been separated as much as possible.

PART I: EXCITATION BY FULLY-DEVELOPED TURBULENT FLOW INSIDE THE PIPE

CHAPTER 1

1.1 INTRODUCTION

The random wall-pressure field, which is associated with fully-developed turbulent flow inside pipes, extends over complete piping lengths and is a continuous source of structural excitation. The intensity of the driving pressure field is proportional to the dynamic pressure of the flow, so that turbulent flow may well control the vibrational response of the pipe for high flow speeds and, in gas flows, for high internal pressures.

It is recognised that more powerful and efficient excitations will exist in most practical piping systems. However, no comprehensive set of experimental data on flow-induced pipe vibration or the resulting acoustic radiation is currently available. Consequently, it was considered desirable to examine initially the simplest flow excitation in order to develop an understanding of the importance of the various parameters involved.

An experimental and theoretical study of the vibrational response of and the acoustic radiation from thin-walled pipes, excited by internal turbulent flow, was begun in order to define the importance of the problem and to develop appropriate theoretical approaches, so that future work with more complex flow excitations representative of real systems would be on a sound basis.

1.2 SURVEY OF PREVIOUS WORK

The general investigation of the vibrational response of structures excited by random pressure environments arose with the development of high-speed jet aircraft for passenger transportation and from the problems of structural fatigue and high interior noise levels, which occur in such circumstances. The prediction of the magnitude of the coupling between

the complex pressure fields acting on the aircraft skin and the skin itself is most difficult for typical structures. By taking idealised structural elements (strings, beams, flat panels) and more simple excitations (progressive acoustic waves and boundary layer pressure fields), it has been possible to develop theoretical analyses to such a level that reasonably accurate response predictions for such situations are possible. These demonstrate the importance of the various physical phenomena involved. Alternative analytical methods are currently being developed by various research organisations to complement the idealised approach in the examination of actual aircraft structures.

These theoretical analyses are essentially directly applicable to the present situation concerning the excitation of thin-walled cylinders by internal fully-developed turbulent flow. Thus the more important developments in the area of the response of structures to random excitation are discussed initially. This includes the problem of the measurement of the properties of the wall-pressure field beneath turbulent flows. Work concerned particularly with the response of flow-excited cylinders is subsequently reviewed, and the survey concludes with a discussion of the coupling between the cylindrical vibrational response and the external acoustic field.

Initial theoretical development was provided by Lyon (1956), who considered the response of a string to excitation by different random noise fields. In particular, the case of the response of an aluminium ribbon, excited by turbulent airflow convected along the ribbon length, was examined both theoretically and experimentally. The pressure field, assumed to be random in space, was represented by a delta function, with a decaying temporal correlation. The condition of hydrodynamic coincidence, that is a matching of the flow convection velocity with the strip bending wavespeed, was predicted to occur only for the situation where the flow excitation was correlated over lengths comparable to or greater than the modal wavelength. Measurements of the mean-square modal response confirmed

this prediction. Large decreases in modal quality factors were observed as the flow velocity increased. The response of an infinite string to a turbulence pressure field convected along its length was considered for comparison with the finite string example. Amplification of the response due to coincidence was again predicted to occur only when the excitation was correlated over a distance greater than the free bending wavelength.

Ribner (1956) considered the problem of the acoustic power radiation from a flow-excited infinite flat plate in a similar manner. Coincidence was found to occur when the excitation flow speed was equal to the free bending wavespeed in the plate. Structural boundary conditions have no influence in this idealisation. Consequently, the response and power radiation vary smoothly with frequency, although it was recognised that, for real finite structures, a reverberant vibration response would occur, which would control the radiation for subsonic convection speeds. The response was predicted to occur primarily as structural running waves.

The method of normal mode analysis was formalised by Powell (1958a) to facilitate the calculation of the response spectrum of finite structures excited by random homogeneous excitation fields. Generalised harmonic analysis was used to find the response in each mode. The spectrum of the spatially averaged response was calculated by summing the space-averaged contribution from each structural mode. The 'joint acceptance' expressed the magnitude of the coupling between the pressure field and the average modal response.

Dyer (1959) used normal mode analysis to formulate an expression for the vibrational response covariance and the mean-square displacement of a flat plate excited by turbulent flow, using an analytical approach similar to Lyon (1956) but extended to the two-dimensional situation. Hydrodynamic coincidence was examined and considered to occur only when the component of the wavespeed of the structural resonant mode in the flow direction was equal to the convection velocity of the excitation pressure field, as with Lyon's ribbon. Again, strong amplification of the response

was predicted to occur provided the pressure field was correlated over a distance greater than the wavelength of the coincident mode. The effectiveness of damping treatment for response reduction was discussed.

The model used by Dyer for the turbulent wall-pressure field assumed a random stationary process of small spatial scale, whose time correlation decayed exponentially as it was convected in the flow direction. Subsequent measurements of the properties (intensity, spectra and space-time correlations) of the wall-pressure field beneath turbulent boundary layers have been made by Willmarth and Wooldridge (1962), Bull (1967) and Corcos (1963) in considerable detail. When presented as cross-spectral densities, they are found to agree closely with the model proposed by Corcos (1963), which has the form:

$$\phi_p(\underset{\sim}{\xi},\omega) = \phi_p(\omega)\ \exp(-a_x|\xi|-a_y|\eta|+i\frac{\omega\xi}{U_c}) \qquad [1.1]$$

where $a_x = c_x k_c$, $a_y = c_y k_c$, $k_c = \omega/U_c$, and U_c is the convection velocity of the pressure field. $\phi_p(\omega)$ is the power spectral density of the pressure field, (ξ, η) represent the longitudinal and lateral separations, and c_x, c_y are decay constants in the (ξ, η) directions. The convection velocity is usually assumed constant, although measurements by Bull (1967) show that U_c depends on ξ at small separations and also varies with frequency: at low frequencies, the narrow-band correlation coefficients become independent of frequency for large separations. Corcos (1962) and Bakewell (1964) have made similar measurements of the properties of the wall-pressure field in pipes carrying fully-developed turbulent flow: these agree closely with the above model.

The effects of pressure gradients on cross-spectral density measurements have been investigated by Schloemer (1967). For mild favourable pressure gradients, the ratio of convection velocity to free stream velocity was observed to increase by approximately 10%, while the pressure field spectral density decreased at higher non-dimensional frequencies

when compared to zero pressure gradient measurements. Such effects are not expected to be significant in the present work.

Space-time pressure correlation measurements are susceptible to large relative errors at large separations and long time delays, so that the above measurements reflect accurately only the convected components of the turbulence pressure field. Blake and Chase (1971), and Farabee and Gieb (1975) have attempted to measure wavenumber - frequency pressure spectra directly with spatial filtering techniques involving arrays of appropriately-phased pressure transducers. Their measurements agree with the Corcos model at the convection wavenumber, but at lower wavenumbers, the Corcos model considerably overestimates the measured spectral levels. When the frequencies of interest are well above the hydrodynamic coincidence frequency, as for thick-shell structures excited by low-speed water flow, this low-wavenumber domain of the turbulence pressure field tends to control the structural vibration response, as discussed by Chandiramani and Blake (1968). Alternative models of the turbulence pressure field, due to Chase (1969) and Chandiramani, have not been extensively verified experimentally, although limited qualitative agreement exists. Consequently, generally the Corcos model has been used in theoretical predictions for comparison with experimental results, even for frequencies well above the hydrodynamic coincidence frequency.

Comprehensive theoretical and experimental studies of the vibrational response of flat panels to random pressure fields have been performed by Wilby (1967) and Maestrello (1965a, 1965b, 1967). Working with acoustic plane waves and fully-developed flow, Wilby presented detailed comparisons of the measured and theoretical low mode order vibration response spectrum. The agreement produced was very reasonable in most cases, considering the assumption of mode shapes corresponding to simply-supported ends and the difficulties involved in accurately determining the effect of flow on modal quality factors. Maestrello investigated turbulent flow excitation exclusively. One-third octave and narrow-band measurements of the response of

and acoustic radiation from a series of panels (both undamped and damped with layers of tape) were made over a Mach number range from 0.34 to 0.75. Running waves, as predicted by Ribner, were observed for those coincident modes for which the pressure field correlation extended over distances greater than a modal wavelength in the flow direction. Measurements of the modal radiation resistances were found to be essentially independent of the flow Mach number, which is consistent with the observation that the radiated power and the vibrational response of each panel have the same dependence on Mach number. In the case of a strong running wave response, the application of rubber and sand mechanical terminations at the downstream panel boundary was shown to reduce the standing wave response significantly. Calculations, based on Dyer's approach but using the measured pressure covariance, predict the vibrational covariance closely, but overestimate the measured response. No experimental measurement of the effect of the flow on the structural damping was reported. Using methods developed by Maidanik (1962) for predicting the radiation resistance of ribbed panels, Maestrello obtained good estimates of the acoustic power radiation for a variety of panel-stiffener configurations. He also achieved substantial reductions in radiated acoustic power by modifying the panel boundary conditions and by adding surface damping treatments.

White (1966) successfully analysed the available experimental measurements of flow-excited panel radiation, including the results of Maestrello (1965a). Assuming light damping, high modal density and equal modal energy, he used the methods of statistical energy analysis (Lyon and Maidanik (1962)) to calculate the average spectral density of the radiated acoustic power. Close agreement with the measured results was obtained especially at high frequencies. The analysis explains the measured change in Mach number dependence with frequency of the radiated power. Davies (1971) has used a similar approach to White and compared it with Powell's normal mode analysis in the analysis of his measurements of the acoustic radiation from thin panels excited by fully-developed turbulent flow.

Improvements were made in the prediction of the panel radiation ratios from those derived by Maidanik (1962). Close agreement between the experimental results and both theoretical predictions was found for all frequencies. Statistical energy analysis can apparently be successfully used in the analysis of panel vibrational response and radiation with a considerable reduction in computational effort.

One of the first sets of published experimental results concerning the response of a structure to turbulent flow involved a thin-walled Mylar cylindrical test section. Weyers (1960) carried out an experimental investigation of the acoustic near field generated by the cylinder response to internal fully-developed turbulent flow. Measurements of the excitation pressure spectrum and intensity were made with a piezo-electric transducer pressed against the outside of the Mylar cylinder. The cylinder dimensions were: length 28 cms, diameter 2.54 cms, and wall thickness 0.0125 mm. Measurements of the pressure spectra and intensity made in this way are consistent with the data of other investigators, for example, Corcos (1962) The acoustic near-field pressure spectral density was measured at a distance of 6.4 mm from the pipe wall in a small anechoic chamber enclosing the pipe. Eight cylinders varying in wall thickness from 0.0125 mm to 0.053 mm were tested over a range of flow Mach number from 0.11 to 0.28. The mean-square acoustic pressure depended on the fifth power of the flow Mach number and was approximately inversely proportional to the square of the wall thickness. The effects of a static pressure differential across the pipe wall, which would exist during operating flow conditions, were predicted closely with existing thin shell theory.

Rattayya and Junger (1964) applied Powell's normal mode analysis to the excitation of cylindrical shells by internal turbulent flow. Expressions derived for the cross-spectral density of the resulting generalised force, which is proportional to the joint acceptance, allowed for the axial symmetry of pipe flow and a homogeneous circumferential pipe vibration response. Approximations made for low flow velocities demonstrated that

the pipe vibrational response is independent of the structural mode order. This corresponds to the case where, at a particular frequency, the fluid convection speed is far smaller than the axial component of the structural wavespeed. The total response spectral density was calculated from the product of the average modal response spectrum and the modal density, assuming light structural damping, so that each mode contributed to the response only at its resonance frequency. It was concluded that hydrodynamic coincidence would occur only for supersonic flow, and would not be important in normal situations.

For the case of water as the excitation fluid, Clinch (1970) presented a theoretical and experimental study of the vibrational response of a thin-walled steel pipe excited by internal turbulent flow. His measurements of the wall-pressure spectral density were consistent with those of Corcos (1962), although significant deviations from the Corcos model exist in his cross-spectral density data. The decay rates of the narrow-band cross-correlation coefficients show a dependence on transducer separation and convection speed, rather than on Strouhal number alone as with Corcos. The theoretical analysis follows that developed by Rattayya and Junger. The joint acceptance was shown to be independent of mode order, although algebraic errors exist in the joint acceptance expressions and no allowance for the symmetry of pipe flow has been made. The measured results and the theoretical predictions show close agreement. The mean-square displacement was found to be proportional to the fourth power of the flow speed.

As Clinch suggests, some doubt exists as to the validity of the structural damping estimate. Clinch took a single measurement of the in-situ structural quality factor to represent the damping of all the resonant modes, although he believed that the response was mainly in one of the n=1 translational modes. The measured value was an order of magnitude smaller than is expected for similar water-loaded steel structures (Junger and Feit (1972)), where any mass loading is mainly reactive. The impulse-decay

method was used to estimate the structural damping, although this approach is now recognised to produce unreliable results (Crocker and Price (1969)). Since a detailed examination of the frequency dependence of pipe quality factors was not carried out for either the water-loaded or unloaded situations, it is not entirely clear that the good agreement obtained was not simply fortuitous.

The acoustic radiation from cylindrical shells has been the subject of continuous research for many years. Junger (1952) derived expressions for the radiation ratios of infinite pipes with periodic axial and circumferential standing wave configurations. Vibration patterns, in which the structural wavespeeds are supersonic with respect to the surrounding acoustic medium, radiate acoustic power with the efficiency of an infinite plane piston, and with a cylindrical directivity pattern. As the structural wavespeed becomes sonic or subsonic, the radiation ratio reduces sharply to zero so that no power is radiated. Smith (1955) and Heckl (1962) demonstrate that the main effect of curvature on the vibration modes of a cylinder is to increase their structural wavespeeds, thus raising a given resonance frequency above that for the same mode on a flat plate of the same dimensions. Supersonic modes were shown to occur at frequencies well below the acoustic coincidence frequency, contrasting with the case of a flat plate of the same thickness in which the wavespeeds of all resonant modes are subsonic below the coincidence frequency.

Maidanik (1962) developed a statistical method for the prediction of the radiation ratios of ribbed panels in situations where the response was resonant and the modal density was high. This was based on a consideration of the radiation properties of panel modal vibration patterns derived from physical arguments involving panel dimensions and relative structural and acoustic wavelengths. Manning and Maidanik (1964) extended this approach to cylindrical shells. They argued that, at those frequencies where the response contains both supersonic and subsonic modes, the acoustic radiation is determined solely by the supersonic modes, that is, the radiation ratio

is zero for subsonic modes but unity for supersonic modes. With the assumption of equal modal energy, the average radiation ratio in a particular frequency band was set equal to the number of supersonic modes divided by the total number of modes in that frequency band. Satisfactory agreement was found with experiment.

Using a simplified form of the resonance frequency equation for cylinders, Heckl (1964) derived an expression for the density of resonance frequencies of a cylindrical shell. Improvements to this formulation have been made by Miller and Hart (1967). The density of supersonic modes was derived by Manning, Lyon and Scharton (1966), but may also be evaluated numerically following Miller and Hart.

Bailey and Fahy (1972) and Yousri and Fahy (1973) have derived exact expressions for the radiation ratios of the transverse bending modes of finite length cylindrical beams. The vibrational response of and acoustic radiation from long small-diameter pipes may be controlled by similar translational modes at low frequencies. A more general analysis by Junger and Feit (1972) allows the calculation of the radiation ratio of any resonant mode on a finite length cylinder. They show that radiation damping may control the response of the more efficiently radiating modes (usually low circumferential order). Little numerical computation and no experimental measurements of the radiation ratios of these modes are available.

1.3 PRESENT INVESTIGATION

As indicated in the literature review in the previous section, a reasonable understanding of the problem of the excitation of structures by random pressure fields exists, at least in general terms. Extensive experimental data have been collected on the vibration response of and the acoustic radiation from various types of structures. Theoretical methods have been developed which explain the more important features of these experimental results. Exact analyses involving the details of the flow

properties and structural configuration may be used for low mode order response investigations, while statistical approaches appear satisfactory for high modal density applications or for more complex geometries.

To date, little theoretical work has been reported in the area of flow-excited pipe vibration response and acoustic radiation. That which has been reported, has been concerned only with the vibration response, and no comprehensive assessment of the various parameters involved has been made. The experimental data presented illustrate solely the dependence of the vibration response on flow speed, and are of limited use due to the omission of detailed information on the structural damping. Theoretical expressions exist for the calculation of the radiation ratios of any pipe vibration mode, although little experimental verification is available. Likewise, statistical estimates of averaged radiation ratios, which were developed originally for short, large-diameter thin-walled shells, require experimental validation before they can be applied to pipes generally. However, the application of such analytical techniques to the present problem would seem straightforward, although experimental confirmation of each assumption is required.

The general aims of this investigation have been detailed in the General Introduction and in section 1.1. The specific aims of the work reported in Part I may now be defined.

(i) The development of suitable analytical techniques for use in a parametric study of the effects of flow and structural variables on the vibrational response of and acoustic radiation from thin-walled pipes, excited by internal fully-developed turbulent flow.

(ii) The construction of a pipe flow facility, which would enable suitable ranges of flow and structural variables to be tested experimentally.

(iii) The experimental measurement of the vibrational response of and acoustic radiation from the various test pipes over the range of

flow speeds to be used, to establish a data base for flow-generated piping noise, and to enable comparisons with the theoretical predictions to be made.

(iv) The comparison of the experimental data for turbulent flow excitation with those measured for excitation by propagating acoustic waves, to facilitate an experimental estimate of the relative joint acceptances of the two excitations.

As suggested in the preceeding paragraphs and described in subsequent chapters, this work represents a detailed experimental and theoretical assessment of turbulent pipe flow as an acoustic noise source; as such, it is the first comprehensive investigation of the complex subject of flow-induced piping noise.

CHAPTER 2

THEORETICAL APPROACH

2.1 INTRODUCTION

In this chapter, expressions are developed for the power spectral density of the vibrational response of and the acoustic radiation from thin-walled pipes, excited by internal turbulent flow. Much of this formalism has been presented previously in a paper by Bull and Rennison (1974a), which is included as Appendix A. The present approach was developed to illustrate the effects of various structural and flow parameters on the pipe response and radiation. From these considerations, a series of experimental situations is devised with the aim of verifying the main conclusions of the analysis and so justifying the assumptions made.

Normal mode analysis is used to predict the pipe vibration response and acoustic radiation. The pipe structure is considered homogeneous over its surface area. The vibrational modes are assumed to be independent and lightly-damped i.e. no modal coupling due to damping occurs. The mode shapes were chosen to correspond to simply-supported end conditions, and therefore are separable into axial and circumferential components. The turbulence pressure field is considered homogeneous and stationary, with a cross-spectral density described by the Corcos model (equation [1.1]). There is assumed to be no interaction between the vibrating pipe and the wall-pressure field.

In a statistical formulation of the radiated power, only those modes whose wavespeeds are supersonic with respect to the external acoustic medium, are considered to contribute to the acoustic power radiation. Statistical estimates of the pipe vibrational response and acoustic radiation, which depend on a simplified pipe resonance frequency equation and an associated modal density expression, are compared with exact and approximate

theories. Wavenumber diagrams are introduced to illustrate the relationships existing for various flow, structural and acoustic parameters.

2.2 GENERAL FORMALISM FOR THE PIPE RESPONSE AND ACOUSTIC RADIATION

The total response of the pipe structure is represented by the response in its resonant modes. Accordingly, as derived by Bull and Rennison (1974a), following Powell (1958b), the spectral density of the displacement response, averaged over the pipe surface, $[[\phi_w(\omega)]]$, to a random stationary homogeneous pressure field is found to be

$$[[\phi_w(\omega)]] = \phi_p(\omega)\ S^2 \sum_\alpha \frac{[[\psi_\alpha^2(\underset{\sim}{r})]]\, j_{\alpha\alpha}^2(\omega)}{|Z_\alpha(\omega)|^2} \qquad [2.1]$$

where $\phi_p(\omega)$ is the power spectral density of the random pressure field acting on the structure of surface area S. $\underset{\sim}{r}$ defines the coordinates of the pipe surface.

$$Z_\alpha(\omega) = M_\alpha[\omega_\alpha^2 - \omega^2 + i\,(\frac{\omega_\alpha \omega}{Q_\alpha})] \qquad [2.2]$$

where $Z_\alpha(\omega)$, M_α, ω_α, Q_α and $\psi_\alpha(\underset{\sim}{r})$ are respectively the generalised obstructance, mass, resonance frequency, quality factor and shape of the αth mode.

The 'joint acceptance' $j_{\alpha\alpha}^2(\omega)$ of the αth mode, which is proportional to the generalised force of the αth mode, expresses the degree of spatial coupling existing between the pressure excitation and the shape of the αth mode, and is defined as

$$j_{\alpha\alpha}^2(\omega) = \frac{1}{S^2} \int_S dS(\underset{\sim}{r_1})\ \psi_\alpha(\underset{\sim}{r_1}) \int_S dS(\underset{\sim}{r_2})\ \psi_\alpha(\underset{\sim}{r_2})\ R_p(\underset{\sim}{\xi},\ 0;\omega) \qquad [2.3]$$

where $\underset{\sim}{\xi} = (\underset{\sim}{r_1} - \underset{\sim}{r_2})$. $R_p(\xi, 0;\omega)$ is the narrow-band correlation coefficient of the pressure field at zero time delay and is the real part of the cross-spectral density of the pressure field, normalised by its power spectral

density $\phi_p(\omega)$.

The total response at a particular frequency ω is the sum of the responses of all the individual modes. For lightly-damped structures, the response will be determined by the resonant contributions of each mode. In particular, the response in a narrow frequency band, whose centre frequency is ω_o, will be determined solely by the modes which are resonant within that band; equation [2.1] may be numerically integrated over the bandwidth, $\Delta\omega$, to give the response in that band. This will involve considerable computational effort for high modal densities and large bandwidths.

When $\phi_p(\omega)$ and $j^2_{\alpha\alpha}(\omega)$ are assumed to be essentially constant over $\Delta\omega$, and if $Q_\alpha >> \omega_o/\Delta\omega$, the resonant contribution of each mode may be represented by a delta function at its resonance frequency, as in Bull and Rennison (1974a). This leads to

$$[[\, \phi_w(\omega) \,]] \simeq \frac{\pi S^2 \phi_p(\omega)}{2\omega^3 \Delta\omega} \frac{[[\, \psi^2 \,]]}{M^2} \sum_{\alpha(\Delta\omega)} j^2_{\alpha\alpha}(\omega)\, Q \qquad [2.4]$$

where, for homogeneous structures and modes shapes corresponding to simply supported ends, $[[\, \psi^2_\alpha(\underset{\sim}{r}) \,]]$ and M_α (now denoted by $[[\, \psi^2 \,]]$ and M) are independent of α.

The mode order α is geometrically related to the structural wave vector through the angle θ which the wave vector makes with the coordinate axes. Thus, at a particular frequency, $j^2_{\alpha\alpha}(\omega)$ may be transformed to $j^2(\omega,\theta)$. Defining $n(\omega,\theta)$ as a continuous modal density function describing the number of modes per unit wave angle per unit frequency, the summation over mode order in equation [2.4] may be replaced for high modal densities by an integration over wave angle, where Q_α is also taken to be a continuous function of ω and θ. Equation [2.4] now becomes

$$[[\, \phi_w(\omega) \,]] \simeq \frac{\pi S^2 \phi_p(\omega)\ [[\, \psi^2 \,]]}{2\ \omega^3\ M^2} \int_\theta Q(\omega,\theta) j^2(\omega,\theta) n(\omega,\theta) d\theta \qquad [2.5]$$

which is the statistical counterpart of the exact formulation, equation [2.1]. Estimates of the modal resonance frequencies, mode shapes and the cross-spectral density of the turbulence pressure field are necessary to evaluate equations [2.1] and [2.5].

2.2.1 Cylinder Dynamics

Fig. 2.1 illustrates the pipe coordinate system. The vector $\underset{\sim}{r} = (x,y)$ defines the axial and circumferential coordinates of points on the pipe surface. (u_1, v, w) are displacements in the axial, tangential and radial directions respectively, at various $\underset{\sim}{r}$. ℓ, a, and h are the pipe length, mean radius and wall thickness respectively.

The mode shapes are given by the separable functions

$$\psi_\alpha(\underset{\sim}{r}) = \psi_{mn}(x,y) = \text{Sin } k_m x \begin{Bmatrix} \text{Sin } k_n y \\ \text{Cos } k_n y \end{Bmatrix} \qquad [2.6]$$

where $k_m = m\pi/\ell$; $k_n = n/a$; m is the number of axial halfwaves in length ℓ; and n is the number of full circumferential waves. As noted by Powell (1964), both sets of modes must be considered for the calculation of a homogeneous vibration response to a circumferentially homogeneous excitation. It should be noted that it will be difficult to identify both mode shapes corresponding to a particular resonance frequency; also $[[\psi^2]] = 1/4$ and $M = \rho_s h\, S/4$ for all modes, where ρ_s is the pipe density.

Resonance frequencies ω_{mn} are non-dimensionalized by the pipe 'ring' frequency as $\nu_{mn} = \omega_{mn}/\omega_r$, where $\omega_r = C_{Lp}/a$. Here $C_{Lp} = (E/\rho_s\gamma^2)^{1/2}$, is the speed of a compression wave in a plate of the pipe material; E and μ are respectively, the pipe elastic modulus and Poisson's ratio; and $\gamma^2 = 1 - \mu^2$. ν_{mn} can be calculated exactly, as required by equation [2.1], from Arnold and Warburton (1953). For the evaluation of equation [2.5], a simple approximate equation, derived from Heckl (1962), may be used. By assuming that $k_n a >> \nu_{mn}$, Heckl's equations lead to

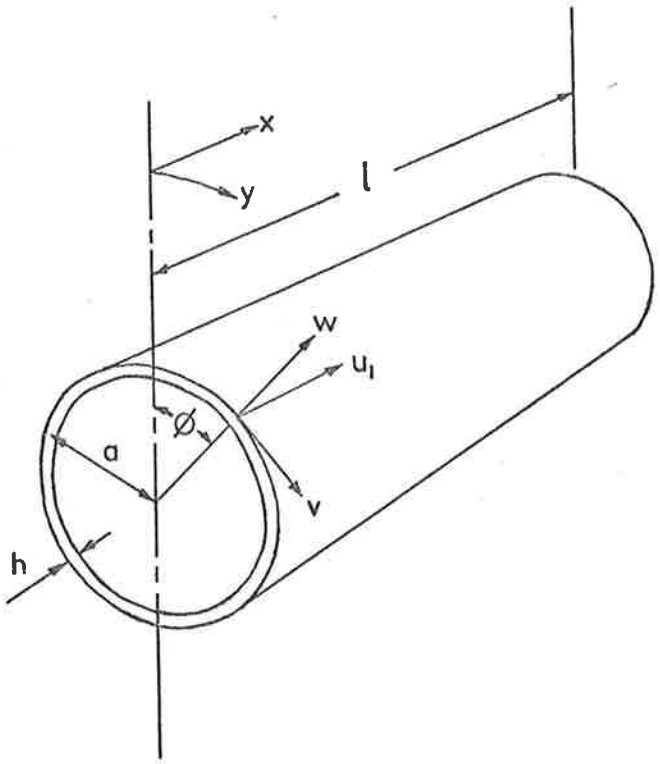

FIG. 2.1 CO-ORDINATE SYSTEM OF CYLINDRICAL PIPE

$$\nu_{mn}^2 = \beta^2 k^4 a^4 + \gamma^2 (k_m/k)^4 \qquad [2.7]$$

where $k^2 = k_m^2 + k_n^2$ and $\beta = (h/\sqrt{12}\,a)$. On comparison with Arnold and Warburton predictions, significant errors only occur for low-order circumferential modes, although the modal density of such modes is closely predicted.

The effect of variations in Poisson's ratio between different materials may be removed by writing equation [2.7] in the following form:

$$\bar{\nu}^2 = \bar{K}^4 + \mathrm{Sin}^4\theta \qquad [2.8]$$

where $\bar{\nu} = \nu/\gamma$, $\bar{K} = \sqrt{\beta/\gamma}\,K$, $K^2 = K_m^2 + K_n^2$, $K_m = k_m a$, $K_n = n$, $\bar{K}_m = \sqrt{\beta/\gamma}\,K_m$ $\bar{K}_n = \sqrt{\beta/\gamma}\,K_n$, and $\theta = \tan^{-1}(k_m/k_n)$. Fig. 2.2 is a non-dimensional structural wavenumber diagram, where lines of constant $\bar{\nu}$ (drawn by varying θ from 0 to $\mathrm{Sin}^{-1}(\sqrt{\bar{\nu}})$) represent the loci of all structural modes with resonance frequencies equal to $\bar{\nu}$. The area under each frequency curve is proportional to the total number of resonance frequencies below that frequency, so that the rate of change with $\bar{\nu}$ of the area beneath each curve of constant $\bar{\nu}$ is proportional to the density of resonance frequencies. The density of resonance frequencies per unit wave angle per unit $\bar{\nu}$ is calculated as

$$n(\nu, \theta) = \frac{\Lambda}{2\pi\beta}\left(1 - \frac{\mathrm{Sin}^4\theta}{\bar{\nu}^2}\right)^{-\frac{1}{2}} \qquad [2.9]$$

where $\Lambda = \ell/a$. Remembering that each resonance frequency corresponds to two resonant modes, the modal density $N(\nu)$ is defined as the density of resonance frequencies, namely

$$N(\nu) = \frac{\Lambda}{2\pi\beta}\int_0^{\theta}\left(1 - \frac{\mathrm{Sin}^4\theta}{\bar{\nu}^2}\right)^{-1/2} d\theta \qquad [2.10]$$

where $\theta = \mathrm{Sin}^{-1}(\bar{\nu}^{\frac{1}{2}})$ for $\bar{\nu} \leq 1$ and $\pi/2$ for $\bar{\nu} > 1$. Equation [2.5] must be multiplied by a factor of 2 to allow for both sets of modes.

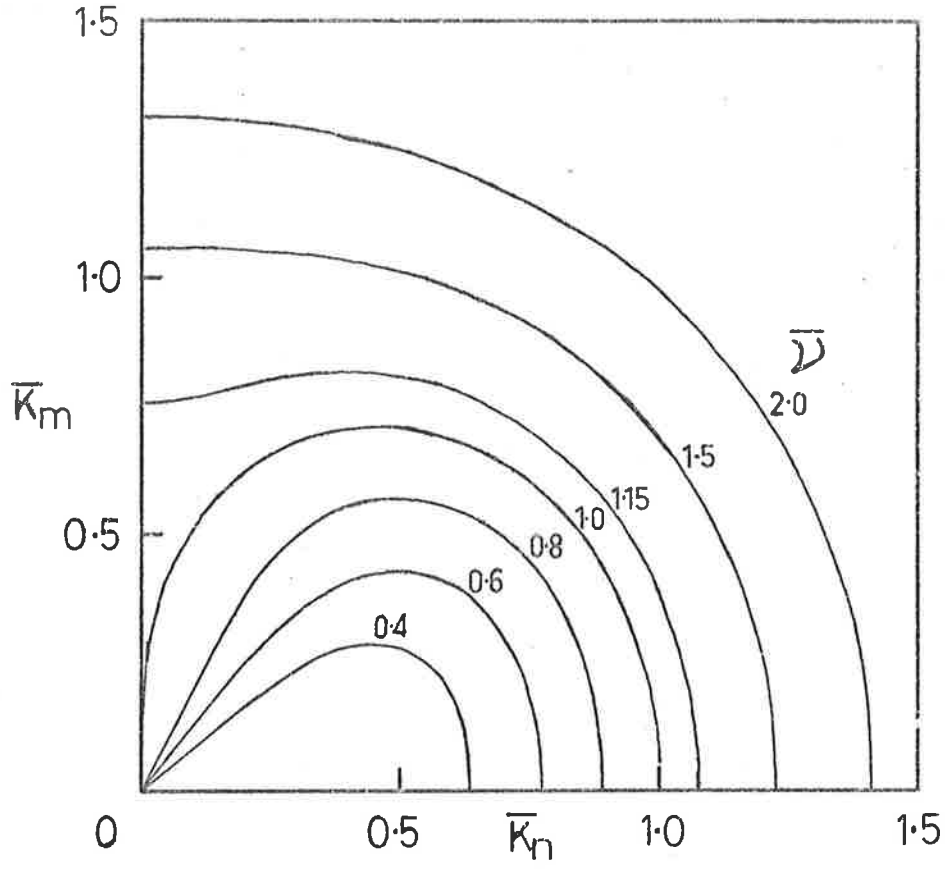

FIG. 2.2 NON-DIMENSIONAL WAVENUMBER DIAGRAM FOR PIPE

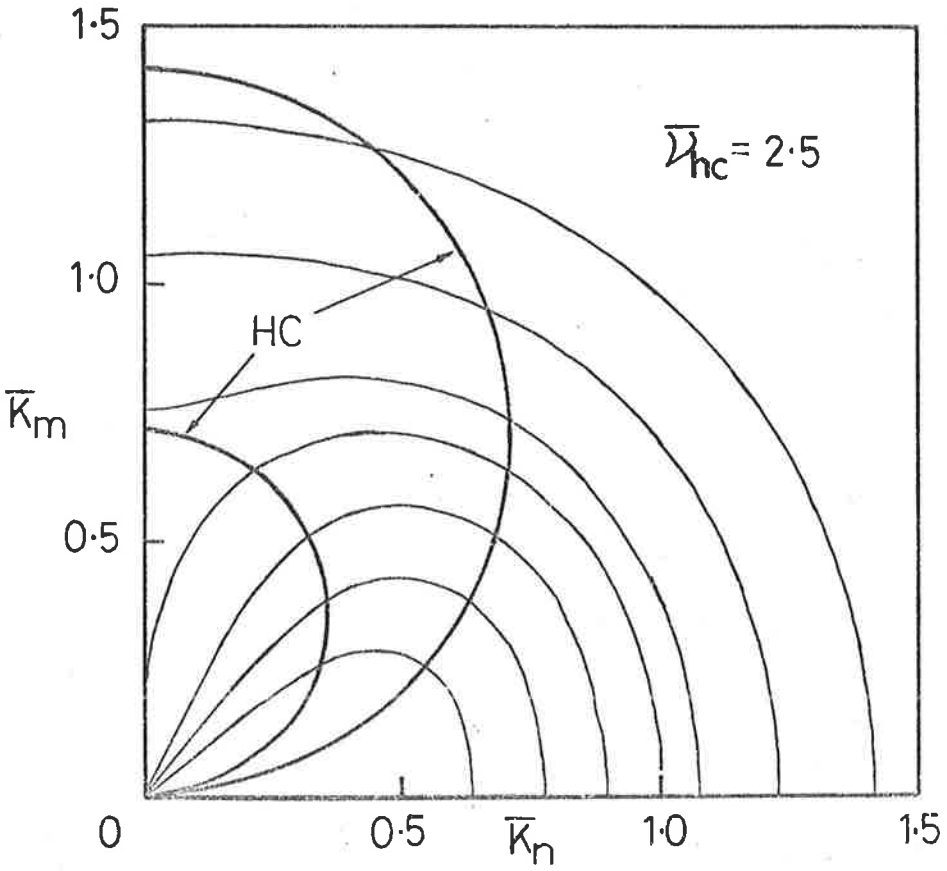

FIG. 2.3 HYDRODYNAMIC COINCIDENCE LINES

The modal density therefore refers to the density of one of the two sets of modes whose shapes are described by equation [2.6]. The modal density per unit wave angle per unit $\bar{\nu}$ is equal to the expression given by equation [2.9].

2.2.2 Properties of the Pressure Field and the Joint Acceptance

The Corcos model (equation [1.1]) has been used to describe the cross-spectral density of the turbulence wall-pressure field. The corresponding narrow-band correlation coefficient $R_p(\xi, \eta, \tau; \omega)$ at $\tau = 0$, is represented by the separable function,

$$R_p(\xi, \eta, 0; \omega) = e^{\left(-c_x \frac{\omega|\xi|}{U_c} - c_y \frac{\omega|\eta|}{U_c}\right)} \cos \frac{\omega|\xi|}{U_c} \qquad [2.11]$$

where the convection velocity U_c is assumed independent of frequency. Thus, $U_c = uU_o$, where U_o is the centreline velocity of the pipe flow: existing experimental data indicate that $u = 0.6$ (Corcos (1962)).

The joint acceptance of the (m,n)th vibrational mode is separable into axial and circumferential functions, as

$$j^2_{mnmn}(\omega) = j^2_{mm}(\omega)\, j^2_{nn}(\omega) \qquad [2.12]$$

Evaluation of the separate functions, as in Bull and Rennison (1974a), gives

$$\begin{aligned} j^2_{mm}(\omega) = \{&2[(K_m^2 - [1-c_x^2]K_c^2)^2 - 4c_x^2 K_c^4][1-(-1)^m e^{-c_x \Lambda K_c} \cos \Lambda K_c] \\ &+ 8c_x K_c^2 (K_m^2 - [1-c_x^2]K_c^2)(-1)^m e^{-c_x \Lambda K_c} \sin \Lambda K_c \\ &+ c_x \Lambda K_c K_m^2 (K_m^2 + [1+c_x^2]K_c^2)\Delta\}/\Lambda^2 K_m^6 \Delta^2 , \end{aligned} \qquad [2.13]$$

and

$$j_{nn}^2 = \frac{c_y K_c [1-(-1)^n e^{-c_y \pi K_c}]}{2\pi(c_y^2 K_c^2 + K_n^2)} \qquad [2.14]$$

where

$$\Delta = [(K_m^2 + [1 + c_x^2]K_c^2)^2 - 4K_m^2K_c^2]/K_m^4,$$

$$K_c = k_c a \text{ and } k_c = \omega/U_c,$$

and where equation [2.14] is the same for both sets of circumferential modes of equation [2.6].

Substitution of these equations in equation [2.5] leads to

$$[[\phi_w(\omega)]] = \frac{4\pi\ \phi_p(\omega)}{\rho_s^2 h^2 \omega^3 \omega_r}\ J(\nu) \qquad [2.15]$$

where

$$J(\nu) = \int_0^\theta Q(\nu,\theta)\ j^2(\nu,\theta)\ n(\nu,\theta)d\theta \qquad [2.16]$$

and $n(\nu,\theta)$ is the modal density per unit θ per unit $\bar{\nu}$. Account has been taken of both sets of modes with a factor of 2 in equation [2.15].

2.2.3 The Occurrence of Hydrodynamic Coincidence

In the literature survey, hydrodynamic coincidence was defined as that condition wherein the convection wavenumber of the turbulence pressure field $\bar{K}_c = \sqrt{\beta/\gamma}\ K_c$ is equal to the axial wavenumber of the structural resonant mode $\bar{K}_m$, where the flow is in the axial direction. Coincidence will result in an amplification of the modal response (see Figs. 1(a) to 1(c) of Appendix A). The hydrodynamic coincidence frequency $\omega_{hc} = (2\sqrt{3}\ U_c^2/hc_{Lp})$ is the highest frequency for which hydrodynamic coincidence may occur for turbulent flow over a flat plate of thickness h. When dealing with pipes, it may be non-dimensionalised by the ring frequency, as

$$\bar{\nu}_{hc} = \nu_{hc}/\gamma = \omega_{hc}/\gamma\omega_r = \frac{1}{\gamma\beta}\left(\frac{U_c}{c_{Lp}}\right)^2 = \frac{u^2 M_o^2}{\beta\gamma M_{Lp}^2} \qquad [2.17]$$

where $M_o = U_o/c$ is the centreline flowspeed, non-dimensionalised by the external speed of sound c; and $M_{Lp} = c_{Lp}/c$.

The conditions controlling coincidence at a particular frequency $\bar{\nu}$ may be examined by setting $\bar{K}_m = \bar{K}_c$ in equation [2.8]. It may then be shown that hydrodynamic coincidence can only occur if $\bar{\nu}_{hc} \geq 2$, in which case 3 possibilities arise:

$$\text{(i)} \quad \text{for } \bar{\nu} \leq \bar{\nu}_1 = \frac{\bar{\nu}_{hc}}{\sqrt{2}} \left[1 - (1 - 4/\bar{\nu}_{hc}^2)^{1/2}\right]^{1/2}$$

$$\simeq 1 + (2\bar{\nu}_{hc}^2)^{-1}, \text{ for } \bar{\nu}_{hc} > 2 ,$$

there will be two coincidence roots, corresponding to $\bar{K}_c = \bar{K}_m$;

$$\text{(ii)} \quad \text{for } \bar{\nu}_1 < \bar{\nu} < \bar{\nu}_2 = \frac{\bar{\nu}_{hc}}{\sqrt{2}} \left[1 + (1 - 4/\bar{\nu}_{hc}^2)^{1/2}\right]^{1/2}$$

$$\simeq \bar{\nu}_{hc}(1 - (2\bar{\nu}_{hc}^2)^{-1}), \text{ for } \bar{\nu}_{hc} > 2,$$

there will be one coincidence root;

(iii) for $\bar{\nu} > \bar{\nu}_2$, there will be no coincidence.

Calculations showing the variation in $j^2(\nu,\theta)$ with ν,θ and ν_{hc} are shown in Figs. 3 & 4 of Appendix 1. When coincidence can occur (i.e. for $\bar{\nu}_{hc} > 2$ and $\bar{\nu} < \bar{\nu}_2$), coincident modes dominate the vibrational response. Such conditions ($\bar{\nu}_{hc} > 2$) rarely arise in practical pipes (see later sections).

A hydrodynamic coincidence (H.C.) line, originally proposed by Chandiramani, Widnall, Lyon and Franken (1966), is the locus of modes for which $\bar{K}_c = \bar{K}_m$. It divides the structural wavenumber diagram into regions where $\bar{K}_c < \bar{K}_m$ and where $\bar{K}_c > \bar{K}_m$, as in Fig. 2.3 where $\bar{\nu}_{hc} = 2.5$. Reductions in computational effort may be achieved for $\bar{\nu} < \bar{\nu}_2$, by integrating the response spectral density (equation [2.15]) only over those modes within the region $\bar{K}_c \leq \bar{K}_m$.

2.2.4 Non-dimensional Response Spectral Densities

Non-dimensional spectral densities of the pipe displacement response $\Phi_w(\omega)$, velocity response $\Phi_{\dot{w}}(\omega)$, and acceleration response $\Phi_{\ddot{w}}(\omega)$, each averaged over the pipe surface, are defined by the following expressions.

$\Phi_w(\omega) = [[\phi_w(\omega)]]\ \omega_r/a^2$, is the spectral density of the pipe displacement response, averaged over the pipe surface;

$\Phi_{\dot{w}}(\omega) = [[\phi_{\dot{w}}(\omega)]]/a^2\omega_r = \Phi_w(\omega)\nu^2$, is the spectral density of the pipe velocity response, averaged over the pipe surface;

$\Phi_{\ddot{w}}(\omega) = [[\phi_{\ddot{w}}(\omega)]]/a^2\omega_r^3 = \Phi_w(\omega)\nu^4$, is the spectral density of the pipe acceleration response, averaged over the pipe surface.

Experimental data of the power spectral density of the turbulence wall-pressure field generally collapse well in the non-dimensional form,

$$\Phi_p(\omega) = \phi_p(\omega)U_o/q_o^2 a$$

where $q_o = \frac{1}{2}\rho_f U_o^2$ is the centreline dynamic pressure and ρ_f is the fluid density. $\Phi_p(\omega)$ is now used, in conjunction with the above definitions, to form ratios of the non-dimensional spectral densities of the pipe vibrational response to the non-dimensional spectral density of the turbulence pressure field.

From equation [2.15] and the above relations, we find

$$\frac{\Phi_w}{\Phi_p} = \frac{\pi}{12}\ \frac{\rho_{fs}^2\ M_o^3}{\beta^2\ M_{Lp}^3}\ \frac{J(\nu)}{\nu^3}\ , \qquad [2.18]$$

$$\frac{\Phi_{\dot{w}}}{\Phi_p}(\omega) = \frac{\pi}{12} \frac{\rho_{fs}^2 M_o^3}{\beta^2 M_{Lp}^3} \frac{J(\nu)}{\nu} \quad , \qquad [2.19]$$

and

$$\frac{\Phi_{\dot{w}}}{\Phi_p}(\omega) = \frac{\pi}{12} \frac{\rho_{fs}^2 M_o^3}{\beta^2 M_{Lp}^3} \nu J(\nu) \quad , \qquad [2.20]$$

In these latter equations, $\rho_{fs} = \rho_f/\rho_s$ and $J(\nu)$ is given by equation [2.16].

2.2.5 Acoustic Power Radiation

The spectral density of the acoustic power radiation from the pipe may be defined as

$$\phi_\pi(\omega) = R_{rad} [[\phi_{\dot{w}}(\omega)]] = R_{rad} [[\phi_w(\omega)]] \omega^2 \quad , \qquad [2.21]$$

where $R_{rad} = \rho c S \sigma$ is the pipe radiation resistance; σ is the radiation ratio; ρ and c are respectively, the density of and the acoustic wave velocity in the acoustic medium surrounding the pipe; and $[[\phi_{\dot{w}}(\omega)]]$ is the spectral density of the velocity response, averaged over the pipe surface.

A lower bound to the acoustic radiation from the pipe may be found by assuming that only those modes, whose structural wavespeeds are sonic or supersonic with respect to the external acoustic medium, contribute to the acoustic radiation, and that $\sigma = 1$ for these modes. (It is assumed $\sigma = 0$ for subsonic modes.) From equations [2.8] and [2.24], it can be shown* that supersonic pipe vibration modes can occur only for frequencies such that $K_a \geq 1$, where $K_a = \omega a/c = \nu M_{Lp}$. The power spectral density of the acoustic radiation from the pipe may then be found from equations [2.15] and [2.16], where the integration is performed over supersonic modes only. Defining the non-dimensional spectral density of the pipe acoustic radiation as $\Phi_\pi(\omega) = (\phi_\pi(\omega)/\rho c^2 S a)$ leads to

* Setting $K = K_a$ and $K_n = 1$ and eliminating $\sin^4\theta$ from equations [2.8] and [2.24] leads to $K_a \geq 1$ for the lowest frequency supersonic mode.

$$\frac{\Phi_\pi}{\Phi_p}(\omega) = \frac{\pi}{12} \frac{\rho_{fs}^2 M_o^3}{\beta^2 \nu M_{Lp}^2} J_s(\nu) , \qquad [2.22]$$

where

$$J_s(\nu) = \int_{\theta_1}^{\theta_2} Q(\nu,\theta)\, j^2(\nu,\theta) n(\nu,\theta) d\theta , \qquad [2.23]$$

and supersonic modes exist only in the range $\theta_1 \leq \vartheta \leq \theta_2$.

The acoustic coincidence frequency ω_{ac} is defined as that frequency at which the wavenumber of a grazing acoustic wave is equal to the wavenumber of a free bending wave in a plate of thickness h; it may be non-dimensionalised by the pipe ring frequency as

$$\bar{\nu}_{ac} = \frac{\nu_{ac}}{\gamma} = \frac{\omega_{ac}}{\gamma \omega_r} = \frac{1}{\gamma\beta} \left(\frac{c}{c_{Lp}}\right)^2 = (\gamma\beta M_{Lp}^2)^{-1}$$

The division of the wavenumber diagram into regions of supersonic and subsonic vibration modes is accomplished by setting $\bar{K} = \bar{K}_a$ in equation [2.8], (noting that $\bar{K}_a^2 = \bar{\nu}^2 / \bar{\nu}_{ac}$), thus constructing the sonic mode (S.M.) line(s). In equation [2.23], θ_2 is defined, for $\bar{\nu} \leq 1$ by the root of equations [2.8] with $K_n = 1$, since according to equation [2.8], no n = 0 modes exist for $\bar{\nu} \leq 1$; $\theta_2 = \pi/2$ for $\bar{\nu} > 1$. For $\bar{\nu} > \bar{\nu}_{ac}$, all modes are supersonic, so that $\theta_1 = 0$. On the other hand, for $\bar{\nu} < \bar{\nu}_{ac}$, θ_1 (and thus the range of supersonic modes) will vary as $\bar{\nu}_{ac} \gtrless 2$.

Following Bull and Rennison (1974a),

$$\theta_1 = \mathrm{Sin}^{-1} \left[\bar{\nu}^2 (1 - (\bar{\nu}/\bar{\nu}_{ac})^2)\right]^{\frac{1}{4}} \qquad [2.24]$$

For $\bar{\nu}_{ac} < 2$, supersonic modes will occur for frequencies where $\theta_1 < \theta_2$ ($K_a \gtrsim 1$) and θ_1 is found from equation [2.24]. There will be a single sonic mode line, since the argument of equation [2.24] is always real. Fig. 2.4(a) shows the wavenumber diagram for $\bar{\nu}_{ac} = 0.8$; modes within the shaded region A below the S.M. line are subsonic, while those in region C are

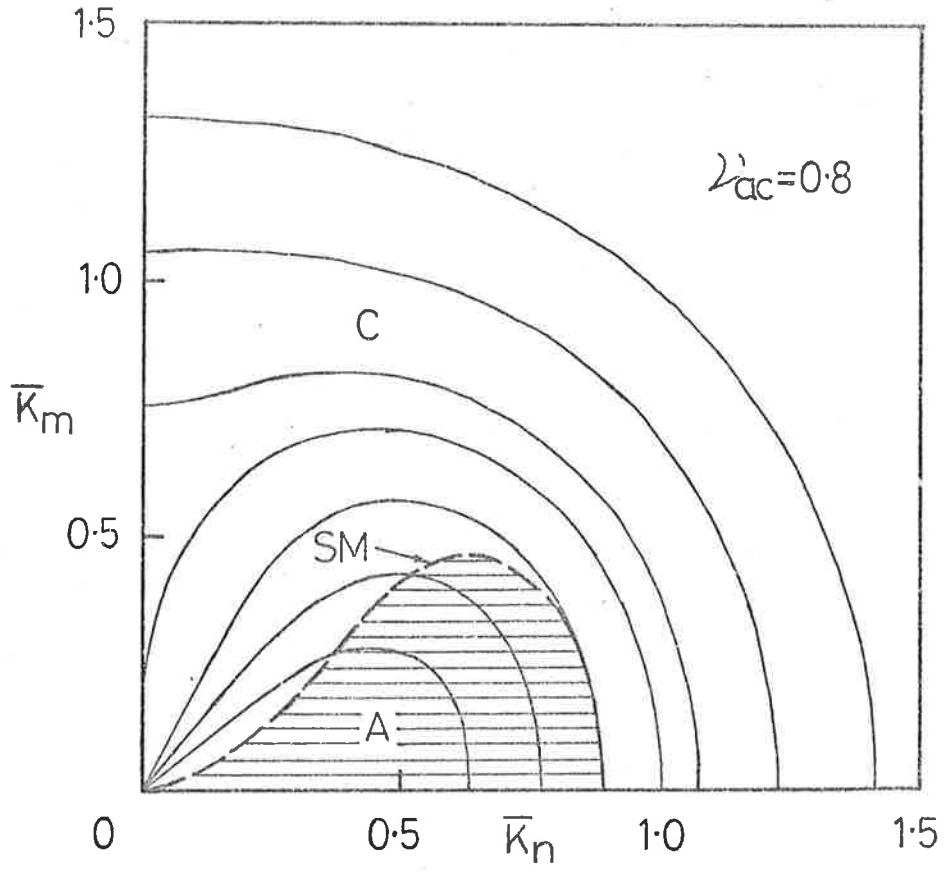

FIG. 2.4(a)

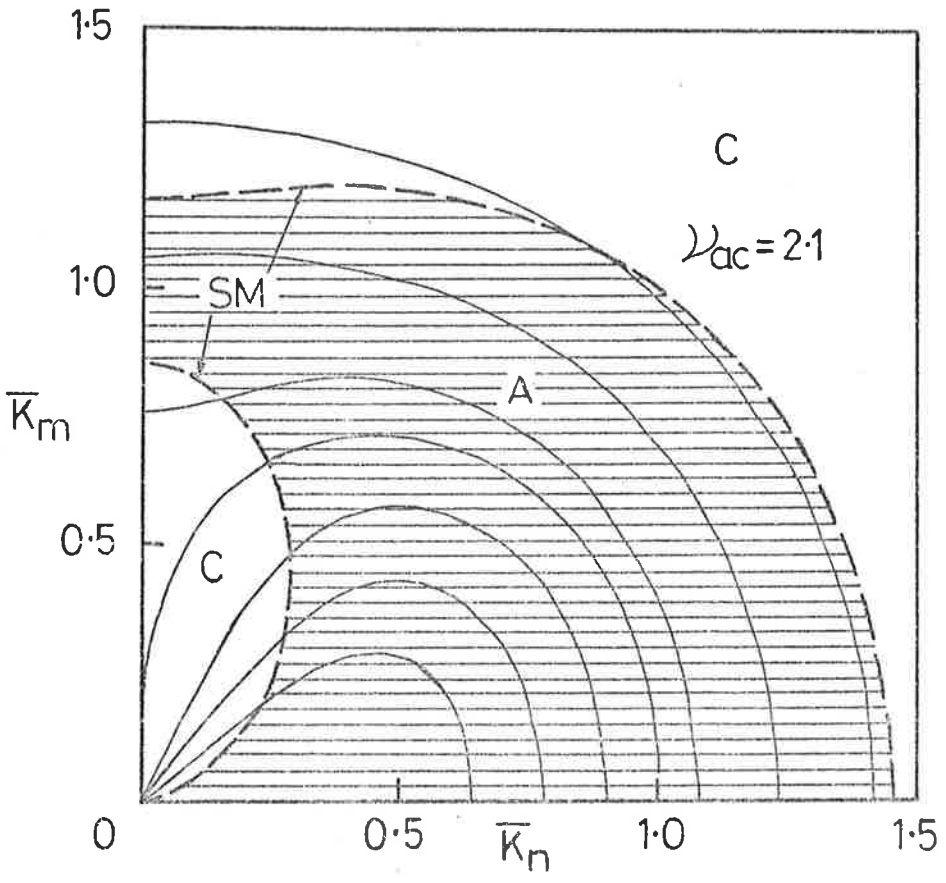

FIG. 2.4(b) SONIC MODE LINES

supersonic. For $\bar{\nu} < \bar{\nu}_{ac} > 2$, no supersonic modes exist over the frequency range $\bar{\nu}_B \leq \bar{\nu} \leq \bar{\nu}_A$, (corresponding to zero power radiation from resonant modes), where

$$\bar{\nu}_{A,B} = \frac{\nu_{ac}}{\sqrt{2}} [1 \pm (1 - 4 / \bar{\nu}^2)^{\frac{1}{2}}]^{\frac{1}{2}} \qquad [2.25]$$

For $\bar{\nu}_{ac} >> 2$, $\bar{\nu}_A \simeq \bar{\nu}_{ac}$ and $\nu_B \simeq 1$. Fig. 2.4(b) shows the situation for $\bar{\nu}_{ac} = 2.1$. Now two S.M. lines are generated defining the region of subsonic modes A ($\bar{\nu}_B = 1.238$ and $\bar{\nu}_A = 1.696$).

At frequencies such that $K_a < 1$, what radiation occurs must result from subsonic modes, since in fact $\sigma \neq 0$ but only $<< 1$. Following Junger and Feit (1972), we may derive an expression for the radiation ratio of any structural mode on a finite length cylinder. In Appendix B, it is shown that, for pipes, the assumption that $\sigma = 0$ for subsonic modes is rather poor unless $K_n >> K_a$. The main analytical result from Appendix B is

$$\sigma_{mn} = \frac{16\Lambda}{\pi^4 m^2} \int_0^{\pi/2} \frac{\text{Cos}^2 \text{ or } \text{Sin}^2 (\frac{K_a \Lambda}{2} \text{Cos } \zeta) \, d\zeta}{\text{Sin}\zeta \left| H_n' (K_a \text{Sin}\zeta) \right|^2 (1 - \{\frac{K_a \Lambda \text{Cos}\zeta}{m\pi}\}^2)^2} \qquad [2.26]$$

where Sin^2 is used when m is even, and Cos^2 used when m is odd.

Equation [2.26] may be used to estimate an upper bound to the acoustic radiation from pipes (i.e. the contribution from subsonic as well as supersonic modes). The exact analysis which sums the contribution from all modes must then be used, rather than the statistical analysis (equation [2.22]), since equation [2.26] may not be readily expressed as a continuous function of wave angle θ. Such an exact approach is discussed in section 2.2.7, where the lower and upper bound calculations are compared.

2.2.6 Approximations to $\Phi_{\ddot{w}}$ and Φ_{π} for Practical Pipes

It has been argued, by Bull and Rennison (1974b), Rattayya and Junger (1964), and Clinch (1970), that for practical pipe flow situations,

$\bar{K}_c >> \bar{K}_m$. Thus convection of the pressure field will play no part in the coupling between the pipe and the excitation. Approximate expressions for the joint acceptance have been developed (Bull and Rennison (1974b)) to give

$$j^2_{mm}(\omega) \simeq \frac{c_x}{\Lambda K_c} = \frac{uc_x M_o}{\Lambda \nu M_{Lp}}$$

$$j^2_{nn}(\omega) \simeq \frac{1}{2\pi c_y K_c} = \frac{uM_o}{2\pi c_y \nu M_{Lp}}$$

(That j^2_{mm} and j^2_{nn} depend on K_c^{-1} results from the assumption of the $\omega\xi/U_c$ and $\omega\eta/U_c$ similarity in spatial coherence present in the Corcos model of the turbulence pressure field cross-spectral density.) Furthermore.

$$j^2(\nu,\theta) \simeq \frac{u^2}{2\pi}\frac{c_x}{c_y}\frac{M_o^2}{\Lambda\nu^2 M_{Lp}^2} \qquad [2.27]$$

which is independent of structural mode order (i.e. θ).

If $Q(\nu,\theta) = Q$, then equation [2.20] becomes

$$\frac{\Phi_{\ddot{w}}}{\Phi_p} \simeq \frac{u^2}{24}\frac{c_x}{c_y}\frac{\rho_{fs}^2 M_o^5 Q}{\Lambda\beta^2 M_{Lp}^5}\frac{N(\nu)}{\nu} \qquad [2.28]$$

This may be re-written as

$$\frac{\Phi_{\ddot{w}}}{\Phi_p} = \frac{u^2}{96}\frac{c_x}{c_y}\frac{\rho_{fs}^2 M_o^5 Q}{\beta^3 M_{Lp}^5}\frac{f(\nu)}{\nu} \qquad [2.29]$$

where $f(\nu) = \frac{2}{\pi}\int_0^{\theta}(1 - \frac{\mathrm{Sin}^4\theta}{\bar{\nu}^2})^{-\frac{1}{2}}d\theta$ and $\theta = \mathrm{Sin}^{-1}(\bar{\nu}^{-\frac{1}{2}})$ for $\bar{\nu} \leq 1$ and $\pi/2$ for $\bar{\nu} > 1$. $f(\nu)/\nu$ is dependent only on $\bar{\nu}$, so that equation [2.29] indicates the theoretical dependence of $\Phi_{\ddot{w}}$ on flow and structural parameters. For example, $\Phi_{\ddot{w}}$ will be proportional to $\Phi_p \rho_{fs}^2 Q$, will depend on the fifth power of the flow speed M_o, but will be inversely proportional to $\beta^3 M_{Lp}^5$. Furthermore, for $\bar{\nu} << 1$, $f(\nu)\alpha\bar{\nu}^{-\frac{1}{2}}$, while for $\bar{\nu} > 1$, $f(\nu) = 1.0$: the theoretical frequency dependence may be predicted over a broad range of $\bar{\nu}$.

If Q_s is the average quality factor of supersonic modes, equation [2.22] approximates to

$$\frac{\Phi_\pi}{\Phi_p} \simeq \frac{u^2}{24} \frac{c_x}{c_y} \frac{\rho_{fs}^2 M_o^5 Q_s}{\Lambda \beta^2 M_{Lp}^4} \frac{N_s}{\nu^3} \qquad [2.30]$$

where $N_s = \int_{\theta_1}^{\theta_2} n(\nu,\theta)d\theta$, and θ_1 and θ_2 are determined as in equation [2.23]. θ_1 and hence N_s depend on β and M_{Lp}, so that, while equation [2.30] expresses the dependence of Φ_π/Φ_p on M_o, ρ_{fs} and Q_s correctly, further approximations to N_s are required to establish the dependence on β, ν and M_{Lp}. Following Bull and Rennison (1974b), for $\bar{\nu} << 1$ and $\bar{\nu} << \bar{\nu}_{ac}$,

$$N_s(\nu) \simeq \frac{\Lambda M_{Lp}^2 \nu^{3/2}}{4 \pi \gamma^{1/2}} \qquad [2.31]$$

while for $\bar{\nu} > \bar{\nu}_{ac}$, $N_s(\nu) = N(\nu)$. Pipes of the same material (M_{Lp} constant) and same length and radius, but with different values of β, will have varying dependence on β, as $\bar{\nu} \gtrless \bar{\nu}_{ac}$. For $\bar{\nu} >> 1 > \bar{\nu}_{ac}$, $N_s \simeq \Lambda/4\beta$, so that Φ_π/Φ_p will be inversely proportional to $\beta^3 M_{Lp}^4 \nu^3$, while for $\bar{\nu} << 1 < \bar{\nu}_{ac}$ Φ_π/Φ_p will be inversely proportional to $(\beta^2 M_{Lp}^2 \nu^{3/2})$.

From such considerations, the dependence of the non-dimensional spectral densities of the acceleration response and the acoustic power radiation on flow and structural parameters can be predicted. The approximate expressions not only provide useful simplifications for estimating the vibrational response and acoustic power radiation for thin pipes, but also indicate the manner in which the experimental results for different flow/structural configurations may be compared.

2.2.7 Numerical Evaluation of the Alternative Analytical Approaches

The nature and magnitude of the errors introduced by the assumptions of the statistical analysis may be demonstrated by comparing exact and statistical calculations of $\Phi_{\dot{w}}/\Phi_p$ and Φ_π/Φ_p. Such calculations are presented for a pipe/flow configuration which is representative of the

experimental work described in the following chapters. The following parameters were chosen: $\Lambda = 100.$; $\mu = 0.3$; $\beta = 0.010$; $M_{Lp} = 15.11$; $M_o = 0.371$; $\rho_{fs} = 0.0001504$ so that $\gamma = 0.954$, $\bar{\nu}_{hc} = 0.0227$ and $\bar{\nu}_{ac} = 0.459$.

Acceleration Response — A non-dimensional form of the exact expression for $\Phi_{\ddot{w}}/\Phi_p$ may be developed from equation (2.1) to give:

$$\frac{\Phi_{\ddot{w}}}{\Phi_p} = \frac{\rho_{fs}^2 M_o^5}{12 \beta^2 M_{Lp}^3} \sum_{\alpha} \frac{j_{\alpha\alpha}^2(\omega)}{[\{1 - (\frac{\omega_\alpha}{\omega})^2\}^2 + (\frac{\omega_\alpha}{\omega Q_\alpha})^2]} \qquad [2.32]$$

where values of ω_α and $j_{\alpha\alpha}^2(\omega)$ are calculated from Arnold and Warburton (1953) and from equations [2.12] to 2.14] respectively. Equation [2.32] may be averaged over $\frac{1}{3}$ - octave bands (by integrating and dividing by the bandwidth) for comparison with the statistical calculations, as given by equation [2.20]. These two calculations are presented in Fig. 2.5(a) : modal quality factors have been assumed constant and equal to 2000 for all modes i.e. $Q_\alpha = Q = 2000$. At low frequencies, the exact analysis (curve (i)) shows the contributions of groups of circumferential modes of low m. The statistical analysis (curve (ii)) smooths this low frequency variation of $\Phi_{\ddot{w}}/\Phi_p$ through the use of the continuous modal density function $n(\nu,\theta)$. As ν increases, the statistical analysis agrees closely with the exact theory: e.g. for $\nu > 0.05$, the two approaches differ by less than 1dB. Under the assumption of light but equal modal damping, the statistical analysis is a good approximation to the exact theory for calculations of the vibrational response.

Acoustic Radiation — On substituting non-dimensional expressions for Φ_π and $\Phi_{\ddot{w}}$ into equation [2.21], it follows that, for each individual mode,

$$\Phi_\pi = \Phi_{\ddot{w}} \sigma M_{Lp}/\nu^2 \qquad [2.33]$$

where σ is the modal radiation ratio. Equation [2.33] may be used to define the average radiation ratio of a group of modes at frequency ν

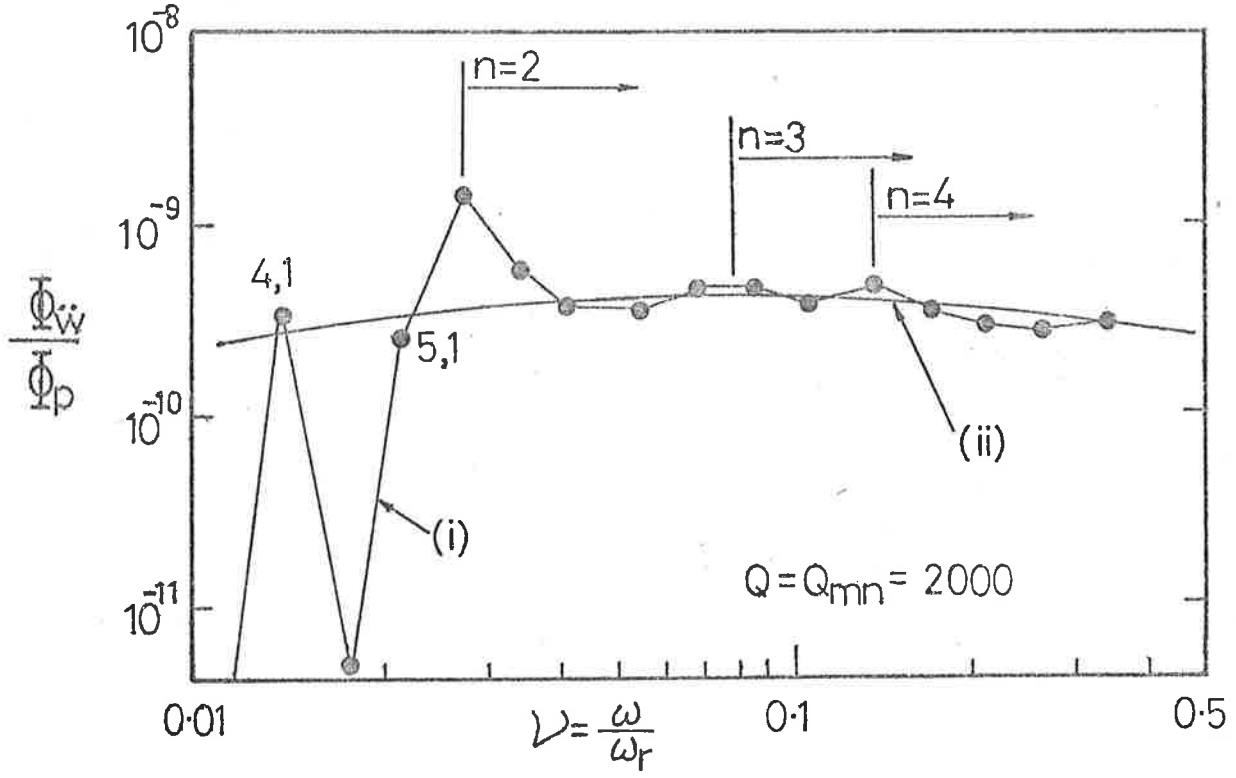

FIG. 2.5(a) EXACT & STATISTICAL CALCULATIONS $\Phi_{\ddot{w}}$

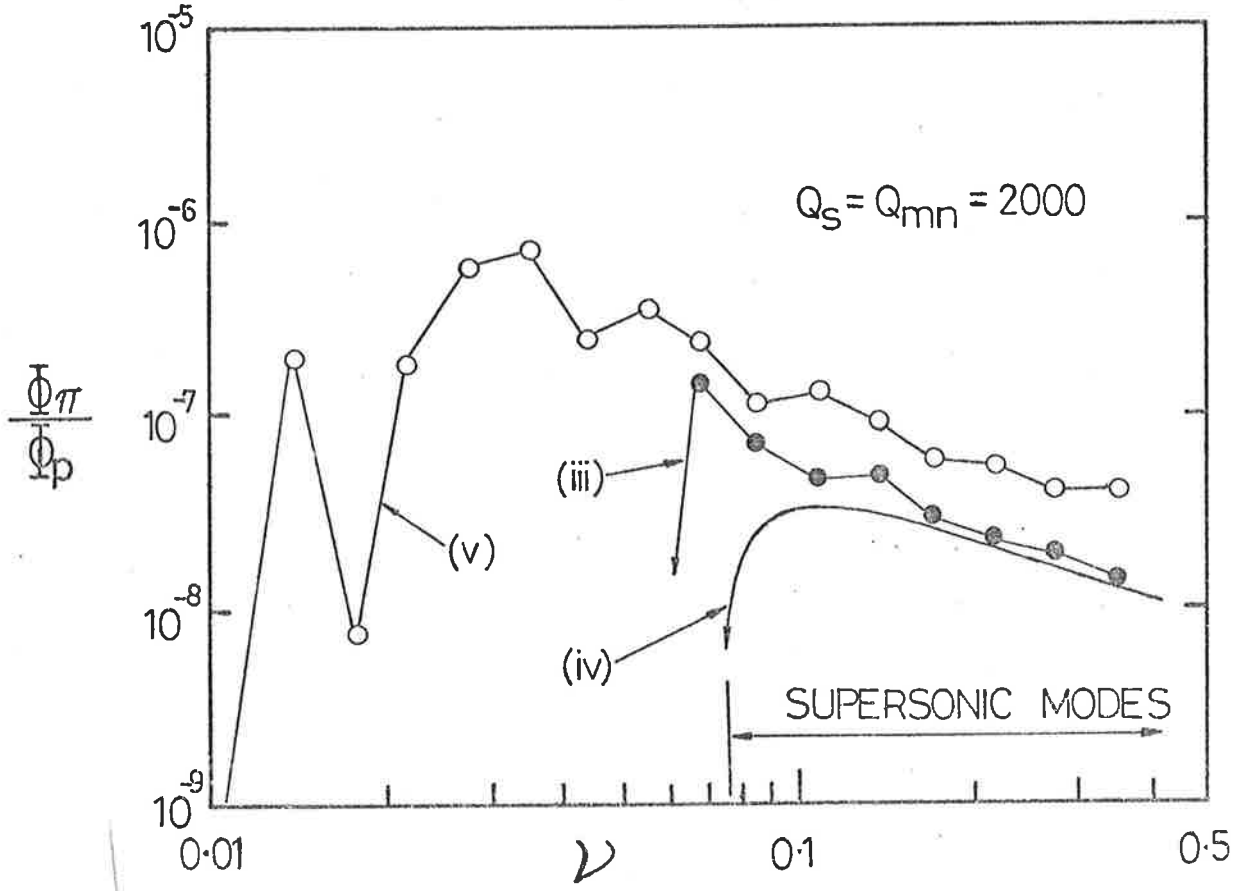

FIG. 2.5(b) EXACT & STATISTICAL CALCULATIONS Φ_{π}

where $\Phi_{\ddot{w}}$ and Φ_{π} are the total vibrational response and power radiation from all the contributing modes at ν. When equation [2.33] is substituted in equation [2.32], the total acoustic power radiated is given by

$$\frac{\Phi_{\pi}}{\Phi_{p}} = \frac{\rho_{fs}^2 M_o^3}{6\nu^2 M_{Lp}^2 \beta^2} \left(\sum_{\alpha} \frac{j_{\alpha\alpha}^2(\omega)\, \sigma_{\alpha}}{[\{1 - (\frac{\omega_{\alpha}}{\omega})^2\}^2 + (\frac{\omega_{\alpha}}{\omega Q_{\alpha}})^2]} \right) \qquad [2.34]$$

where values of σ_{α} are found from equation [2.26].

The statistical analysis of the acoustic radiation assumes that only supersonic modes radiate significant acoustic power, and that these modes have unit radiation ratio. In order to verify this assumption, the summation of equation [2.34] has been restricted to supersonic modes to give a direct comparison with the statistical approach of equation [2.22]; Q_s in the statistical analysis and Q_{α} in the exact approach are taken to be constant and equal to 2000. In Fig. 2.5(b), the two calculations are seen to give similar results; the statistical calculation (curve (iv)) lies slightly below the exact (curve (iii)), reflecting the choice of upper integration limit corresponding to n = 1 modes in equation [2.23] for J_s. As ν increases, the two calculations agree closely. The onset of supersonic modes actually occurs at a slightly lower frequency than predicted statistically, but the difference is less than 5%. It is concluded that the statistical analysis is a good approximation to the exact analysis of the acoustic radiation from supersonic modes, especially for $K_a > 2$.

The contribution of subsonic modes to the total radiation may be found from equation [2.34], when the summation is taken over all modes, using appropriate values of σ_{α}. This calculation is shown in Fig. 2.5(b) as curve (v): all modes have $Q_{\alpha} = 2000$. Significant acoustic radiation results from subsonic modes at all frequencies up to ν_{ac} (above which all modes are supersonic). At frequencies below the first supersonic mode in these calculations, the additional acoustic radiation is produced mainly by subsonic n = 1 modes; these have relatively higher radiation ratios than

higher circumferential order modes which occur at the same ν and which strongly influence $\Phi_{\ddot{w}}/\Phi_p$.

Effect of Realistic Variations in Q_α In practical situations involving lightly-damped pipe materials, radiation damping tends to reduce the influence of those modes with high radiation ratios: i.e. the assumption $Q(\nu,\theta) = Q$ is not generally valid.

To include this effect in the exact calculations of $\Phi_{\ddot{w}}/\Phi_p$ and Φ_π/Φ_p, the overall modal quality factors Q_α have been calculated from the relation

$$\frac{1}{Q_\alpha} = \frac{1}{Q_i} + \frac{1}{Q_{rad}} \qquad [2.35]$$

where Q_i is the internal quality factor associated primarily with material damping for pipes (see section 4.3) and has been set equal to 2000 for all modes, and Q_{rad} is the quality factor resulting from acoustic radiation damping, and is calculated from

$$Q_{rad} = \frac{\omega M}{R_{rad}} = \frac{\omega \rho_s h}{\rho c \sigma_\alpha} \qquad [2.36]$$

using values of σ_α calculated from equation [2.26].

In calculations of $\Phi_{\ddot{w}}/\Phi_p$ using the statistical analysis, the average quality factors Q have been set equal to 2000, since for $\nu < \nu_{ac}$, subsonic modes (of generally lower radiation ratio) control the vibrational response. However, in calculations of Φ_π/Φ_p, the average quality factors of supersonic modes Q_s have been found from

$$Q_s = \frac{\omega \rho_s h}{\rho c} \qquad [2.37]$$

since $\sigma = 1$ for these modes and $Q_s << Q$ for $\nu < \nu_{ac}$ for the present pipe.

These various calculations are shown in Fig. 2.5(c) to (e). In the calculation of $\Phi_{\ddot{w}}/\Phi_p$ (Fig. 2.5(c)), close agreement between the two

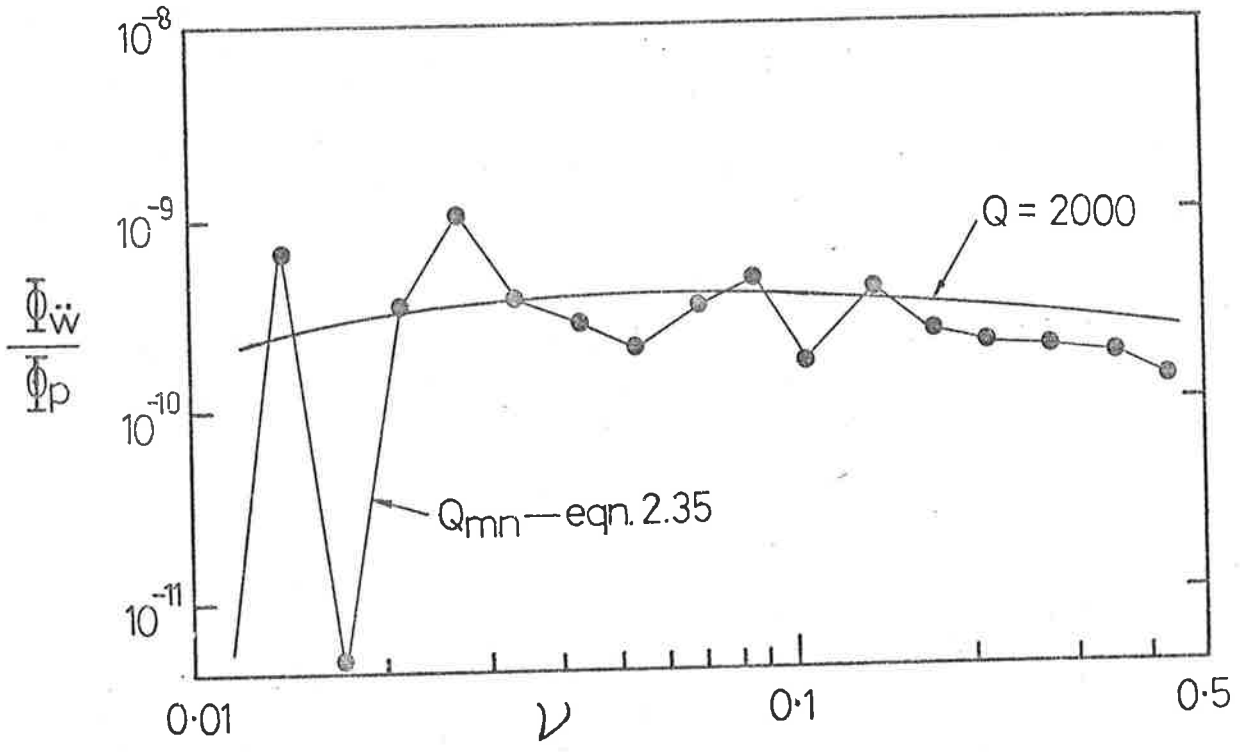

FIG. 2.5(c) $\Phi_{\ddot{w}}$ CALCULATIONS ALLOWING FOR RADIATION DAMPING

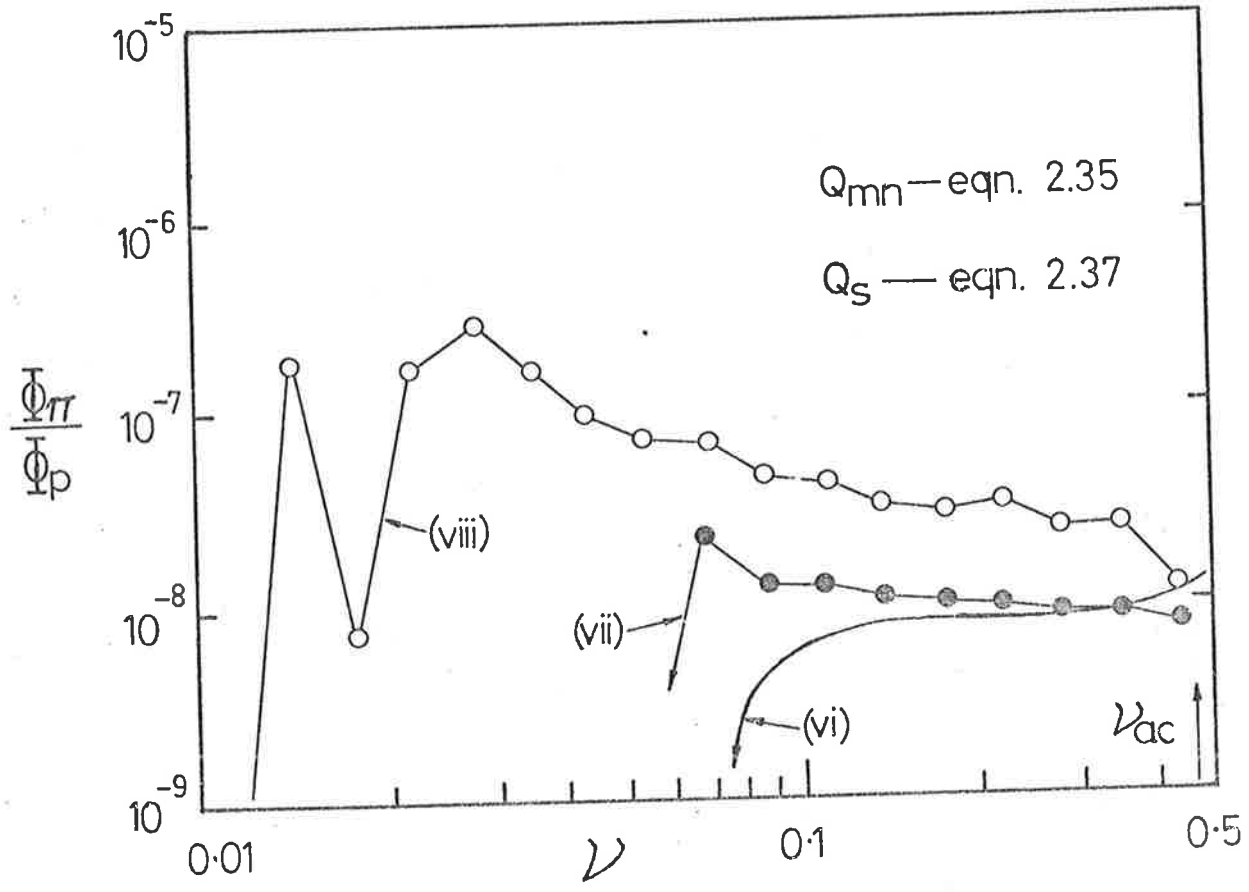

FIG. 2.5(d) $\Phi_{\pi\pi}$ ALLOWING RADIATION DAMPING

analyses still exists, suggesting that modes which are significantly damped by acoustic radiation losses, do not greatly influence the response for this pipe: however, referring to Figs. 2.5(a) and 2.5(c), we see that the additional differences between the two analyses, result directly from the radiation damping of subsonic modes, e.g. at $\nu = 0.055$ and 0.11, and for $\nu > 0.2$. In Fig. 2.5(d), the inclusion of radiation damping is seen to cause the values of Φ_π/Φ_p from the statistical analysis (curve (vi)) and the exact analysis based on supersonic modes only (curve (vii)) to decrease relative to the total acoustic radiation from all modes (curve (viii)). In fact, curve(viii) is also lower than the level of curve (v) in Fig. 2.5(b) as a result of radiation damping. The acoustic radiation produced by subsonic modes is significantly greater than that produced by the radiation-damped supersonic modes for all ν up to ν_{ac}.

This may be more clearly demonstrated by plotting the average radiaton ratios for the various calculations using equation [2.33] as a basis. The statistical analysis calculation (curve (ix)) lies 2dB below the exact analysis which is based on supersonic modes only (curve (x)). The inclusion of the contribution by lightly-damped subsonic modes to the acoustic radiation is seen to lead to large increases in the average radiation ratio for all ν up to ν_{ac}.

2.2.8 Significance of Different $\bar{\nu}_{ac}$ and $\bar{\nu}_{hc}$ Combinations

Hydrodynamic coincidence will only occur for $\bar{\nu}_{hc} \geq 2$. In practical terms, this corresponds to unusually high flow speeds and very thin-walled pipes. For example, since

$$\bar{\nu}_{hc} = u^2 M_o^2 \bar{\nu}_{ac} = M_c^2 \bar{\nu}_{ac} \qquad [2.37]$$

it can be seen that, for a thin-walled steel pipe (h = 1.0mm, a = 15cms, $\beta = 0.00192$), $\bar{\nu}_{ac} = 2.34$, requiring that $M_o \geq 1.54$ for coincidence to occur at all. In fact, four different combinations of $\bar{\nu}_{ac}$ and $\bar{\nu}_{hc}$ arise, as

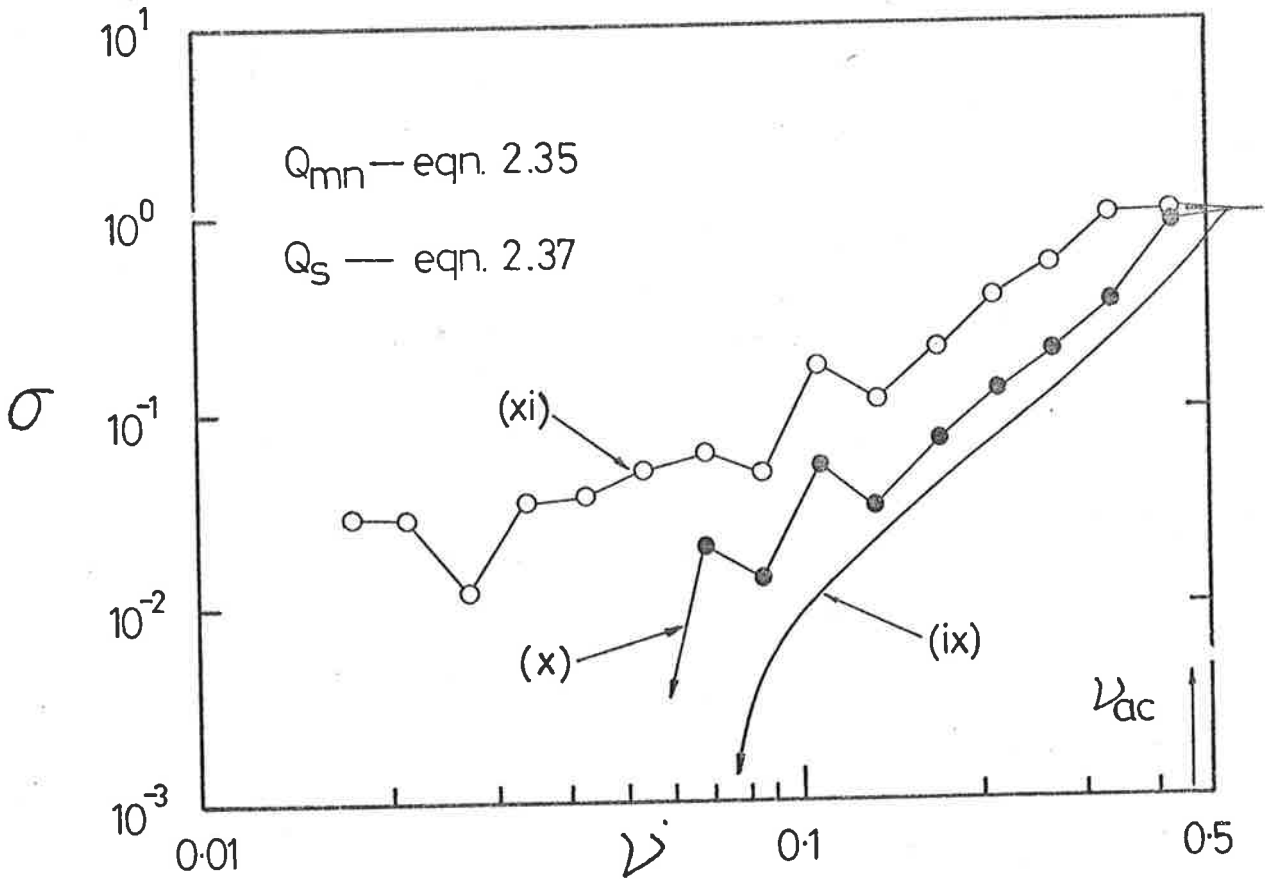

FIG. 2.5(e) σ ALLOWING FOR RADIATION DAMPING

$\bar{\nu}_{ac} \lessgtr 2$ and $\bar{\nu}_{hc} \lessgtr 2$. These cover the full range of pipe-flow situations, as discussed in some detail in Bull and Rennison (1974c). To illustrate the effects of different combinations of $\bar{\nu}_{ac}$ and $\bar{\nu}_{hc}$, H.C. and S.M. lines may be superimposed on a wavenumber diagram, to generate four different classifications of modes.

Case 1 : both $\bar{\nu}_{hc}$ and $\bar{\nu}_{ac} < 2$ Hydrodynamic coincidence cannot occur for $\bar{\nu}_{hc} < 2$, so that $K_c > K_m$ for all modes. There will be no H.C. lines on the wavenumber diagram. Since $\bar{\nu}_{ac} < 2$, supersonic modes will exist for all frequencies, and there will be only a single S.M. line. Figure 2.4(a) is a typical example of an industrial steel pipe; here $\bar{\nu}_{ac} = 0.8$ while $\bar{\nu}_{hc} < 2$. Region A contains only subsonic modes for which $K_c > K_m$ and region C contains only supersonic modes for which $K_c > K_m$.

Case 2 : $\bar{\nu}_{hc} < 2 < \bar{\nu}_{ac}$ Hydrodynamic coincidence cannot occur and $K_c > K_m$ for all modes. Since $\bar{\nu}_{ac} > 2$, the wavenumber diagram is divided, as in Fig. 2.4(b) where $\bar{\nu}_{ac} = 2.1$, into two regions of supersonic modes (C) and one region of subsonic modes (A), as discussed in section 2.2.5. A rigid P.V.C. pipe at subsonic flow speeds would belong in this category.

Case 3 : Both $\bar{\nu}_{hc}$ and $\bar{\nu}_{ac} > 2$ Restricting the example to subsonic convection speeds, then $\bar{\nu}_{ac} > \bar{\nu}_{hc} > 2$. Choosing $\bar{\nu}_{hc} = 2.5$ and $\bar{\nu}_{ac} = 10.$, we draw Fig. 2.6. Region B contains only subsonic modes for which $K_c < K_m$. The response of modes in region B will be amplified by hydrodynamic coincidence; however, following the assumption of the statistical analysis (that $\sigma = 0$ for subsonic modes), the power radiation will be confined to supersonic modes (region C), for which hydrodynamic coincidence cannot occur, as $M_c < 1$ in this case. Acoustic radiation is confined to $\nu \leq 1$ under these assumptions, which were shown , in fact, to provide a considerable underestimate for real pipes. For the purposes of an experimental examination, case 3 could be achieved with high subsonic internal flow speeds and an extremely thin-walled pipe.

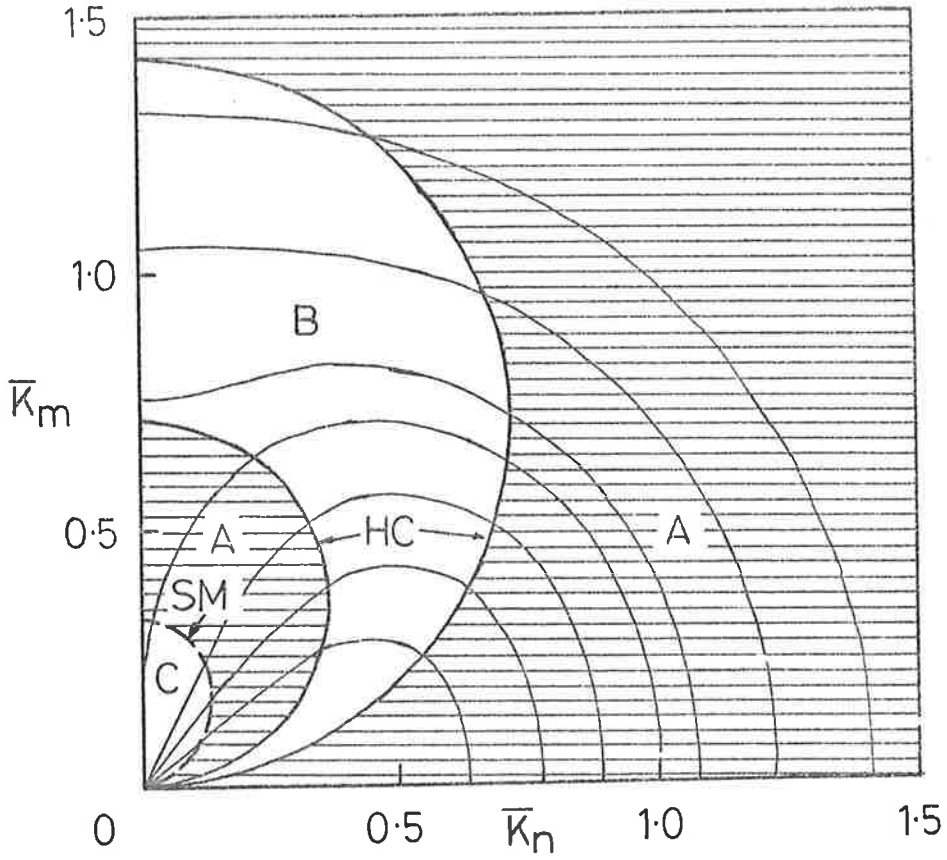

FIG. 2.6 H.C. & S.M. LINES: $\lambda_{hc}=2{\cdot}5$ $\lambda_{ac}=10{\cdot}$

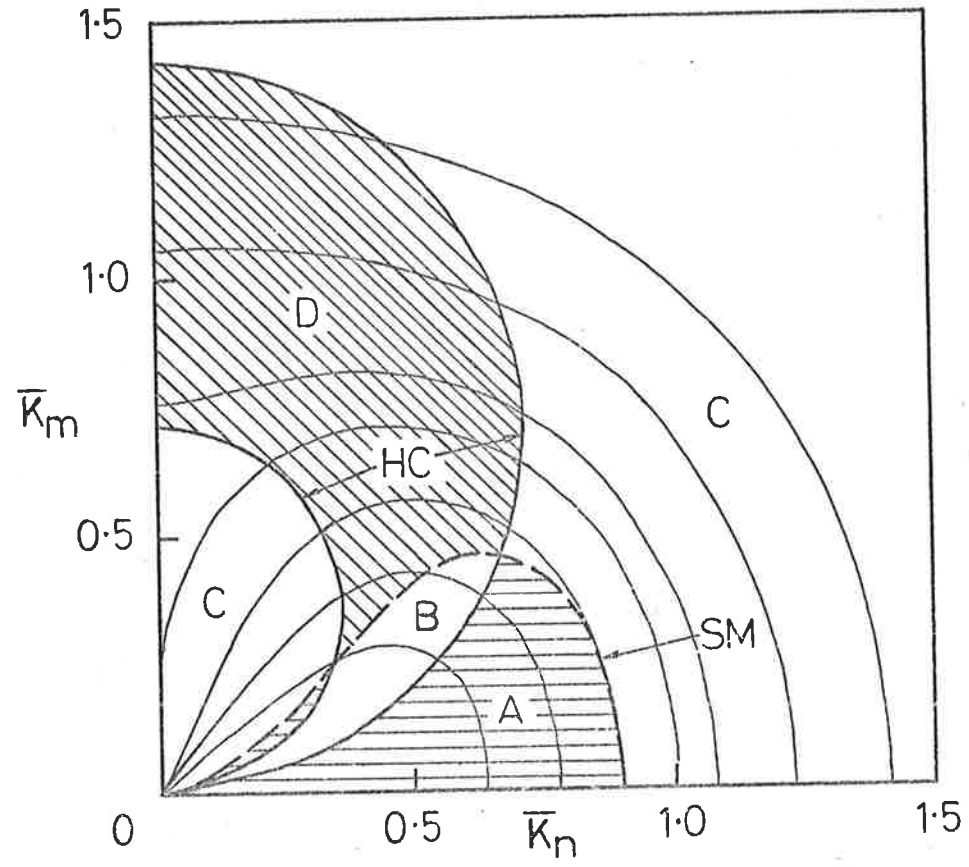

FIG. 2.7 H.C. & S.M. LINES: $\lambda_{hc}=2{\cdot}5$ $\lambda_{ac}=0{\cdot}8$

Case 4 : $\bar{\nu}_{hc} > 2 > \bar{\nu}_{ac}$ This case corresponds to supersonic internal flow and as such would represent a case rarely met in practice, except perhaps for short lengths of pipe immediately downstream of valves. Combination of Fig. 2.3 ($\bar{\nu}_{hc} = 2.5$) and Fig. 2.4(a) ($\bar{\nu}_{ac} = 0.8$) as in Fig. 2.7 illustrates that,in this case, a region D of supersonic modes for which $K_c \leq K_m$ will exist. Since their response is amplified by coincidence and they have unit radiation ratio, they will control the acoustic radiation.

Cases 1 and 2 cover the broad range of industrial piping systems, while cases 3 and 4 occur only in extreme circumstances. However, it was desirable to attempt an examination of each case in order to verify the theoretical model presented. As described in later chapters, experimental work was concentrated mainly on case 1, where steel pipes of varying wall thickness were used to provide different values of $\bar{\nu}_{ac} < 2$. The investigation was extended to case 2 by changing the pipe material. Rigid P.V.C. with a value of $\bar{\nu}_{ac} = 2.04$ was used. Case 3 was examined in a complex experimental arrangement, in which a very thin-walled brass tube was restrained from collapsing during the experiment by pre-tensioning the tube within a small anechoic box with a static pressure differential greater than that created during the operation of the flow. It was not possible to achieve supersonic flow with the experimental apparatus, so that case 4 which involves hydrodynamic coincidence of supersonic modes remains untested. The detailed experimental work is described in succeeding chapters.

2.3 SUMMARY

A statistical analysis of the vibrational response of and the acoustic radiation from thin-walled pipes excited by fully-developed turbulent flow has been presented. This analysis has been based on the normal mode method, the various assumptions of which have been verified extensively in previous investigations. A statistical approach becomes

useful at frequencies above those of the lowest resonant modes i.e. when boundary conditions become less important to the response. The concept of the structural modal density can be used directly in the calculation of the average response spectral density by numerical integration of a straightforward algebraic function : this is in contrast to the exact approach in which the detailed modal response spectral density, found by summing the response over all modes at the frequencies of interest, must be integrated over frequency to give meaningful average results.

For practical pipe/flow configurations, which in general are well removed from the condition of hydrodynamic coincidence, various approximations to the pipe vibrational response and acoustic radiation may be readily made. From these, the parametric dependence of the pipe response and radiation can be predicted.

For example,

(i) the non-dimensional acceleration response is predicted to depend on the fifth power of the pipe flow speed, to be proportional to the average pipe quality factors, and to be inversely proportional to the cube of the pipe wall thickness.

(ii) The non-dimensional acoustic power radiation is predicted to depend also on the fifth power of the pipe flow speed, to be proportional to the average quality factors of the supersonic modes, and to be inversely proportional to the cube of the pipe wall thickness for $\bar{\nu} > \bar{\nu}_{ac}$ but to the square of the pipe wall thickness for $\bar{\nu} << \bar{\nu}_{ac}$.

The exact and statistical analyses have been shown to lead to equivalent results for calculations of the vibrational response of pipes excited by turbulent flow. On the other hand, calculations of the acoustic radiation using the exact and statistical analyses demonstrate that subsonic modes tend to control the acoustic radiation for all $\bar{\nu} < \bar{\nu}_{ac}$: thus, if the exact theory is valid for prediction of the acoustic radiation, the assumption of the statistical analysis, that only supersonic vibration modes contribute to the radiation, is expected to lead to significant errors in acoustic radiation estimates.

Finally, the statistical analysis provides a convenient analytical framework, from which the concepts of hydrodynamic and acoustic coincidence may be examined. This leads to important predictions concerning the influence of various parameters in practical circumstances, and also directly to a series of differing experimental situations, which are the subject of subsequent chapters.

CHAPTER 3

THE EXPERIMENTAL FLOW FACILITY AND ITS CALIBRATION

3.1 INTRODUCTION

The aim of the experimental programme was to make reliable measurements of the vibrational response of and the acoustic radiation from a series of pipes, excited by fully-developed turbulent flow. For this purpose a high-speed, intermittent, induced flow pipe facility was constructed across the laboratory anechoic chamber, where measurements were to be made. Extraneous acoustic excitation within the flow was to be avoided so that the measured data resulted exclusively from fully-developed turbulent flow. A wide range of flow speeds was required, and interchangeable pipe test sections, of varying wall-thickness and material but of the same internal diameter, were to be incorporated.

This chapter presents the layout of the experimental facility, defines its capabilities and describes the measurement procedures used during the experimental programme.

3.2 PHYSICAL DETAILS

An induced-flow configuration, incorporating a sonic choke, was used to minimize the level of acoustic noise within the test pipe and for speed control. Economic considerations determined that only intermittent operation was possible. The pipe facility was mounted across the anechoic chamber between a reverberation chamber (the source of air at atmospheric conditions) and a $17m^3$ vacuum tank system, which could be evacuated to 25kPa. The system layout is shown in Fig. 3.1.

Most of the testing was to be done with steel pipes. A nominal 75 mm internal pipe diameter was chosen - the result of a compromise between the restricted running times predicted for larger pipe diameters and the requirement to measure at frequencies above the ring frequencies of the

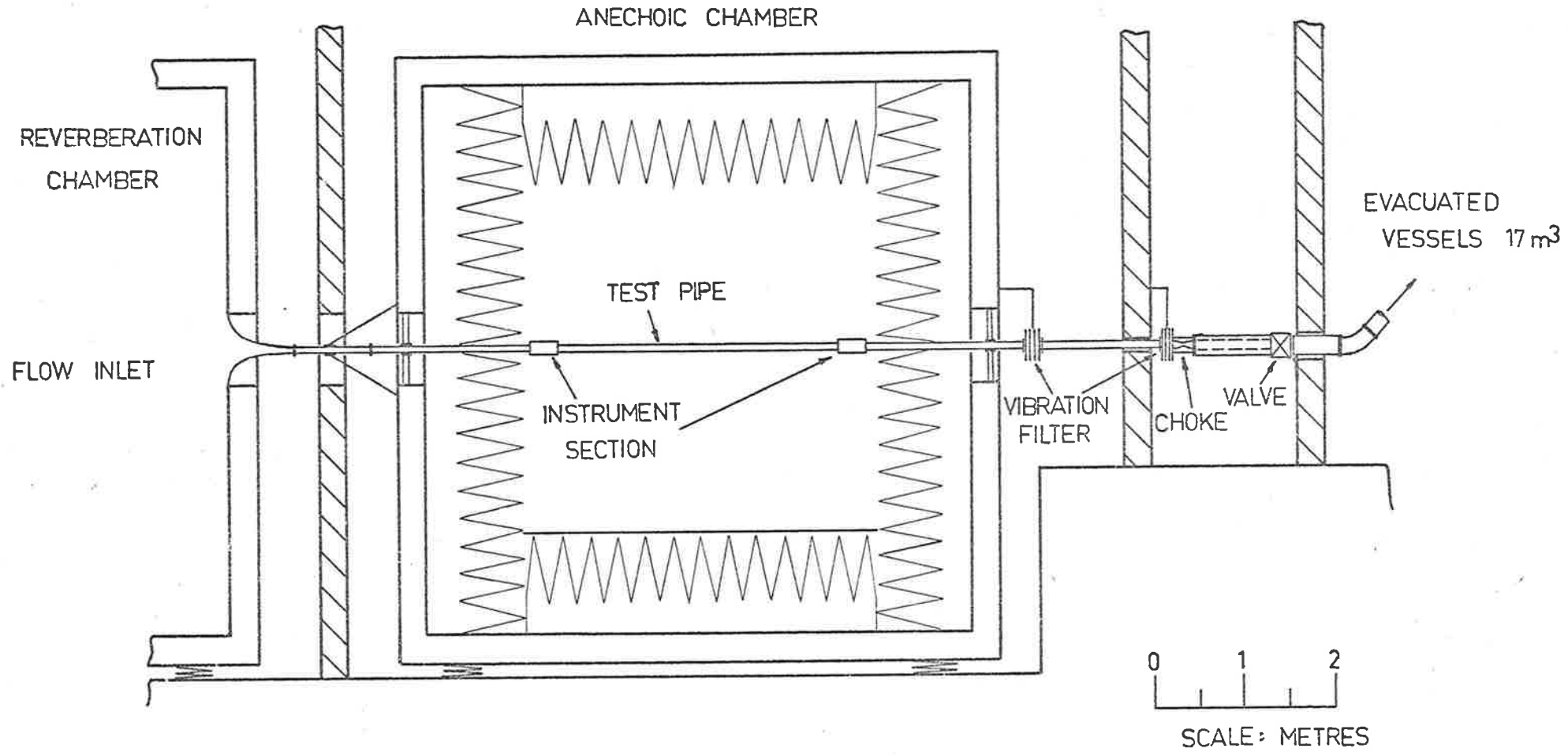

FIG. 3.1 GENERAL ARRANGEMENT OF EXPERIMENTAL PIPE FLOW-NOISE EQUIPMENT

various pipes to be tested.

Air is drawn into the pipe through a smooth inlet which is mounted flush with, yet vibration isolated from, the reverberation chamber wall. A heavy-wall steel pipe (h ≃ 6 mm) of the same internal diameter as the test section connects the inlet and the upstream instrumentation section, the latter being located inside the anechoic chamber. The upstream end of the test section lies about 45 pipe diameters downstream of the inlet. A 3 m test section spans the chamber between upstream and downstream instrumentation sections.

The instrumentation sections were designed to allow measurements of the relevant flow properties and their variation over the test section length. These properties include the mean static pressure on the pipe wall, flow velocity profiles, and the spectra of the fluctuating component of the wall static pressure. Furthermore, the test section can be replaced by a heavy-wall pipe section, instrumented with seven static pressure stations to allow the measurement of the static pressure drop over the test section length as required for the calculation of the wall shear stress.

The five test sections are interchangeable, having been drawn to the same internal diameter as the heavy-wall pipe (and the instrumentation sections). A system of spigots, dowels and a spacer plate allows the test section to be changed without disconnecting the complete pipe rig. The three steel test sections were manufactured from cold-drawn, seamless mild steel stock, while the rigid P.V.C. test section was extruded to the same internal diameter. The shorter brass test section requires an insert of heavy-wall pipe to complete the span between instrumentation sections. Details of the test sections are given in Table 3.1; Fig. 3.2 shows the layout inside the anechoic chamber.

The heavy-wall pipe extends from the downstream instrumentation section to the sonic choke section, broken only by two vibration isolators. The piping section upstream of the vibration isolator nearest the test section is bolted rigidly to the wall of the concrete anechoic chamber,

Table 3.1 : Details of Experimental Test Section Pipes

Test Pipe Number	1	2	3	4	5
Material	Steel	Steel	Steel	Rigid PVC	Brass
E (GPa)	196	196	196	5.5	104
μ	0.28	0.28	0.28	0.40	0.37
γ	0.960	0.960	0.960	0.917	0.929
ρ_s (kg/m)	7800	7800	7800	1560	8500
c_{Lp} (m/s)	5222	5222	5222	2048	3765
Pipe length, ℓ (m)	2.94	2.92	2.92	2.91	0.38
External Diameter (mm)	74.04	74.32	75.10	75.31	72.65
Internal Diameter (mm)	72.54	72.54	72.54	71.71	72.54
a (mm) (mean)	36.6	36.7	36.9	36.8	36.3
h (mm)	0.75	0.89	1.28	1.80	0.056
β	0.0059	0.0070	0.0100	0.0141	0.000445
$\Lambda = \ell/a$	80.3	79.4	78.9	79.2	10.5
f_r (kHz)	22.7	22.6	22.5	8.8	16.5
$*M_{Lp}$	15.3	15.3	15.3	6.0	11.0
$\bar{\nu}_{ac}$	0.75	0.64	0.44	2.14	19.8

* c = 341 m/s

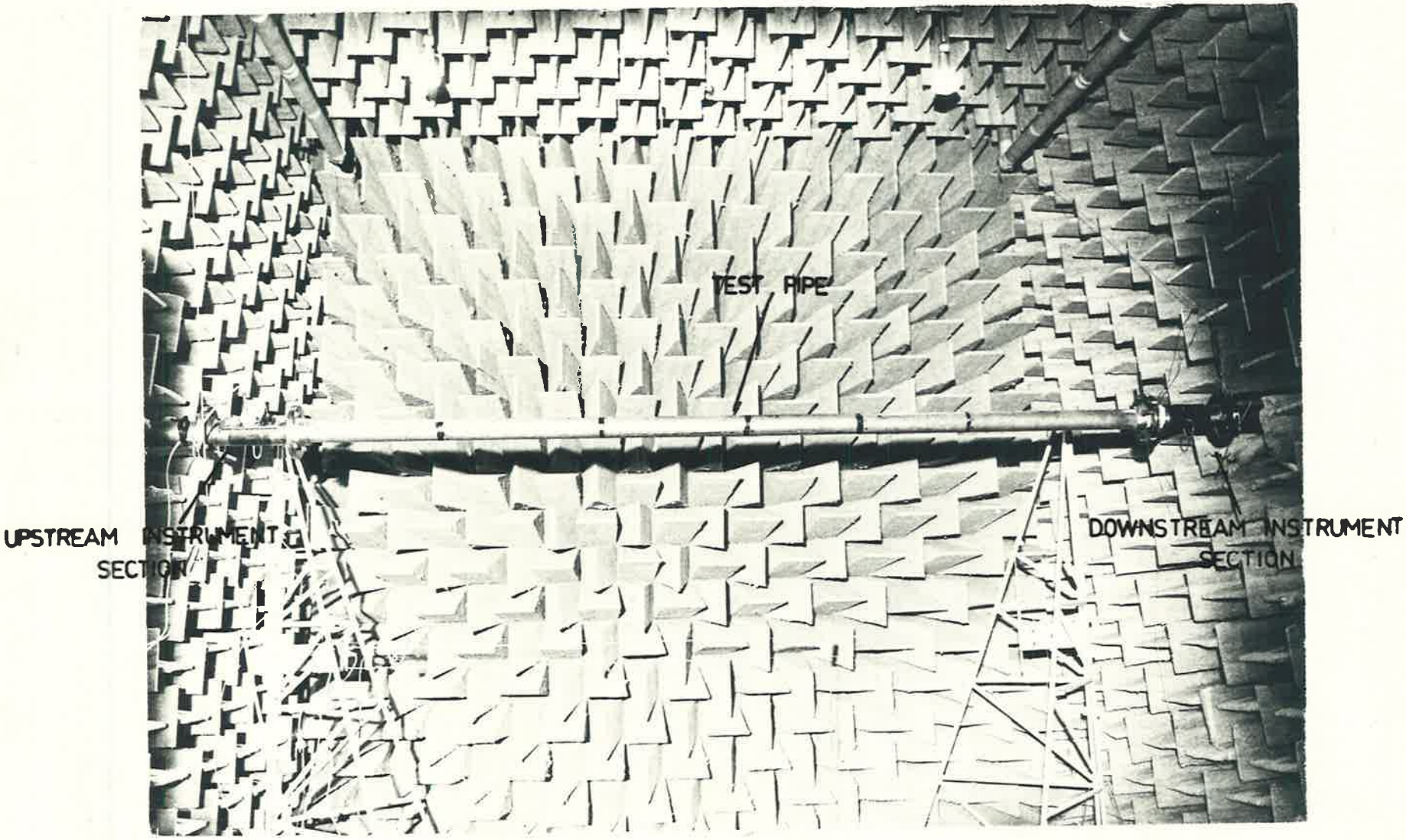

FIG. 3.2 STEEL PIPE IN FLOW RIG INSIDE ANECHOIC CHAMBER

which itself is isolated from any ground vibration. The internal bore of each pipe is hydraulically smooth. All joints are sealed with rubber O'rings to prevent leakage and are spigotted concentric with the pipe internal diameter, so that potential acoustic sources due to wall discontinuities are avoided. The maximum misalignment existing at any pipe joint between the inlet and the upstream isolator is less than 0.05 mm.

The vibration isolators (Fig. 3.3) are designed to act as low-pass filters for any vibration generated near the sonic choke. Each consists of a series of four steel plates (6.5 mm thick and 250 mm square) separated from each other and the enclosing flanges by soft rubber gaskets, 6 mm thick. A hole of the same diameter as the internal diameter of the test sections was bored in each plate and in the enclosing flanges. The rubber gaskets of the same internal diameter were cast of moulding rubber. A removable steel dowel, used to align the plates and flanges as they are glued to the spacing gaskets, maintains the relative position of the isolator components between experimental runs. Negligible distortions to the internal bore exist across the isolators. The insertion loss of each vibration isolator was measured to be greater than 40dB over the frequency range from 200Hz to 20kHz.

The flow velocity in the test section may be varied in fixed steps by means of a series of sonic throats. Seven smooth axi-symmetric nozzles of different throat areas to give seven fixed flow conditions were made to fit inside the sonic choke body and are easily interchangeable. Measurements of the centre-line velocity at the instrumentation sections with a hot-wire anemometer confirm that steady flow conditions are attained within 1 second from commencing the opening of the quick-acting pneumatically-operated valve. The running time, defined as the time during which steady flow conditions exist, is determined by monitoring the noise level adjacent to the flow inlet in the reverbation chamber: as the nozzle velocity drops below sonic, a sudden increase in inlet noise level occurs. The measured flow properties are presented in the next section.

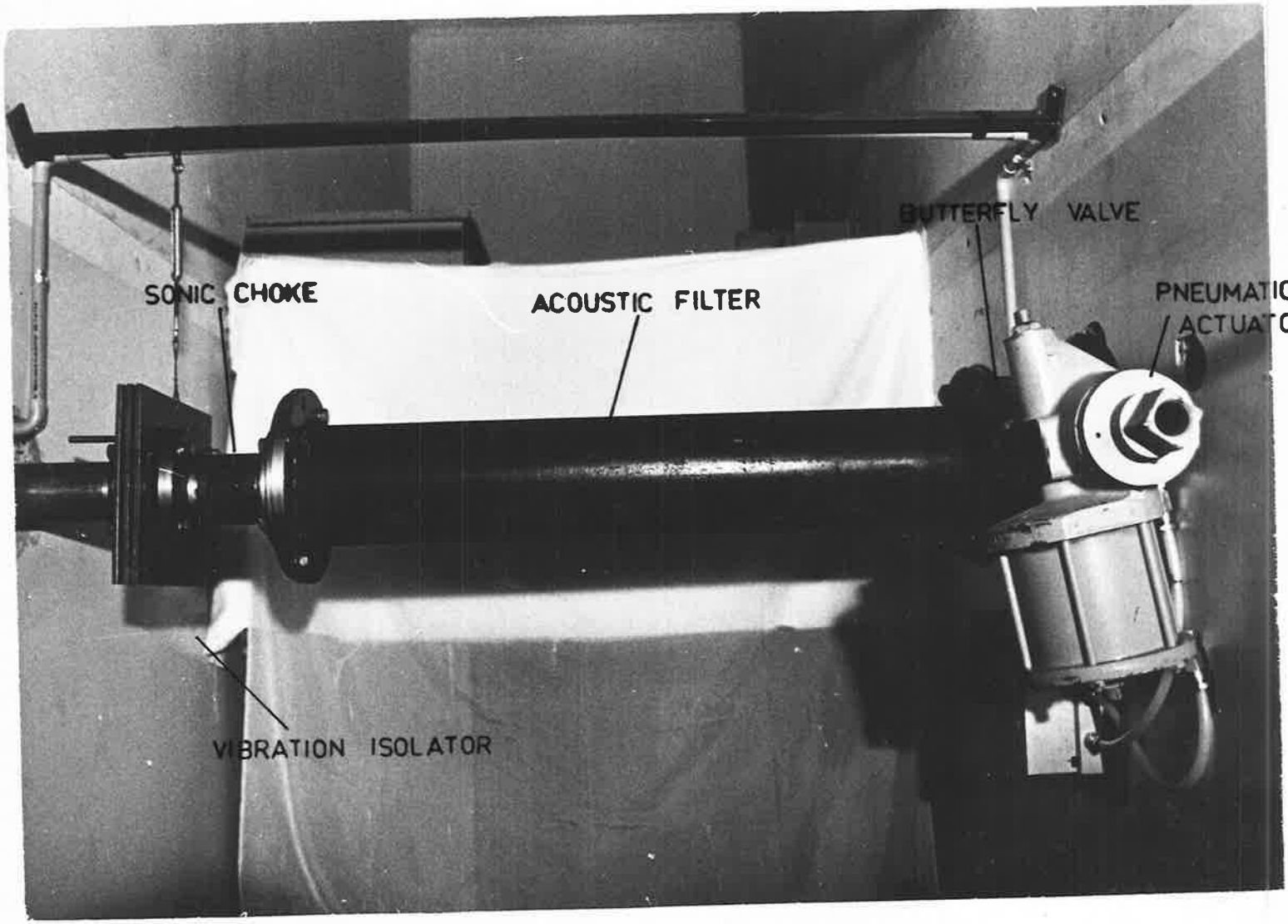

FIG. 3.3 FLOW CONTROL EQUIPMENT: INDUCED-FLOW RIG

An acoustic filter, made by packing glass wool behind a cylindrical perforated sheet-metal liner inside a 150 mm diameter steel pipe, was mounted directly downstream of the sonic choke to attenuate the flow noise produced downstream of the choke. The flow expands gradually from the sonic choke through the filter and the valve station to the 150 mm diameter steel pipe which connects to the vacuum tanks. The pneumatically-operated butterfly valve (Fig. 3.3) may be remotely controlled from either chamber or from an instrumentation control room. Thus the test section is isolated from any mechanical or acoustic disturbances generated by the choke or by flow downstream of it. The measurements taken and the procedures followed are described in the next section.

3.3 INSTRUMENTATION AND FACILITY PERFORMANCE

Measurements of the mean flow properties of the induced-flow facility were made to determine the range of flow speeds for which fully-developed turbulent flow existed over the test section length. The procedures followed and the conclusions reached are presented in this section. Measurements of the properties of the wall-pressure field and of the pipe wall materials are given; techniques for measuing the vibrational response and acoustic radiation are discussed.

3.3.1 Mean Flow Properties

The mean flow properties were calculated from measurements of radial total pressure profiles. A small pitot tube was used to obtain the total pressures, and the wall static pressure was assumed constant across the pipe diameter.

A wall static pressure station was located slightly upstream of the pitot tube position at each instrumentation station. The circumferential variation of static pressure was investigated by using several circumferential positions at each axial station: the diameter of the static holes was 0.75 mm. The variation in circumferential static pressure was less than 1% from the mean value, implying axi-symmetric flow. At each station, an

average value was measured by interconnecting two static holes. Thirteen axial static pressure stations were used: 3 in each instrumentation section, and 7 in the heavy-wall pipe insert. The axial variation in wall static pressure was measured for each flow speed and is shown in Fig. 3.4. The static pressure decreases smoothly (almost linearly) with distance in the flow direction; small accelerations of the flow are indicated by the changes in slope of the curves as the flow progresses down the pipe.

The nose of the pitot tube was flattened to a thickness of 1.5 mm and projected 50 mm upstream of the probe support. A National pressure transducer (LX1702G), with a sensitivity of 0.0673 volts/kPa and a frequency response flat to 1kHz, was used for pressure measurements. The calibrated output was fed to the vertical coordinates of a pen recorder. A simple positioning mechanism allowed the pitot tube to be traversed away from the pipe wall across the pipe centreline, while a resistance potentiometer produced a voltage proportional to the pitot tube position: this voltage was fed to the horizontal coordinates of the pen recorder. Traversing the pitot tube from the pipe wall to the pipe centreline produced a graph of total pressure against radial distance. The wall static pressure was measured directly after each traverse, both with the pitot tube immersed in the flow and withdrawn; the presence of the pitot tube produced small variations in the wall static pressures but these were less than 3% of the centreline dynamic pressure. The static pressure measurement with the pitot tube at the pipe centreline was used in all calculations.

The velocity profiles were calculated from pitot tube total pressure measurements and corresponding wall static pressures, using compressible flow relations. The velocity profiles compare favourably with those of Schlichting (1968, p.562). Both small accelerations of the flow and a slight broadening of the velocity profiles occur over the test section length, the effects increasing with flow speed. Table 3.2 shows the calculated mean flow properties at the two instrumentation sections. Frictional choking of the flow near the sonic shoke limited the maximum achievable test section flow speed. The velocity profiles at the upstream and downstream instrumentation

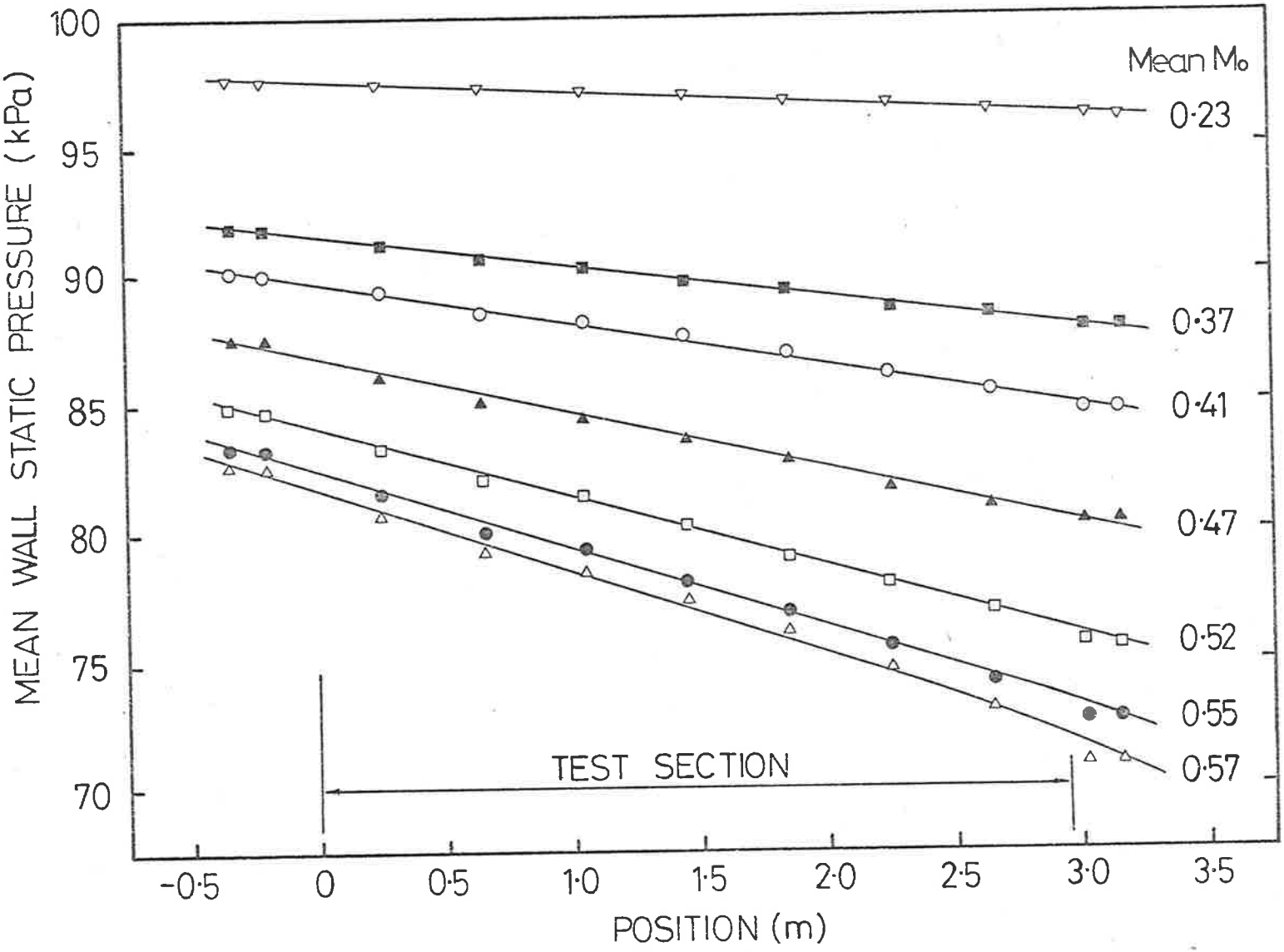

FIG. 3.4 VARIATION OF WALL STATIC PRESSURE WITH Mo OVER PIPE LENGTH

TABLE 3.2 SUMMARY OF MEASURED FLOW DATA

Throat Number	1	2	3	4	5	6	7
Upstream Instrument Section							
M_o	0.226	0.365	0.405	0.457	0.495	0.518	0.531
q_o (kPa)	3.55	8.92	10.8	13.4	15.4	16.7	17.4
U_o (m/s)	77.6	126.	139.	157.	170.	178.	183.
U_τ (m/s)	2.66	4.21	4.68	5.10	5.57	5.92	5.95
R_e ($x10^{-5}$)	3.95	6.50	7.24	8.23	8.97	9.42	9.68
Downstream Instrument Section							
M_o	0.219	0.378	0.417	0.472	0.534	0.582	0.608
q_o (kPa)	3.30	9.11	10.8	13.3	16.7	18.7	20.0
U_o (m/s)	75.4	130.	143.	162.	187.	200.	209.
U_τ (m/s)	2.63	4.34	4.78	5.37	6.15	6.6	6.76
R_e ($x10^{-5}$)	3.85	6.75	7.47	8.52	9.92	10.7	11.2
Mean Values Over Test Section Length							
M_o	0.223	0.371	0.411	0.465	0.515	0.550	0.569
q_o (kPa)	3.43	9.02	10.8	13.4	16.1	17.0	18.7
U_o (m/s)	76.5	128.	141.	160.	179.	189.	196.

sections are plotted in universal form in Fig. 3.5, where close agreement with the universal velocity distribution law (Schlichting (1968, p. 567)) is found. Friction velocities have been calculated both from measurements of the pressure drop along the pipe and from the velocity profiles, following the method suggested by Clauser (1954) - good agreement was found.

While some spread in the data exists, the flow appears to be essentially fully-developed at both instrumentation sections for all flow speeds.

3.3.2 Fluctuating Wall-Pressure Field Measurements

Measurements of the spectral density of the random fluctuating pressure field acting on the internal pipe wall were made, although considerable documentation of the properties of the pressure field on the boundary of turbulent flows already exists. Considering the observed accelerations occurring at all flow speeds, it was felt necessary to compare the measured and assumed form of the non-dimensional spectral density of the turbulence pressure field.

A piezo-electric transducer, constructed from a 0.75 mm diameter lead zirconate disk, and a pre-amplifier were mounted in a 40 mm diameter instrument plug. This was profiled to the same curvature as the bore of the instrumentation section. No surface discontinuities existed within the instrumentation section. The output from the transducer preamplifier was passed to a Brüel and Kjær (B & K) 2604 Microphone Amplifier, and then fed to both a Nagra IVL tape-recorder and a B & K 3347 Real Time Analyser (RTA). The RTA was used both to monitor the transducer output during the experiments and for the analysis of tape-recorded data. The latter process involved the construction of tape loops to obtain signal averaging times longer than the experimental running times: the 20 second time constant averaging circuit of the RTA was used for this purpose, whereas the 0.5 second time constant was used during direct recording. In general, the differences in spectral levels between the direct RTA analysis and those obtained from the tape-recorded

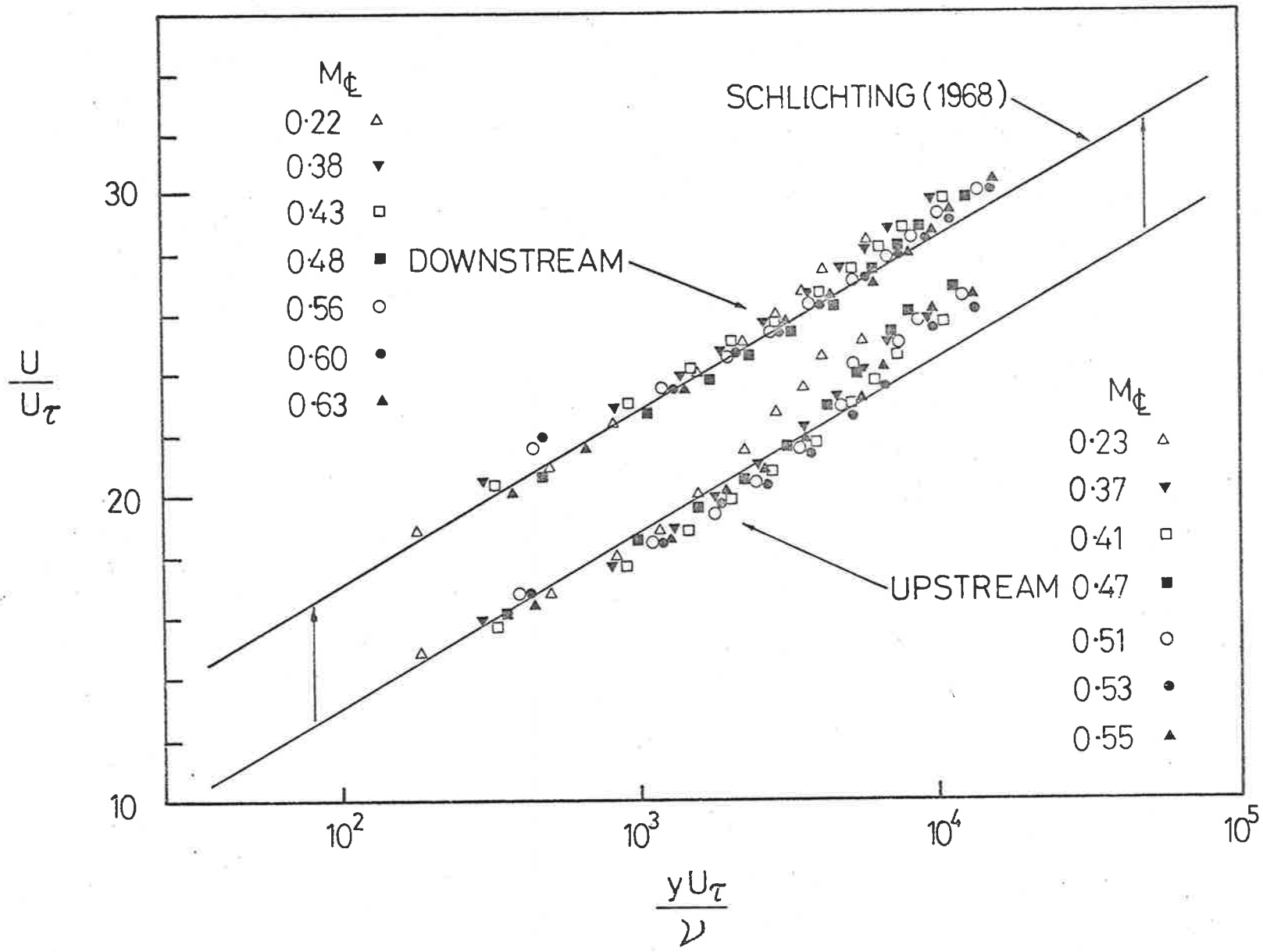

FIG. 3.5 VELOCITY PROFILES IN UNIVERSAL FORM

data were less than 1dB over the frequency range from 250Hz to 40kHz.

Calibration procedures were designed so that the transducer did not have to be removed from the instrumentation plug and therefore remained flush with the plug surface throughout experiments. In the initial calibration, the instrumentation section was connected for the end of a 40 mm x 65 mm rectangular shock tube, but mechanically isolated from it by one of the vibration isolators used in induced-flow rig. Shocks of various strengths were passed down the instrumentation section to determine the sensitivity, linearity, and frequency response of the in-situ transducer. The sensitivity of the transducer (including preamplifier) was 0.058V/kPa, and was linear over a range of shock strengths from 3. to 40.kPa, with a flat frequency response from 100Hz to 50kHz. In addition, an acoustic coupler was used both to verify the low-frequency calibration and to provide a simple alternative to the shock tube calibration during experimental work. The coupler was constructed so that the in-situ transducer, a reference B & K 4136 6.35 mm microphone and a small earpiece oscillator all faced into a cavity, the dimensions of which were all less than 7 mm. With this arrangement, the calibration could be verified for frequencies up to 2kHz, being limited by wave effects in the coupler at higher frequencies. Close agreement was obtained between the two methods.

The transducer is sensitive to any acoustic noise present in the pipe and responds to any vibration of the instrumentation plug. Both of these sources will tend to contaminate the true turbulence pressure signal, as will the electrical noise of the preamplifier. The spectral density of the electronic noise was less than 1% of the measured pressure for all frequencies above 200Hz for all flow speeds. The vibrational response of the transducer system was investigated by blanking off the mounted transducer from the flow. This was done by retracting the transducer 3 mm from the pipe internal surface and clamping in the resulting hole, a steel slug and then sealing any gaps with beeswax. The spectral density of the vibration signal so obtained was generally less than 1% of the signal measured with

the transducer open to the flow. Data were rejected at the frequencies where the signal-to-noise ratio was less than 5 (this only occured for the lowest flow speed).

During an experiment, acoustic noise is radiated to the reverberation chamber from the inlet bell-mouth. This noise seems to be generated by turbulent mixing within the pipe, rather than at the inlet plane where the flow was smooth or downstream of the choke, which would have implied propagation of high noise levels through the very thin boundary layer at the throat. An investigation of the acoustic noise within the pipe was attempted to determine whether it contributed significantly to the excitation spectral density. Measurement of acoustic noise within high speed flows is difficult, since the interaction between the turbulent flow and the transducer will cause significant contamination of the true acoustic signal. An alternative procedure is to measure the cross-correlation between two flush-mounted transducers, spaced sufficiently widely so that the turbulent pressure signal is uncorrelated. The processes involved are time consuming and susceptible to electronic noise for low acoustic signals, and were not used.

An alternative approach involved the measurement of the acoustic intensity at various axial inlet positions beginning at the inlet plane (where the flow velocity is low) and progressing further into the pipe until significant levels of flow noise are produced by the measuring probe. For this purpose, a B & K 4136 microphone with B & K 2168 Pre-amplifier was shielded within a 12.7mm diameter, long hollow cylinder with a streamlined tail. The cylinder entered the inlet, tail first from the reverberation room. The acoustic signal was sensed through four circumferentially-placed, 3 mm diameter holes, which were 100 mm upstream of the cylinder tail. The diameter of the holes was small, so that the frequency of any hole-generated flow noise would be high: any surface-or tail-generated flow noise would be of a low level, since the cylinder was faired and axi-symmetric.

As the probe entered the inlet and up to positions of constant area duct cross-section, the measured intensity increased as the cross-

section area decreased, and when the constant area section of the inlet was entered, the intensity remained constant. Thus the major acoustic source appeared to be located further into the pipe and to be radiating predominantly plane waves to the inlet. The intensity remained constant for approximately 300 mm within the constant area section of the inlet. As the probe was traversed further into the pipe than this, significant probe noise was generated. This same behaviour was found for each of the three flow speeds tested (M_o = 0.22, 0.37 and 0.46). The intensities measured at frequencies less than 4kHz (above which significant flow noise was generated) were used as estimates of the acoustic noise present. These were comparable to the flow signal only for the lowest flow speed at frequencies less than 300Hz. Consequently, little acoustic correction to the wall-pressure spectral density need be made.

The measured spectral densities of the turbulence pressures for the various flow speeds are presented in non-dimensional form in Fig. 3.6(a) and (b) for the upstream and downstream flow conditions respectively. Measured centreline parameters (q_o and U_o) and the internal pipe radius, a, have been used. Comparison with the measurements of Bull (1967) for turbulent boundary layer flow (where a is equivalent to the boundary layer thickness δ) and with the measurements of Corcos (1962) for turbulent pipe flow, demonstrate considerable consistency. The experimental collapse over the wide range of flow conditions is quite close. No significant differences between the upstream and downstream spectral densities occur, suggesting that for present purposes, the flow may be considered fully-developed over the test section for the whole range of flow speeds. Additional comparisons of the measured values of the ratio of the root-mean-square pressure to the centreline dynamic pressure and to the wall shear stress (calculated from pressure drop measurements) compare closely with other published data, as shown in Figs. 3.7(a) and (b).

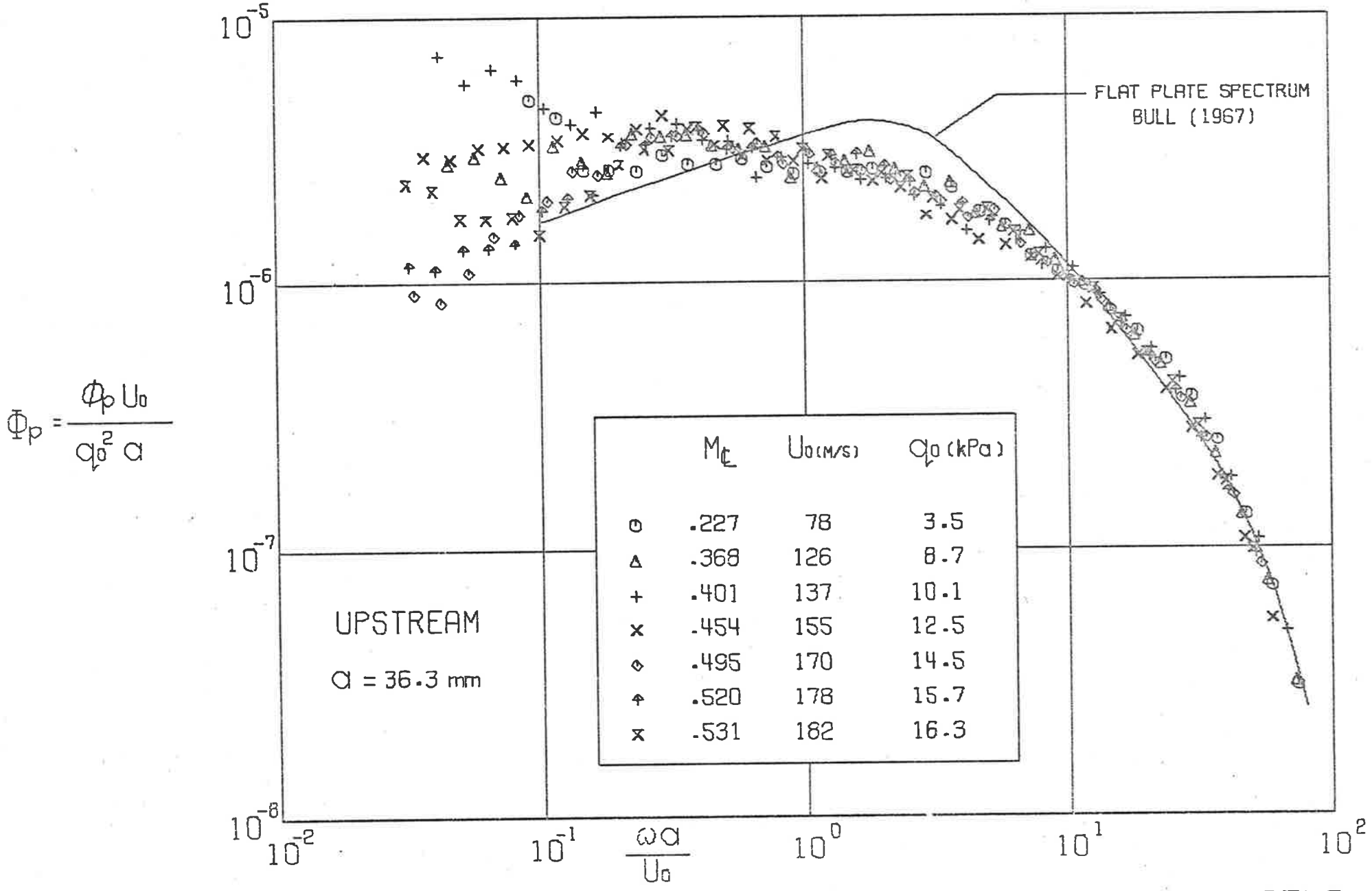

FIG. 3.6(a) SPECTRAL DENSITY OF WALL-PRESSURE FIELD

$$\Phi_p = \frac{\phi_p U_0}{q_0^2 a}$$

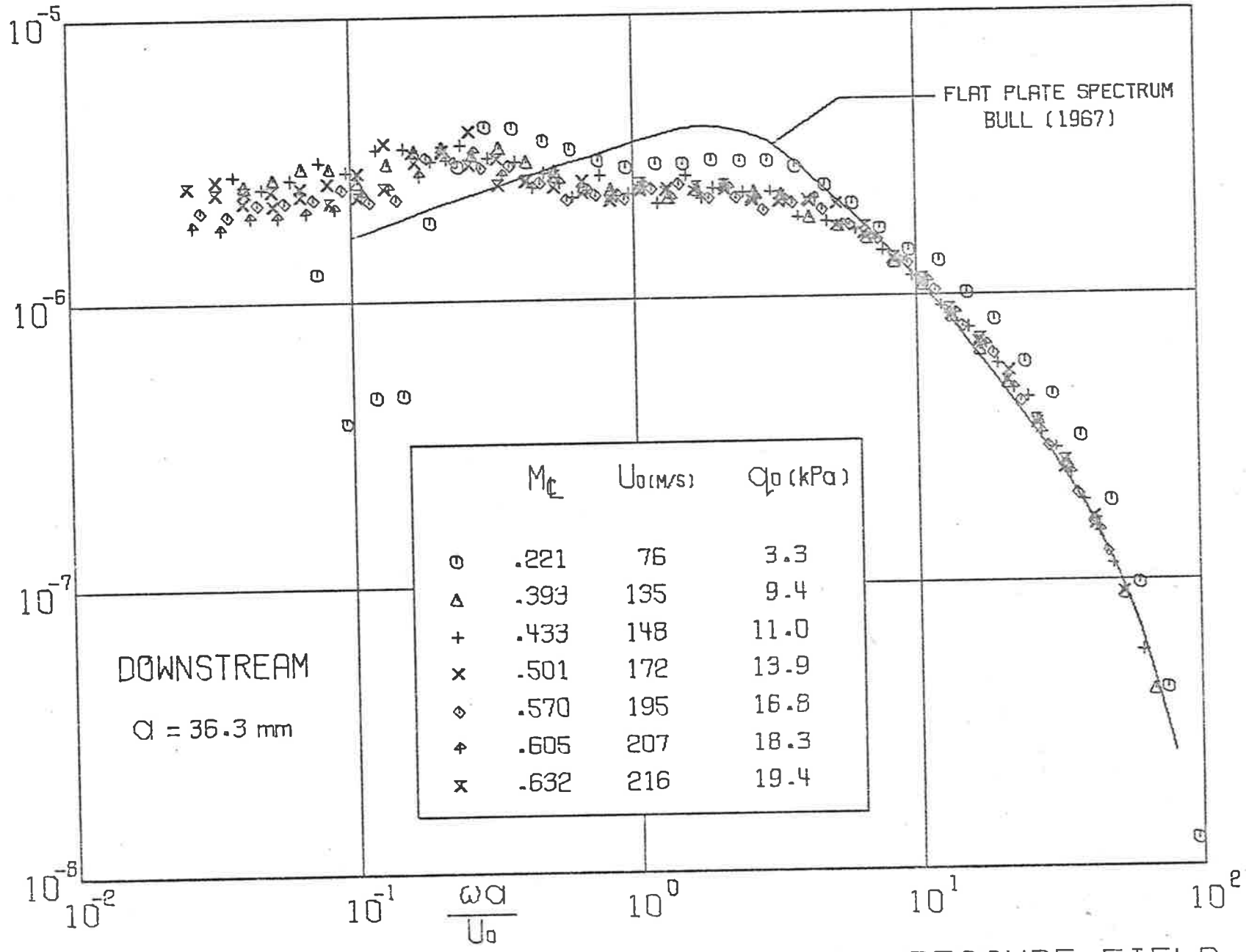

FIG. 3.6(b) SPECTRAL DENSITY OF WALL-PRESSURE FIELD

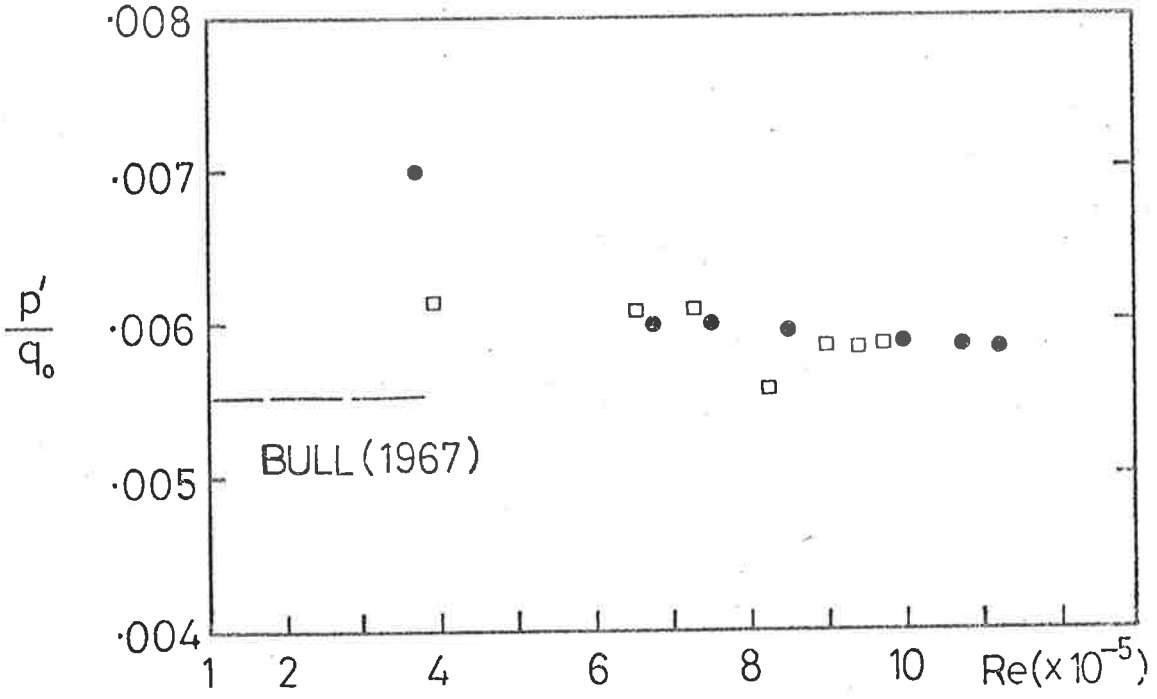

FIG. 3.7(a) VARIATION OF p'/q_o WITH Re NUMBER

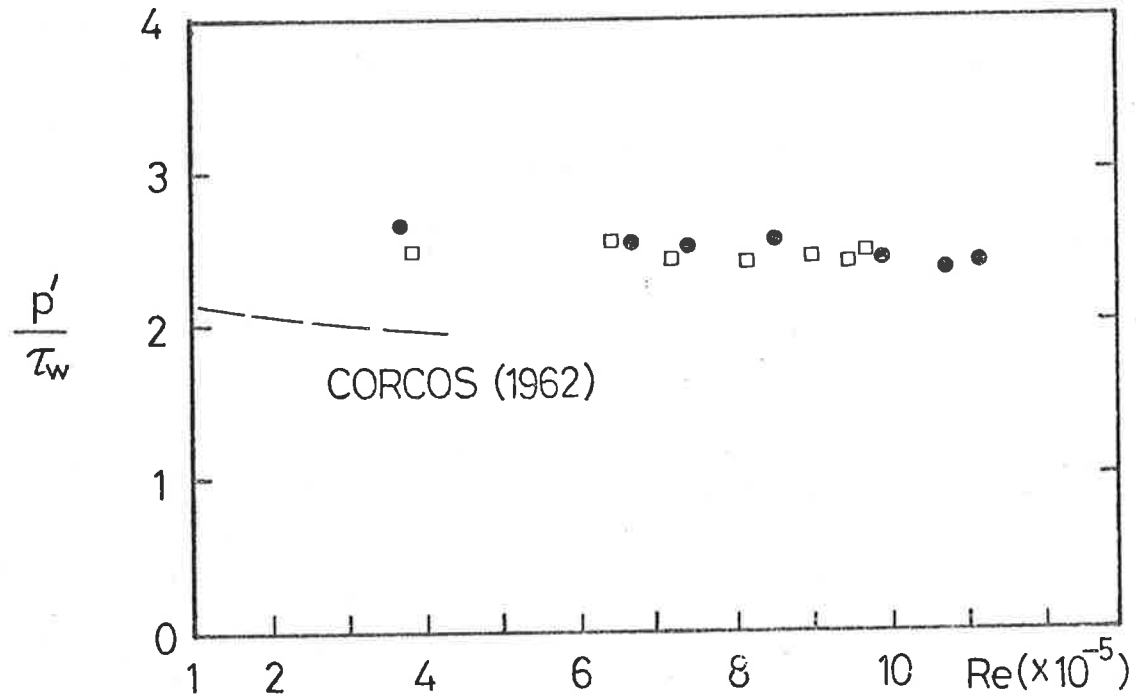

FIG. 3.7(b) VARIATION OF p'/τ_w WITH Re NUMBER

3.3.3 Structural Properties of Test Sections

Values of elastic modulus E, density ρ_s and Poisson's ratio μ of each test section are required for calculations of the longitudinal wave-speed in the wall of each test pipe and for the non-dimensional presentation of experimental data. E and ρ_s are readily measured, while μ can be found from tabulated data. Usually E is determined from a static tensile text. However, for plastics, E can vary considerably with frequency and temperature. For the P.V.C. test section, in addition to a tensile test, E was measured with an alternative method: this depended on the fact that the resonance frequencies of a beam with clamped ends, which are proportional to E, can be predicted exactly (Morse and Ingard (1968, p. 185)).

For the static tensile tests, test strips (6.5 mm wide and 400 mm long) were milled from spare test section material. As they retained some of the circumferential curvature of the original test sections, a 75 mm length in the middle of each strip was reduced to a width of 4 mm: measurements of the strain in a 25.4 mm gauge length in the necked portion were made with an Ingstron Strain Gauge Extensometer G-51-11M. The applied load was plotted automatically against the strain by the Ingstron TT-1115 Universal Testing instrument; E was determined from the slope of the graphs. The data for the steel test strips agreed within 2% of tabulated data in Kinsler and Frey (1962, p. 502) and Marks (1967, p. 6-7).

The value of E for P.V.C. from the tensile test was 4.GPa. An alternate value of E for P.V.C. was obtained by measuring the resonance frequencies of an un-necked tensile test strip, whose ends were clamped rigidly in massive supports. Values of E calculated from low-order mode resonances were found to exceed the tensile test measurement and to asymptote, for higher mode order, to a value 37% higher than the tensile test result. This difference between the two determinations is believed to have resulted from a real variation of E with frequency: the result from the beam resonance experiment, which agrees with tabulated data (Cremer, Ungar and Heckl (1973, p. 216)), has been used for calculation purposes.

Measurements of the properties of the brass test material were not attempted, but were taken from Kinsler and Frey (1962, p. 502). All structural properties data used are shown in Table 3.1.

3.3.4 Measurement Procedures

Experimental measurements were taken only during periods for which steady state conditions of pipe vibrational response and acoustic radiation existed. On monitoring the pipe wall acceleration and acoustic radiation spectra on the Real Time Analyser, this was found to be only slightly shorter than the running time of each flow configuration.

The pre-amplified transducer output was amplified by a B & K 2114 Spectrometer and recorded on both the RTA and the Nagra IV tape recorder. Tape loops of the central portion of the recorded data were replayed into the RTA for comparison with directly-stored data. The differences in spectra obtained from the two methods were usually less than 1dB. Data were recorded over the frequency range 200Hz to 40kHz.

Pipe Wall Response Miniature B & K 8307 0.5g accelerometers were used in the measurement of the acceleration response of the thin-walled pipes tested. While mass loading reduced their high frequency sensitivity, they were found to be robust and convenient instruments for continuous use in the collection of data from many points over the pipe surface. Calibration was performed with a B & K 1606 Vibration Pickup Preamplifier. The 8307 accelerometer, which has a nominally flat frequency response up to frequencies in excess of 40kHz for a rigid mounting, was to be fastened to the pipe surface with a thin layer of beeswax. In order to determine the response of the mounting at high frequencies, the accelerometer was attached with beeswax to the top surface of a B & K 4290 Calibration Exciter in an identical manner to that for the pipe acceleration measurements. The output from the reference accelerometer housed within the calibration exciter was maintained constant by feeding it to the active compressor circuit of a B & K 1014 Beat Frequency Oscillator. The resulting response curve was flat to 40kHz, indicating that

for 0.5g accelerometers at least, a beeswax layer provides a satisfactory mount for the whole range of pipe response measurements. Double-sided adhesive tape also produced a flat frequency response to 40kHz for a 0.5g accelerometer.

At high frequencies, even the small mass of a 0.5g accelerometer will cause a reduction in the acceleration response of light-weight structures. An assessment of this 'mass-loading' was made by measuring the reductions in the pipe acceleration response following the addition of several small masses to the 0.5g accelerometer attached to the test pipes, for a constant electromagnetic excitation power input in one-third octave frequency bands. The measurements were extrapolated back to the case of zero mass-loading to give estimates of the necessary corrections to be applied for the 0.5g accelerometer. These are presented in Fig. 3.8 for the steel and P.V.C. test pipes. For each of the steel pipes, the mass-loading correction increases at 6.5dB/octave for frequencies greater than the 'break' frequency i.e. that frequency at which mass-loading becomes important. The P.V.C. mass-loading curve has a similar form to the steel curves. Corrections to spectra measured with the 0.5g accelerometer were taken from these curves.*

The background electronic and vibration noise spectra were usually at least 20dB below the acceleration spectra for frequencies greater than 1kHz; only for the lowest flow speed were corrections necessary and then only in those frequency bands containing few resonant modes.

Acoustic Radiation The background level for acoustic measurements in the anechoic chamber was determined by the electronic noise of the B & K microphone/preamplifier/power supply equipment. By appropriate combination of B & K 4131 (25.4 mm) and B & K 4133 (12.7 mm) condensor microphones, measurements of pipe acoustic radiation were possible over the complete frequency range from 250Hz to 40kHz for all pipes and all flow speeds. Some measurements for the lowest flow speed required corrections for electronic noise, but the vast majority of measurements lay well above the background levels.

* The accuracy of these corrections to the measured acceleration spectra is $\pm$ 1 dB for $\nu < 1$ and $\pm$ 3 dB for $\nu > 1$.

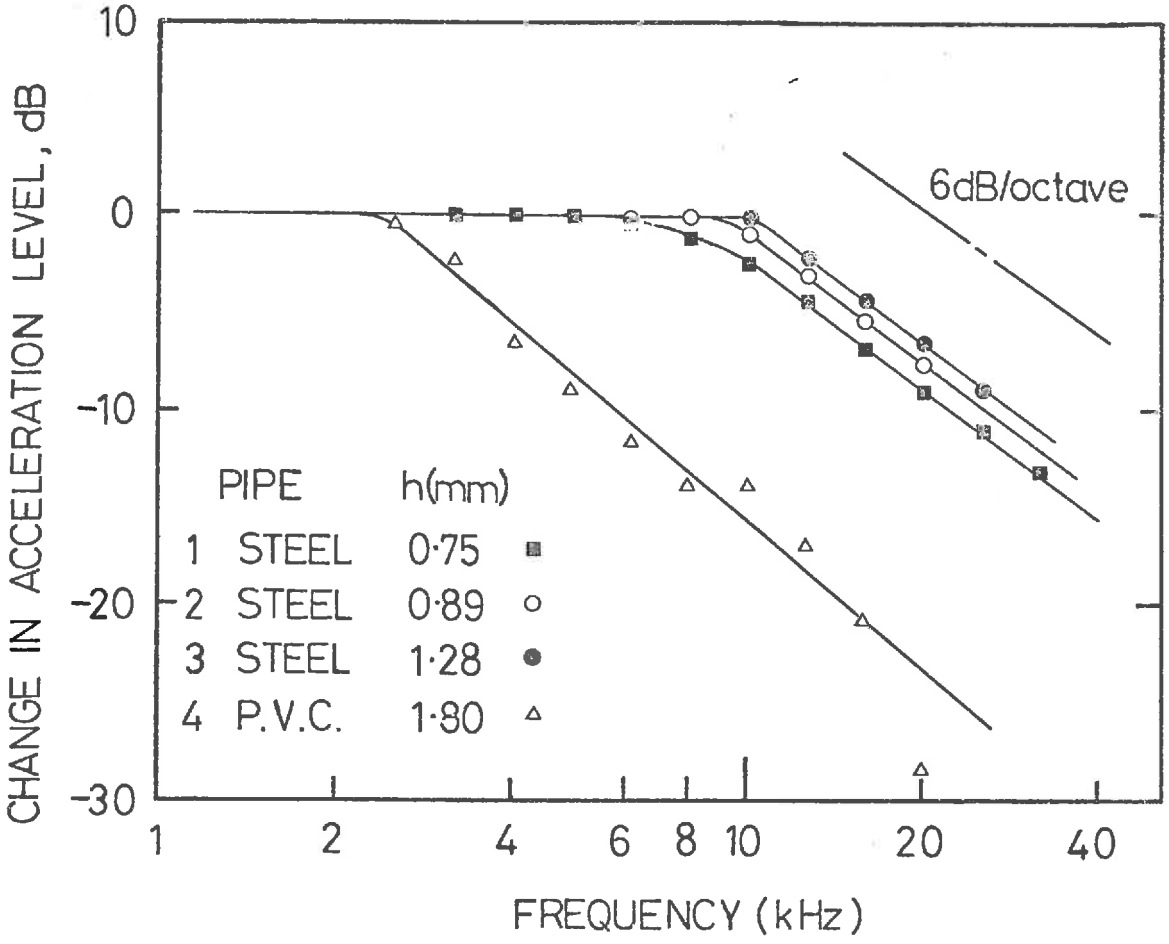

FIG. 3·8 MASS-LOADING EFFECTS OF B&K 8307 0·5g ACCELEROMETER

Previous work on the characteristics of the anechoic chamber has shown that the chamber may be considered as a free-field environment for one-third octave band acoustic measurements from 200Hz to above 40kHz: it can therefore be used to determine the directivity of the pipe radiation. This is discussed in section 4.5.

3.4 SUMMARY

Details of the construction and operating characteristics of the induced flow pipe facility have been described to demonstrate its capabilities for the measurement of flow-induced pipe noise.

The operation is intermittent with running times for steady state conditions generally in excess of five seconds for the pipe diameter used. Seven flow configurations, corresponding to centreline velocities (averaged over the test section length) of 77, 127, 141, 160, 179, 189 and 196 m/sec are available: these conditions correspond to mean centreline non-dimensional flow speeds M_o ranging from 0.22 to 0.57 i.e. a factor of 2.55 between maximum and minimum values. Fully-developed flow conditions have been shown to exist over the test section length for all tested flow speeds, as demonstrated by comparisons of the non-dimensionalised velocity profiles and the universal velocity-distribution law.

Similarly, measurements of the non-dimensional power spectral densities of the turbulence wall-pressure field associated with these flows agree closely with established experimental data. No significant extraneous flow or acoustic excitations appear to be present within the test section pipes.

Procedures have been described, which allow for satisfactory collection of experimental data on the vibrational response of and the acoustic radiation from pipes excited by fully-developed turbulent flow, over a broad frequency range from 200Hz to 40kHz for all the above flow speeds.

CHAPTER 4

EXPERIMENTS WITH STEEL PIPES

4.1 INTRODUCTION

Steel test sections were used in the initial set of experiments. For the thicknesses chosen and flow speeds available, $0.45 \lesssim \bar{v}_{ac} \lesssim 0.75$ and $0.0081 \lesssim \bar{v}_{hc} \lesssim 0.088$, corresponding to case 1 discussed in section 2.2.8. The conditions are far removed from coincidence, so that the dependence of the non-dimensional pipe vibrational response $\Phi_{\ddot{w}}/\Phi_p$ and acoustic radiation Φ_π/Φ_p on structural and flow parameters should be predicted closely by the approximate expressions, equations [2.28] and [2.30].

The dependence of $\Phi_{\ddot{w}}/\Phi_p$ and Φ_π/Φ_p on flow speed and structural dimensions can be isolated by using a single pipe material. For steel pipes in case 1, $\Phi_{\ddot{w}}/\Phi_p$ and Φ_π/Φ_p are both theoretically independent of Λ: thus Λ was maintained constant during experiments with steel pipes to reduce the number of experimental variables. As shown in Table 3.1, three steel pipes of different wall thickness were used to explore the β dependence of the pipe vibration response and acoustic radiation. Seven different flow speeds were tested. Modal resonance frequencies and quality factors were measured in considerable detail for a variety of boundary conditions, ranging from free to rigid ends.

The experimental measurements, appropriately reduced to non-dimensional form, are presented in the subsequent sections of this chapter. Comparisons are made of the predicted and measured values of the non-dimensional spectral densities of the response and radiation, and of their predicted and measured parametric dependence.

Damping treatments were applied to the surface of the thickest pipe. The resulting changes in quality factors, vibrational response and acoustic radiation are reported to show the capacity of such treatments

for noise control purposes. The relative effectiveness of flow and acoustic excitations in producing external acoustic radiation is also considered.

4.2 PIPE RESONANCE FREQUENCIES AND MODAL DENSITY

The modal density function, as given by equation [2.10], is fundamental to the statistical analysis of the resonant pipe response and the associated acoustic radiation. Considering the assumptions involved in the derivation of the modal density equation, an experimental verification was necessary to examine the magnitude of any differences between theoretical and measured results.

The axial symmetry of a cylinder means that, for each resonance frequency, two resonant modes will exist, corresponding to the mode shapes described by equation [2.6]. The theoretical analyses of Chapter 2 has allowed for this by defining the modal density as the density of resonance frequencies and multiplying the response equation by a factor of 2. In general, it will not be possible to differentiate between the two mode shapes at each resonance frequency, although on at least one occasion, the response-amplitude curve was found to have two closely-spaced peaks, each of which corresponded to the same order mode.

Comparisons of theoretical pipe resonance frequencies, predicted by the 'exact' resonance frequency equations derived by Arnold and Warburton (1953) and by the simplified form of Heckl's equation (equation [2.7]), show that the latter is inaccurate for low circumferential-order modes, producing overestimates of the 'exact' resonance frequencies of approximately 50% for the n = 1 and n = 2 modes. Consequently, the total number of modes below a certain frequency is underestimated. In spite of this, the frequency rate of change of the number of modes below a certain frequency (i.e. the modal density) is predicted quite well, as has been reported by Heckl (1962) and Miller and Hart (1967).

A series of exploratory experiments with two lengths of steel

pipe of test section 1 was carried out to investigate the accuracy of the application of the modal density function to pipe vibration analysis. The additional effects of a variation in pipe end conditions and of a static pressure differential across the pipe wall were examined. While these results are not all used directly in the analysis of the flow experiments, they allow general conclusions to be made about the likely importance of such variations.

An initial experiment involved a 3.5 m length of steel pipe, whose other dimensions corresponded to those of test section 1. Free end conditions were achieved by suspending the pipe at its vibration nodes nearest the ends in light-gauge wire loops. An electromagnet, placed beneath one pipe end, was driven from a narrow-band Muirhead-Wigan Oscillator D-650-B. Pipe resonance frequencies were detected aurally and from peaks in the response-amplitude curve as sensed by a B & K 8307 0.5g accelerometer, which was attached with beeswax to the opposite end of the pipe. The wires were adjusted manually to the nodal lines so that energy dissipation through the structural supports was minimised. The order of each particular resonant mode was determined by traversing the accelerometer smoothly over the pipe surface and counting the number of axial and circumferential nodes. During all these experiments, modal damping measurements were made, as described in the next section.

It was possible to isolate the first 13 axial modes of circumferential order $n = 1$, and the first 20 to 30 axial modes of each circumferential order $n = 2$, $n = 3$ and $n = 4$. The modal overlap increased at high frequencies ($\nu > 0.2$), making the isolation of modes of order $n \geq 5$ difficult. The spacing of resonant modes in frequency is illustrated in the graphs of modal quality factor for this pipe, as in Fig. 4.2(a). Large groups of low axial-order modes of fixed circumferential order n occur at certain frequencies, determined principally by the bending stiffness of the nth circumferential-order modes, to produce an irregular density of modes.

The theoretical approach of Arnold and Warburton (1953) was found to predict the pipe resonance frequencies accurately. The modal resonance frequencies of a cylinder with free ends are essentially the same as those of a cylinder with clamped ends, where the length of the free-free cylinder is taken equal to the distance between axial node lines nearest the cylinder ends. The maximum error in resonance frequency was 8%, and the agreement improved as the axial order m increased.

Calculations of the experimental modal density at low frequency were made in one-third octave bands: these are compared with the theoretical prediction (equation [2.10]) in non-dimensional form in Fig. 4.1. The experimental values are distributed evenly about the theoretical prediction. This scatter, which is rather large at low frequencies, decreases as $\bar{\nu}$ increases beyond 0.1. The experimental peaks are associated with the 'grouping together' of low axial-order modes of fixed circumferential order. As the total number of modes in a band increases, these groupings have less influence on the experimental modal density.

To examine the changes in resonance frequencies produced by fixing the pipe ends in this exploratory situation, the experiment was repeated for a 'clamped' end condition. Here the ends of the same test pipe were fastened in massive 15kg supports in tight cylindrical push-fit joints: however the joints were not as rigid as they would be if the ends were welded or brazed to the supports. This small flexibility in the joint increased the damping of the higher axial-order modes for $n \geq 2$, so that fewer modes could be isolated than with the free-free end condition. Nevertheless, only minor variations in the modal resonance frequencies from those observed with free-free end conditions were produced; no changes in modal density were found.

The end conditions used during all flow experiments corresponded closely to these 'clamped' ends i.e. the test pipes were fastened into the end flanges with push-fit joints. The three steel test sections were now 'clamped', each in turn, in the induced-flow rig in the anechoic chamber

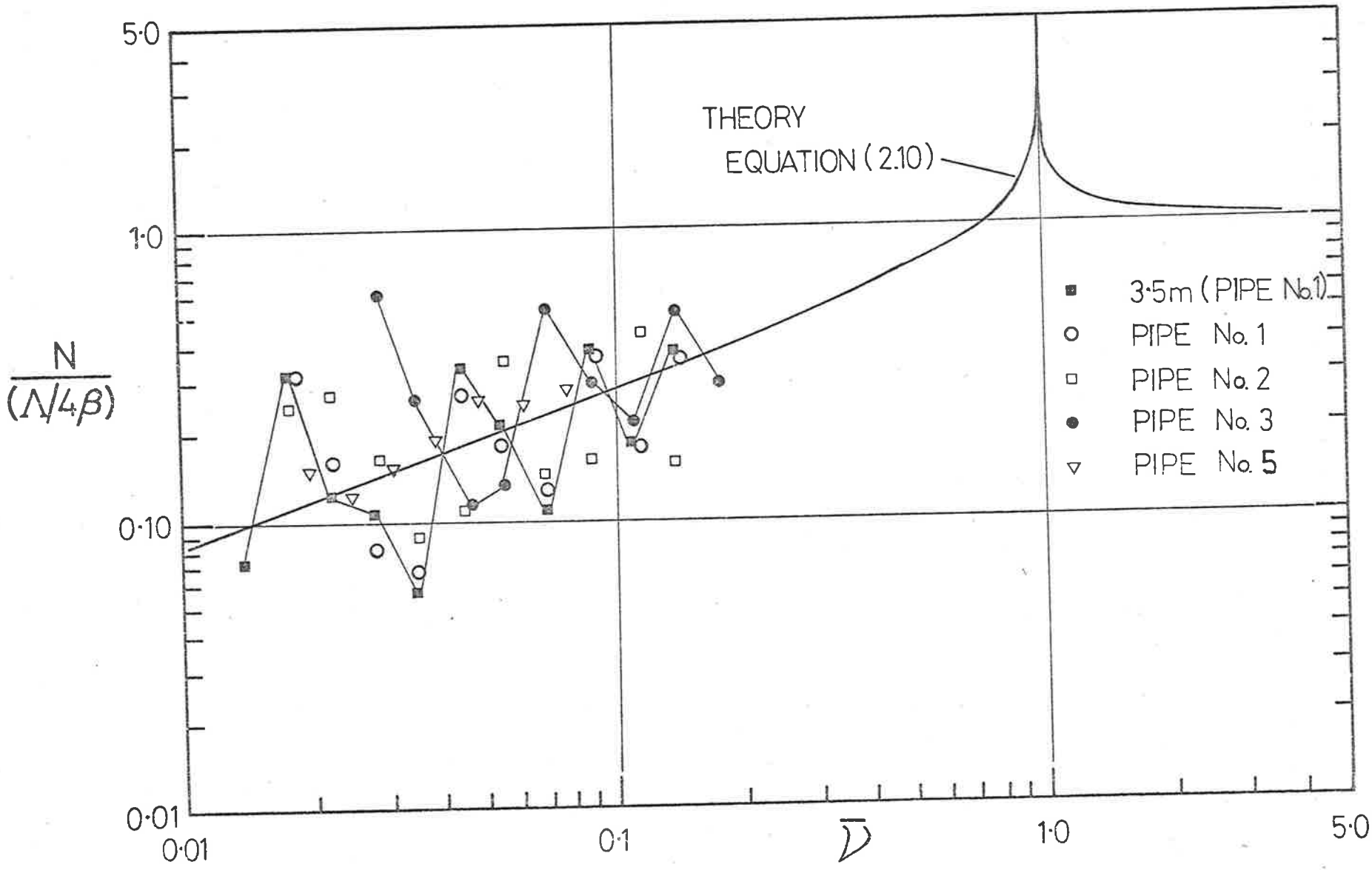

FIG. 4.1 MODAL DENSITY OF EXPERIMENTAL TEST PIPES

for flow testing. Resonance frequency distributions (and modal quality factors) were measured, as shown in the graphs of quality factors in Figs. 4.4(a) to (c). The resulting calculated modal densities are shown in Fig. 4.1. Similar scatter as occurred for the free-free end condition is present in the results of all test sections: the theory represents a good mean curve for the experimental data.

It was not possible to measure the density of the supersonic modes, due to increasing modal overlap at higher frequencies. Close agreement was found, however, between the measured resonance frequencies of the low axial-order n = 1 modes of all test pipes and theoretical predictions using the equations of Arnold and Warburton. (n = 1 modes are supersonic at lower frequencies than all other order n modes). Calculations from these latter equations and the approximate supersonic modal density equation (N_s in equation [2.30]) of the density of supersonic modes agree closely: consequently, it is expected that the experimental density of supersonic modes will be predicted with at least the accuracy of the prediction of the modal density of the total number of modes.

During the operation of the induced-flow rig, a static pressure reduction of up to 25kPa occurs inside the pipe, which will tend to reduce the vibrational membrane stresses in the pipe wall and also decrease the resonance frequencies: these changes were investigated experimentally. The induced-flow rig was sealed at the inlet and the choke. A vacuum pump was used to apply a series of constant pressure differences across the pipe wall, while the changes in resonance frequencies were monitored. The resulting reductions were found to be directly proportional to both the circumferential mode order and the reductions in internal pressure (up to 50kPa), but were always less than 5% as shown in Fig. 4.3. Consequently, no important changes in modal density are expected to occur during the flow-testing of the steel pipes.

4.3 DAMPING OF STEEL PIPES

4.3.1 Introduction

Theoretical estimates of the vibrational response of and acoustic radiation from structures depend on estimates of the structural damping. For example, the response of a single structural mode is proportional to its modal quality factor Q_α, as well as to the coupling between the excitation and the mode. Similarly, the response of a group of modes contained in a narrow frequency band may be considered proportional to an 'average quality factor' Q, and to the average coupling existing between the excitation and the resonant modes. For those situations where the coupling is independent of the actual mode, the average quality factor is equal to the arithmetic mean of the quality factors of the modes in the band. When the joint acceptance varies significantly over the resonant modes in a band, the average quality factor may be controlled by the most strongly-coupled, lightly-damped modes. In general, therefore, different excitations will produce different effective Q values, requiring that the actual excitation under investigation be used in the measurement of the average quality factors, in order that the appropriate modal energy levels (on which Q depends) are produced.

Measurement of the decay of steady-state vibrational energy levels on removal of the excitation will give correct estimates of the average quality factors for mechanical or acoustic structural excitation. This approach is not practical, however, for turbulent flow excitation of structures since the excitation will not decay sufficiently quickly. Several rather complex methods exist for the measurement of individual modal quality factors for flow-excited structures, but these are suitable only for low-order, widely-spaced, lightly-damped modes. In the excitation of low-order modes of thin panels by turbulent flow, Wilby (1967) found that the flow increased the damping by an average of 50% over the values measured by single-frequency electromagnetic excitation with no flow over the panels.

No methods exist for the direct measurement of average quality factors of lightly-damped structures of high modal density, which are excited solely by turbulent flow. Since the present steel pipes have larger wall thicknesses than the panels used by Wilby, we have assumed that no important increases in modal damping will be produced by the action of the flow: even if the Q's decreased by 50%, this would imply errors in theoretical response predictions of only 3dB.

Introductory experiments were performed to determine the most suitable method for measuring the modal and average quality factors. These were followed by investigations of the effects of variations in pipe end conditions and of a static pressure differential across the pipe wall. While such a detailed investigation was perhaps not necessary for the analysis of the experimental results, the effects observed seemed sufficiently interesting in their own right to justify a detailed examination.

The 'response-amplitude' and the 'response-decay' methods were compared. In the response-amplitude method, the frequency bandwidth ($\Delta\omega_\alpha$) of each individual resonant mode is measured at the half-power points of the response-amplitude curve; the modal quality factor is then given by $Q_\alpha = (\omega_\alpha/\Delta\omega_\alpha)$, where ω_α is the mode resonance frequency. This method requires that the oscillator frequency is stable over the measurement period and can be varied over small discrete intervals. Likewise the mode resonance frequency must not drift with time. Any non-resonant vibration should be minimized by the appropriate placement of the exciter and vibration transducer. For lightly-damped modes at low frequencies, the modal bandwidths can be very small so that large inaccuracies may be produced by small errors in bandwidth measurement. The method is extremely time consuming when many modes are to be investigated.

The response-decay method involves a measurement of the rate of decay of the pipe vibration from its initial steady-state level after the excitation has been removed. To accomplish this, the amplified accelerometer signal is passed to a linear-log converter and then to a variable

time-base storage C.R.O., where the decay rate is measured with a calibrated protractor. The same limitations regarding non-resonant contributions to the modal decay apply to this method as to the response-amplitude method. The results are more accurate for small bandwidths and are not sensitive to resonance frequency drift. The two methods were found to give identical results; however, the latter was adopted since it is more convenient to use, and has the advantage that it may also be used in the measurement of average quality factors, where the excitation is with bands of random noise.

4.3.2 Measurements on a Pipe with Free Ends

For lightly-damped steel structures, only structural damping and acoustic radiation will contribute significantly to the decay of vibrational energy levels. Structural energy dissipation will be associated both with material internal-damping mechanisms and with losses occuring at the structural boundaries; of the latter mechanisms, viscous damping arising from the pumping of gas around the joints can be important in non-rigid joints (Ungar and Carbonell (1966)). As discussed in section 2.2.7, significant acoustic damping will occur when the structural radiation ratio of light-weight structures is high, so that Q_{rad} (defined by equation [2.36]) may be less than the quality factor produced by other damping mechanisms. First a pipe with free ends was tested: the influence of the structural supports was removed, so that internal and acoustic damping could be examined. The 3.5 m section of steel pipe (section 4.2) was excited at one end with an electromagnet driven by the Muirhead Oscillator at those frequencies corresponding to pipe resonant modes. The supporting wire loops were adjusted to the nodal positions to minimize the energy lost through the supports. The 0.5g accelerometer, located at the pipe end opposite the excitation, sensed the decay of the pipe acceleration level on removal of the excitation. The modal decay rate was found to be independent of the position of both the exciter and the accelerometer,

and of the amplitude of the excitation (as indicated by straight-line logarithmic decay curves).

The modal quality factors for the pipe with free ends are shown in Fig. 4.2(a). The greater majority of the low-frequency modes ($\nu < 0.13$) have been located: smooth mean curves can be drawn. A remarkable order exists in the variation of Q_{mn} with m, for fixed n. Consider the n = 1 modes. As m increases, Q_{mn} increases initially (associated perhaps with a small but decreasing energy transfer through the supporting wires), and then decreases smoothly from a peak value of $Q_{m1} \simeq 2300$ to a minimum measured value of approximately 350. The n = 1 modes have the highest structural wavespeeds at a particular frequency. In this case, as m increases, the radiation ratio of the n = 1 modes increases sharply and the resulting acoustic damping increases, so that Q_{rad} decreases. Assuming that the material quality factor is approximately 2300, equation [2.35] may be used to calculate Q_{mn} as Q_{rad} decreases with mode order: for example,

$$\frac{1}{Q_{mn}} = \frac{1}{Q_i} + \frac{1}{Q_{rad}} \qquad \text{where } Q_i = 2300.$$

These calculations are presented for n = 1 to 4 in Figs. 4.2(b) to (d), where Q_{rad} has been calculated using equation [2.36]: mean experimental curves from Fig. 4.2(a) are included for comparison. From Fig. 4.2(b), for n = 1 modes, the acoustic radiation is seen to control the quality factor of modes $m \geq 4$.

Similar trends are found with modes of circumferential order n = 2 and n = 3. An initial increasing portion of the Q_{mn} curve is followed by a flat plateau of constant Q_{mn} of approximately 2300. The acoustic quality factors of the n = 2 and n = 3 modes control the plateau width (Figs. 4.2(c) and (d)). After an initial increase, the measured quality factors of the n = 4 circumferential modes remain essentially constant for the range of m measured. Calculations predict that significant acoustic damping will not occur for n = 4 modes until $m > 75$ or $\nu > 0.31$.

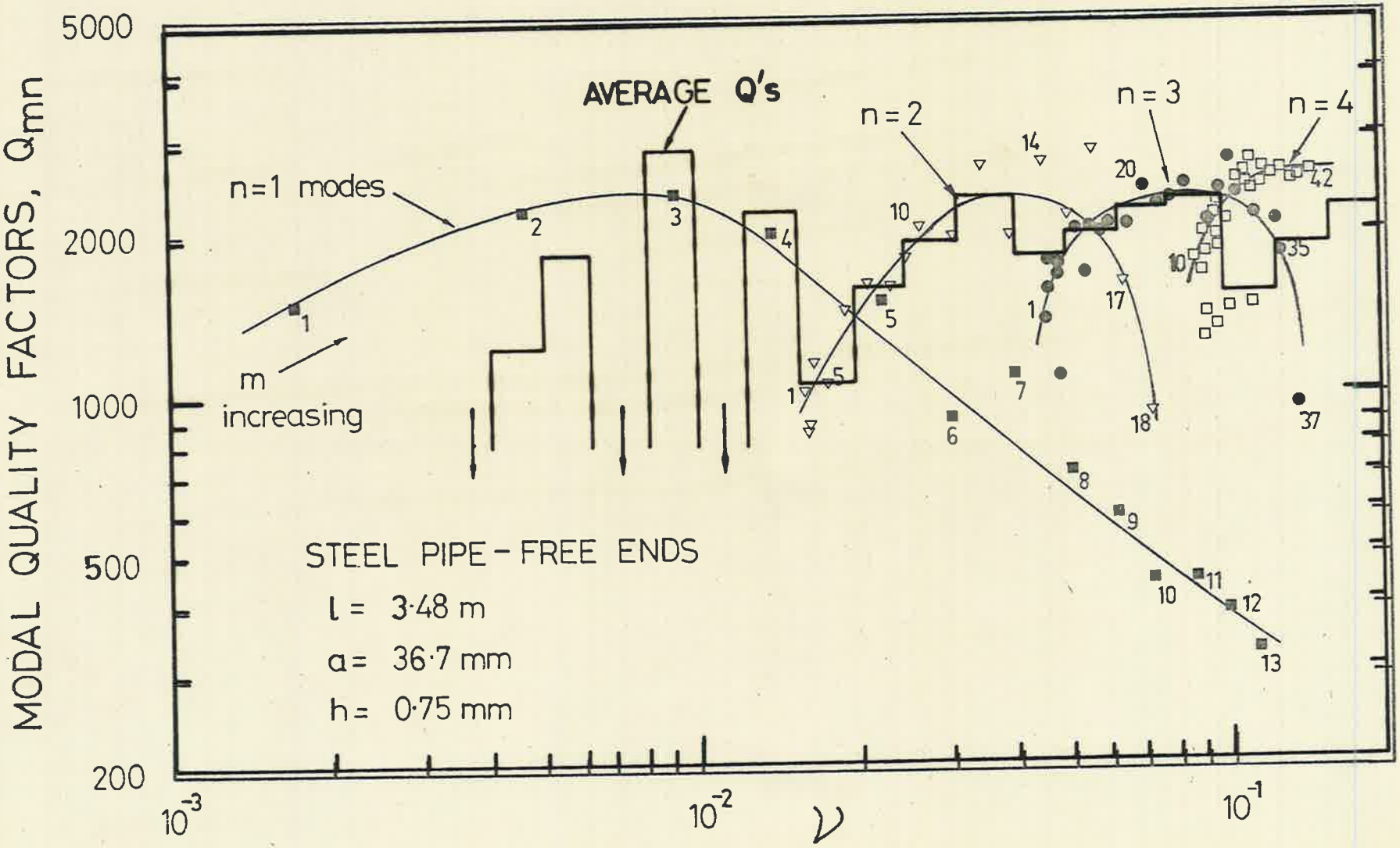

FIG. 4.2(a) MODAL RESONANCE FREQUENCIES & Q's - FREE ENDS - STEEL PIPE

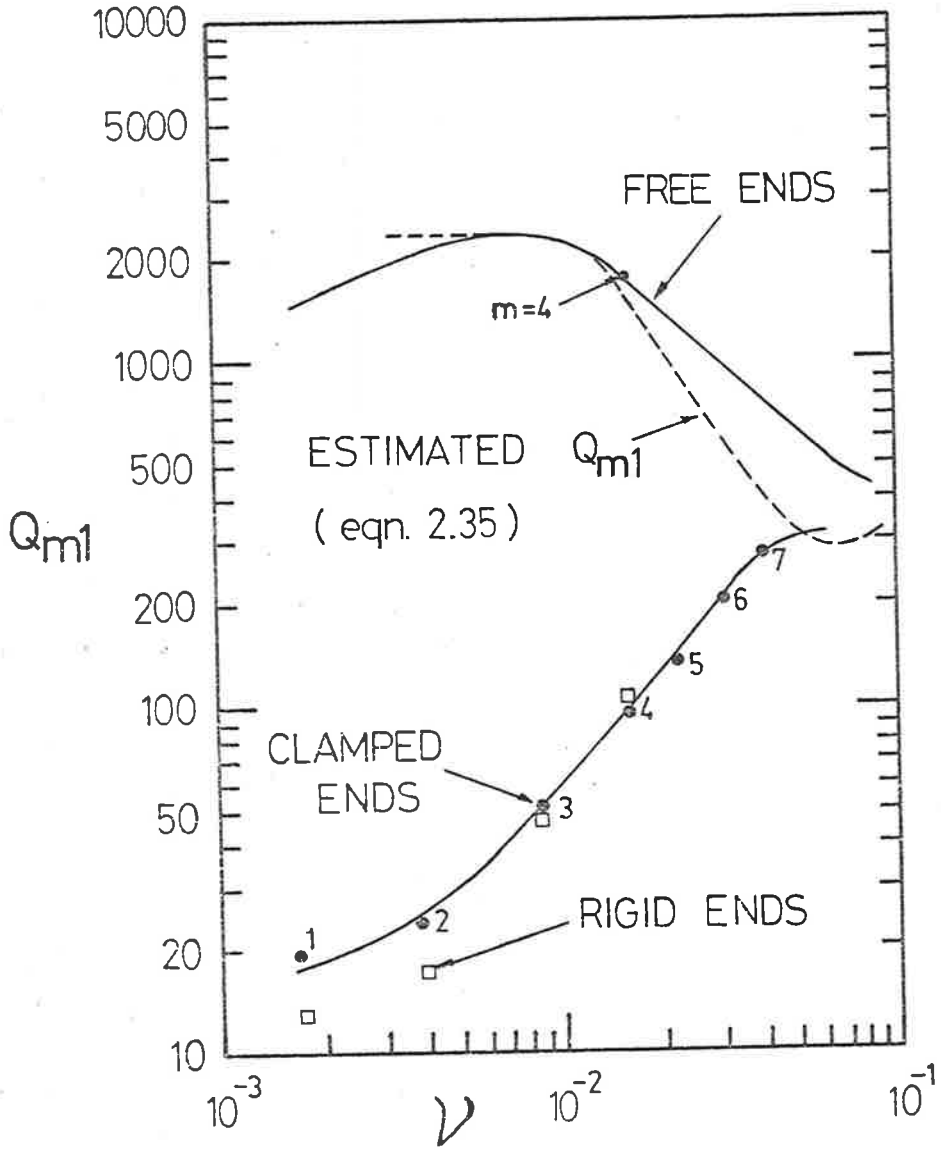

FIG. 4.2(b) Q_{m1} FOR VARIOUS END CONDITIONS

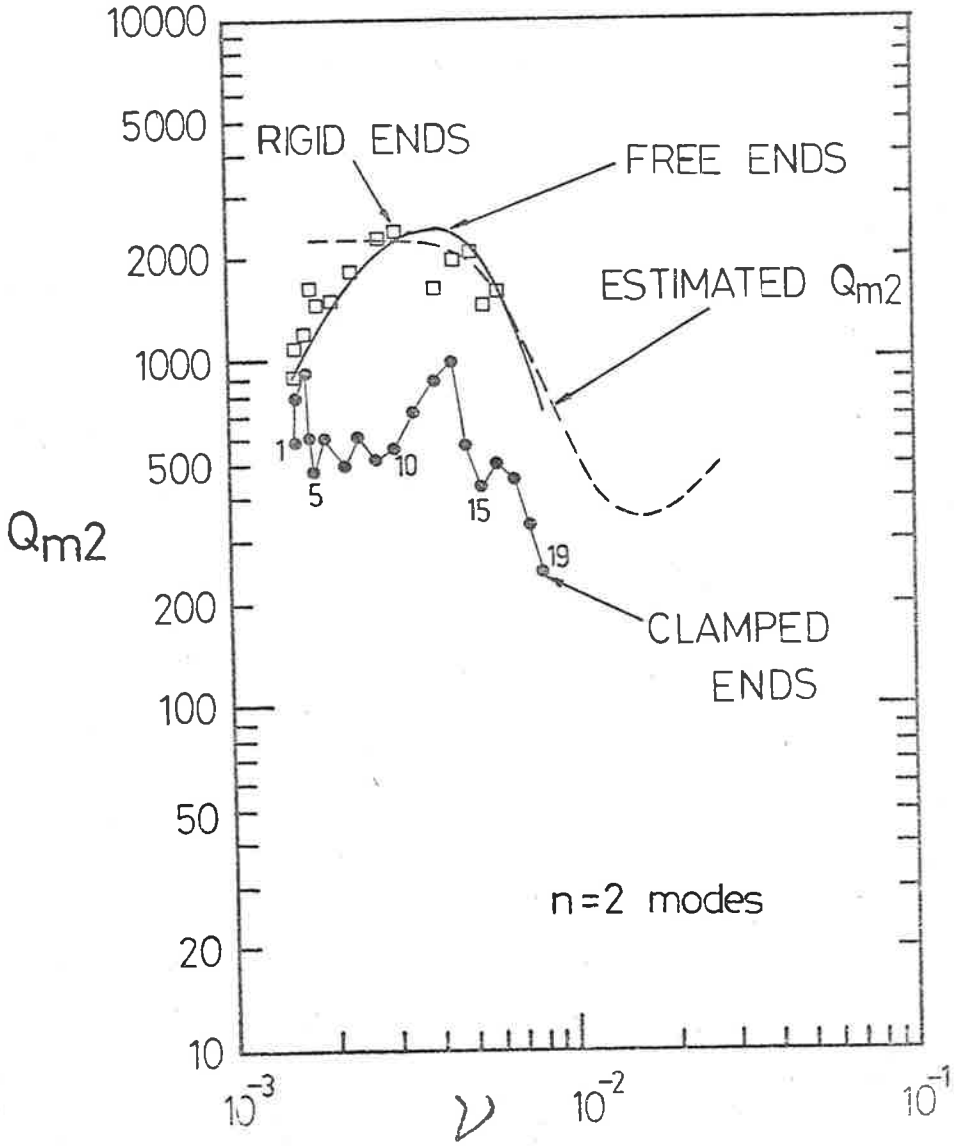

FIG. 4.2(c) Q_{m2} FOR VARIOUS END CONDITIONS

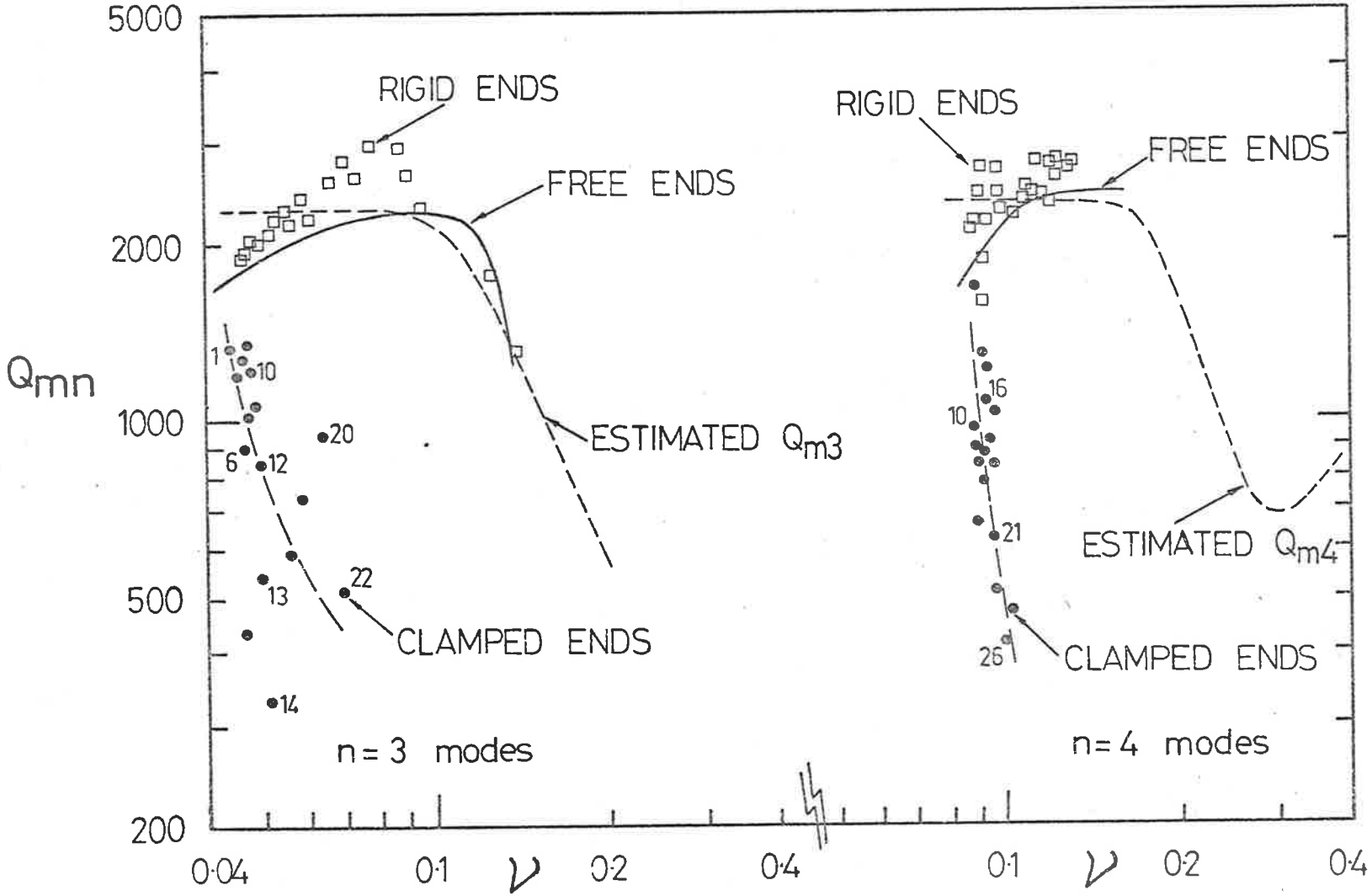

FIG. 4.2(d) Q_{m3} & Q_{m4} FOR VARIOUS END CONDITIONS

From these results, it follows that the response of low-frequency supersonic modes will be determined primarily by the acoustic damping presented by the surrounding acoustic medium. The actual measurement of the quality factors of these supersonic modes is difficult, since they are more heavily damped than other subsonic modes present. However, reasonable estimates of the quality factors of these modes may be made by assuming unit radiation ratio.

The same pipe was excited with one-third octave bands of random noise from a B & K 1402 Random Noise Generator, and average quality factor measurements were made using the response-decay method. The initial slopes of the decay curves were taken to represent the average quality factors - these are shown on the overlay in Fig. 4.2(a). Calculations of the arithmetic mean of the modal quality factors in each band agree closely with these measurements, even for bands containing a range of modes of different circumferential order.

4.3.3. Measurements on a Pipe with 'Clamped' Ends

The ends of the 3.5 m steel pipe were 'clamped' in massive supports as described in section 4.2. Measurements of the modal and average quality factors were repeated; for clarity, only the modal results are shown in Figs. 4.2(b) to 4.2(d), although it was found that the measured average quality factors of the modes in a particular band were equal to the arithmetic mean of the quality factors of the individual modes.

Substantial increases in structural damping occur for modes of each circumferential order. Vibration in the n = 1 'translational' modes involved displacements of the pipe centre of mass (normal to the pipe axis), so that considerable energy is dissipated by vibration of the pipe end-supports. This additional damping decreases as m increases, as shown in Fig. 4.2(b) by the curve of Q_{m1}, which increases smoothly from a minimum value of Q_{11}=20 to Q_{71}. Furthermore, it was found that Q_{m1} ($m < 4$) could be reduced to less than 10, by placing a rubber O-ring between the outside

diameter of the pipe ends and an enlarged clamping support, thus creating a flexible, simply-supported end condition. Shearing of the O-ring support provided additional damping. However, for the clamped end, the additional damping occuring at the ends for the n = 1 modes, presumably the most severe case, has disappeared completely by m ≃ 6. At higher m (and ν), the increasing radiation damping probably causes the 'clamped' Q_{ml} curve to fall in a similar manner to the free end case, as shown in Fig. 4.2(b), although it was not possible, especially at frequencies where n = 3 modes occur (ν ≃ 0.044), to isolate n = 1 modes of axial order greater than 7.

Modes of circumferential order n ≥ 2 do not involve a translation of the pipe axis, so that their quality factors should not be influenced by the pipe end conditions in the same strong manner as n = 1 modes: in fact, as seen in Fig. 4.2(c) and (d), the increases in damping of the low axial-order modes for n ≥ 2 are quite small. It was noted that no significant changes in the quality factors of the low m, n = 2 modes from the free end results were produced by the O-ring supports; this reinforces the opinion that the n ≥ 2 modes do not dissipate significant energy by support vibration. Contrary to the behaviour observed for n = 1 modes (Fig. 4.2(b)), the additional damping produced by the 'clamped' end condition increases as m increases, for modes of constant circumferential order n. The increases in additional damping become larger and more ordered as n increases, as shown in Figs. 4.2(c) and (d). A possible explanation of this behaviour is that the process of 'gas-pumping' is involved in the push-fit joints at the pipe ends. Ungar and Carbonell (1966) have investigated this phenomenon as it occurs in bolted beam-plate structures, while Maidanik (1966) has developed a satisfactory explanation of the dependence of the average quality factors on frequency, gas pressure, and separation distance between plate and beam: however, the model does not appear readily applicable to the present situation. We note that, for 'clamped' ends, values of Q_{mn} decrease with increasing ν(or m) for constant n, and that the frequency dependence of Q_{mn} decreases as n increases. The

modal quality factors were reduced by up to 10dB over the range of observed modes, the largest reductions occurring for the highest order modes.

To examine whether, in fact, the increased damping was related to the type of joint, the push-fit joints for the same pipe were glued with epoxy cement to form 'rigid' joints; the measurements of modal quality factors were repeated, though this phase of the work was not attempted until all other experimental work was completed. It was found that the modal quality factors increased above the 'clamped' end condition measurements, to the values found for the free-free end condition, except for the n = 1 modes. These results for the 'rigid' end condition are shown in Figs. 4.2(b) to 4.2(d) for comparison with the other end conditions. This increase in modal quality factor confirms that phenomena inside the push-fit joints were responsible for the strong frequency dependence of the Q_{mn} curves (for constant n). In practical situations, the pipe ends will usually be welded and therefore quite rigid: then, it appears likely that, except for n = 1 modes of low axial order and for those modes damped by acoustic radiation, all modes will be essentially lightly damped with quality factors in excess of 1000.

During all experiments, the 'clamped' end condition of push-fit joints was used. Measured quality factors of test sections in-situ are required in the reduction of results and for theoretical predictions of $\Phi_{\ddot{w}}/\Phi_p$ and Φ_{π}/Φ_p.

4.3.4. Effects of a Static Pressure Differential

An experiment to examine whether a static pressure differential would alter the modal quality factors in any way was performed. The experimental arrangement was similar to that described in section 4.2; test section 1 (β = 0.00591) was 'clamped' in the induced-flow rig in the anechoic chamber.

The modal and average quality factors were measured for two static pressure differences: (a) 25kPa and (b) 50kPa. In Fig. 4.3

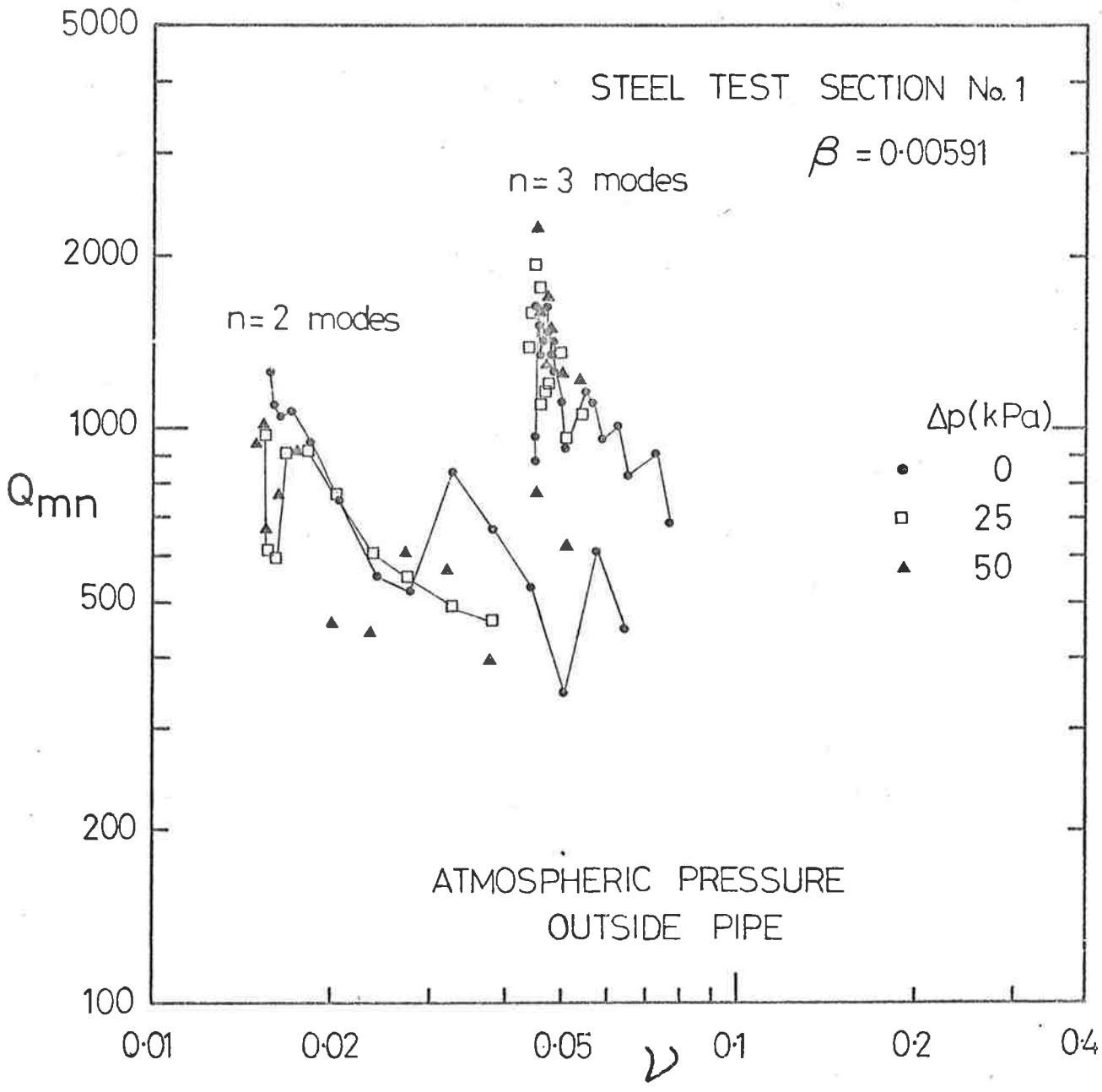

FIG. 4.3 VARIATION OF Q_{mn} WITH STATIC PRESSURE DIFFERENTIAL

the modal results are compared with measurements for zero static pressure difference. A small reduction in the resonance frequency of each mode occurs, as previously noted, but there are no systematic or significant variations in the quality factors. Likewise, the variations in the average quality factors were small and showed no dependence on the pressure difference. It is concluded that the static pressure differential which will exist across the pipe during operation of the flow rig will not influence the results in any important way.

4.3.5. Measurements on Test Section Pipes

Detailed investigations of the modal and average quality factors for all test sections in-situ were carried out as an integral part of the testing programme. Average quality factors were measured before and after each series of flow tests, while the individual modal data were measured before flow testing only. No differences in the average quality factor measurements made before and after flow testing were observed. In all cases, the 'clamped' end condition corresponding to push-fit joints was used.

The measured quality factor information (i.e. Q_{mn} and Q) is plotted in Figs. 4.4(a), (b) and (c) for steel test sections 1,2 and 3 respectively (which correspond to values of β = 0.00591, 0.0070, 0.0100). The average quality factors for supersonic modes Q_s are estimated from the actual values of Q_{mn} of modes as they tend to become supersonic, qualified by calculations of Q_s from equation [2.37] and by measured values of Q. Q and Q_s are required for theoretical estimates of the vibrational response and acoustic power radiation from the tested pipes.

Similar trends in the behaviour of the modal and average quality factors to those previously described were found for the three steel test sections. For all test sections, the same remarkable order in Q_{mn}, as shown in Figs. 4.2(b) to (d), occurred. In particular, values of Q_{mn} (for constant n) decrease as ν(or m) increases, the rate of decrease increasing with n.

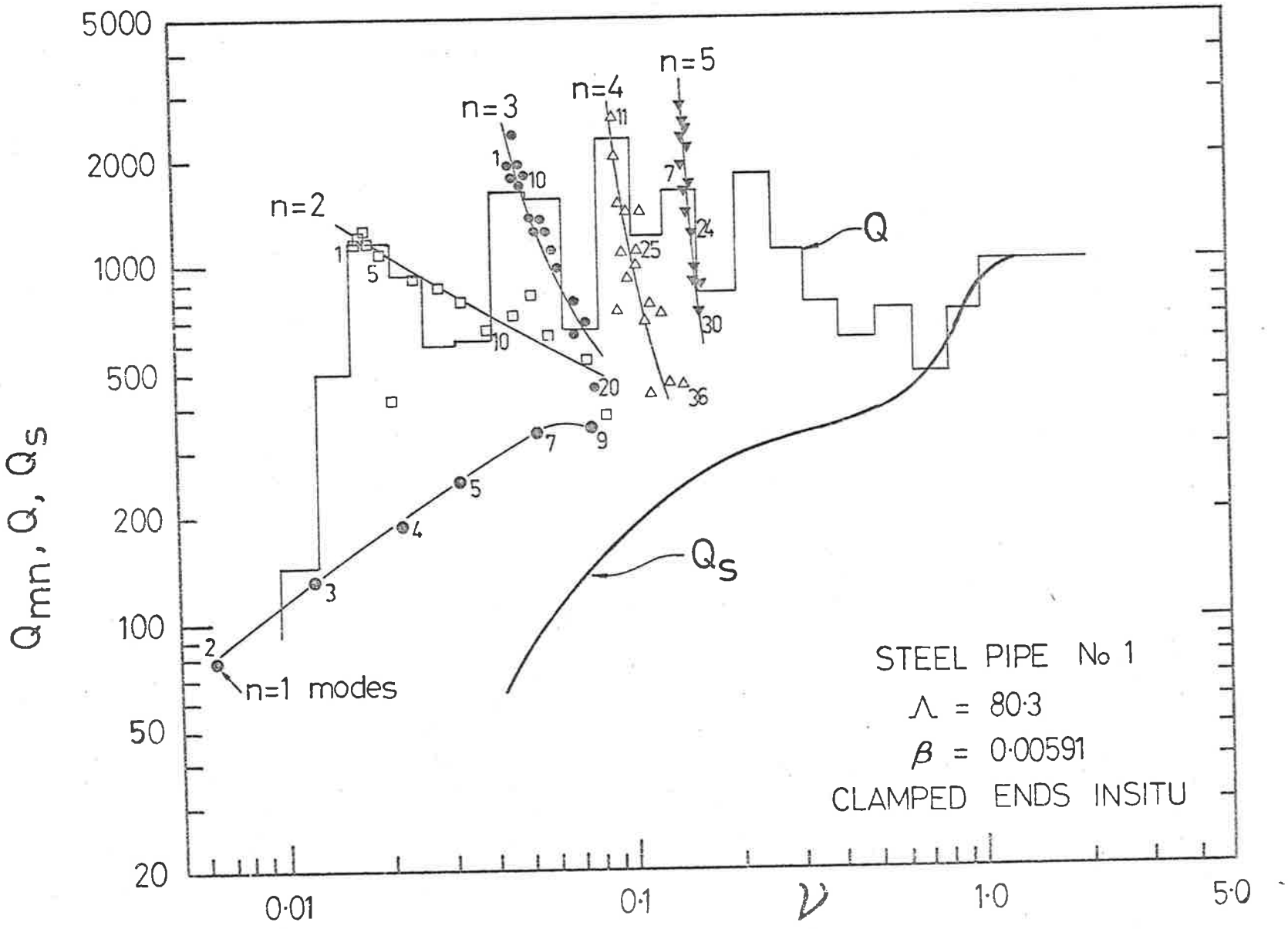

FIG. 4.4(a) QUALITY FACTORS FOR PIPE No. 1 $\beta = 0{\cdot}00591$

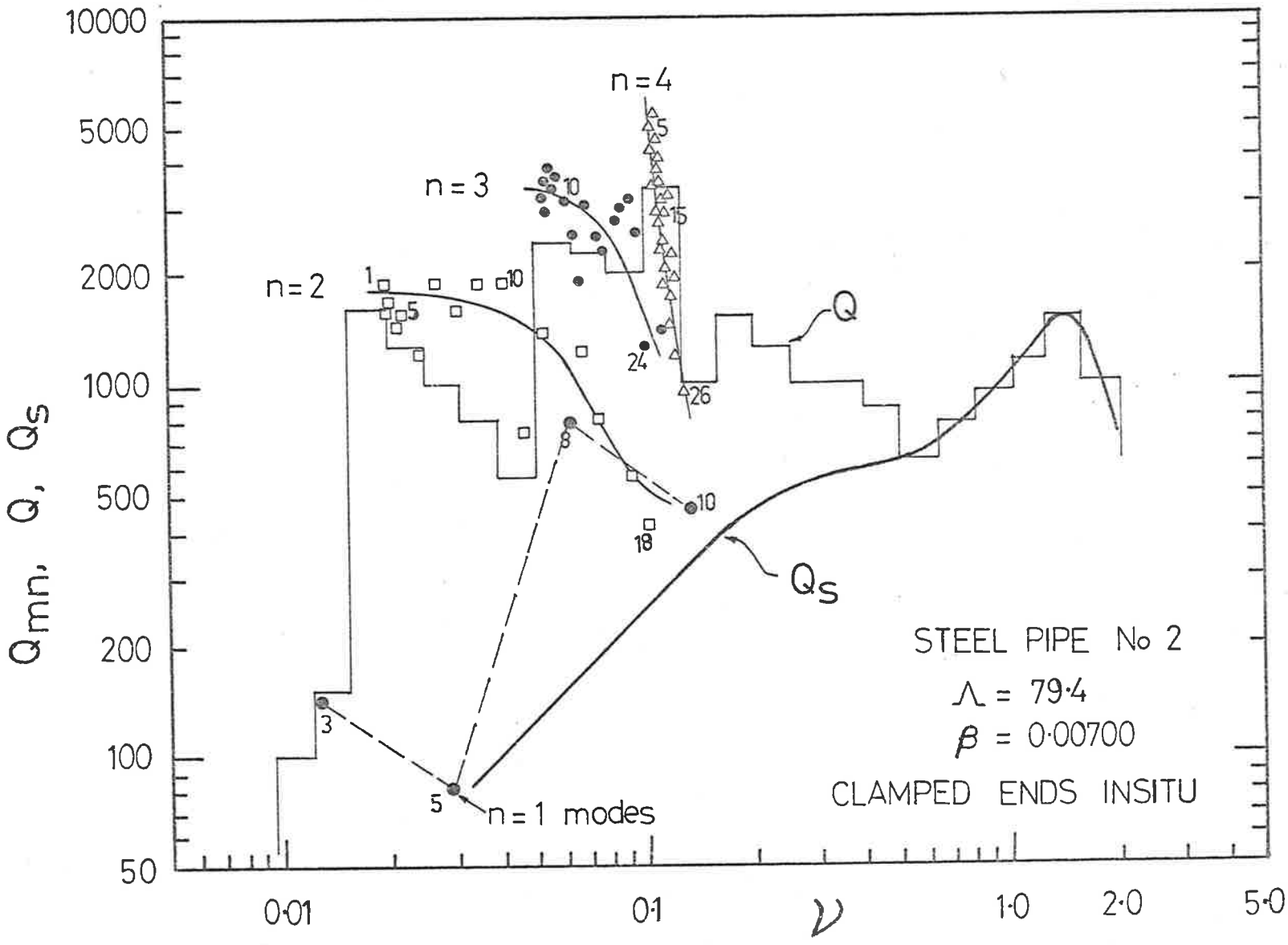

FIG. 4.4(b) QUALITY FACTORS FOR PIPE No. 2 $\beta = 0{\cdot}00700$

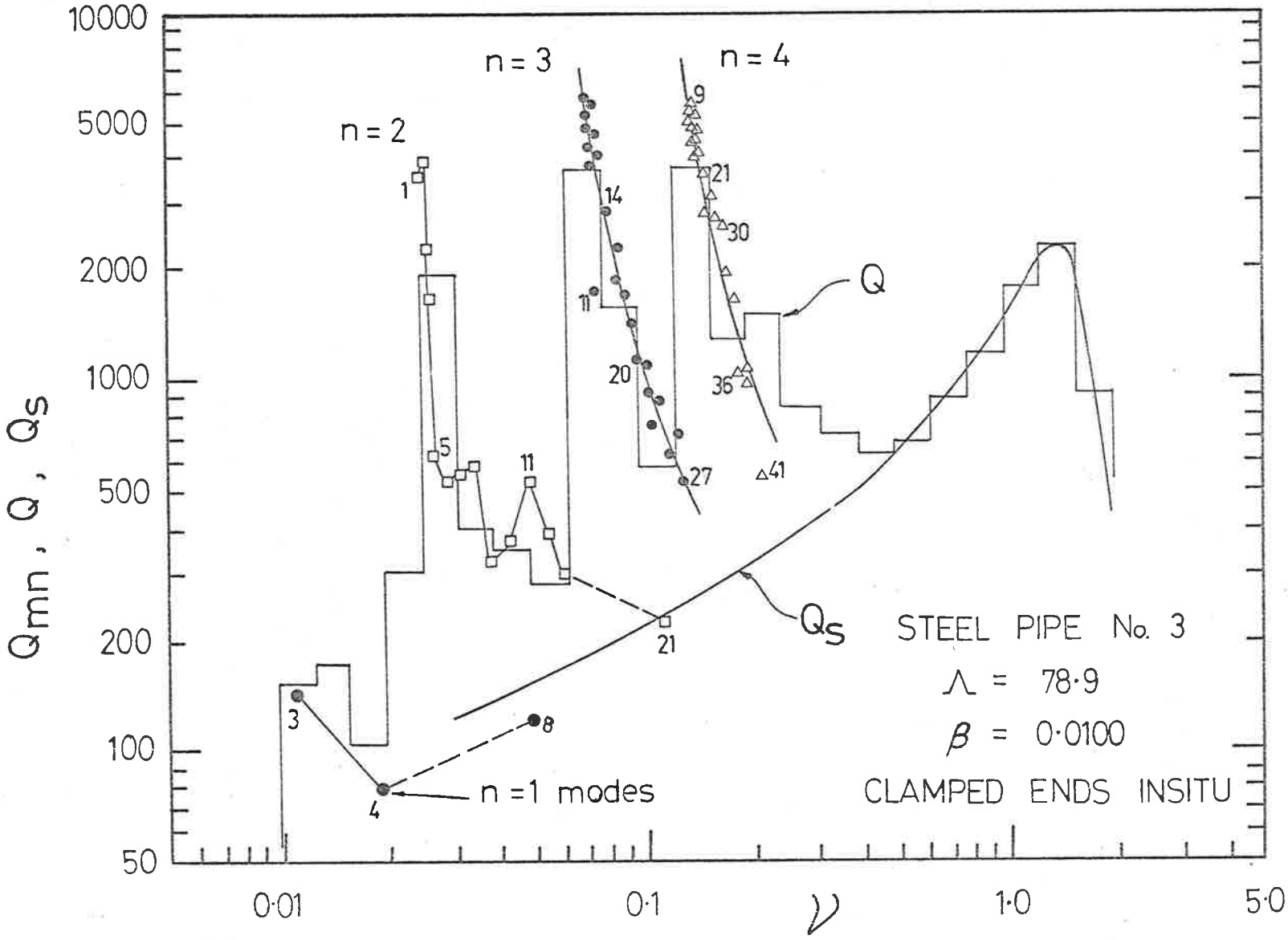

FIG. 4.4(c) QUALITY FACTORS FOR PIPE No 3 $\beta = 0{\cdot}0100$

The average quality factor Q, as given by the initial slope of the log-decay curve, was found to equal to arithmetic mean of the modal quality factors.

4.3.7. Summary

The resonant modes of the tested steel pipes were found to be essentially lightly damped. Considerable variations in the modal quality factors existed between modes of different order, however, depending on the nature of the pipe end conditions and on the value of the modal radiation ratio.

Initial experiments on pipes with free-free end conditions demonstrated that the quality factors of modes of low radiation ratio were approximately independent of the mode order. It was seen that as the modal radiation ratios approached unity values, the modal quality factors (which are inversely proportional to the radiation ratios) decreased as they became progressively more controlled by the acoustic radiation away from the pipe.

For push-fit end conditions (termed 'clamped' in the present experiments) which allow some relative motion between the end supports and the pipe surface, large amounts of additional damping (up to 10dB) occurred. For each set of circumferential modes of order $n \geq 2$, the modal quality factor Q_{mn} decreased as m (or ν) increased: also the frequency dependence of Q_{mn} decreased as n increased. Pumping of gas around the end joints was probably responsible for these observed increases in damping above the levels found for the free-free end condition. It was found that rigidly fixing the push-fit joints with epoxy cement caused the modal and average quality factors to increase to values corresponding to free-free end conditions. It seems that, in welded piping systems, rigid end conditions will exist most frequently, so that high modal quality factors can be expected in the absence of significant acoustic radiation damping or other damping mechanisms (such as attached structures).

During experimental flow testing, the quality factors of test sections in-situ were measured for use in the data reduction process and for theoretical predictions: the end conditions corresponded to 'clamped' push-fit joints. For the pipe wall thicknesses investigated, the presence of a small static pressure difference across the pipe wall failed to produce any significant changes in pipe quality factors. It has been assumed that the presence of turbulent flow inside the pipe will have negligible effect on the structural damping.

4.4 ACCELERATION RESPONSE

4.4.1. Introduction

For the purpose of making a detailed examination of the vibrational response of steel pipes and of providing a comparison with the theoretical predictions of Chapter 2, an extensive set of measurements of the acceleration response of steel pipes to flow excitation has been taken.

The measured data are presented in non-dimensional form as $\Phi_{\ddot{w}}/\Phi_p$, as suggested by equation [2.20]. The general characteristics of the acceleration response are described in detail and with reference to the measurements of the pipe modal densities and quality factors. The dependence of $\Phi_{\ddot{w}}/\Phi_p$ on the internal flow speed and the pipe wall thickness is examined following the predictions of equation [2.29]. Comparisons of the experimental non-dimensional response spectral densities and the theoretical predictions, using the statistical analysis, are discussed.

4.4.2. Spatial Uniformity of the Pipe Response

The random turbulence pressure field acting on the inside wall of the test pipes is homogeneous; it should produce a circumferentially homogeneous vibrational response in the pipe, as discussed in section 2.2.1. To examine this conclusion and to decide the more general question of the minimum number of measurement positions required to give a satisfactory spatial average, an investigation of the spatial uniformity of the pipe vibrational response was carried out.

Acceleration response spectra of test section 1 for M_o=0.37 were measured at eight equally-spaced circumferential measurement positions at each of five equally-spaced axial stations. (The two end axial stations were 50cms from the pipe ends). At any one axial station, the circumferential variation in acceleration spectral density was always less than $\pm$ 1dB for frequencies greater than 1kHz($\nu > 0.044$) and always less than $\pm$ 3dB for lower frequencies. The axial variation in the circumferential mean values of the acceleration spectral densities was always less than 1dB for $\nu > 0.044$. The overall standard deviation of the acceleration spectral density was less than 1.4dB for all $\nu > 0.044$. As a result of this spatial uniformity in response for this steel pipe, subsequent measurements were taken at a single mid-span position. The same conclusions were reached for the other two steel test sections, as each was tested during the course of experimental work.

It would appear that, given the accuracy of the instrumentation ($\pm$ 0.5dB), the vibrational response can be considered not only essentially circumferentially homogeneous as predicted, but also uniform over most of the pipe surface (provided measurements are made at positions away from the pipe ends).

4.4.3. Spectral Characteristics and Parametric Dependence

The experimental non-dimensional spectral densities of the acceleration response of test section 1 (β = 0.00591) (averaged over the pipe surface), divided by the appropriate measured values of the non-dimensional power spectral densities of the turbulence pressure field (Fig. 3.6), are presented in Fig. 4.5(a) for all the flow speeds tested. Usually measurements were analysed in one-third octave bands, although a narrow-band analysis (1% bandwidth) of the M_o = 0.52 results was performed: this clearly demonstrated that each resonant mode contributes to the response predominantly at its own resonance frequency. In Fig. 4.5(a) at low frequencies ($\nu < 0.1$), the spectral densities $\Phi_{\ddot{w}}/\Phi_p$ display sharp

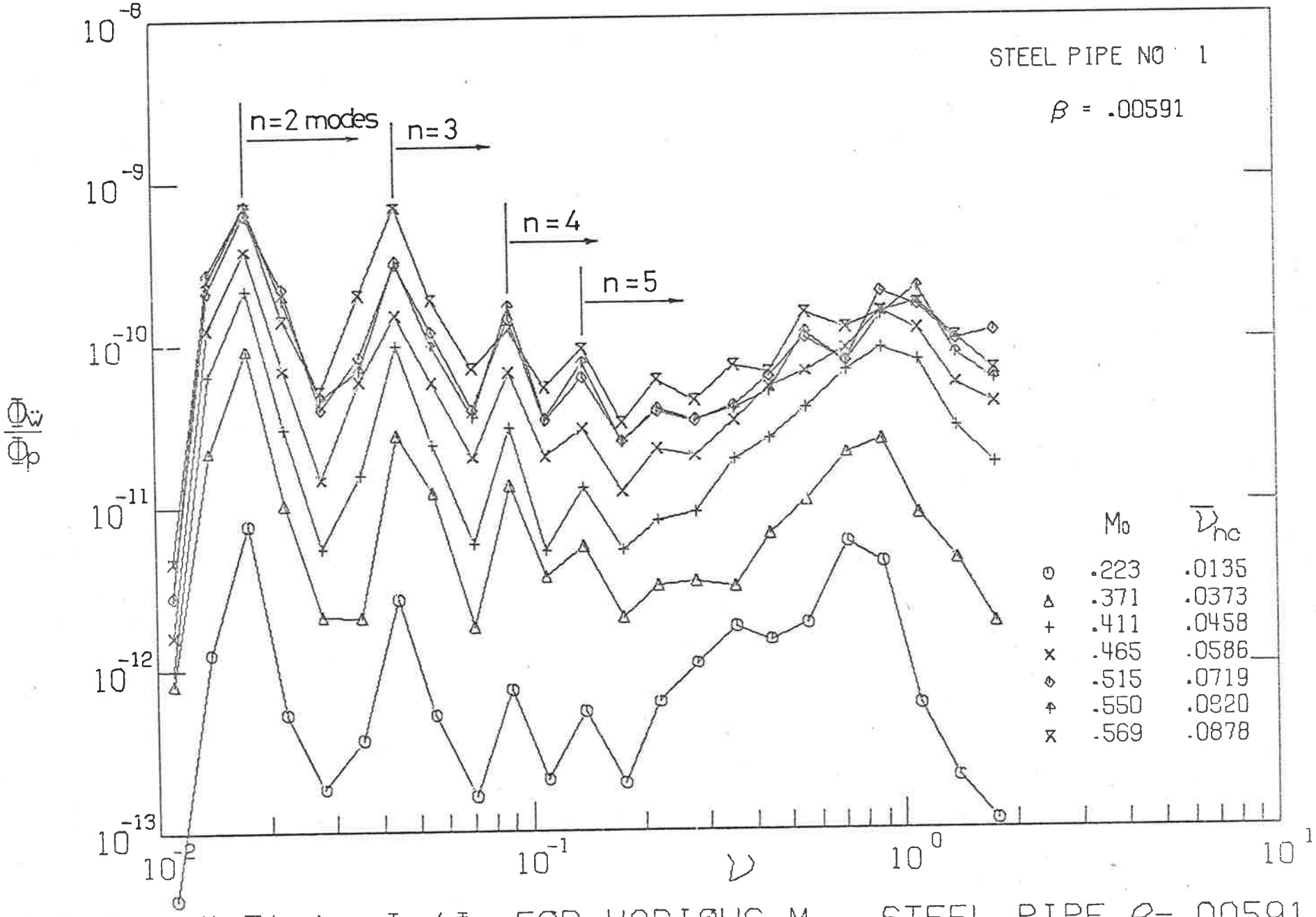

FIG. 4.5(a) $\Phi\ddot{w}/\Phi_p$ FOR VARIOUS M_o. STEEL PIPE β=.00591

peaks, reflecting the variations in modal density data (Fig. 4.1) and average quality factor (Fig. 4.4(a)) with ν for this pipe. The frequencies corresponding to the initial occurrence of the various sets of modes of different n are indicated in Fig. 4.5(a) for low n.

For $\nu < 0.2$, the mean $\Phi_{\ddot{w}}/\Phi_p$ levels tend to decrease as ν increases, but for $\nu \gtrsim 0.3$, the slopes of $\Phi_{\ddot{w}}/\Phi_p$ curves begin to increase with ν; the levels of $\Phi_{\ddot{w}}/\Phi_p$ reach their maximum values close to the ring frequency. The general spectral levels increase with increasing M_o, except at higher values of M_o, where some intersection of the various curves occurs.

For the present experimental configuration, $\bar{\nu}_{hc} << 2$ for all flow speeds. The approximate expression for the acceleration response (equation [2.29]) may be used to examine the parametric dependence for the various steel pipes. Equation [2.29] may be rearranged as

$$\frac{\Phi_{\ddot{w}}}{\Phi_p \, Q\rho_{fs}^2 \, M_o^5} = \frac{u^2}{96} \, \frac{c_x}{c_y} \, \frac{f(\nu)}{\beta^3 \, M_{Lp}^5 \, \nu} \qquad [4.1]$$

The dependence of $\Phi_{\ddot{w}}/\Phi_p$ on M_o may be examined by replotting the results in the form of equation [4.1]. Values of Q are included to remove the frequency dependence of Q from the results, while ρ_{fs}^2 is weakly dependent on M_o. This approach is shown in Fig. 4.5(b). for the whole range of M_o. The remaining irregular low-frequency variations result from deviations of the experimental modal density from the predicted values. The data collapse is reasonably close for $\nu > 0.2$ (except for $M_o = 0.22$), but for lower frequencies, $\Phi_{\ddot{w}}/\Phi_p$ appears to depend more closely on M_o^6 rather than M_o^5. The variation with frequency of the closeness of the collapse perhaps reflects the different variation of K_c/K_m with ν which occurs compared to that predicted statistically. Since the approximations to $j^2(\nu,\theta)$ are only valid for $K_c/K_m >> 1$, variations from the predicted M_o^5 dependence may occur as K_c/K_m tends to 1. This will occur mainly for low ν, where the approximate frequency equation (equation [2.8]) does not predict K_m correctly.

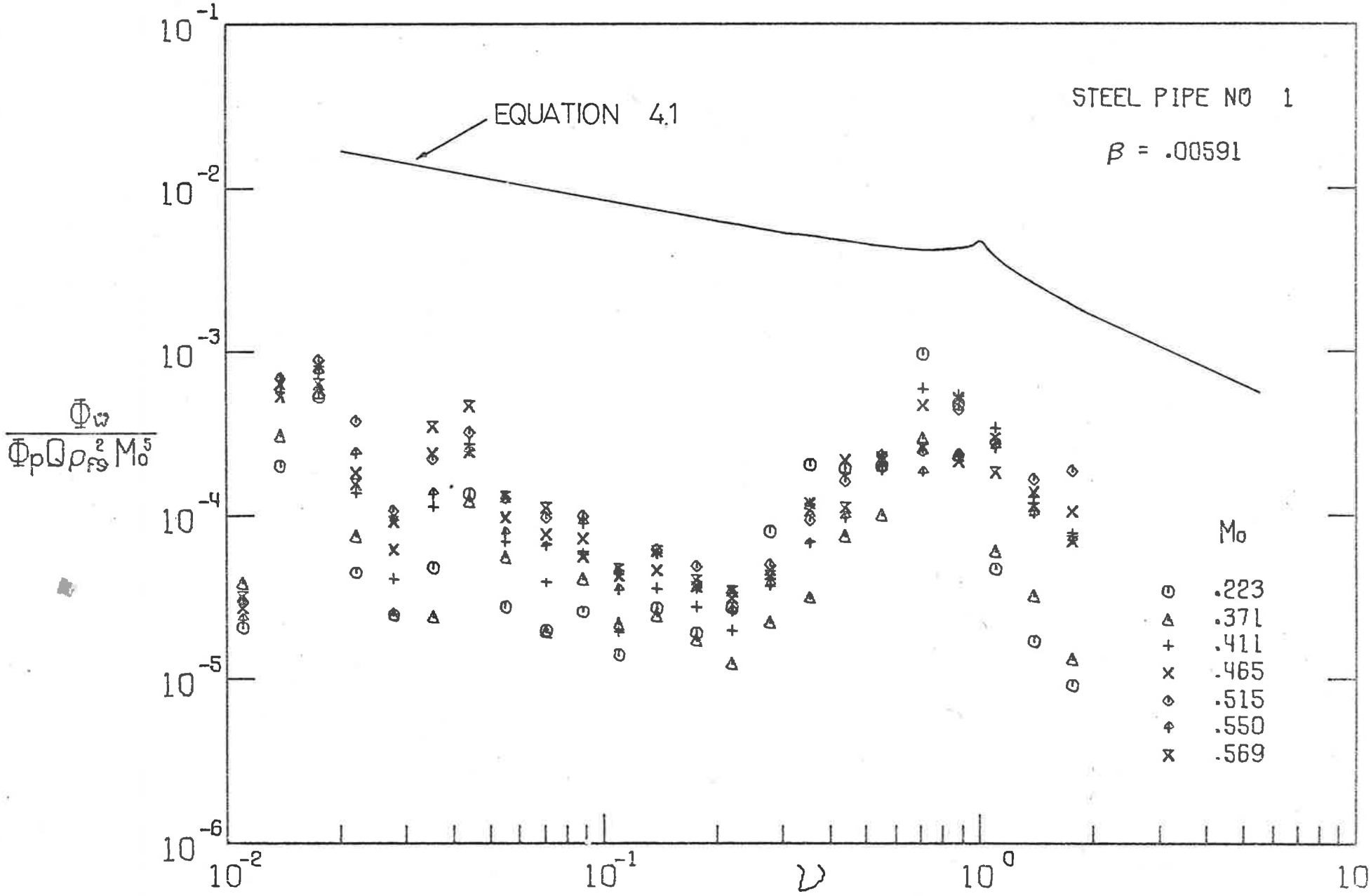

FIG.4.5(b) EFFECT OF FLOW SPEED ON Φ_w/Φ_p. STEEL PIPE β=.00591

The theoretical approximation given by equation [4.1], is included in Fig. 4.5(b) for comparison with the experimental results. Large differences exist between the mean of the experimental data and the theoretical curve, even though the approximations made should be valid for this situation. The difference is approximately 13dB at the ring frequency, increasing to a maximum of 25dB at $\nu = 0.1$, but decreasing for lower ν. For $\nu < 0.3$ and $\nu > 1$, the frequency dependence is well predicted, in spite of the poor absolute agreement. It should be noted that for $M = 0.22$, $\Phi_{\ddot{w}}/\Phi_p$ for $0.3 < \nu < 0.7$ is inconsistent with the general dependence on M_o, suggesting some extraneous acoustic excitation was present at higher frequencies for this lowest flow speed.

Measurements of the acceleration response of test section 2 are presented in the same way. Curves of $\Phi_{\ddot{w}}/\Phi_p$ for each M_o are shown in Fig. 4.6(a); again the frequency variation of these curves may be related to the irregular variations in modal density and average quality factor for this test pipe. In Fig. 4.6(b), the dependence on flow speed is examined by plotting $\Phi_{\ddot{w}}/(\Phi_p Q \rho_{fs}^2 M_o^5)$: a more compact collapse occurs than in Fig. 4.5(b), even for low ν. Again in the mid-frequency range, the data for $M_o = 0.22$ tend to lie significantly above the mean curve. Similar discrepancies with the approximate theoretical equation [4.1] are found: the frequency dependence is not as well predicted.

The experimental data for test section 3 are shown in Figs. 4.7(a) and 4.7(b), where the same general characteristics as for test section 1 are found: the collapse produced by assuming a fifth power dependence on flow speed is the closest of the steel test sections, while similar discrepancies between the approximate theory and the mean data curve still exist. The change in frequency dependence for $\nu > 0.2$ is again observed.

Equation [4.1] indicates that $\Phi_{\ddot{w}}/\Phi_p$ is inversely proportional to β^3, β^{-2} resulting from the pipe wall thickness and β^{-1} from the modal density. Equation [4.1] may be re-written as

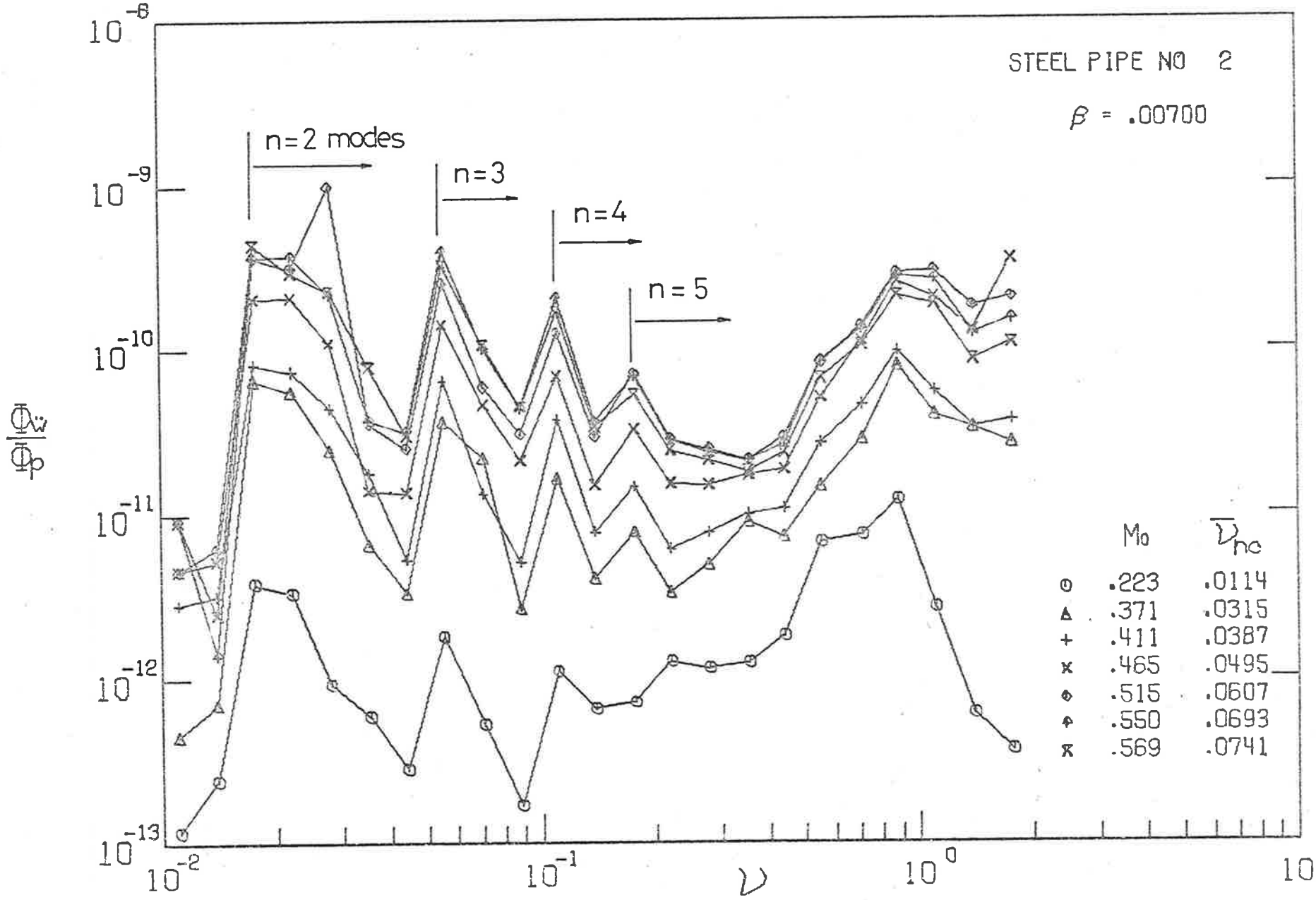

FIG. 4.6(a) $\Phi_{\ddot{w}}/\Phi_p$ FOR VARIOUS M_0. STEEL PIPE β=.00700

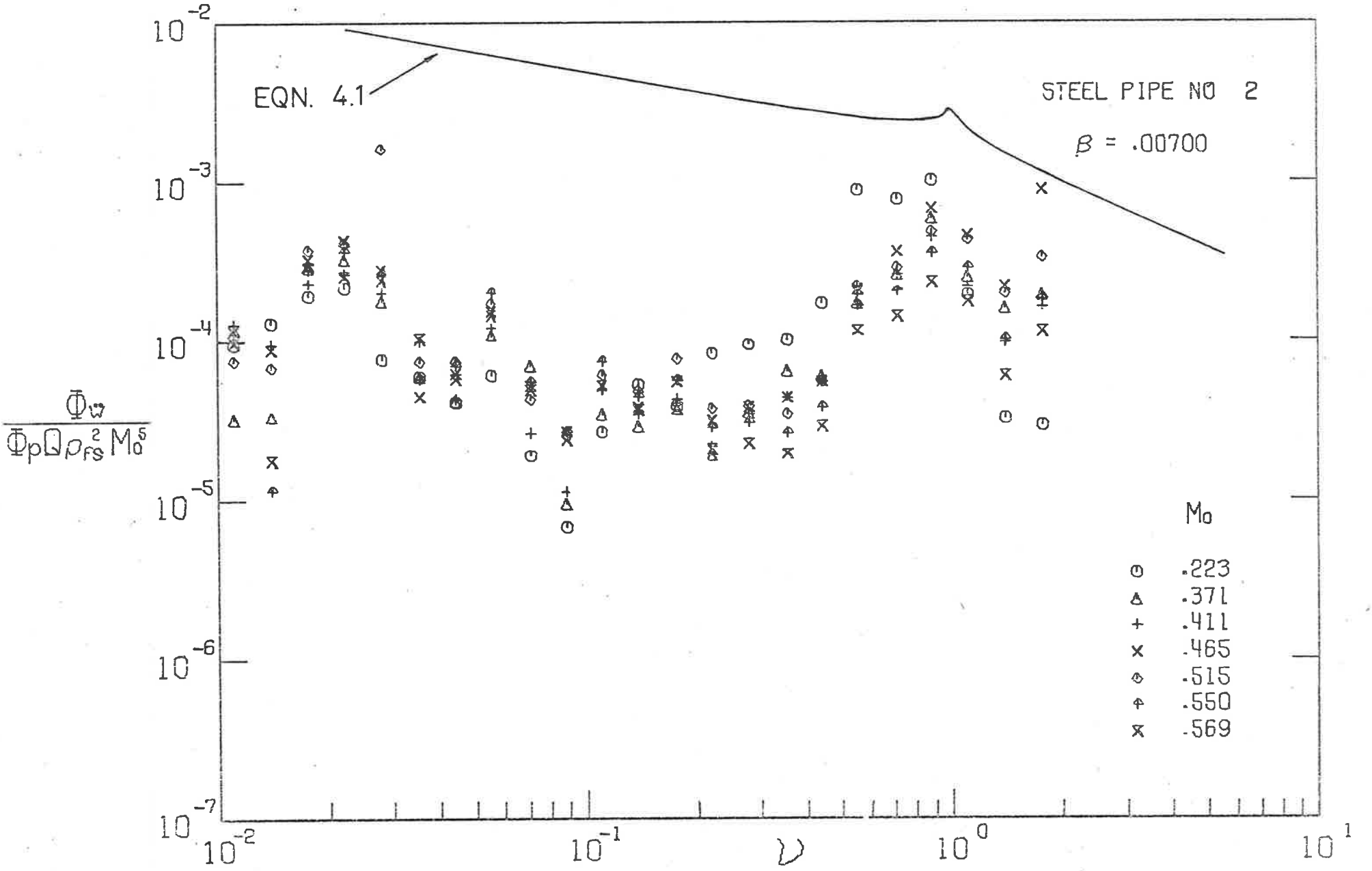

FIG.4.6(b) EFFECT OF FLOW SPEED ON Φ_w/Φ_p. STEEL PIPE β=.00700

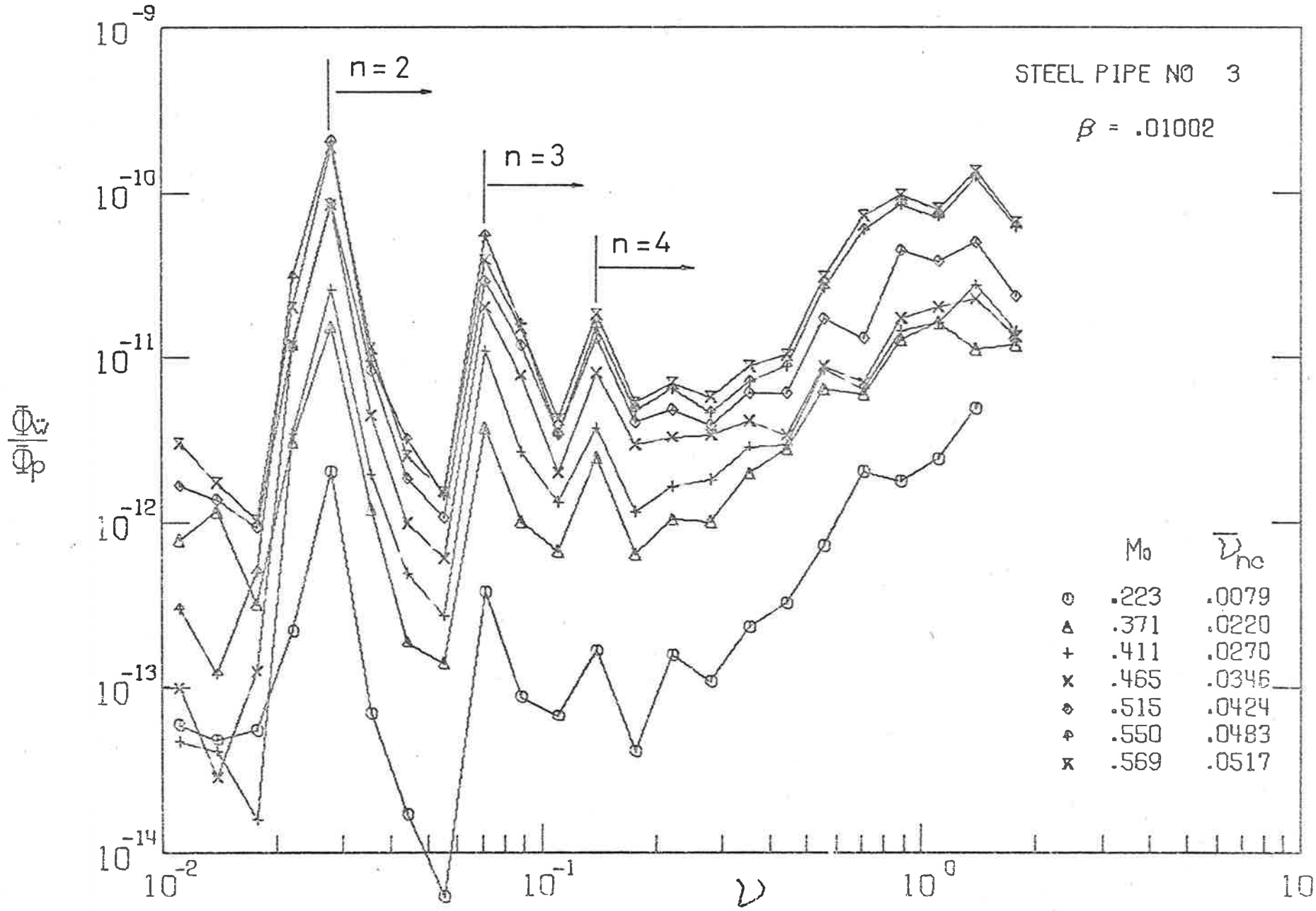

FIG. 4.7(a) $\Phi\ddot{w}/\Phi_p$ FOR VARIOUS M_o. STEEL PIPE β=.01002

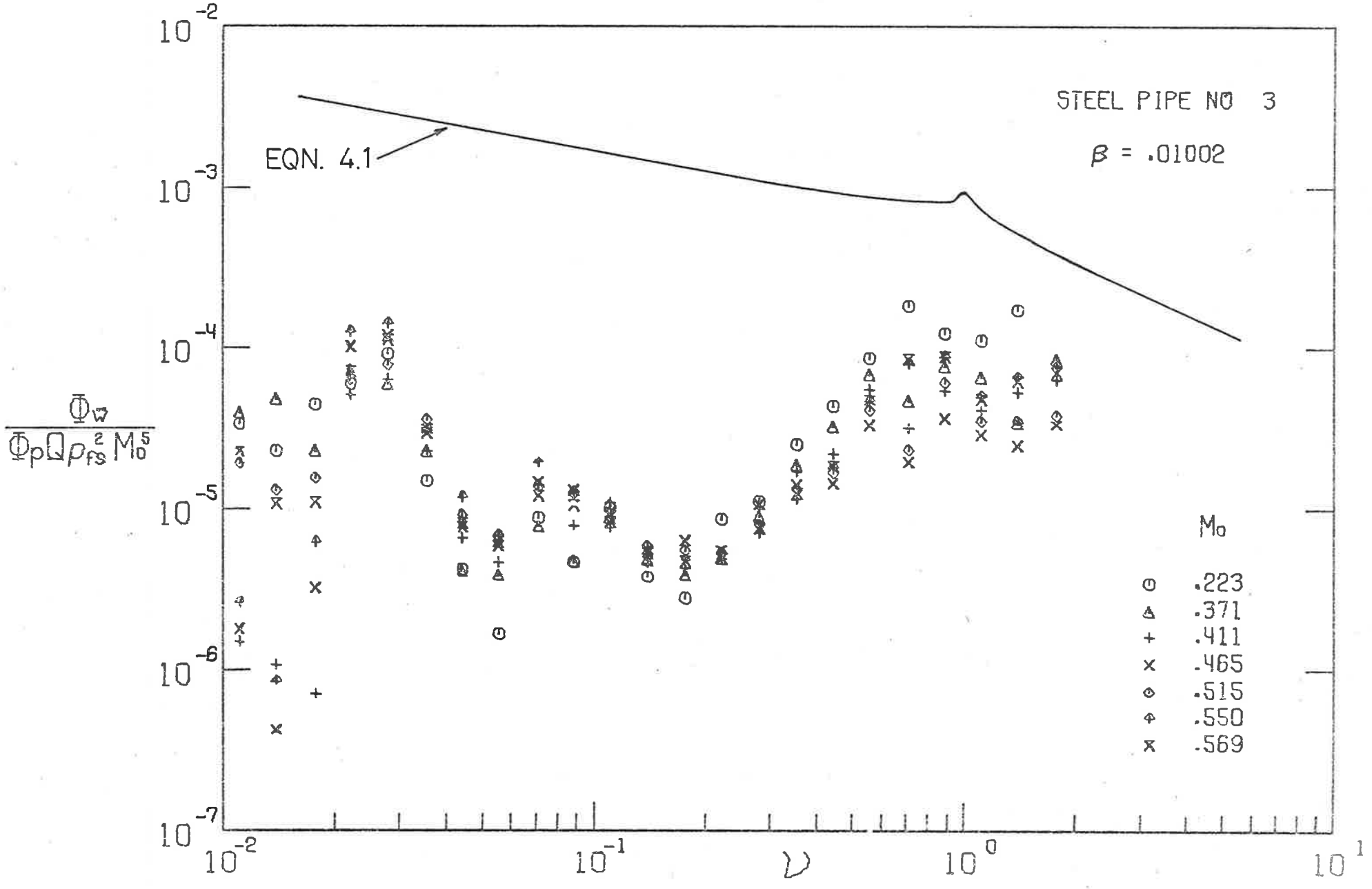

FIG.4.7(b) EFFECT OF FLOW SPEED ON Φ_w/Φ_p. STEEL PIPE β=.01002

$$\frac{\Phi_{\ddot{w}}\ \beta^3 M_{Lp}^5}{\Phi_p\ Q\ \rho_{fs}^2 M_o^5} = \frac{u^2}{96}\ \frac{c_x}{c_y}\ \frac{f(\nu)}{\nu} \qquad [4.2]$$

The data from the three test pipes may be compared by re-plotting in this latter form and the β dependence is thereby investigated. Mean values of the 6 highest M_o data sets $(\Phi_{\ddot{w}}\ \beta^3\ M_{Lp}^5)/(\Phi_p\ Q\ \rho_{fs}^2\ M_o^5)$ have been calculated for each test section i.e. $M_o = 0.22$ data are not included; these curves are shown in Fig. 4.8. A close collapse is produced over the whole frequency range, supporting the predicted β^3 dependence. The $M_o = 0.22$ data for each pipe have been omitted since they appear to result from acoustic excitation for $\nu > 0.3$: this rejection lowers the mid-frequency average data by approximately 1dB. The approximate theoretical prediction (equation [4.2]) shows similar lack of absolute agreement with the experimental data in Fig. 4.8 to that found in previous comparisons, although the frequency dependence is predicted reasonably, at least for $\nu < 0.3$.

The sharp change in frequency dependence for $\nu > 0.3$ is believed to result partly from the presence of a weak acoustic field within the flow. The presence of such a field has been indicated by measurements at the pipe inlet of the intensity of sound radiated from within the pipe : the inferred intensity of the acoustic field acting on the pipe wall is much less than the intensity of the fluctuating turbulence wall-pressures, although the acoustic field may result purely from the turbulent flow in the pipe (Davies and Ffowcs-Williams (1968)). It is not possible to estimate however, at which flow speeds (at these higher frequencies) the acoustic excitation has significant influence on $\Phi_{\ddot{w}}/\Phi_p$, although from Fig. 4.5(a), the frequency dependence of $\Phi_{\ddot{w}}/\Phi_p$ decreases as M_o increases suggesting that the acoustic field is only important for low M_o.

4.4.4. Additional Comparisons of Experimental and Theoretical Results

The statistical theoretical expression, equation [2.20], is used to provide a comparison with the measured results, using measured values

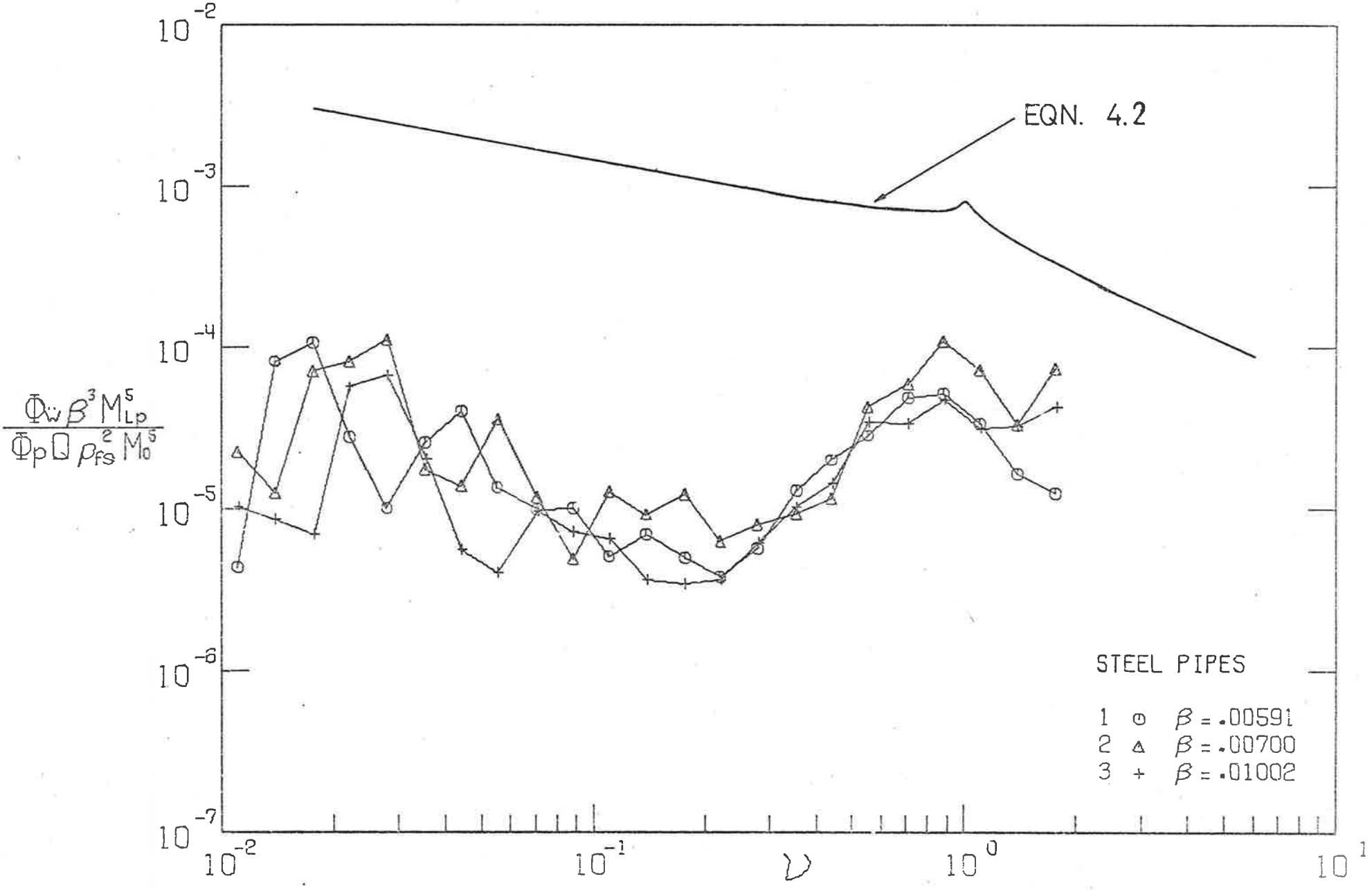

FIG. 4.8 EFFECT OF WALL THICKNESS ON Φ_w/Φ_p FOR STEEL PIPES

of Q from Figs. 4.4(a) to (c). Exact calculations (equation [2.32]), using measured values of modal quality factors and resonance frequencies, may be included to complement the analysis at low frequencies, although in section 2.2.7, the statistical analysis was shown to give equivalent estimates to those of the exact approach. A set of exact calculations is given for each section. The comparison for each test section is presented for only two excitation flow speeds, in order to simplify the diagrams; similar observations can be made at other flow speeds.

Figures 4.9(a), (b) and (c) show the measured results and theoretical calculations for test pipes 1, 2 and 3 respectively, for M_o = 0.22 and 0.55. Generally, the agreement for the three test pipes is poor. For $\nu \simeq 0.02$, the differences between theory and experimental results are approximately 10dB; for $0.05 < \nu < 0.5$, differences of 15 to 25dB exist; as ν increases to 1, the differences tend to decrease to 12dB, as found in previous comparisons. The differences generally decrease with increasing M_o and $\bar{\nu}_{hc}$, especially for $\nu < 0.3$. However, they are not explained by the small errors inherent in the measurement process: M_{Lp}, M_o, β and ρ_{fs} have each been measured to accuracy of 2%, while $\Phi_{\ddot{w}}$ and Φ_p are accurate to within 10%. The maximum total measurement error should be less than 3dB. The effect of flow on Q is believed to be small, producing no more than a 3dB theoretical overestimate in $\Phi_{\ddot{w}}/\Phi_p$. Theoretical assumptions not verified experimentally involve the mode shapes and the form of the cross-spectral density of the turbulence pressure field.

The calculations of the modal mass, the space-averaged square of the mode shape and the modal joint acceptance have used mode shapes corresponding to simply-supported ends. In practice, the mode shapes will correspond more closely to those of clamped rather than simply-supported boundary conditions. The choice of mode shape does not affect the value of $[[\psi_\alpha^2(\underset{\sim}{r})]]/M_\alpha^2$ in equation [2.1], so that the joint acceptance is the only term, in which errors generated by the choice of mode shape, can be important. Using expressions for the joint acceptance with either simply-supported or clamped

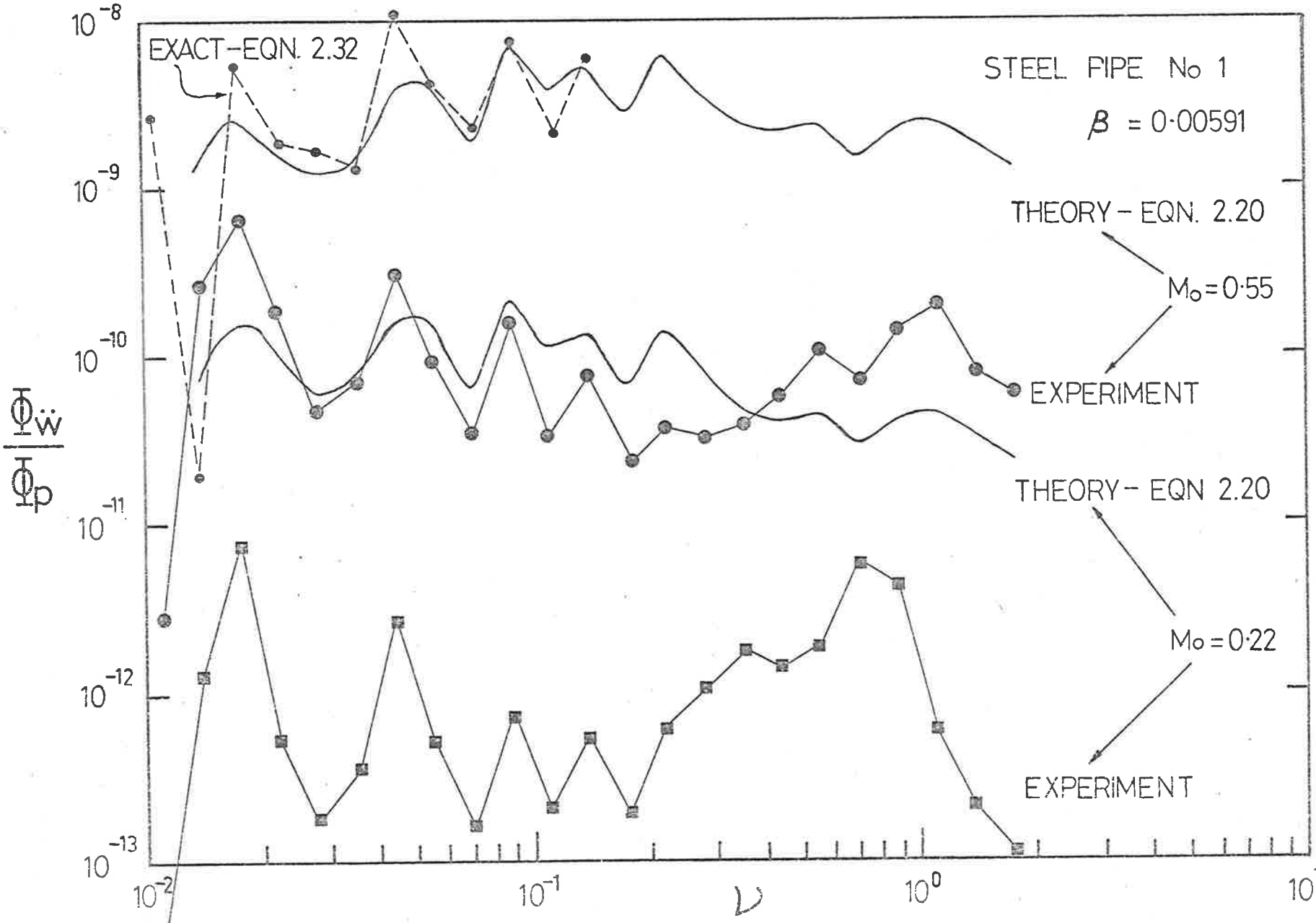

FIG 4.9(a) $\Phi_{\dot{w}}/\Phi_p$ — COMPARISON OF EXPERIMENT & THEORY — STEEL PIPE β = 0·00591

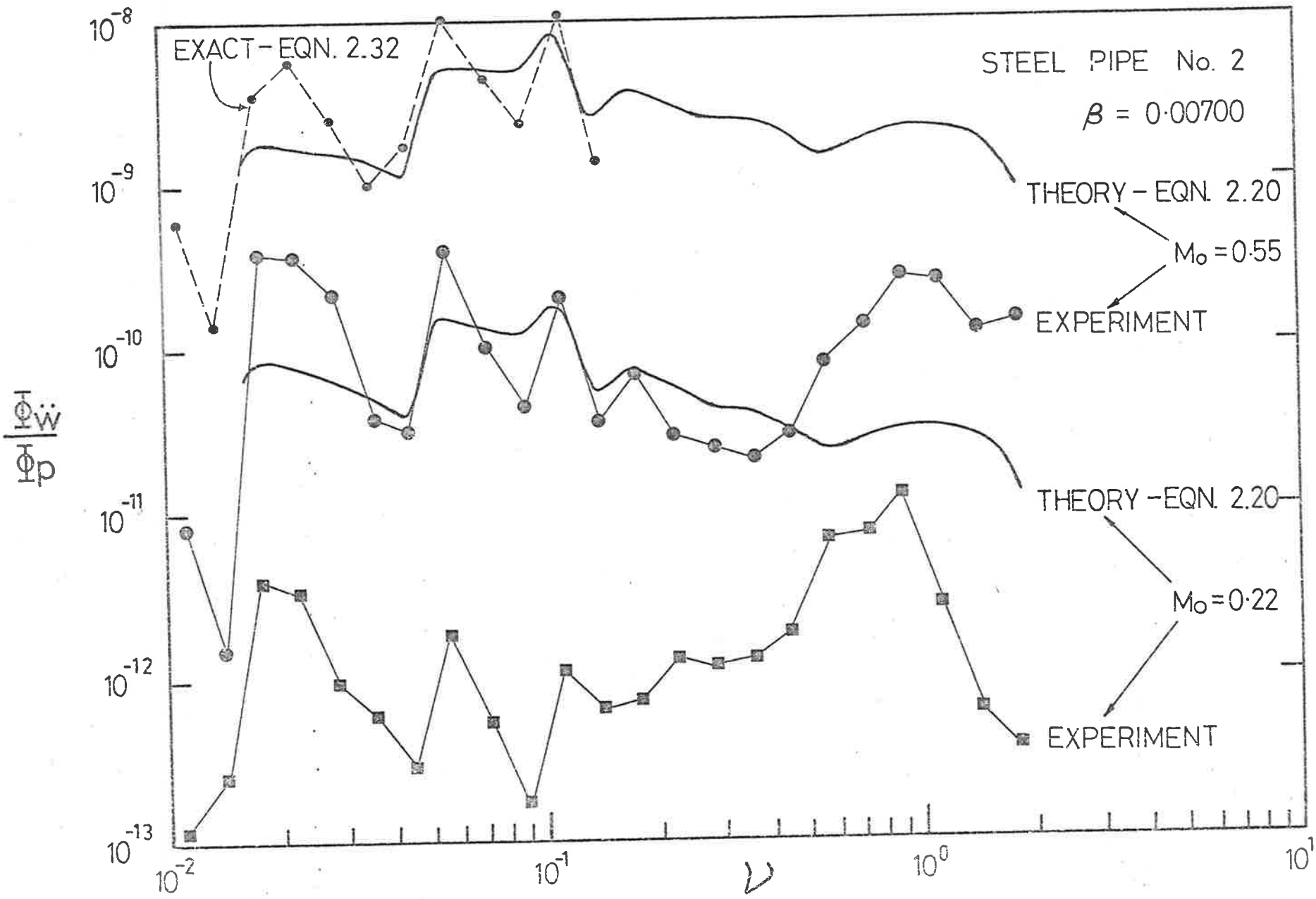

FIG 4.9(b) $\Phi_{\ddot{w}}/\Phi_p$ — COMPARISON OF EXPERIMENT & THEORY — STEEL PIPE $\beta = 0{\cdot}00700$

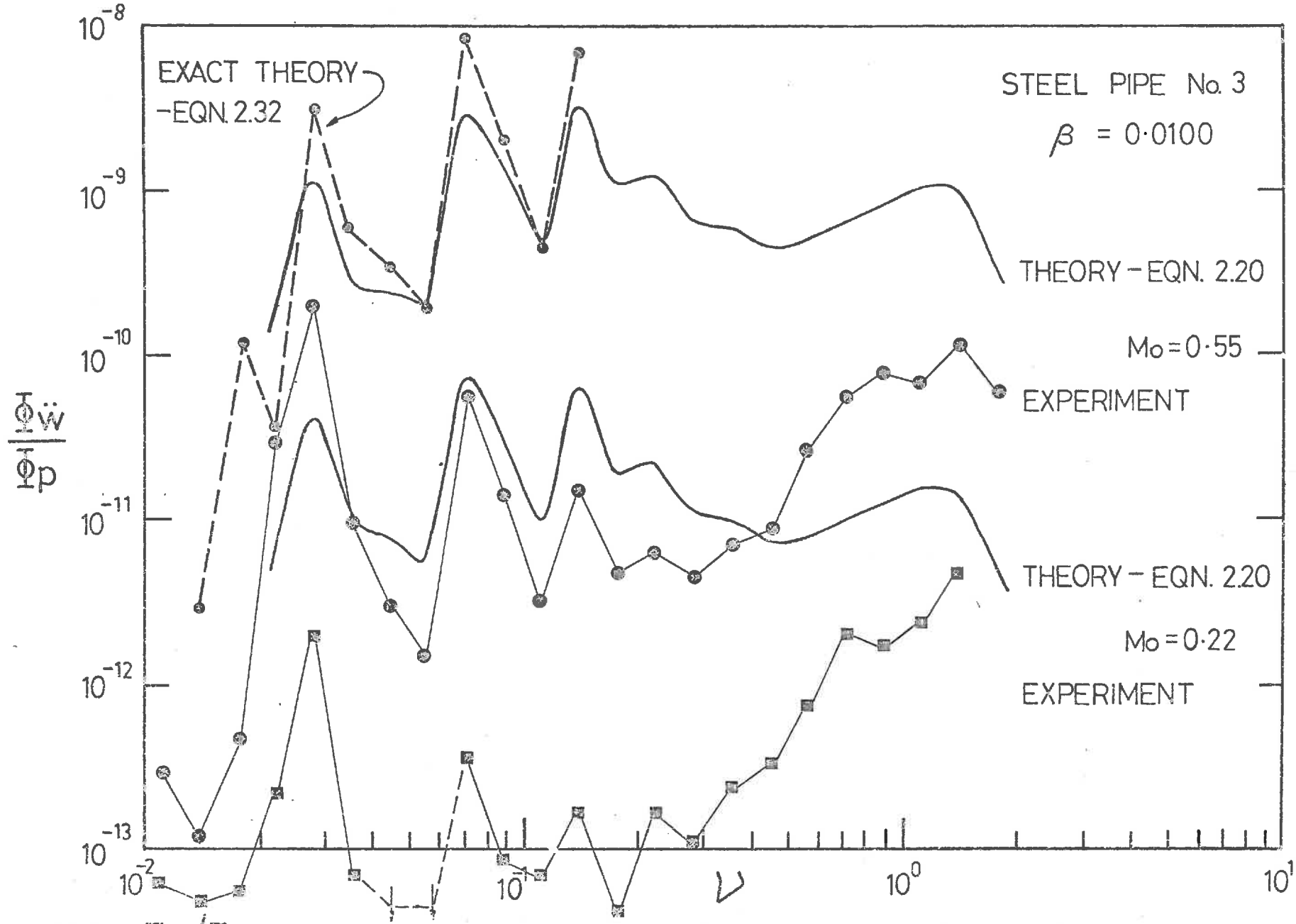

FIG. 4.9(c) $\Phi\ddot{w}/\Phi p$ — COMPARISON OF EXPERIMENT & THEORY — STEEL PIPE β=0·0100

ends, Bozich (1964) has shown that the joint acceptance of the structural modes of a flat plate, excited by a random pressure field which decays quickly in the flow direction, is essentially independent of the boundary conditions; the differences in $j^2_{\alpha\alpha}(\omega)$ for the two sets of mode shapes were calculated to be less than 2dB. The calculated modal mass will be increased if the axial and tangential components of the structural displacement of the pipe wall are taken into account for the various vibration modes (Forsberg (1966)); the effect is not important for other than n = 1 modes, which contribute little to $\Phi_{\ddot{w}}/\Phi_p$ when higher-order circumferential modes are present in the same frequency band.

The Corcos model for the cross-spectral density of the turbulence pressure field is widely used in predictions of the vibrational response of and acoustic radiation from flow-excited structures, particularly where hydrodynamic coincidence occurs over a wide frequency band. Hydrodynamic coincidence implies a matching in wavenumber and frequency between the turbulence pressure field and the structural mode. The convected components of the turbulence pressure field are then important: the Corcos model agrees well with existing experimental data in this wavenumber domain, as demonstrated by Bull (1967) and Wills (1970).

For $\omega > \omega_{hc}$, hydrodynamic coincidence cannot occur and the vibrational response of flow-excited structures tends to depend increasingly on the low-wavenumber domain of the turbulence pressure field. Measurements of the pressure fields beneath turbulent boundary layers by Chandiramani and Blake (1968), Blake and Chase (1969), and Farabee and Gieb (1975) have demonstrated that the Corcos model leads to severe overestimates of these low-wavenumber components of the spectral density of the fluctuating wall-pressures Furthermore, Aupperle and Lambert (1975) have argued that the use of the Corcos model in estimates of the acoustic power radiation from flow-excited flat plates for $\omega > \omega_{hc}$, can lead to overestimates of up to approximately 14dB for $\omega \simeq 8\omega_{hc}$. Due to pipe curvature, the resonant frequencies of pipe vibration modes are raised above those in plates of the same dimensions:

thus errors in the low-wavenumber domain of the turbulence pressure field will produce larger errors in estimates of the vibrational response of pipes than of plates of the same size for constant ω_{hc}.

In section 4.6, following the presentation of the measurements of the acoustic power radiation from steel pipes, the observed differences between the theoretical estimates and the experimental measurements of $\Phi_{\ddot{w}}/\Phi_p$ and Φ_π/Φ_p of the present pipes will be discussed by examining the wavenumber-frequency spectral densities of the excitation and response in more detail. Alternative models for the low-wavenumber domain of the pressure field will be used to produce a theoretical upper bound to the observed differences.

4.4.5. Summary

The acceleration response of three thin-walled steel pipes to excitation by fully-developed turbulent flow has been investigated experimentally for flow conditions which were well removed from hydrodynamic coincidence. Data were obtained for seven flow speeds for each pipe.

The response of each pipe was determined by the contributions of pipe resonant modes at their own frequencies. However, when measured in one-third octave bands, the vibration response was found to be not only circumferentially homogeneous as predicted but also essentially uniform over the pipe surface, due to the high modal densities existing for most frequencies.

Reductions of the experimental data for each pipe were made following the theoretical predictions of Chapter 2; these calculations tended to confirm that, for the steel pipes tested, the non-dimensional spectral density of the space-averaged acceleration response $\Phi_{\ddot{w}}$ was

(i) proportional to the power spectral density of the exciting turbulence wall-pressure field Φ_p;

(ii) proportional to the average quality factors of each pipe;

(iii) proportional to the fifth (or higher) power of the internal flow speed;

and,

(iv) inversely proportional to the cube of the pipe wall thickness.

The frequency dependence of the non-dimensionalised experimental data showed some agreement with the approximate theoretical predictions, particularly at low frequencies and above the ring frequency. However, as far as absolute values were concerned, the theoretical predictions exceeded the experimental measurements by approximately 12dB at low and high values of ν and by approximately 20dB in the mid-frequency range.

4.5 ACOUSTIC POWER RADIATION

4.5.1 Introduction

In general, the accurate assessment of the power radiated from an acoustic source may be performed most conveniently within a reverberation chamber, where the power levels can be related to measurements of the intensity of the essentially diffuse pressure field and to the room geometry and absorption characteristics. Information concerning the directivity of the source radiation is inevitably lost.

In contrast, the accurate determination of the power radiated from the source when situated within the free-field environment of an anechoic chamber requires a detailed knowledge of the source directivity characteristics.

In the present experiments, the test sections were located in an anechoic chamber. An investigation of the directivity of the pipe radiation was carried out to select an accurate and efficient method for the measurement of the acoustic power radiation. Measurements of the acoustic power radiation for the seven flow speeds for the three test sections were then made: these are presented in non-dimensional dorm for each of the three steel test sections. The dependence of these results on flow speed and pipe wall thickness is examined.

As discussed in Chapter 2, a lower bound to the acoustic power radiated from pipes can be developed by assuming that only those pipe

vibration modes, whose wavespeeds are supersonic with respect to the surrounding acoustic medium, radiate significant power. Theoretical predictions based on such an assumption are used for comparison with the experimental measurements. Radiation ratios determined for flow, electromagnetic and acoustic excitation are compared with various statistical estimates based on the approximations made in Chapter 2. Exact calculations are also included for additional comparisons with the experimental results and statistical predictions.

4.5.2 Directivity of the Acoustic Radiation from the Steel Pipes

The far-field directivity pattern of acoustic radiation from an infinite pipe supporting a vibration configuration, which is periodic in the axial and circumferential directions and whose resultant wavespeed is supersonic with respect to the surrounding acoustic medium, will correspond to that of an infinite line source composed of incoherent sources i.e. cylindrical symmetry will exist, so that the intensity of the acoustic field will decrease by 3dB for each doubling of the radial distance and will be independent of axial or circumferential co-ordinate for constant radial distance. Essentially the same conclusions will apply for a finite pipe supporting a supersonic structural mode provided the far-field oberver is located within an imaginary cylindrical volume, whose length is equal to the pipe length, whose radius is less than half the pipe length, and which is axi-symmetric with the pipe centreline. The radiation field of subsonic pipe modes will be expected to display different directionality characteristics. For example, the wavespeeds of low axial-order vibration modes of fixed circumferential order, for pipes where $\Lambda >> 1$, will be supersonic in the axial direction but subsonic circumferentially for $K_a << K_n$, so that a pronounced circumferential directivity may exist.

These characteristics were investigated for steel pipes by traversin a B & K 4133 12.7mm microphone axially, circumferentially and radially in the radiation field of test section 1, during flow excitation at

a flow speed of $M_o = 0.37$. The microphone was aligned to that the radial vector from the pipe centreline was normal to the microphone diaphragm. The radial dependence was investigated at three positions by observing the decreases in radiated Sound Pressure Level (SPL) spectra as the radial distance from the pipe axis was successively doubled from 0.125 m to 1.0 m. For all frequencies greater than 800Hz, 3dB decreases in SPL spectra were measured between each successive radial position. Subsequent far-field acoustic measurements were made at radial distances (r) $\geq$ 0.25 m. The microphone was maintained at a constant radial distance, while measurements of the axial and circumferential SPL spectra were made at various points in a cylindrical pattern surrounding the pipe. Curve (i) of Fig. 4.10 represents a set of such SPL measurements taken at pipe mid-span at eight equally-spaced circumferential positions at r = 0.50 m. The variations in circumferential SPL from the mean values are always less than $\pm$ 1dB for $\nu > 0.06$ and less than $\pm$ 3dB for lower frequencies. Similar results but with smaller variations were found for the spectra at five different axial positions, as shown by curve (ii) of Fig. 4.10, where now the radial distance and circumferential angle have been kept constant.

Supersonic vibration modes are predicted to exist for $\nu > M_{Lp}^{-1} = 0.06$ for steel pipes: the lowest frequency supersonic mode for this pipe is the (9,1) mode, which is resonant at 1820Hz or $\nu = 0.080$ (Fig. 4.4(a)). Above this frequency, supersonic modes will occur in all one-third octave frequency bands, so that the radiation should become progressively more controlled by the supersonic modes which have a cylindrical radiation pattern; on the other hand, for $\nu < M_{Lp}^{-1}$, subsonic modes may combine to produce a radiation pattern which is not cylindrical. In fact, for electromagnetic single frequency excitation, such characteristics could be clearly observed aurally for individual modes at low ν. This argument ignores the conclusions of section 2.2.7, which suggest that in fact subsonic modes with high radiation ratios (<1) will control the radiation for all $\nu < \nu_{ac}$. However, it is probable that the directivity of such high σ subsonic modes is essentially

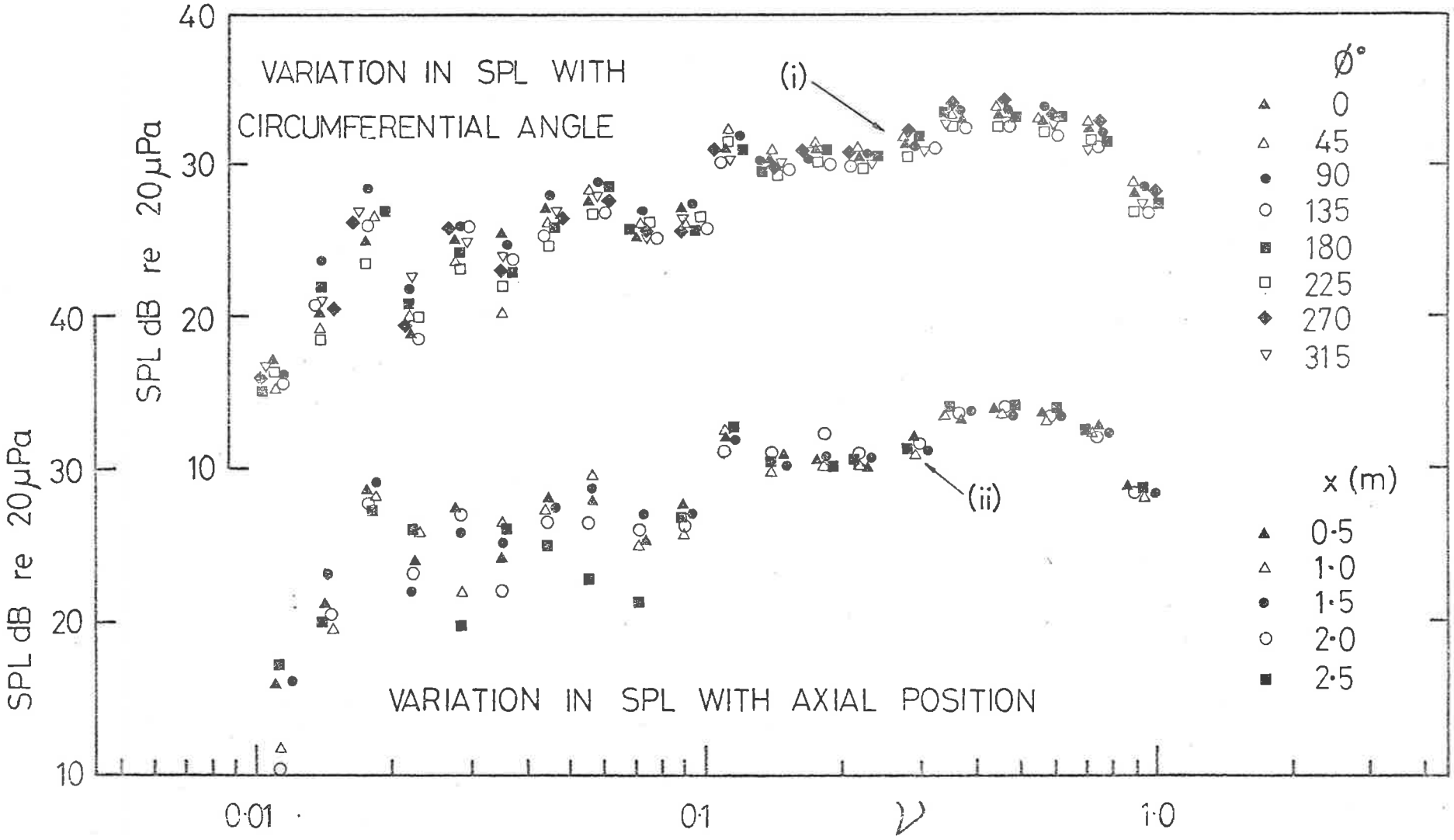

FIG. 4.10 DIRECTIVITY OF ACOUSTIC RADIATION—STEEL PIPE No. 1

cylindrical in any case.

The measurements suggest that, for those frequencies where supersonic modes exist, the acoustic radiation field is indeed cylindrical and that, then, a single measurement of the radiated intensity will enable an accurate estimate of total acoustic power radiation to be made. For other frequencies, the errors produced by assuming a cylindrical radiation pattern are small. In a single frequency band, many modes contribute to the intensity at the measurement point. The acoustic radiation from strongly directional modes tends to be submerged in the total radiation pattern when averaged over all the modes in the band, just as the vibration response tends to be homogeneous circumferentially and also uniform over the pipe surface.

4.5.3. General Characteristics and Parametric Dependence

The experimental results for test section 1 are presented in Fig. 4.11(a) in the reduced non-dimensional form suggested by equation [2.22]; the non-dimensional spectral density of the acoustic power radiation is divided by the measured non-dimensional power spectral density of the turbulence pressure field taken from Fig. 3.6. For $\nu < 1$, the curves of Φ_π/Φ_p are approximately independent of ν, especially for higher flow speeds. The spectral densities of Φ_π/Φ_p for $\nu < 0.1$ are smoother than the corresponding $\Phi_{\dot{w}}/\Phi_p$ spectral densities shown in Fig. 4.5(a). In fact, the peaks are broader and do not always correspond to groups of circumferential modes, as do the peaks in the $\Phi_{\dot{w}}/\Phi_p$ curves. This reflects the differences in the radiation ratios of subsonic modes of varying circumferential order. The n = 1 modes, although not important in the vibrational response when higher-order circumferential modes are present in the same frequency band, will make significant contributions to the acoustic radiation, due to their faster (though still subsonic) wavespeeds and corresponding higher radiation ratios, despite their higher damping and lower modal density.

The peak at $\nu = 0.018$ is due to the n = 2 modes, while the (5,1) mode is resonant at $\nu \simeq 0.028$. The broad peak extending from $\nu = 0.04$ to $\nu = 0.07$ is associated not only with the group of n = 3 modes but also

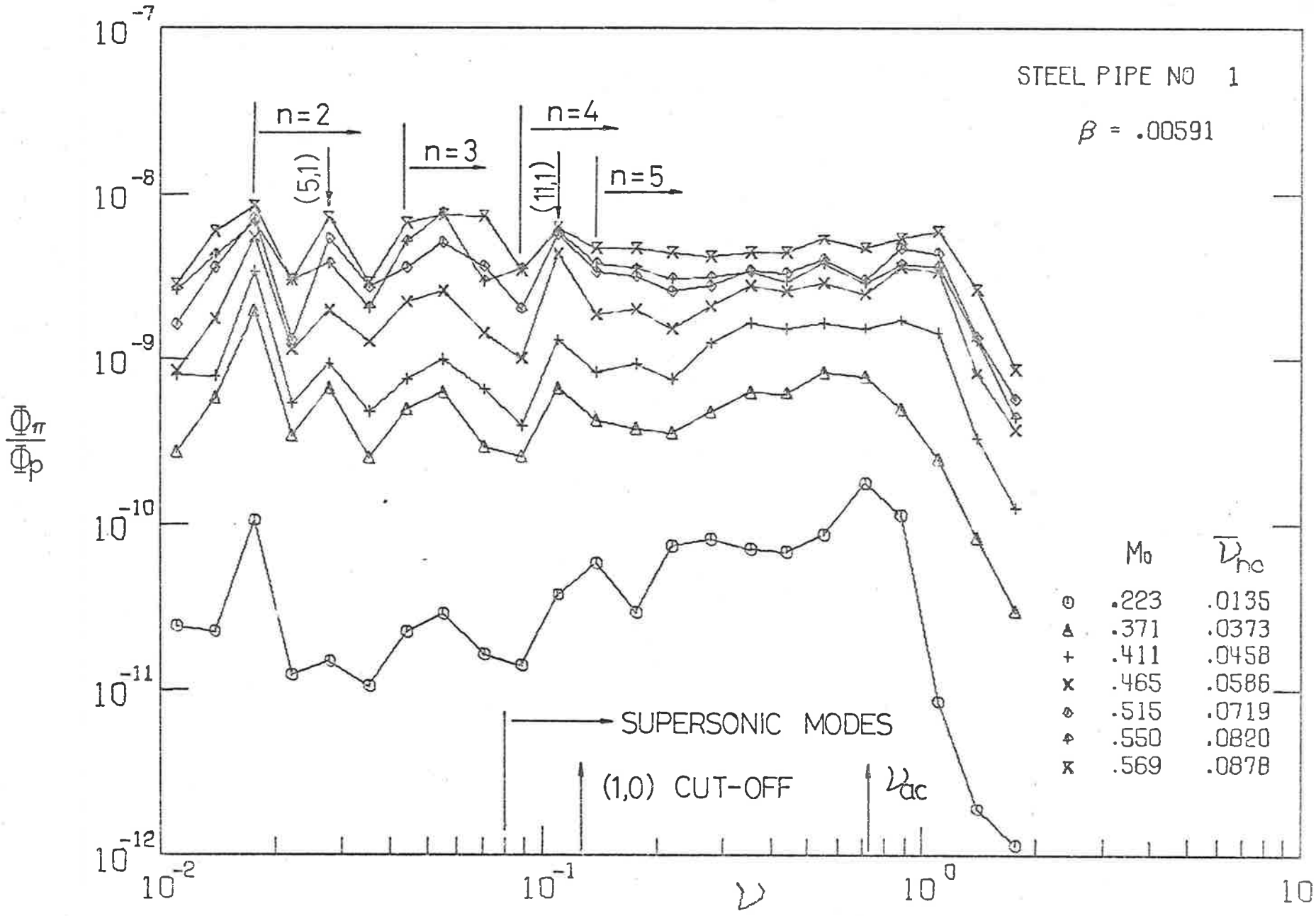

FIG. 4.11(a) Φ_π/Φ_p FOR VARIOUS M_0. STEEL PIPE β= .00591

with several n = 1 modes, which will be supersonic for $\nu > 0.080$. There is no outstanding radiation from the n = 4 and n = 5 modes. The frequency of the first acoustic cross mode inside the pipe of order greater than the plane wave (i.e. the (1,0) mode) corresponds for low M_o, to $K_a = 1.83$ or $\nu = 1.83/M_{Lp}$; the peak at $\nu = 0.11$ may indicate that a small acoustic contribution occurs at this frequency, although the (11,1) pipe vibrational mode is resonant at this frequency also.

Such interpretations are demonstrated more clearly by plotting the experimental radiation ratios, averaged in one-third octave bands, for all M_o. These values of σ, which are calculated as $(\Phi_\pi \nu^2/\Phi_{\ddot{w}} M_{Lp})$ from equation [2.33], are shown in Fig. 4.11(b) for the present pipe. Groups of subsonic resonant modes are seen to occur at frequencies which correspond to minima in the curves for pipe radiation ratio; it would appear therefore, that the low frequency peaks in σ result from the radiation from n = 1 modes, which have higher radiation ratios. The curves of radiation ratio are essentially independent of the pipe flow speed, suggesting that no important changes in the modal quality factors occur as M_o varies. For this pipe, $\nu_{ac} = 0.75$; for $\nu \geq \nu_{ac}$, all vibrational modes are supersonic and $\sigma_{rad} \simeq 1$. This is seen to be qualitatively verified by experiment.

Following Manning and Maidanik (1964), who assumed that all modes had equal vibrational energy levels and that any acoustic radiation was due to supersonic modes only, we may show that

$$\sigma = \frac{N_s}{N} \qquad [4.3]$$

where N_s and N are respectively, the density of supersonic modes and the pipe modal density (given by equation [2.10]). Equation [2.10] is also used to calculate N_s, provided the integration is confined to the range of waveangles corresponding to supersonic modes as discussed in section 2.2.5. The assumption of equal modal energy is clearly not correct for these steel pipes, as shown by the large variations in modal quality factor which occur between the various modes resonant within a frequency band. To allow for the differences in quality factors between the radiating modes and the modes

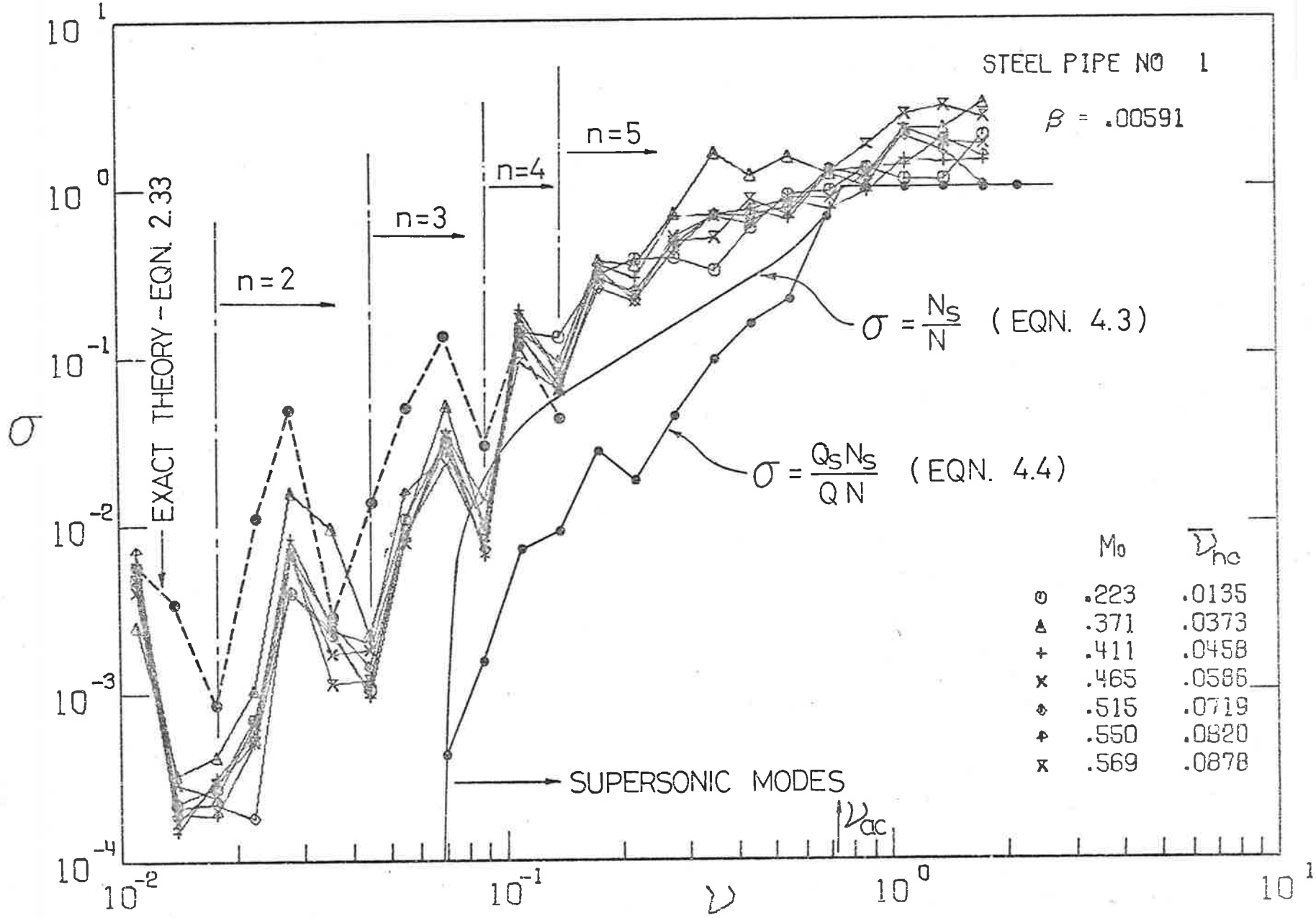

FIG. 4.11(b) σ FOR VARIOUS Mo . STEEL PIPE β=.00591

controlling the response, equation [4.3] is modified to

$$\sigma = \frac{Q_s N_s}{Q N} \qquad [4.4]$$

Equation [4.4] also follows directly by substituting the approximate equations [2.28] and [2.80] in equation [2.33].

Calculations from equations [4.3] and [4.4] are shown in Fig. 4.11(b). The theoretical curves generally lie 3 to 10dB below the experimental data for $\nu < \nu_{ac}$; for $\nu < \nu_{ac}$, the prediction from equation [4.4] lies below that from equation [4.3] since usually $Q_s < Q$ in this frequency range. It appears from the differences between the experimental data and the curve for equation [4.3], that the statistical approach, based on supersonic modes and equal modal energies, will cause significant underestimates in the acoustic power radiation from pipes for $\Lambda > 1$ for $\nu < \nu_{ac}$. When the appropriate quality factors are included in the σ estimate, as in equation [4.4], the differences further increase, suggesting that subsonic modes control the radiation from pipes for $\nu < \nu_{ac} < 1$. Calculations of the exact values of σ from equations [2.33], [2.34] and [2.32], using experimental values of resonance frequencies and quality factors, are also included: the agreement between the experimental and exact theoretical values is close, which further supports the proposition that subsonic modes control the acoustic radiation from pipes for $\nu < \nu_{ac}$.

To provide an added confidence in the experimental measurements, comparisons are made with the radiation ratios measured for both electromagnetic and far-field acoustic excitation. The procedure for the far-field acoustic excitation is described in section 4.8 of this chapter. The microphone and accelerometer positions were identical for the three excitations. One-third octave bands of random noise were used. The accuracy of the absolute measurements was checked by repeating the radiation ratio measurements for the same pipe in a reverberation chamber, using standard techniques, for the case of electromagnetic excitation. The differences between the anechoic and reverberation chamber determinations were generally less than

2dB for $\nu > 0.1$. The results are shown in Fig. 4.11(c), where the curve representing the average for the various flow speeds is presented. Electromagnetic and flow excitation produce essentially the same results, although the flow data lie approximately 3dB above the electromagnetic data for $0.1 < \nu < 0.4$. It sould seem that comparisons of the radiation ratio for different excitations may enable the controlling source to be determined in a complex situation, providing significant differences in σ occur between the different excitations. The acoustic data peak sharply at the frequency of the (1,0) acoustic cross mode. Then the vibrational response was resonant with an amplitude far greater than the forced response expected for acoustic (1,0) excitation. The (11,1) pipe mode is resonant at $\nu = 0.11$ and will be strongly coupled to the (1,0) acoustic mode, under an acoustic coincidence condition. If significant acoustic excitation was immersed within the flow, it should be reflected by a peak in the radiation ratio as for pure acoustic excitation: from this comparison, it would appear that no important acoustic excitation is present at the frequency of the (1,0) acoustic mode. Above this frequency the method is not useful since the curves coalesce as ν approaches ν_{ac}.

It is seen, however, that flow excitation produces consistent radiation ratio results. The conclusions made regarding the contribution of subsonic modes to the radiated power appear to be based on valid measurements.

The approximate expression for Φ_π/Φ_p, equation [2.30], may be used to find the parametric dependence for the present case ($\bar{\nu}_{hc} << 1$): it may be re-arranged as

$$\frac{\Phi_\pi}{\Phi_p \; Q_s \; \rho_{fs}^2 \; M_o^5} = \frac{u^2}{24} \; \frac{c_x}{c_y} \; \frac{N_s}{\Lambda \; \beta^2 \; M_{Lp}^4 \; \nu^3} \qquad [4.5]$$

The experimental data of Fig. 4.11(a) are presented in this form in Fig. 4.11(d); the resulting collapse is close for $\nu > 0.1$ and approximately independent of frequency for $\nu < 1$. The theoretical approximation,

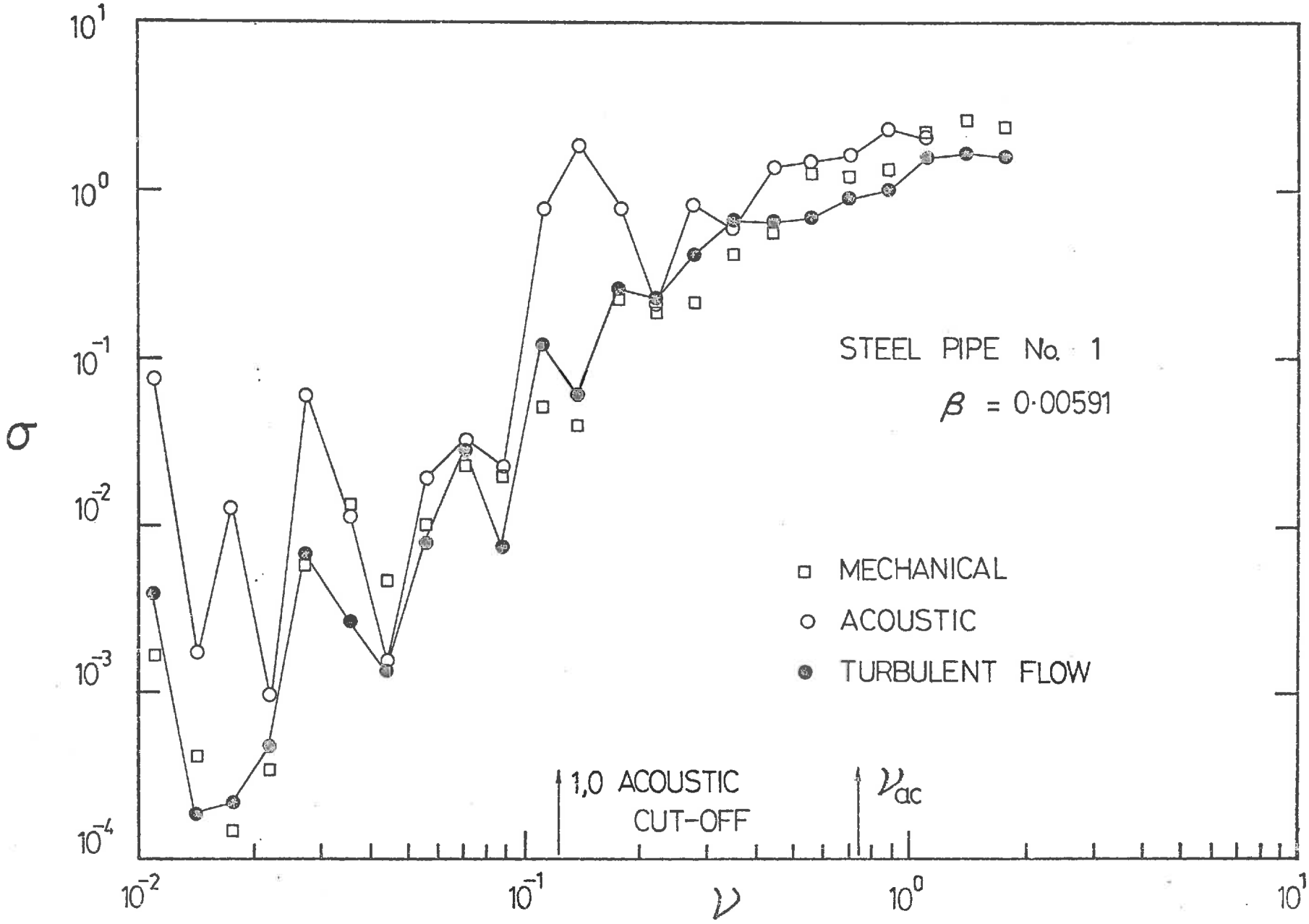

FIG. 4.11(c) σ FOR DIFFERENT EXCITATIONS – STEEL PIPE β = 0·00591

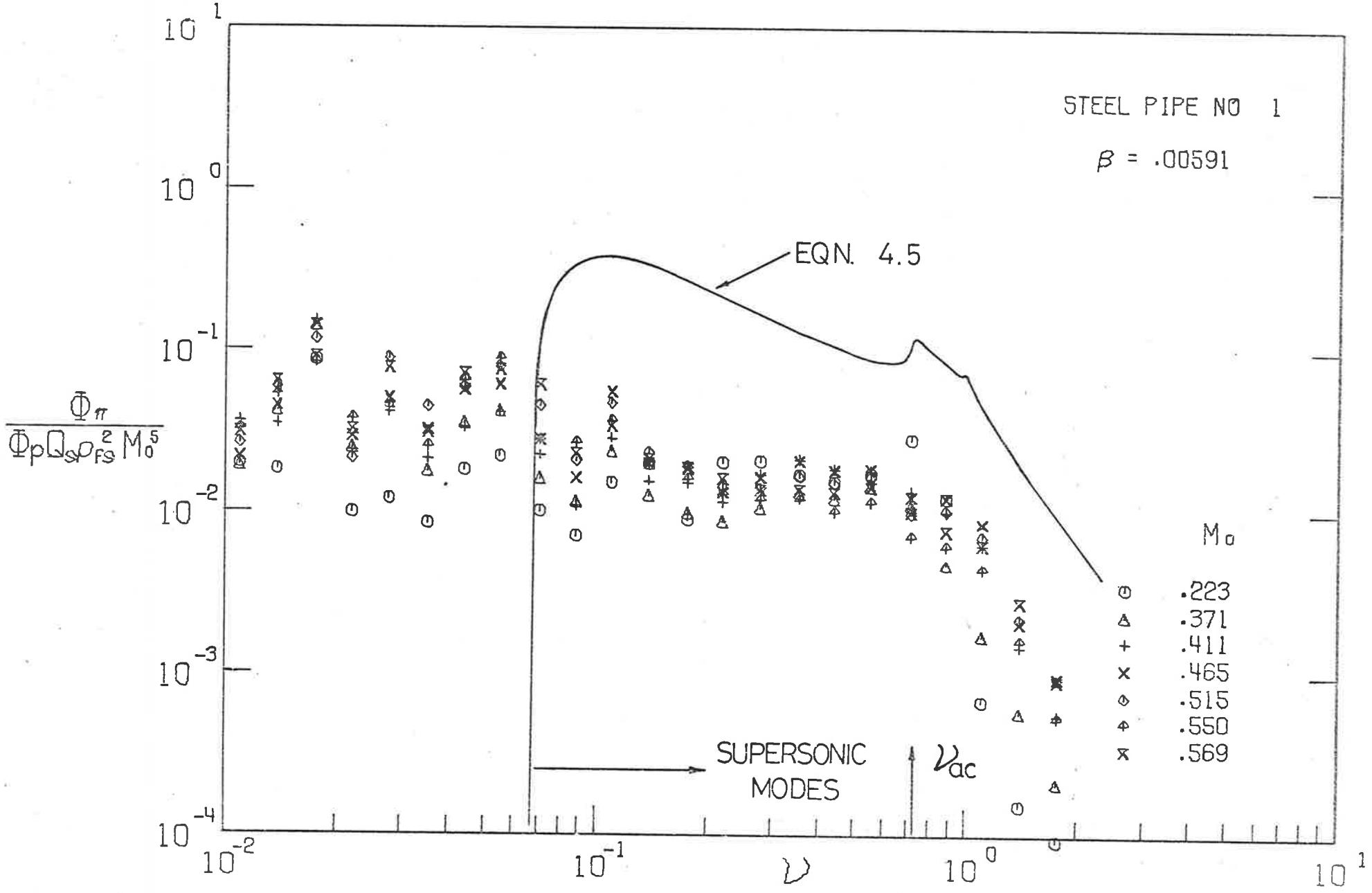

FIG.4.11(d) EFFECT OF FLOW SPEED ON Φ_π/Φ_p. STEEL PIPE β=.00591

equation [4.5], is also shown. While the data confirm the predicted fifth power dependence on flow speed, large differences exist between the theory and the experimental data. These differences vary from approximately 13dB at the cut-on frequency for supersonic modes, to 10dB in the region of the ring frequency and above, although the frequency dependence of the experimental data shows reasonable agreement with the theoretical prediction over the range of supersonic modes. In the light of the discussion presented in section 2.2.7 and in the present section on the expected contribution of subsonic modes to the overall acoustic radiation, the similarity is deceptive, at least for $\nu < \nu_{ac}$.

The acoustic radiation data for test sections 2 and 3 are presented in Figs. 4.12(a) and 4.12(d) and in Figs. 4.13(a) to 4.13(d) respectively, where the results are seen to have similar characteristics to those of section 1. Groups of $n \geq 2$ circumferential modes are perhaps more prominant in the curves of Φ_π/Φ_p for $\nu < 0.2$; however, strong peaks in the radiation ratio curves at other frequencies suggest the important contributions made by those modes with the highest wave-speeds, even though still subsonic. Comparisons of radiation ratios for different excitations suggest that there is no significant contribution to the acoustic radiation from acoustic sources in the region of the (1,0) acoustic mode. In all cases, the experimental radiation ratio reaches a unity value at a frequency $\nu < \nu_{ac}$: this behaviour is common to each excitation and has been predicted in section 2.2.7, suggesting that equations [4.3] and [4.4], although explaining observed trends in σ_{rad} with ν_{ac} variations, are not accurate for pipes for which $\nu_{ac} < 1$, since large contributions to the acoustic radiation may be produced by lightly-damped subsonic modes whose modal density and radiation ratio are high.

The acoustic power radiation depends on the fifth power of the flow speed for test sections 2 and 3 as shown in Figs. 4.12(d) and 4.13(d). The agreement between the approximate expression [4.5] and the reduced data is

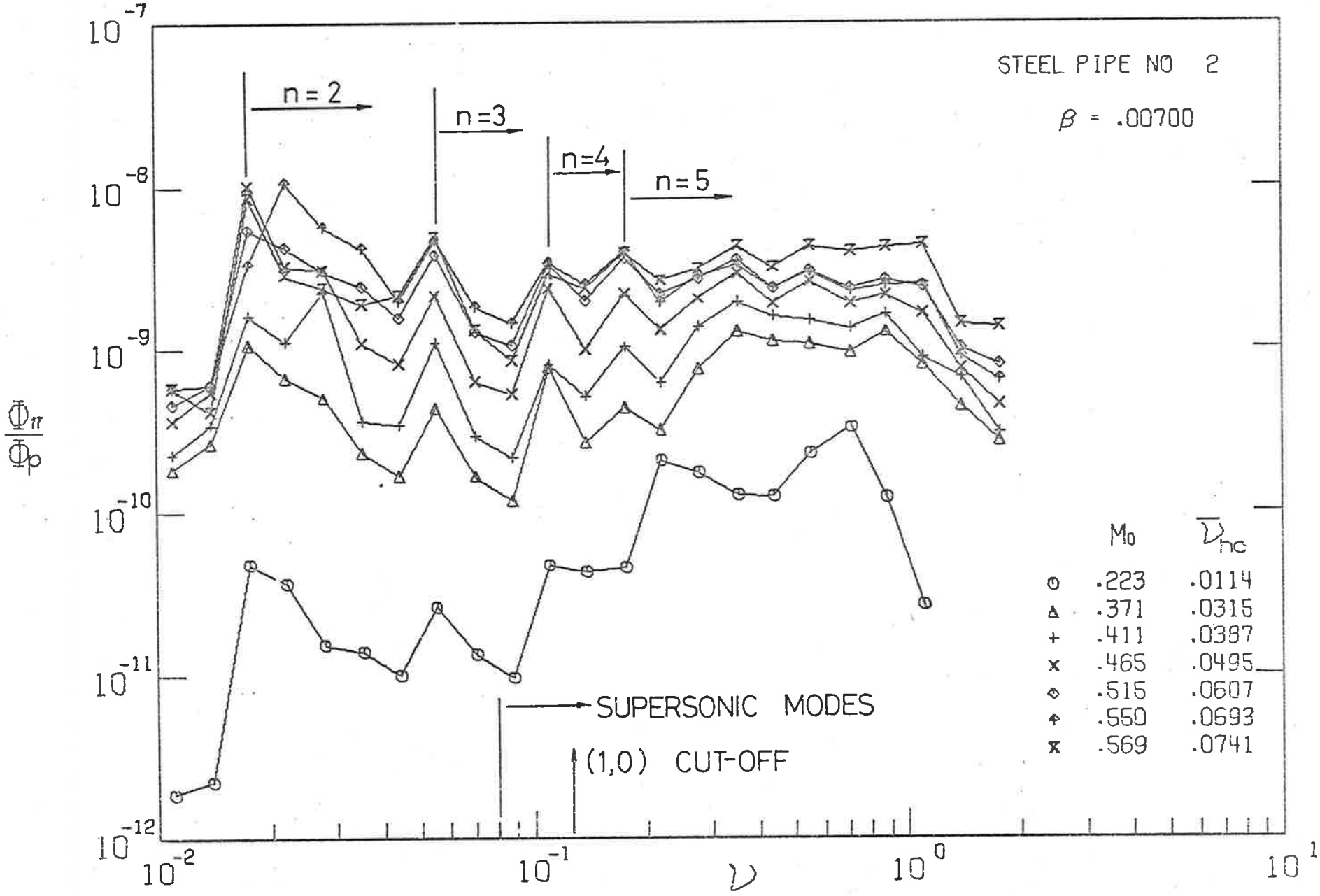

FIG. 4.12(a) Φ_π/Φ_p FOR VARIOUS M_0. STEEL PIPE β= .00700

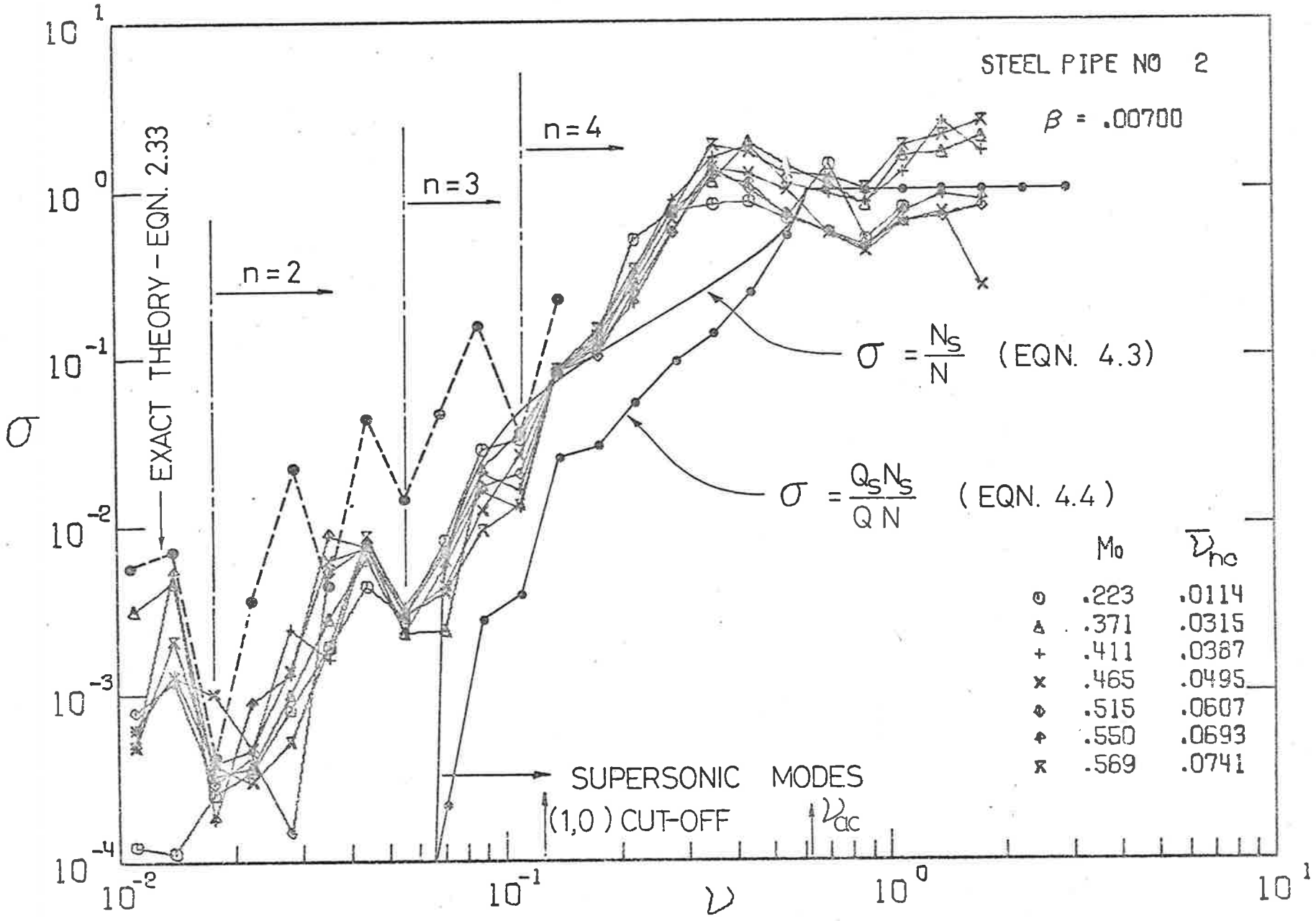

FIG. 4.12(b) σ FOR VARIOUS Mo. STEEL PIPE β = .00700

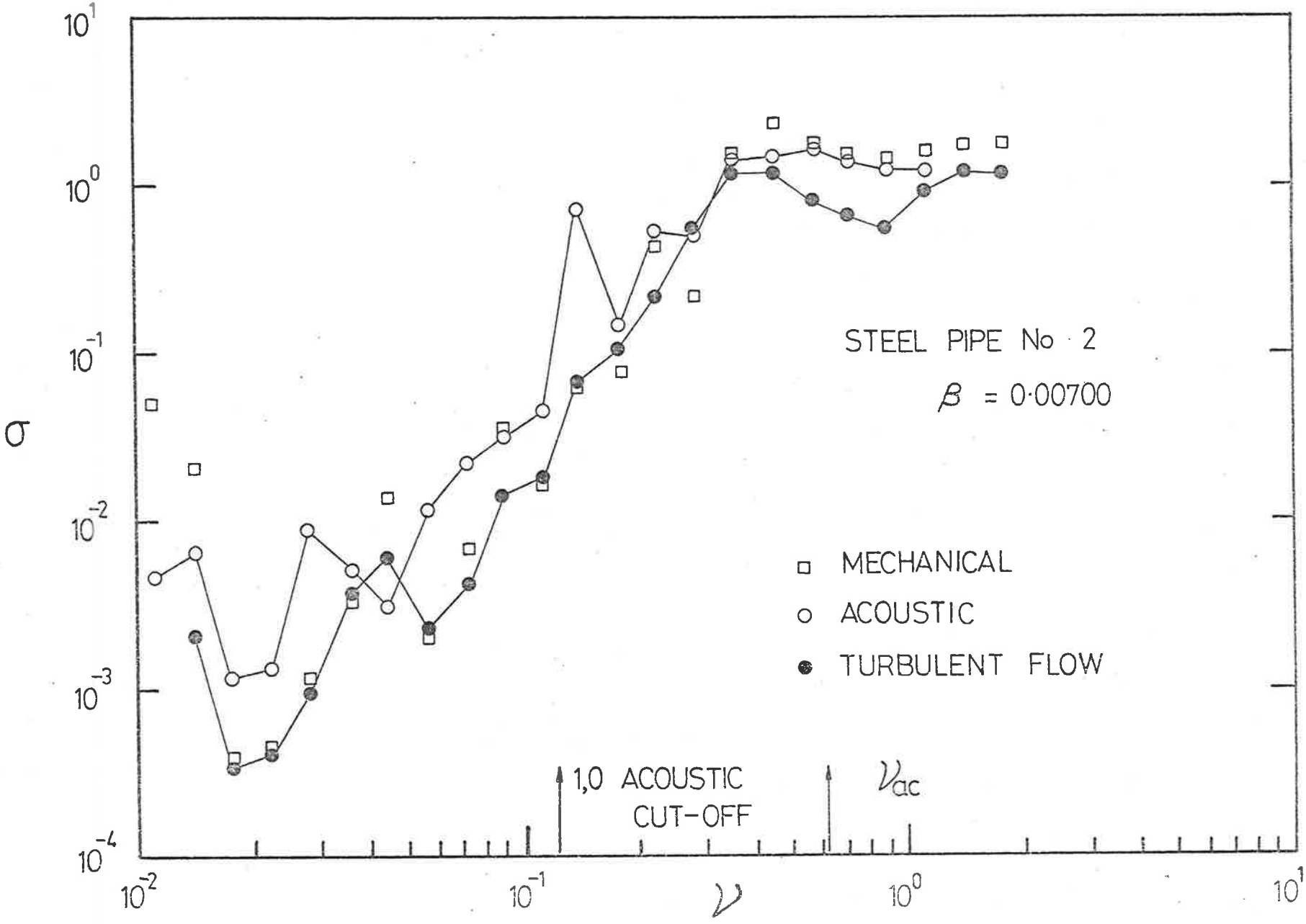

FIG. 4.12(c) σ FOR DIFFERENT EXCITATIONS – STEEL PIPE β = 0·00700

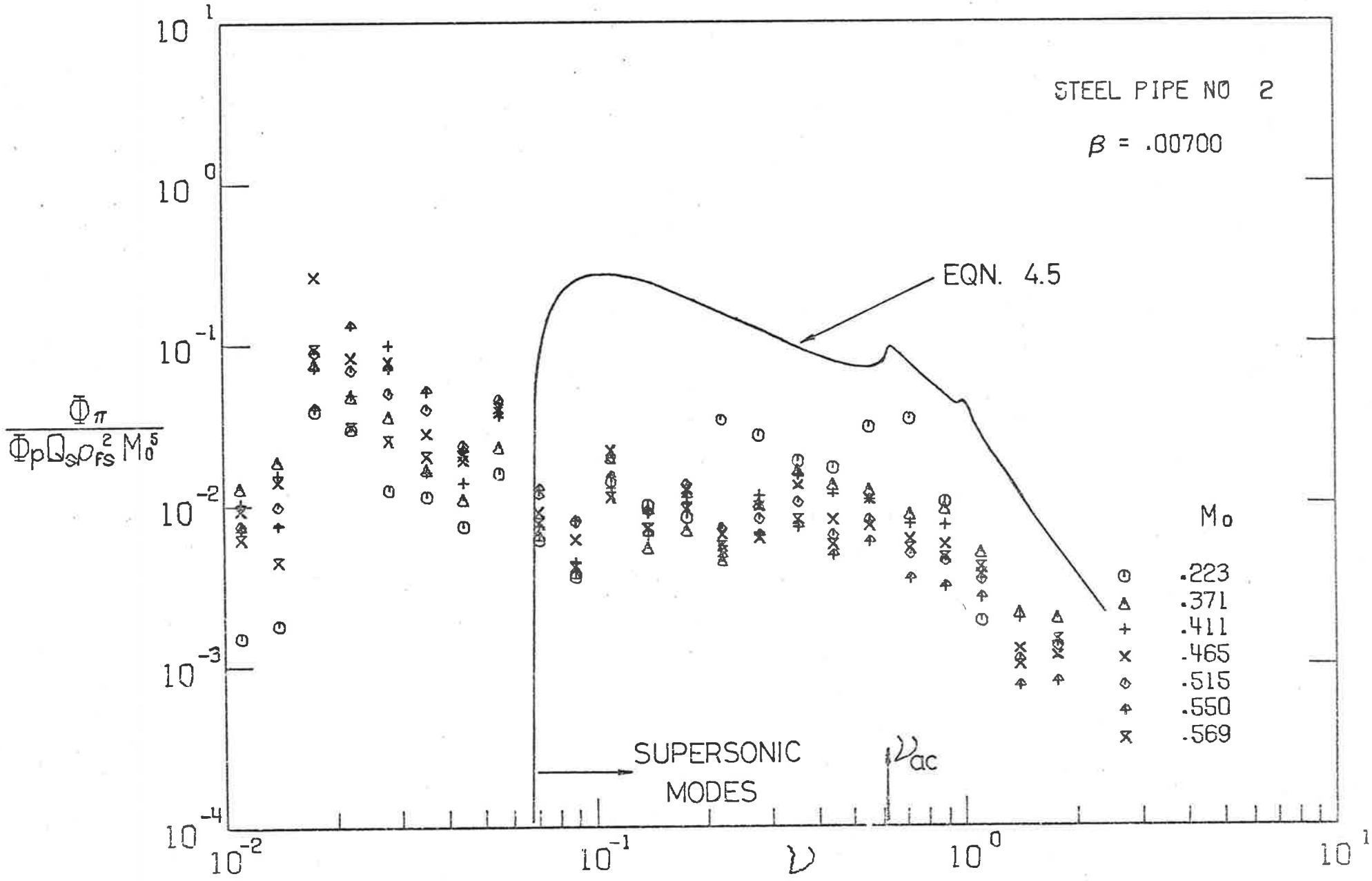

FIG.4.12(d) EFFECT OF FLOW SPEED ON Φ_π/Φ_p . STEEL PIPE β=.00700

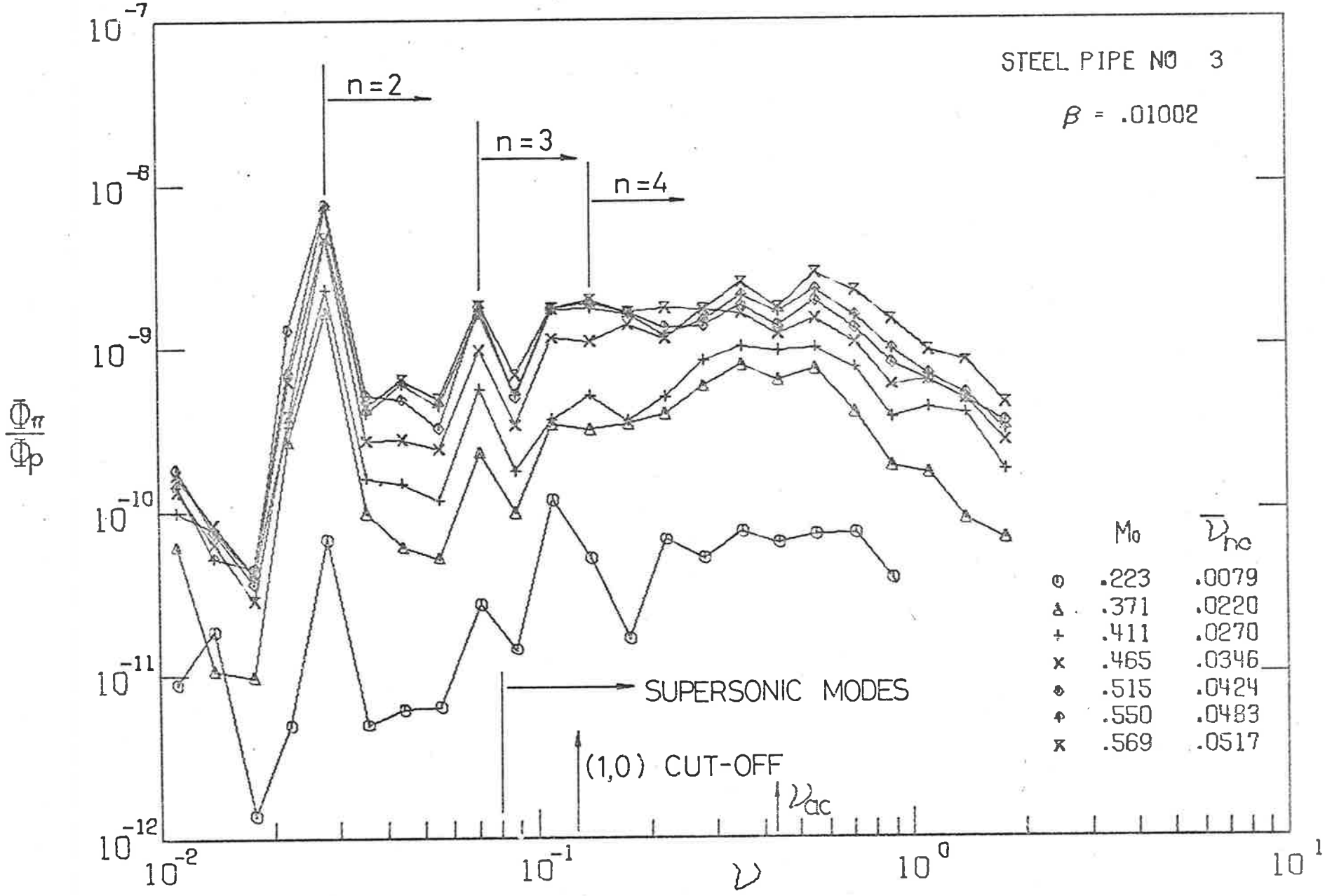

FIG. 4.13(a) Φ_π/Φ_p FOR VARIOUS M_0. STEEL PIPE β= .01002

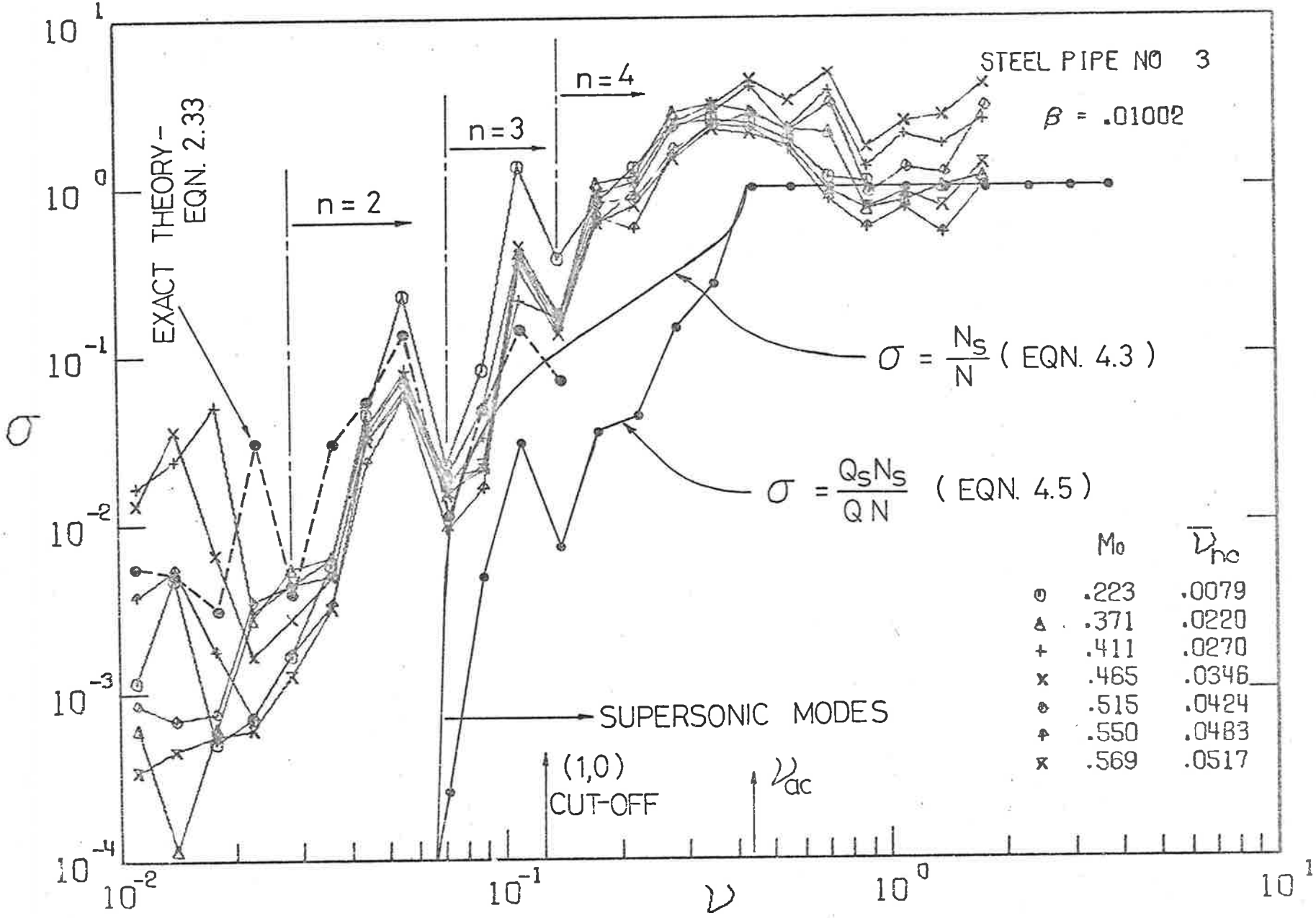

FIG. 4.13(b) σ FOR VARIOUS M_0 . STEEL PIPE $\beta = .01002$

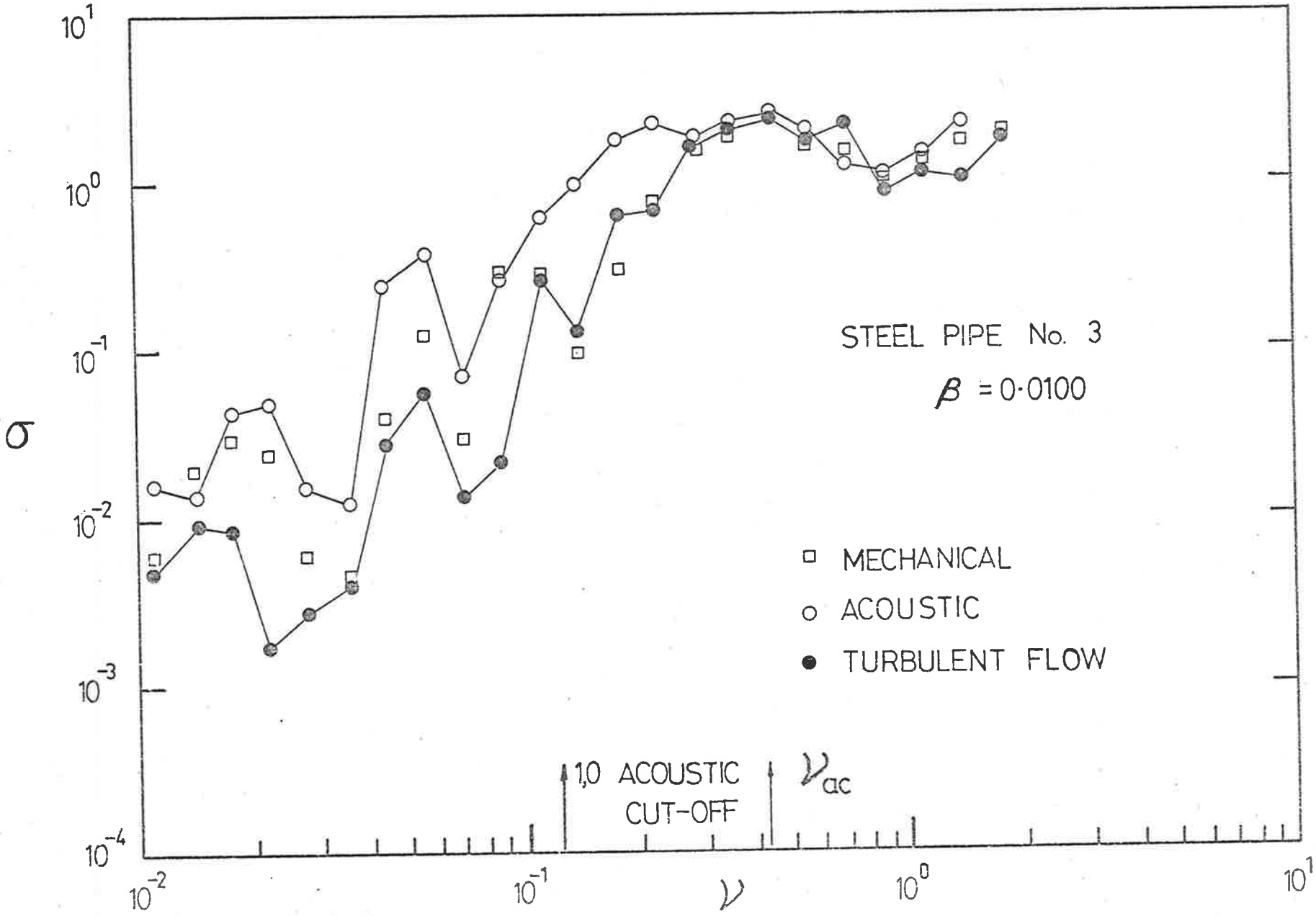

FIG. 4.13(c) σ FOR DIFFERENT EXCITATIONS - STEEL PIPE β = 0·0100

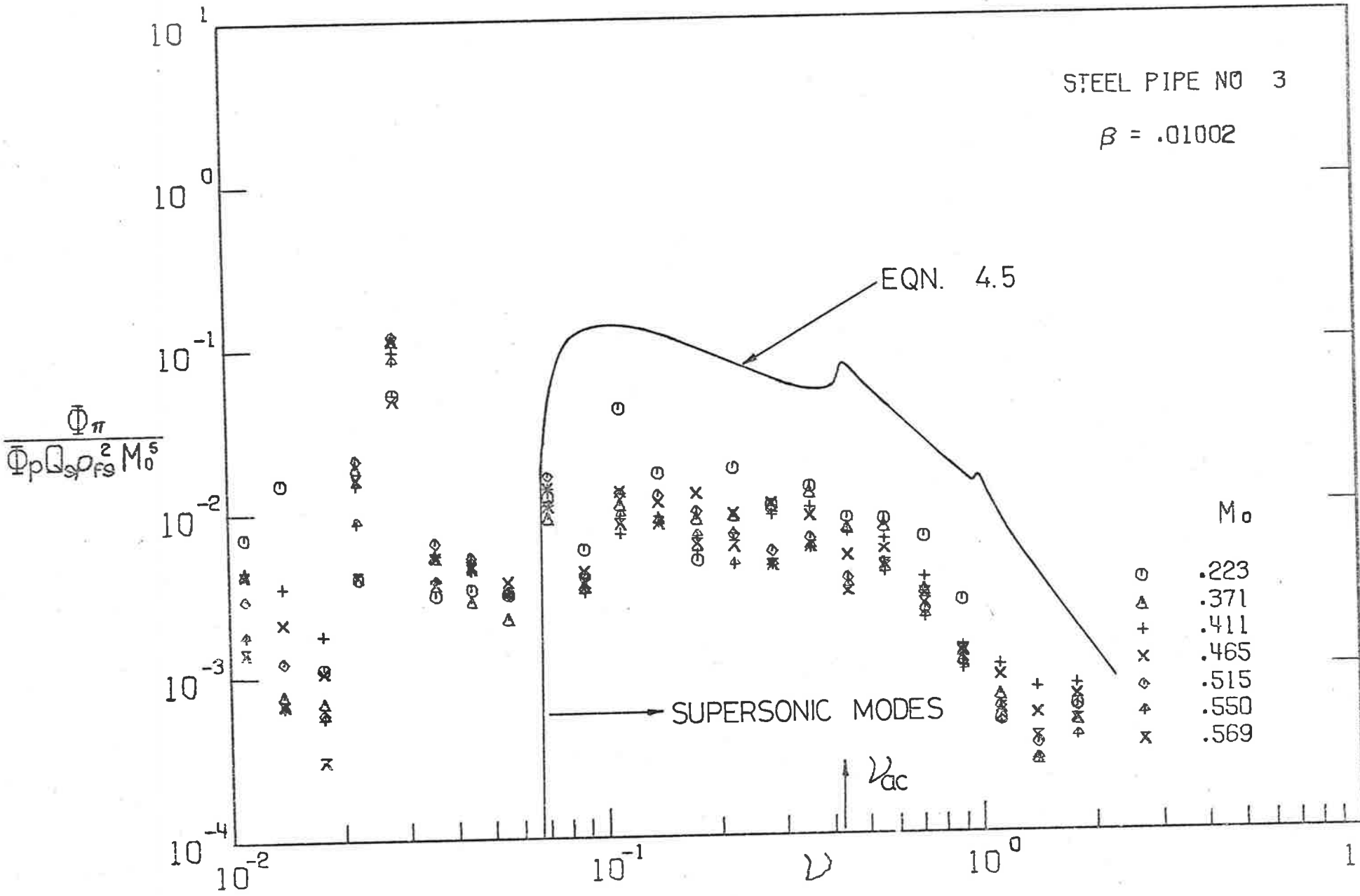

FIG.4.13(d) EFFECT OF FLOW SPEED ON Φ_π/Φ_p . STEEL PIPE β=.01002

poor, with differences of 10 to 15dB existing over the whole frequency range. As discussed in section 2.2.7, by taking the radiation from subsonic modes properly into account, the discrepancies between theory and experiment will increase, approaching those found for the vibrational response.

Equation [4.5] may be re-arranged to examine the β dependence of Φ_π/Φ_p for the present pipes: this gives

$$\frac{\Phi_\pi \ \beta^2 \ M_{Lp}^4}{\Phi_p \ Q_s \ \rho_{fs}^2 \ M_o^5} = \frac{u^2}{24} \ \frac{c_x}{c_y} \ \frac{N_s}{\Lambda \nu^3} \qquad [4.6]$$

From section 2.2.6, N_s is independent of β for $\nu \ll \nu_{ac}$ but inversely proportional to β for $\nu \geq \nu_{ac}$: consequently, the theoretical curves for the 3 test sections found from equation [4.6] will diverge for $\nu > \nu_{ac}$, as shown in Fig. 4.14. The experimental data on the acoustic radiation, averaged over all flow speeds for each pipe in the form suggested by equation [4.6] are also shown. The collapse produced is rather close over all frequencies. As previously suggested, much of the measured acoustic radiation for $\nu < \nu_{ac}$ is produced by subsonic modes, while the contributions made by these modes will vary between different test sections. It is not clear whether the compact collapse produced accurately describes the β dependence of the acoustic radiation, or simply reflects the fortuitous choice of average quality factors Q_s, for the various pipes: if the acoustic radiation in a particular band is controlled by lightly-damped subsonic modes, then the values of Q_s should perhaps correspond to those modes and not the supersonic modes present. These problems exist for $\nu < \nu_{ac}$ only; for $\nu > \nu_{ac}$, $Q_s = Q$, as all modes are supersonic. The measured acoustic radiation depends on β^{-2} or β^{-3}.

4.5.3 Additional Comparison of Experimental and Theoretical Results

The statistical analysis of Chapter 2 presents a method for conveniently estimating to the acoustic power radiation from pipes excited by internal turbulent flow. This was based on the assumption that only supersonic vibration modes contribute significantly to the acoustic power radiation. However, it was shown that subsonic vibrational modes tend to dominate the

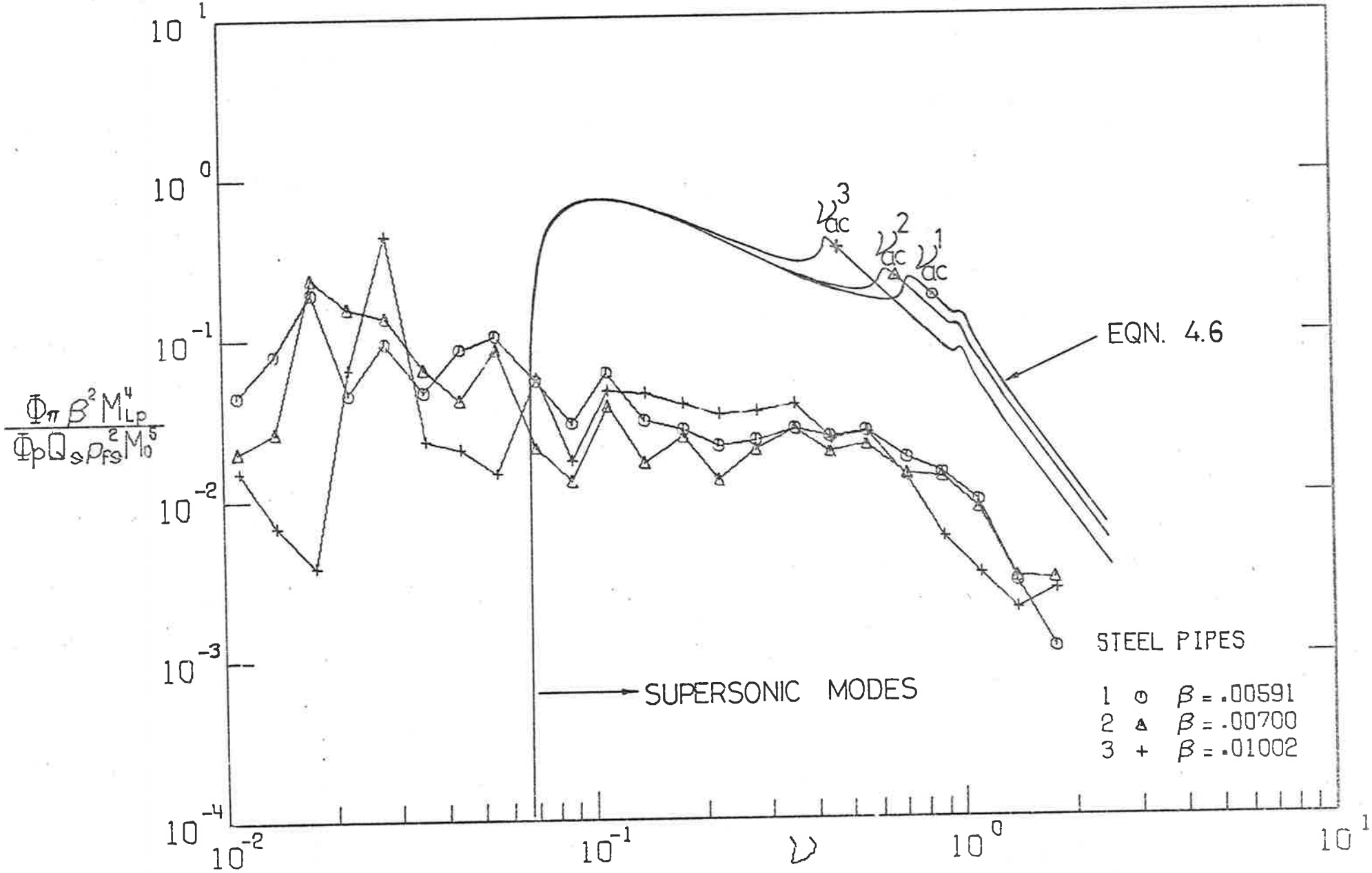

FIG. 4.14 EFFECT OF WALL THICKNESS ON Φ_π/Φ_p FOR STEEL PIPES

acoustic radiation, especially at low frequency: for example, in Fig. 2.5(d) for frequencies where several supersonic modes exist together in a band, the statistical calculation lies approximately 6dB below the exact estimate. In the present discussion, exact calculations (equation [2.34]) are presented for frequencies up to those where supersonic modes begin to exist. These complement the statistical calculations, indicating the magnitude of the contribution of subsonic modes to the power radiation.

The experimental results in non-dimensional form Φ_π/Φ_p are compared with the theoretical predictions from equation [2.22] in Figs. 4.15(a) to 4.15(c). Appropriate values of the one-third octave band quality factors for the supersonic modes have been chosen from Figs. 4.4(a) to 4.4(c) for the steel test sections. Two well-separated flow speeds (M_o = 0.22 and 0.55) are shown for each test section.

In Fig. 4.15(a) (test section 1), it can be seen that, at the lowest frequency for which supersonic modes exist, the sharp cut-off in radiation predicted by the statistical analysis (curve (i) for M_o = 0.55) does not occur; the experimental spectral densities are essentially independent of ν for $\nu < 1$. We note however that this behaviour is generally predicted by the exact analysis (curve (ii) for M_o = 0.55), which is based on measured resonance frequencies and quality factors. At ν = 0.1 for M_o = 0.55, the experimental data lie approximately 11dB below the statistical estimate but 19dB below the exact estimate. For ν = 0.04, where the radiation is from subsonic modes only, the experimental data lies approximately 20dB below the exact estimate, while for $\nu \simeq 1$ the statistical estimate lies only 10dB above the measured results. Similar results are found for all the steel test section pipes. We also note, on comparing the exact calculations and the experimental measurements for $\nu < 0.1$ for both flow speeds, that the theoretical overestimates decrease significantly with increasing M_o (and $\bar{\nu}_{hc}$) as found in the case of the acceleration response (for example, Fig. 4.9(c)).

For the steel pipes used, as $\nu_{ac} < 2$, supersonic modes exist for all ν greater than the cut-on frequency for supersonic modes. The statistical

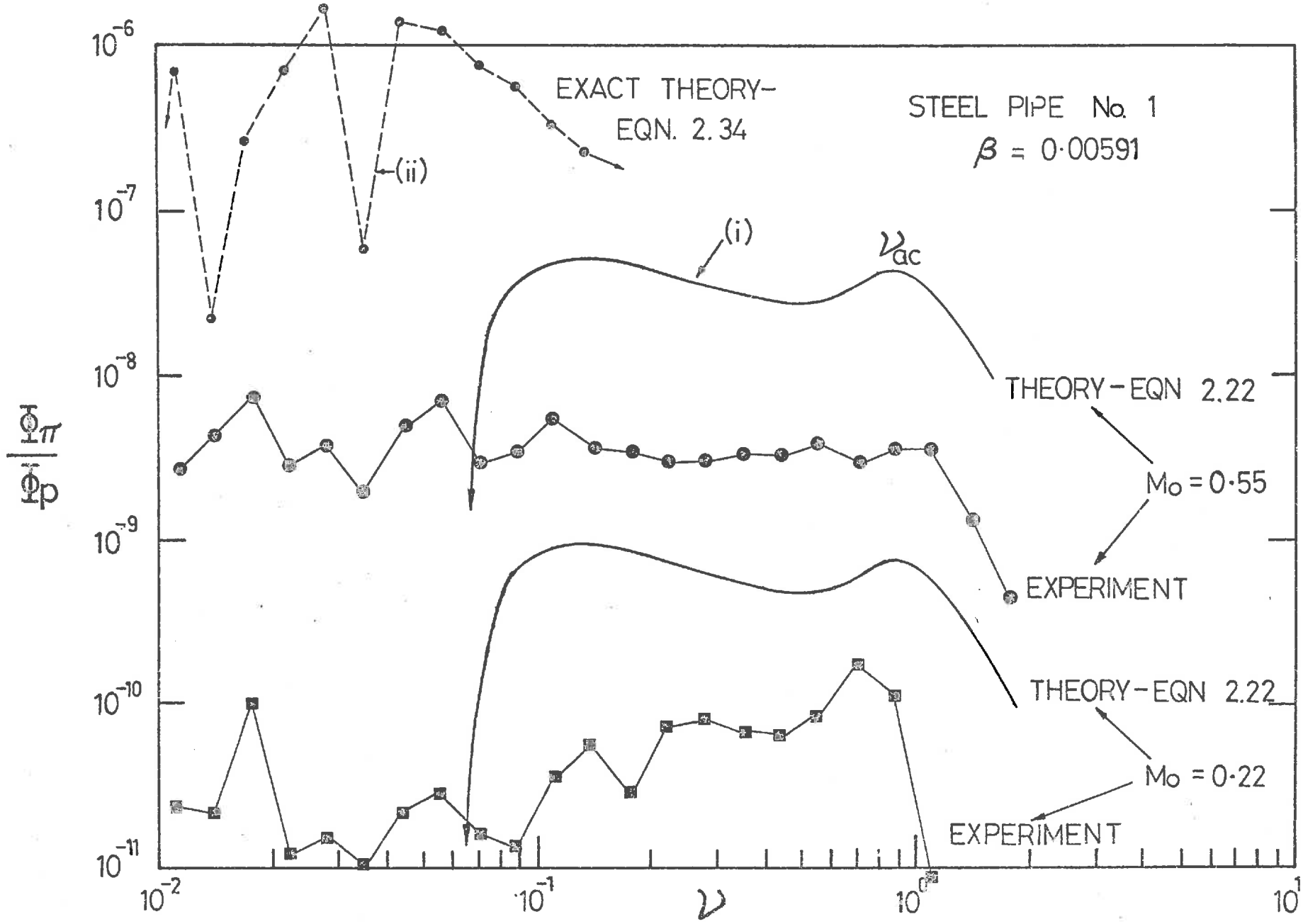

FIG.4.15(a) $\frac{\Phi\pi}{\Phi p}$ – COMPARISON OF EXPERIMENT & THEORY – STEEL PIPE β=0·00591

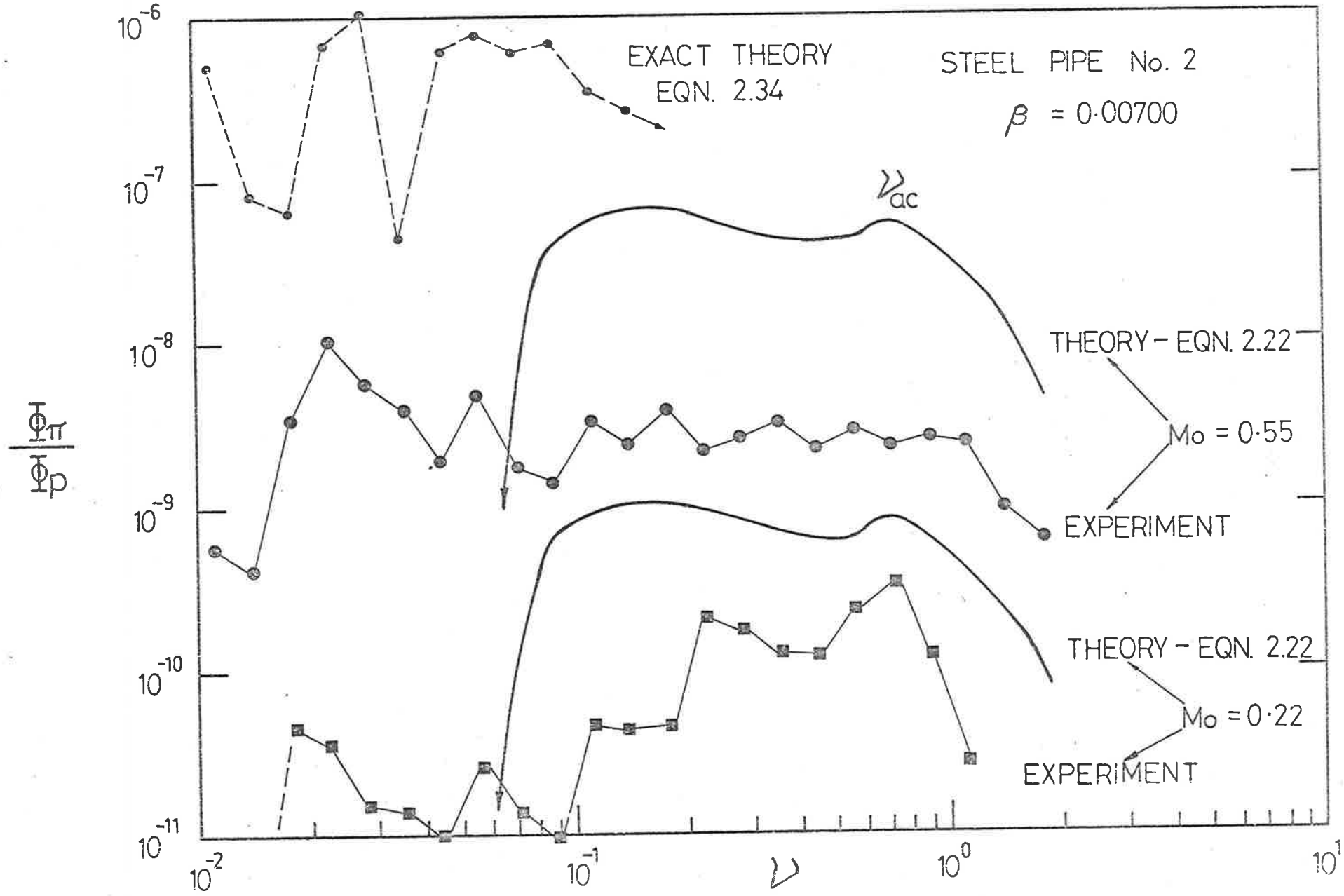

FIG. 4.15(b) Φ_π/Φ_D – COMPARISON OF EXPERIMENT & THEORY – STEEL PIPE $\beta = 0{\cdot}0070$

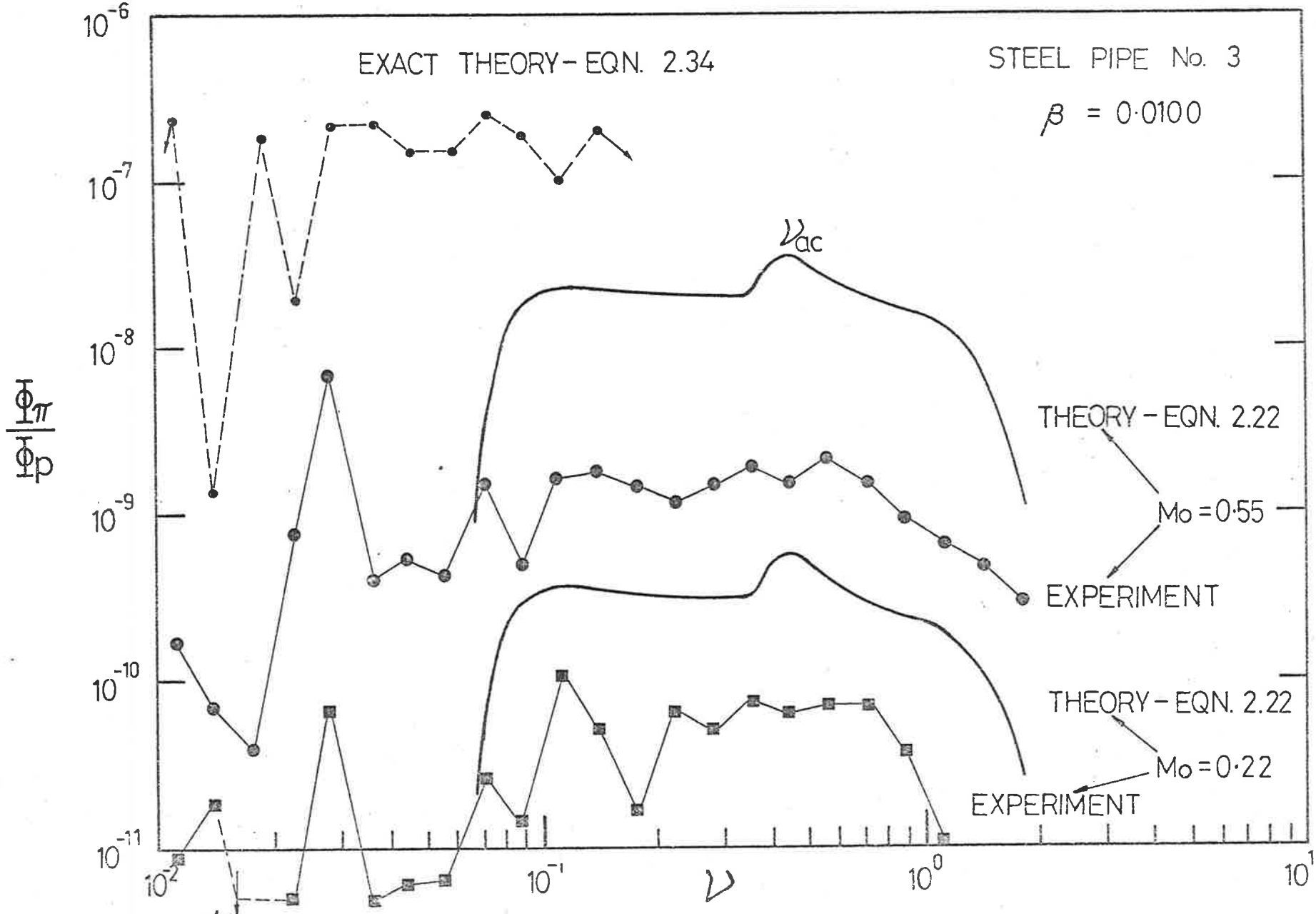

FIG. 4.15(c) Φ_π/Φ_p — COMPARISON OF EXPERIMENT & THEORY – STEEL PIPE β=0·0100

analysis may be validly used for $\nu > \nu_{ac}$ where all modes are supersonic, but where $\nu < \nu_{ac}$, it should significantly underestimate the total radiation due to the neglect of subsonic modes. In contrast with this expectation, a large overestimate occurs. It has been argued previously (section 4.4.4) that the errors involved in the experimental measurements of Φ_π, $\Phi_{\ddot{w}}$, Φ_p, β, ρ_{fs}, M_{Lp}, M_o and Q_s are small, and that the errors produced in the calculations due to the choice of a sinusoidal function for the axial mode shape will be less than 2dB. The cross-spectral density of the turbulence pressure field has not been verified experimentally. It is proposed again, that for the present investigation where $\bar{\nu}_{hc} << 2$, large overestimates of the low-wavenumber spectrum of the turbulence pressure field are produced by using the Corcos model of the cross-spectral density of the wall-pressure field, resulting in similar overestimates in Φ_π/Φ_p. This is discussed in section 4.6 in detail.

4.5.4 Summary

The acoustic radiation from thin-walled steel pipes, excited by fully-developed turbulent flow, has been investigated experimentally for configurations representative of case 1 of section 2.2.8 i.e. both $\bar{\nu}_{hc}$ and $\bar{\nu}_{ac} < 2$. Hydrodynamic coincidence did not occur, while supersonic vibrational modes existed for all frequencies above the cut-on of supersonic modes.

The acoustic radiation from the pipes displayed cylindrical symmetry at frequencies where supersonic modes existed, in that the radiated intensity was independent of axial or circumferential coordinate, but was inversely proportional to the radial distance from the pipe centreline. Both supersonic and subsonic modes contributed to the acoustic radiation, although for all $\nu < \nu_{ac}$, subsonic modes tended to dominate the radiation: since the subsonic modes were more lightly damped than supersonic modes at the same frequency and possessed a higher modal density, they radiated relatively more acoustic power than supersonic modes, even though their radiation ratios were lower than those of supersonic modes. This was shown by measurements of

the radiation ratios of the various pipes, which were found to be higher by up to 10dB than the theoretical estimates from the statistical analysis, but were found to agree reasonably closely with exact theoretical estimates.

Reduction of the experimental data of each pipe in accordance with the predicted dependence on flow and structural parameters show that the non-dimensional acoustic power radiation Φ_π was

(i) proportional to the power spectral density of the exciting turbulence wall-pressure field Φ_p;

(ii) proportional to the average quality factor of the radiating modes;

(iii) proportional to the fifth power of the flow speed; and

(iv) inversely proportional to the square or cube of the pipe wall thicknes for $\nu > \nu_{ac}$, close to theoretical predictions. For $\nu < \nu_{ac}$, the choice of quality factor for supersonic modes obscures the precise dependence on β, although it seems likely that Φ_π will also depend on β^{-2} or β^{-3}.

The frequency dependence of the non-dimensionalised experimental data showed considerable agreement with the exact theoretical predictions. However, as far as any absolute agreement was concerned, the theoretical predictions exceeded the experimental measurements by approximately 20dB at low ν and by 10dB at the ring frequency. The differences seemed to reduce with increasing M_o and $\bar{\nu}_{hc}$.

4.6 DISCUSSION OF DIFFERENCES BETWEEN PREDICTIONS AND EXPERIMENTAL MEASUREMENTS

Measurements of narrow-band cross-correlation coefficients of the pressure field beneath turbulent boundary layers by Corcos (1962) and Bull (1963) are found to be consistent with the Corcos model for the cross-spectral density of the wall-pressure field (equation [1.1]), at least for high frequencies and small transducer separations. Then the measurements are dominated by wavenumbers in the convective domain (i.e. $k_x \simeq k_c$, where k_x is the longitudinal wavenumber) which contain most of the energy of the turbulence pressure field. The low-wavenumber components of the pressure field ($k_x << k_c$) will

contribute to the correlation measurements only at large transducer separations: here the experimental data are most subject to error and the actual contributions from low-wavenumber components are indistinguishable in the experimental scatter normally encountered.

Later experimentalists have resorted to wavenumber-frequency filtering techniques to measure directly in the low-wavenumber domain. For example, the results of Chandiramani and Blake (1968), who used large transducers to remove the contribution from the convected domain, indicate that the Corcos model overestimates the low-wavenumber contribution to the spectral density of the turbulence pressure field by at least 10dB for $\omega\delta^*/U_o \simeq 10$ (δ^* is the displacement thickness). Blake and Chase (1971) and Farabee and Gieb (1975) have used longitudinal arrays of appropriately-phased transducers to measure particular wavenumber components of the wall-pressure field. From the results of Blake and Chase (which were subject to some acoustic interference), the Corcos model may be shown to lead to overestimates of approximately 20dB in the low-wavenumber components of the spectral density for $\omega\delta^*/U_o \simeq 10$. Using improved equipment, Farabee and Gieb determined an upper bound to the low-wavenumber contribution of the spectral density which was 20dB below the level suggested by Blake and Chase. Substantial evidence exists therefore which suggests that the true levels of the low-wavenumber components of the spectral density of the wall-pressure field lie at least 40dB below those estimated with the Corcos model.

Under conditions removed from hydrodynamic coincidence, such model overestimates will generate response overestimates. To demonstrate the likely magnitudes, it is useful to formulate the joint acceptance between a structural mode and a homogeneous random pressure field in its wavenumber-frequency components. It may be shown (Richards and Mead (1968, p.314)) that the spectral density of the joint acceptance between a random homogeneous pressure field and driven structural mode with shape $\psi_\alpha(\underset{\sim}{r})$ is

$$j^2_{\alpha\alpha}(\omega) = \frac{1}{\phi_p(\omega)S^2} \int_S \int_S \phi_p(\underset{\sim}{\xi},\omega)\psi_\alpha(\underset{\sim}{r})\psi_\alpha(\underset{\sim}{r}^1)\ d\underset{\sim}{r}\ d\underset{\sim}{r}^1 \qquad [4.7]$$

where $\underset{\sim}{r} = (x,y)$ and $\underset{\sim}{\xi} = \underset{\sim}{r}^1 - \underset{\sim}{r}$. We define the Fourier transform pair for the cross-spectral density of the turbulence pressure field as

$$\phi_p(\underset{\sim}{\xi},\omega) = \frac{1}{(2\pi)^2} \int_{-\infty}^{\infty}\int \Phi_p(\underset{\sim}{k},\omega)e^{i\underset{\sim}{k}\cdot\underset{\sim}{\xi}}d\underset{\sim}{k} \qquad [4.8]$$

$$\Phi_p(\underset{\sim}{k},\omega) = \int_{-\infty}^{\infty}\int \phi_p(\underset{\sim}{\xi},\omega)e^{-i\underset{\sim}{k}\cdot\underset{\sim}{\xi}}d\underset{\sim}{\xi} \qquad [4.9]$$

where $\Phi_p(\underset{\sim}{k},\omega)$ is the wavenumber-frequency spectral density of the turbulence pressure field and $i^2 = -1$. Similarly, the filtering function of the αth mode shape is the Fourier transform of $\psi_\alpha(\underset{\sim}{r})$

$$H_\alpha(\underset{\sim}{k}) = \int_S \psi_\alpha(\underset{\sim}{r})e^{-i\underset{\sim}{k}\cdot\underset{\sim}{r}}d\underset{\sim}{r} \qquad [4.10]$$

The latter integration limits are finite since $\psi_\alpha(\underset{\sim}{r}) = 0$ outside structural boundaries. Substituting equation [4.8] into [4.7] gives

$$j^2_{\alpha\alpha}(\omega) = \frac{1}{\phi_p(\omega)S^2} \int_S \int_S \frac{1}{(2\pi)^2} \int_{-\infty}^{\infty}\int \Phi_p(\underset{\sim}{k},\omega)e^{i\underset{\sim}{k}\cdot\underset{\sim}{\xi}}d\underset{\sim}{k}\psi_\alpha(\underset{\sim}{r})\psi_\alpha(\underset{\sim}{r}^1)\ d\underset{\sim}{r}\ d\underset{\sim}{r}^1 \qquad [4.11]$$

Reversing the order of the integration and using equation [4.10] leads to

$$j^2_{\alpha\alpha}(\omega) = \frac{1}{\phi_p(\omega)S^2 4\pi^2} \int_{-\infty}^{\infty}\int \Phi_p(\underset{\sim}{k},\omega)\ H_\alpha(\underset{\sim}{k})\ H^*_\alpha(\underset{\sim}{k})\ d\underset{\sim}{k} \qquad [4.12]$$

$$= \frac{1}{4\pi^2 S^2} \int_{\infty}^{\infty}\int \Phi'_p(\underset{\sim}{k},\omega)\left|H_\alpha(\underset{\sim}{k})\right|^2\ d\underset{\sim}{k} \qquad [4.13]$$

where $\Phi'_p(\underset{\sim}{k},\omega) = \Phi_p(\underset{\sim}{k},\omega)/\phi_p(\omega)$ and $H^*_\alpha(\underset{\sim}{k})$ is the complex conjugate of $H_\alpha(\underset{\sim}{k})$. For mode shapes corresponding to simply-supported ends (equation [2.6]) and for axial and circumferential wavenunbers (k_x and k_y), we find

$$|H_{mn}(k_x,k_y)|^2 = |H_m(k_x)|^2 |H_n(k_y)|^2 \qquad [4.14]$$

where $$|H_m(k_x)|^2 = L_x^2 \left(\frac{k_m}{k_m + k_x}\right)^2 \left(\frac{\mathrm{Sin}[(k_m - |k_x|)L_x/2]}{[(k_m - k_x)L_x/2]}\right)^2 ,$$

$$|H_n(k_y)|^2 = L_y^2 \left(\frac{k_n}{k_n + k_y}\right)^2 \left(\frac{\mathrm{Sin}[(k_n - |k_y|)L_y/2]}{[(k_n - k_y)L_y/2]}\right)^2 ,$$

and $k_m = m\pi/L_x$, $k_n = n\pi/L_y$, $L_x = \ell$, $L_y = 2\pi a$, $n = 0,2,4,\ldots..$ for pipes (since only an even number of half-wavelengths may stand around the pipe circumference).

The joint acceptance $j_{\alpha\alpha}^2(\omega)$ is the integral over all $\underset{\sim}{k}$ of the product of the wavenumber-frequency spectrum $\Phi_p'(\underset{\sim}{k},\omega)$ of the pressure field and the modal filtering function $|H_\alpha(\underset{\sim}{k})|^2$. $|H_\alpha(\underset{\sim}{k})|^2$ rises sharply as $\underset{\sim}{k}$ tends to $\pm\, \underset{\sim}{k}_\alpha$, while for wall-pressure fields beneath turbulent flows, $\Phi_p'(\underset{\sim}{k},\omega)$ has a pronounced peak at $\underset{\sim}{k} = (k_c,0)$. When hydrodynamic coincidence occurs, k_c matches the axial structural wavenumber k_m and $j_{\alpha\alpha}^2(\omega)$ has a maximum value for the αth mode. On the other hand, for $\omega > \omega_{hc}$, the low-wavenumber components of the pressure field will determine $j_{\alpha\alpha}^2(\omega)$ for $k_m << k_c$, since $|H_m(k_x)|^2$ tends to zero as k_x varies significantly from $\pm\, k_m$.

To illustrate these effects, $\Phi_p'(k_x,0,\omega)$ and $|H_m(k_x)|^2$ can be plotted against k_x. $\Phi_p'(\underset{\sim}{k},\omega)$ is derived from the Corcos model for $\phi_p(\underset{\sim}{\xi},\omega)$ of the turbulence wall-pressure field as

$$\Phi_p'(k_x,k_y,\omega) = \frac{\Phi_p(\underset{\sim}{k},\omega)}{\phi_p(\omega)} = \left(\frac{2a_x}{a_x^2 + (k_c - k_x)^2}\right)\left(\frac{2a_y}{a_y^2 + k_y^2}\right) \qquad [4.15]$$

where $a_x = c_x k_c$, $a_y = c_y k_c$, $c_x = 0.1$ and $c_y = 0.7$. In Fig. 4.16(a), curve (i) represents $|H_m(k_x)|^2$ for $m = 10$, $n = 2$, $\ell = 2.94$ m and $a = 36.3$ mm. Curve (ii) shows $\Phi_p'(k_x,0,\omega)$ for $k_c = k_m$ i.e. where hydrodynamic coincidence occurs. Then $j_{\alpha\alpha}^2(\omega)$ will be determined essentially by contributions from

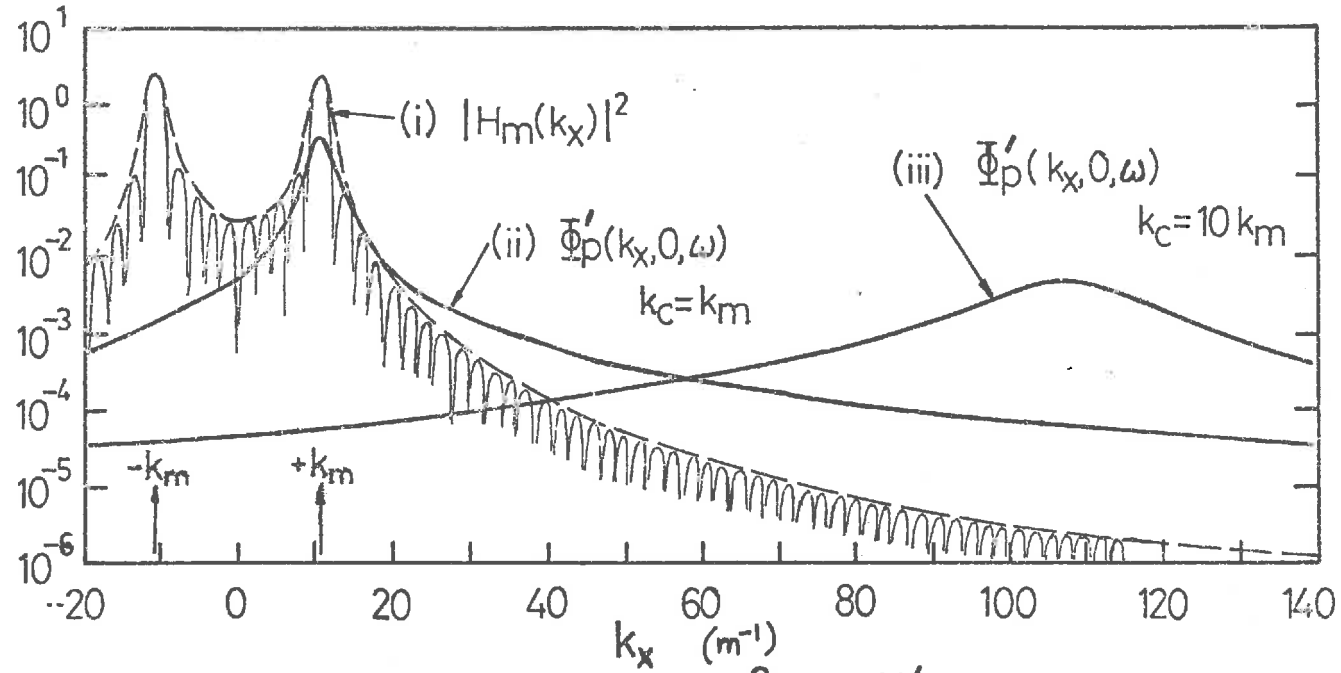

FIG. 4.16(a) VARIATION OF $|H_m|^2$ & Φ'_p WITH k_x

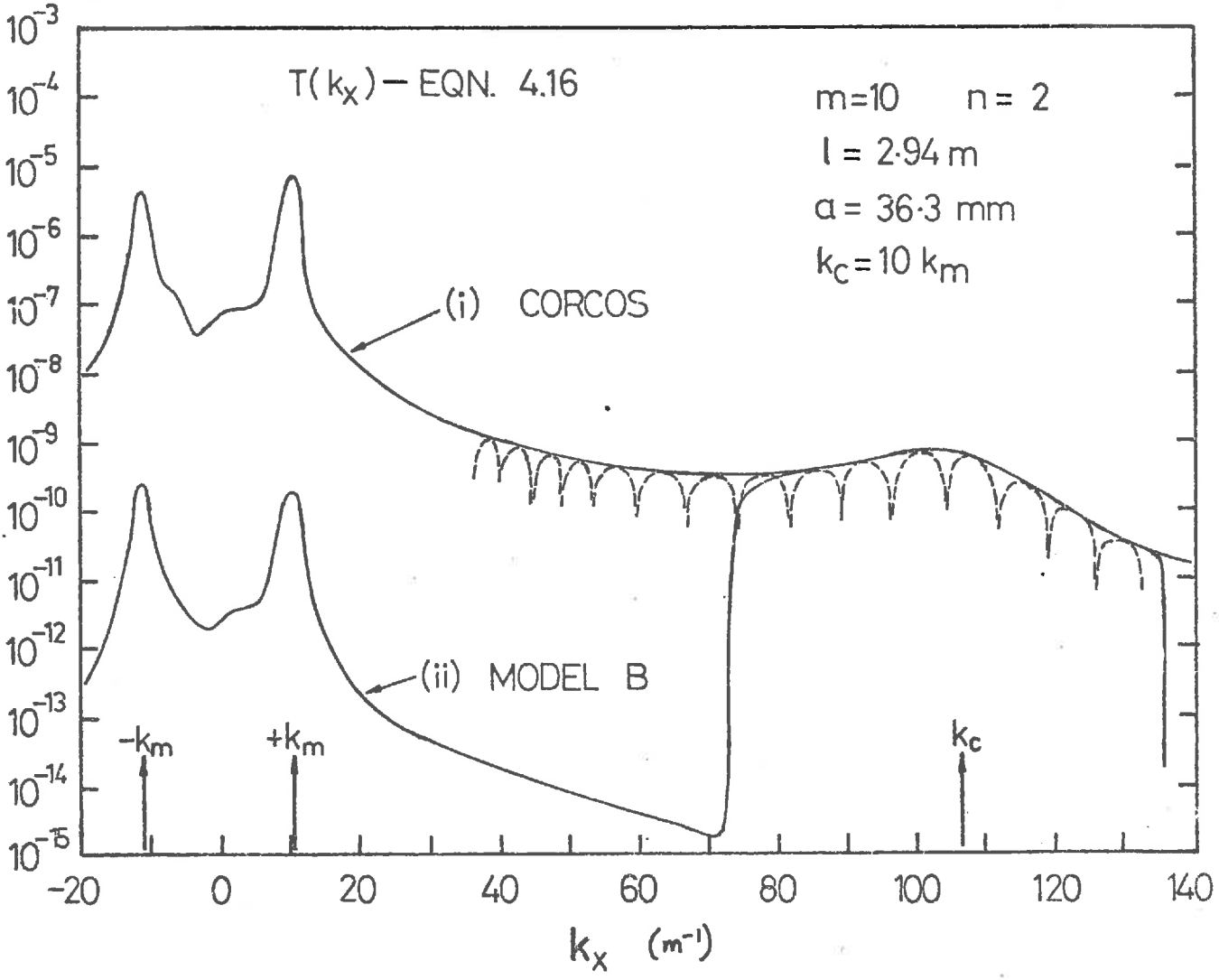

FIG. 4.16(b) VARIATION OF $T(k_x)$ WITH AXIAL WAVENUMBER

the bandwidth of wavenumbers centred on $k_x \simeq k_m = k_c$. Curve (iii) shows $\Phi_p'(k_x,0,\omega)$ for $k_c = 10k_m$: now $j_{\alpha\alpha}^2(\omega)$ will depend relatively more on the low wavenumber components $k_x \simeq \pm k_m$ of $\Phi_p'(k_x,0,\omega)$. This trend will increase as k_c/k_m increases, for the Corcos model.

As discussed earlier, large differences between predictions based on the Corcos model and measured values of $\Phi_p'(\underset{\sim}{k},\omega)$ have been found for these low wavenumbers: but it is precisely this range of wavenumbers which determines the vibrational response of and acoustic radiation from the steel pipes tested in the experimental work described earlier in this chapter. This is shown clearly in Fig. 4.16(b) by curve (i), where $T(k_x)$ is plotted against k_x for the same conditions as in Fig. 4.16(a) with $k_c = 10km$, where

$$T(k_x) = |H_m(k_x)|^2 \int_{-\infty}^{\infty} \Phi_p'(k_x,k_y,\omega)\,|H_n(k_y)|^2 dk_y \qquad [4.16]$$

and

$$j_{\alpha\alpha}^2(\omega) = \frac{1}{4\pi^2 S^2} \int_{-\infty}^{\infty} T(k_x)\,dk_x \qquad [4.17]$$

$T(k_x)$ (found by numerical integration) has maximum values at $k_x = \pm k_m$; we note that $T(k_c)$ is approximately 40dB below $T(k_m)$.

Assuming that $\Phi_p'(k,\omega)$ is described correctly by the Corcos model when $0.7 < k_x/k_c < 1.3$ (i.e. when $\Phi_p'(k_x,0,\omega)/\Phi_p'(k_c,0,\omega) \gtrsim 0.1$), an estimate of the lower bound to $j_{\alpha\alpha}^2(\omega)$ can be made, by setting $\Phi_p'(\underset{\sim}{k},\omega) = 0$ for $k_x/k_c < 0.7$ and > 1.3, and defining $\Phi_p'(\underset{\sim}{k},\omega)$ by equation [4.15] otherwise: we call this, model A. This lower bound to $j_{\alpha\alpha}^2(\omega)$ will be determined by components of $\Phi_p'(\underset{\sim}{k},\omega)$ with $k_x \simeq k_c$. Additionally, the empirical model of Farabee and Gieb may be used to estimate $\Phi_p'(\underset{\sim}{k},\omega)$ for $k_x < 0.7k_c$. Farabee found that

$$\Phi_p(\underset{\sim}{k},\omega)\frac{U_o}{q_o^2\delta^{*3}} \simeq 2 \times 10^9 \left(\frac{\omega\delta^*}{U_o}\right)^{-4} \text{ for low } \underset{\sim}{k}\,.$$

For $\omega\delta^*/U_o > 1.2$, $\quad \phi_p(\omega) \simeq 6 \times 10^{-5} \dfrac{q_o^2\delta^*}{U_o} \left(\dfrac{\omega\delta^*}{U_o}\right)^{-3}$ (Strawdermann (1969)).

Thus $\Phi'_p(k,\omega) = \Phi_p(k,\omega)/\phi_p(\omega) \simeq 5.6 \times 10^{-5} \left(\frac{a}{k_c}\right)$, which is known as model B. Curve (ii) in Fig. 4.16(b) compares $T(k_x)$ using model B with calculations from the Corcos model: the convected wavenumber domain determines the lower bound of $j^2_{\alpha\alpha}(\omega)$ for model B. Further, in order to express a reasonable transition from the Corcos model at $k_x \simeq k_c$ to the measured behaviour of $\Phi'_p(k,\omega)$ at low k, we assume that $\Phi'_p(k,\omega)$ has the form

$$\Phi'_p(k,\omega) = \left(\frac{2a_x^5}{a_x^6 + (k_c - k_x)^6}\right)\left(\frac{2a_y^5}{a_y^6 + k_y^6}\right)$$

which is known as model C. These alternatives are compared with the Corcos model in Fig. 4.16(c) where $\Phi'_p(k_x,0,\omega)$ is plotted against k_x for $k_c = 100\ m^{-1}$.

In Fig. 4.16(d), the results of calculation of $j^2_{\alpha\alpha}(\omega)$ are presented for $m = 10$, $n = 2$, $\ell = 2.94$ m and $a = 36.3$ mm, where $0.1 < k_c/k_m < 100$. Curve (i) represents the results of exact calculations using the exact equations [2.12 to [2.14], which incorporate the Corcos model of $\phi_p(\xi,\omega)$. Curves (ii) to (v) were calculated by using alternative models for $\Phi'_p(k,\omega)$ in equation [4.13] and integrating numerically over all k. The Corcos model (equation [4.15]) was used to find curve (ii): this agrees closely with curve (i) for all k_c/k_m, demonstrating the accuracy of the integration procedure. Curve (iii) uses model A for $\Phi'_p(k,\omega)$: the differences between curves (i) and (iii) indicate the magnitude of the contribution to the joint acceptance made by those components of the wall-pressure field with $k_x \simeq k_m$ as k_m differs from k_c. In particular, these differences show the maximum overestimates in $j^2_{\alpha\alpha}(\omega)$ that may be generated by using the Corcos model of $\phi_p(\xi,\omega)$ as k_c/k_m varies. For $k_c/k_m = 10$ the maximum overestimate will be 32dB. Curve (iv), based on model B, is identical with (iii) for $k_c/k_m < 10$, but (iv) becomes independent of k_c/k_m as the Farabee components in B make the dominant contribution. This suggests that large differences between measured and calculated values of $j^2_{\alpha\alpha}(\omega)$ will occur in practice

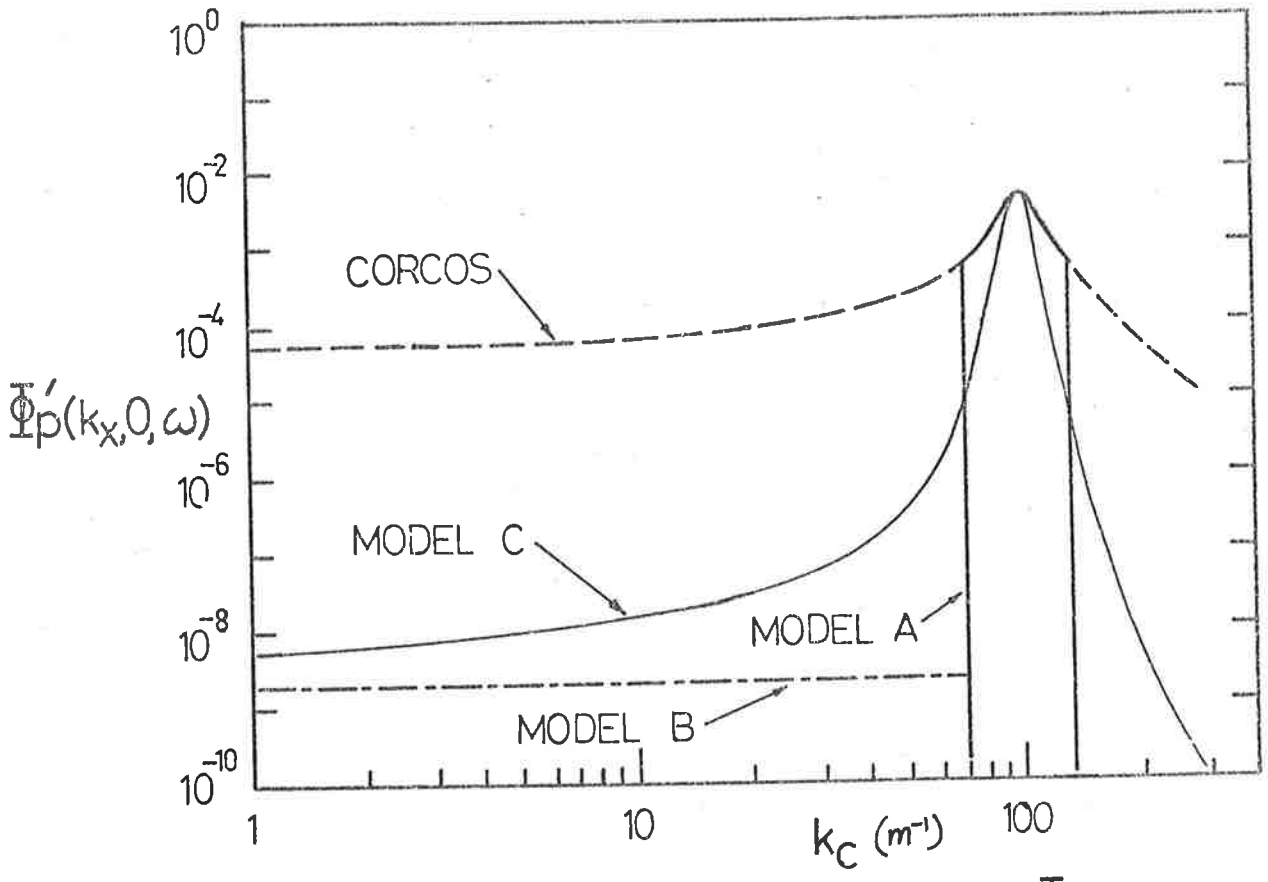

FIG. 4.16(c) VARIOUS MODELS FOR $\Phi p(k_x,0,\omega)$

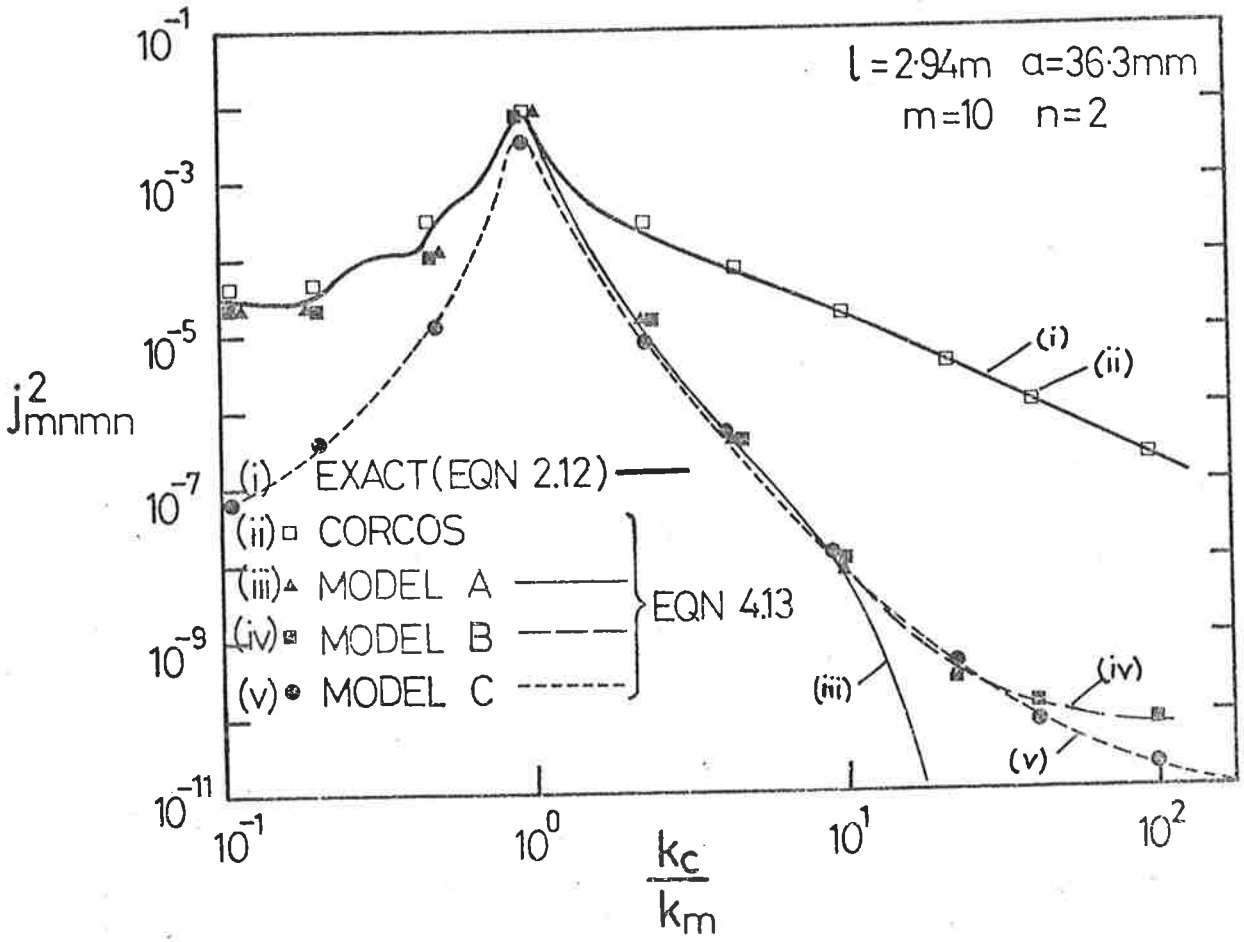

FIG. 4.16(d) MODAL JOINT ACCEPTANCE

when $k_c >> k_m$. Curve (v), based on model C, shows the effect of smoothing $\Phi'_p(k,\omega)$ between the Corcos model at $k_x = k_c$ and the measured spectra at low k_x: significant differences between curves (ii) and (v) still occur.

Now we consider the range of k_c/k_m encountered during the present experiments with steel pipes. From equation [2.8], it can be shown that, for $\bar{\nu} < \sqrt{2}$,

$$\bar{K}_{m_{max}} = \bar{\nu}/\sqrt{2} ,$$

where $\bar{K}_{m_{max}}$ is the maximum value $\bar{K}_m$ may have at $\bar{\nu}$. Then

$$(\frac{\bar{K}_m}{\bar{K}_c})_{max} = (\frac{\bar{\nu}_{hc}}{2})^{\frac{1}{2}} \qquad \text{for } \bar{\nu} < \sqrt{2} ,$$

or in present terminology, $(k_c/k_m)_{min} = (2/\bar{\nu}_{hc})^{\frac{1}{2}}$. Thus, as $\bar{\nu}_{hc}$ decreases, $(k_c/k_m)_{min}$ increases: it has just been argued that the maximum possible overestimate in $j^2_{\alpha\alpha}(\omega)$ using the Corcos model increases as (k_c/k_m) increases (Fig. 4.16(d)).

Considering the steel pipes tested experimentally, for test pipe 3(β = 0.0100), values of $\bar{\nu}_{hc}$ are 0.00797 and 0.0519 for minimum and maximum M_o respectively, while the mean differences in $\Phi_{\ddot{w}}/\Phi_p$ between measured data and predictions for $0.05 < \nu < 0.2$ are approximately 25 and 20dB respectively: this shows some support for the concept that, as $(k_c/k_m)_{min}$ decreases (or equivalently, as $\bar{\nu}_{hc}$ increases), the overestimate in theoretical $j^2_{\alpha\alpha}(\omega)$ produced with the Corcos model decreases. These values of $(k_c/k_m)_{min}$ will be inaccurate at low ν, where equation [2.8] is only approximately correct. In Figs. 4.9(a) to (c), the differences between the measured and predicted values of $\Phi_{\ddot{w}}/\Phi_p$ depend on ν: the differences at low and high ν are much less than the differences in the middle range of ν. This results from the variation in k_c/k_m between modes at different ν and the associated variations in overestimates of $j^2_{\alpha\alpha}(\omega)$. For example, in Fig. 4.9(c) at $\nu \simeq 0.028$, $\Phi_{\ddot{w}}/\Phi_p$ is determined by n = 2 modes, whose mean m is 3: thus k_c/k_m is equal

to 26.7 for $M_o = 0.22$ and to 10.5 for $M_o = 0.57$, corresponding to differences of 12dB and 7dB respectively. At $\nu = 0.138$, $\Phi_{\ddot{w}}/\Phi_p$ is determined by $n = 4$ modes, whose mean m is 9: k_c/k_m is equal to 45.1 for $M_o = 0.22$ and to 17.5 for $M_o = 0.57$, corresponding to differences of 25dB and 21dB respectively. At $\nu = 1.09$, $(k_c/k_m)_{min} = 6.5$ for $M_o = 0.57$, corresponding to 9dB difference between the theoretical estimate and measured data (acoustic excitation influences $\Phi_{\ddot{w}}/\Phi_p$ at $\nu \simeq 1$ for $M_o = 0.22$). The observed variations in differences between experimental data and theoretical predictions with ν are associated with variations in k_c/k_m between the modes at different ν: as k_c/k_m decreases, so the differences between theory and experiment decrease, in qualitative agreement with the variation in $j^2_{\alpha\alpha}(\omega)$ calculations which are produced when different models of $\Phi'_p(\underset{\sim}{k},\omega)$ are used. Similar conclusions can be drawn from Figs. 4.9(b) and (c) for the other steel pipes.

The differences between the exact theoretical predictions and the experimental data of Φ_π/Φ_p are of a similar nature to those observed for $\Phi_{\ddot{w}}/\Phi_p$, as discussed in the preceeding paragraph. The arguments used there apply equally to these radiation differences, since the measured values of the radiation ratio are independent of M_o. In the general case however, the acoustic radiation should be weighted towards the supersonic modes by the action of the radiation ratio function, which filters out the contribution of the modes controlling the response so that the mean k_m will tend to decrease and k_c/k_m will tend to increase; thus the differences between experimental data and theoretical predictions of Φ_π/Φ_p should tend to exceed those for $\Phi_{\ddot{w}}/\Phi_p$ at the same ν. This appears to be so - compare Figs. 4.9(a) & 4.15(a) etc.

We note that variations in the flow speed dependence from the M_o^5 prediction, as were found particularly for test section 1 at low ν, appear to be associated with variations in the values of k_c/k_m at fixed ν and the differing theoretical overestimates which occur for different k_c/k_m: also the approximations to $j^2_{\alpha\alpha}(\omega)$ are invalid as k_c/k_m tends to 1, so that the dependence on M_o will increase above the fifth power prediction.

Thus, we observe that as both $(k_c/k_m)_{min}$ and local values of

(k_c/k_m) decrease, the differences between experimental data and theoretical predictions of both $\Phi_{\ddot{w}}/\Phi_p$ and Φ_π/Φ_p decrease. The theoretical predictions have been made using the Corcos model of the cross-spectral density of the wall-pressure field. This model, while predicting the dominant convected characteristics of the wall-pressure field, produces large overestimates in the low-wavenumber components of $\Phi_p(k,\omega)$: these, in turn, cause large overestimates in the joint acceptance of structural modes for which $k_c >> k_m$. Alternative models have been used to estimate the maximum values of these overestimates as k_c differs from k_m. The observed differences between experimental measurements and theoretical predictions based on the Corcos model are less than these maximum values for all k_c/k_m.

4.7 SURFACE DAMPING TREATMENTS

A study of the various effects of light-weight surface damping treatments on the pipe vibrational response and acoustic power radiation was undertaken. It was of interest to determine the extent of reductions in the pipe quality factor, response and radiation arising from the application of such treatments, and the dependence of these reductions on frequency and mode order.

To begin with, several alternative treatments were applied in turn to test section 3. These included single and double layers of cloth masking tape (Norton No.220); a 3mm thick layer of Selleys butyl mastic plastic putty which was bound onto the pipe surface with masking tape; and single and double layers of adhesive Silastic 732 RTV silicone rubber bound with masking tape: in each case, 30%, 50% and 100% surface area coverages were investigated. The maximum increase in surface mass was less than 15% and occurred for the bound double layer of silicone rubber. Modal and one-third octave band average quality factors were measured using the methods described in section 4.3. Only the results for the 100% coverage of the bound double layer of silicone rubber will be described since this treatment was found to be the most effective; it should be noted however, that the reductions in quality factors increased

with the area of pipe treated and that the treatments tested are listed in order of increasing effectiveness.

The resonance frequencies and quality factors of 20 modes of various circumferential order from n = 1 to n = 4, were monitored: a maximum reduction in resonance frequency of 3% was observed, while, in general, dramatic changes in quality factors were produced. The Q's of the n = 1 modes remained essentially constant at ≃ 150, but the Q's of the n = 2 modes were reduced from ≃3500 by factors of greater than 20 to values of ≃ 50. The Q's of the n = 3 and n = 4 modes underwent similar reductions to values of ≃ 100. These results are presented in Fig. 4.17(a). The changes in average Q's reflect the changes in the Q's of the modes present in each frequency band, as also shown in Fig. 4.17(a). The minimum average Q's are determined apparently by the presence of the n = 1 modes, which, for this pipe, are relatively unaffected by surface damping treatment. As discussed previously, the n = 1 modes involve essentially only a translation of the pipe centre of mass and are often called 'translational' modes. No circumferential bending occurs, so that little additional damping will be produced by surface treatments unless the axial wavelength (and therefore the axial radius of curvature) are comparable with the pipe radius i.e. m ≃ Λ. For higher-order circumferential modes n ≥ 2, the motion is predominantly circumferential bending, at least for low m. Then large changes in circumferential radius of curvature occur, producing large strains in surface damping treatments.

The vibrational response of and the acoustic radiation from the treated test section 3, when excited by turbulent flow at M_o = 0.371, were measured and the results are presented in non-dimensional form in Figs. 4.17(b) and (c), together with the results from the undamped pipe for the same flow speed, taken from Figs. 4.7(a) and 4.13(a). It was assumed that no significant changes in the directivity of the acoustic radiation were produced by the damping treatment; from examination of the curve of radiation ratio for the damped pipe in Fig. 4.17(d), this appears dubious since $\sigma > 5$ for

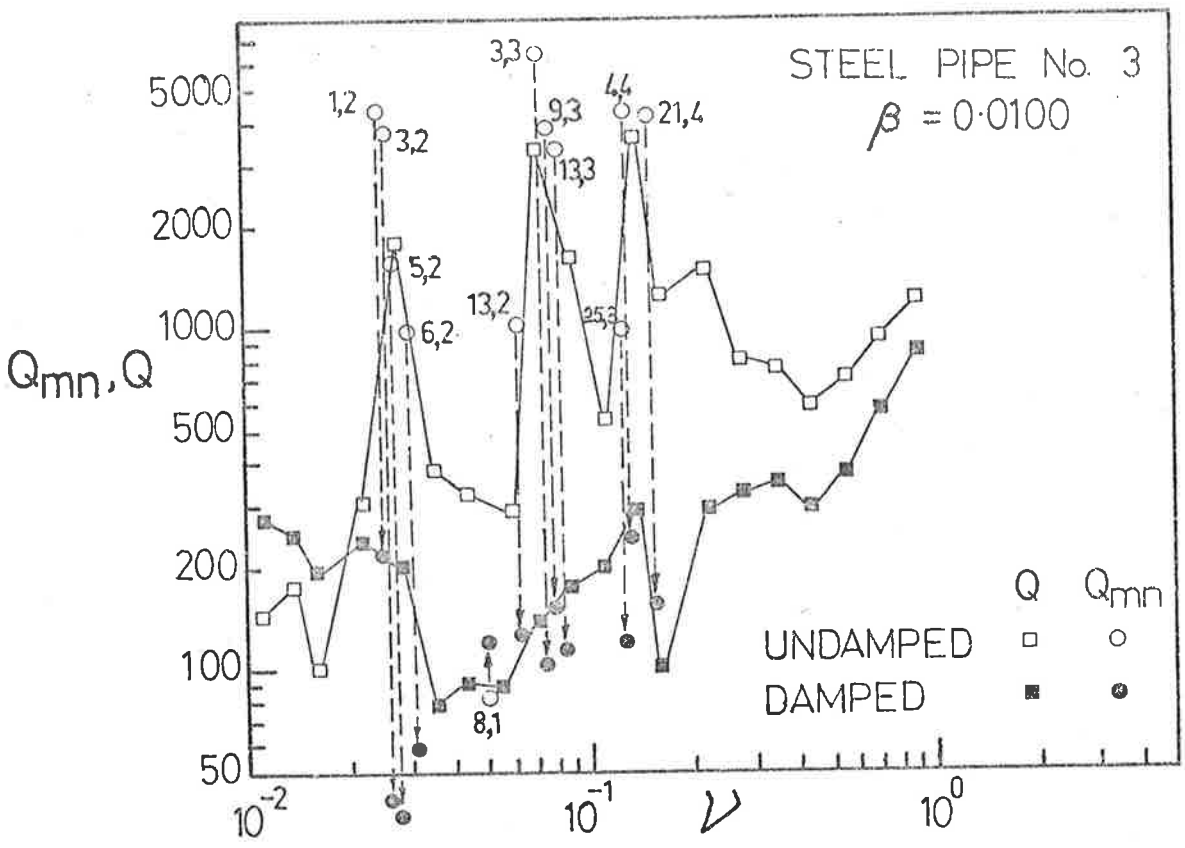

FIG. 4.17(a) EFFECT OF DAMPING TREATMENT ON Q's

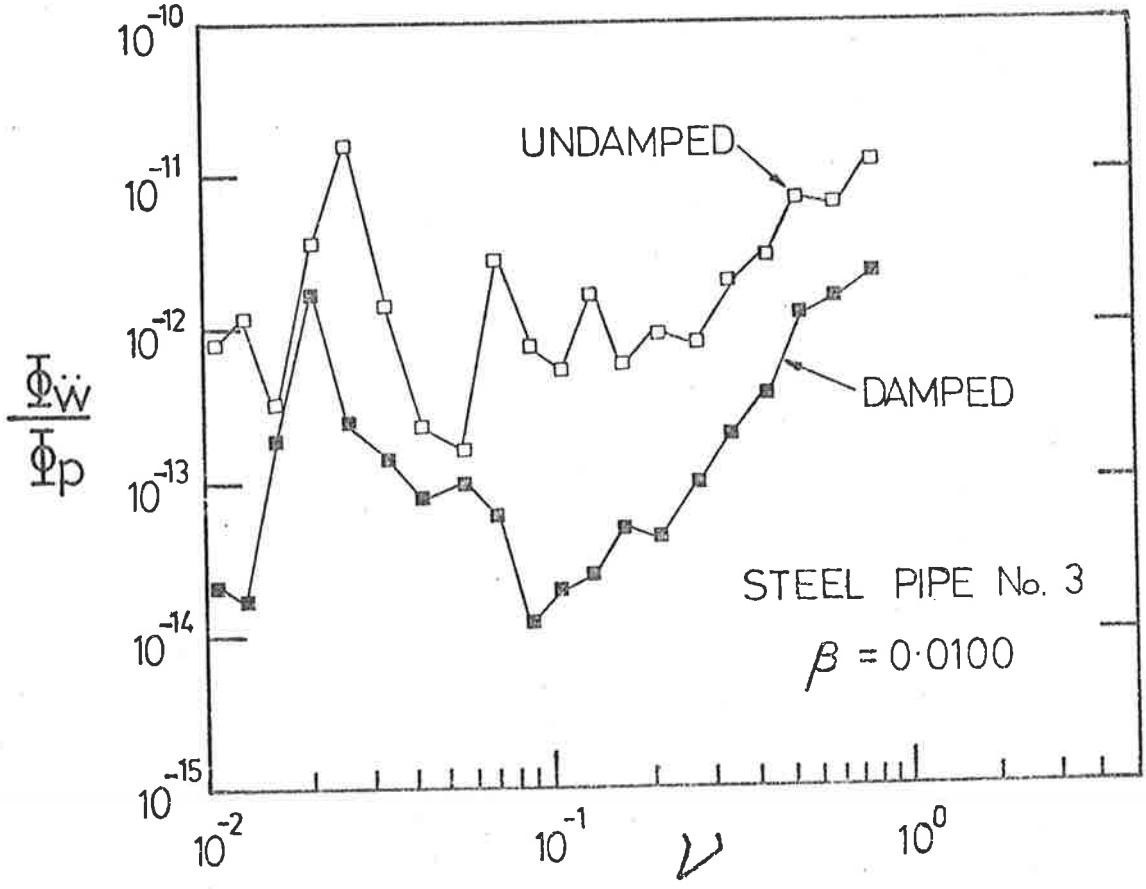

FIG. 4.17(b) EFFECT OF DAMPING TREATMENT ON $\Phi\ddot{w}$

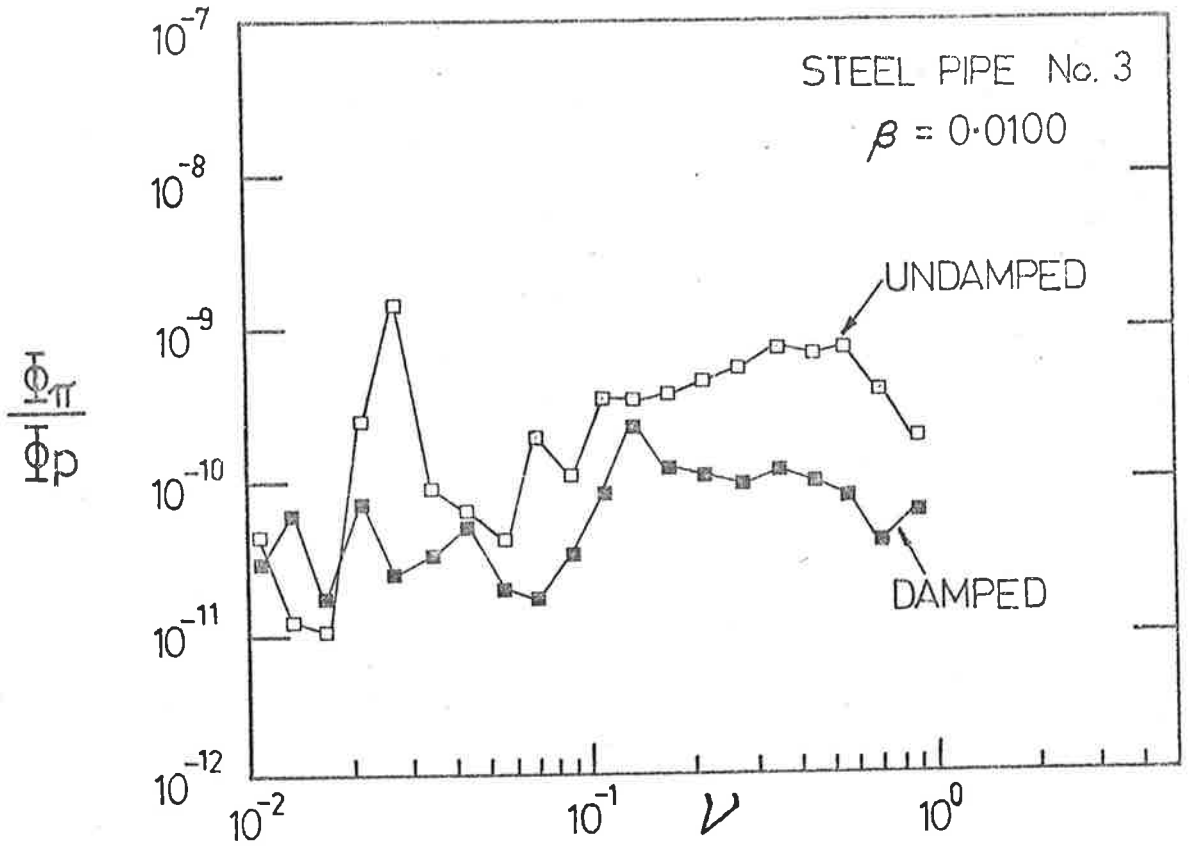

FIG. 4.17(c) EFFECT OF DAMPING TREATMENT ON Φ_π

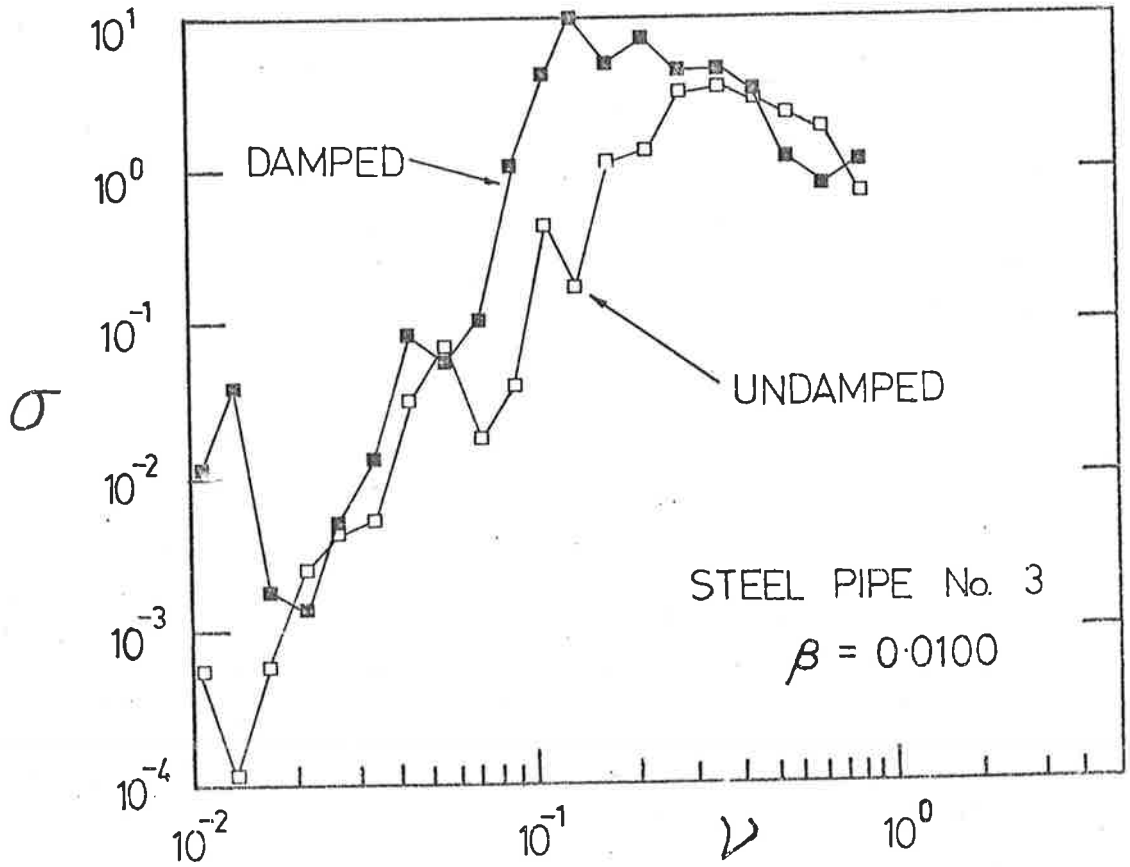

FIG. 4.17(d) EFFECT OF DAMPING TREATMENT ON σ

$0.1 < \nu < 0.4$. The application of the damping treatment produced reductions in $\Phi_{\ddot{w}}/\Phi_p$ and Φ_π/Φ_p over the complete frequency range. The maximum reductions occurred in those bands where groups of low circumferential-order modes (n = 2,3 and 4) exist. For example, 17dB, 16dB, and 18dB reductions in $\Phi_{\ddot{w}}/\Phi_p$ occur at $\nu = 0.028$, 0.070 and 0.141 respectively. These reductions correspond to measured changes in averaged Q's from 2000 to 200 for $\nu = 0.028$, from 3400 to 140 for $\nu = 0.070$, and from 3600 to 300 for $\nu = 0.141$. Other bands at low frequency contained n = 1 and other higher circumferential-order modes with lower undamped Q's: the damping treatments were relatively less effective and produced smaller changes in $\Phi_{\ddot{w}}/\Phi_p$. At higher frequencies, the reductions in $\Phi_{\ddot{w}}/\Phi_p$ vary between 5 and 10dB, but are similar to the variations in Q in Fig. 4.17(a).

The reductions in Φ_π/Φ_p are similar to the reductions in $\Phi_{\ddot{w}}/\Phi_p$ and Q at most frequencies, particularly for $\nu > 0.4$. For $0.07 < \nu < 0.4$, slightly smaller reductions occur in Φ_π/Φ_p than in $\Phi_{\ddot{w}}/\Phi_p$: for example, at $\nu = 0.070$, the reduction in Φ_π/Φ_p is 6dB less than the reduction in $\Phi_{\ddot{w}}/\Phi_p$, while at $\nu = 0.141$, only a 2dB reduction in Φ_π/Φ_p occurs compared with an 18dB reduction in $\Phi_{\ddot{w}}/\Phi_p$. At these two frequencies, the n = 1 modes tend to control the acoustic radiation and are much less affected by damping treatment than the higher circumferential-order modes which control the vibrational response when undamped. For $\nu > 0.3$, higher-order ($n \geq 2$) circumferential modes, which are easily damped, contribute significantly to the radiation as they become supersonic i.e. the n = 1 modes radiate relatively less acoustic power. At these frequencies, reductions in Φ_π/Φ_p tend to be the same as reductions in $\Phi_{\ddot{w}}/\Phi_p$, since the damping treatment acts equally on most radiating and non-radiating modes.

The comments may be demonstrated further by examining the changes in radiation ratio which occur with the application of damping treatment. In Fig. 4.17(d), only small changes in σ occur for $0.2 < \nu < 0.06$ and for $\nu > 0.4$, reflecting the equal reductions in $\Phi_{\ddot{w}}/\Phi_p$ and in Φ_π/Φ_p, while for $0.07 < \nu < 0.3$, significant increases in σ occur suggesting that radiating

modes have not been damped to the same extent as the modes which control the vibrational response.

In summary, on the application of light-weight damping treatments, reductions of up to 10dB in $\Phi_{\ddot{w}}/\Phi_p$ and Φ_π/Φ_p have been achieved over a broad range of frequencies. However, the reductions in Φ_π/Φ_p tended to be limited at low frequencies (where n = 1 modes contributed significantly to the radiation) by difficulties in effectively damping the motion of the n = 1 modes. Referring to section 4.3.3, the Q's of pipes with rigid ends were independent of ν (except when damped by acoustic radiation): thus we expect that, on the application of light-weight damping treatments, greater reductions in both $\Phi_{\ddot{w}}/\Phi_p$ and Φ_π/Φ_p than those presently reported would probably be achieved for pipes with rigid ends.

4.8 COMPARISON WITH FAR-FIELD ACOUSTIC EXCITATION

It is of some interest to know for what frequencies and flow speeds, turbulent flow excitation is likely to produce higher levels of radiated acoustic power than an acoustic excitation acting on the wall with the same intensity. As an initial investigation of the relative efficiency of the two excitations, the spectral densities of the acoustic power radiated from the steel test sections, when excited by fully-developed turbulent flow, were compared with those produced by a far-field acoustic excitation in the absence of flow inside the pipe. At low flow speeds, the distribution of acoustic energy across a pipe radius will be relatively unaffected by the presence of flow inside the pipe, although important changes in modal distribution will occur as M_o increases. For steel pipes, no such investigation of the effect of flow on the acoustic energy distribution was made.

On completion of the flow testing of each steel pipe, the sonic choke was replaced by a 30 watt horn driver mounted axi-symmetrically on the pipe axis. An acoustic termination was placed in the pipe inlet. The horn driver was mechanically isolated from the test pipes by the vibration filters described in section 3.2. The excitation was from acoustic propagating waves only. An initial survey determined that, as with excitation

by turbulent flow, the pipes' vibrational responses were resonant and the acoustic power radiation had essentially cylindrical radiation patterns. The theoretical joint acceptance of circumferential pipe modes of order $n \geq 1$ for plane wave excitation is zero, so that only a forced axi-symmetric response is expected for those frequencies where $K_a < 1.83$. However, a strong resonant vibrational response was produced at all frequencies, and this was found to control the radiation for these lightly-damped steel pipes, as discusses in greater detail in Part II. In an analogous situation Wilby (1967) found that similar unpredicted resonant responses occurred for plane-wave excitation of theoretically uncoupled even-order lateral modes of flat panels.

Single point measurements of the vibrational response and acoustic radiation were made at the same pipe and acoustic field positions as for the flow excitation. The intensity of the acoustic pressure field was measured with a flush-mounted B & K 4136 6.35 mm microphone. The spectral densities of the acoustic radiation produced by unit excitation pressure spectral density ϕ_π / ϕ_p, were calculated for both flow and acoustic excitations to give $(\phi_\pi / \phi_p)F$ and $(\phi_\pi / \phi_p)A$ respectively. The relative effectiveness of the flow and acoustic excitations can be found by dividing $(\phi_\pi / \phi_p)F$ by $(\phi_\pi / \phi_p)A$, for each flow speed, to produce an estimate of the relative joint acceptances, X, between the flow and acoustic excitations. These results are shown in Figs. 4.18(a), (b) and (c) for the three steel test sections. As expected from the conclusions of Chapter 2, as the value of $\bar{\nu}_{hc}$ increases, X increases, reflecting the increases in modal joint acceptance as K_c/K_m decreases. X ranges from values greater than 1 at low frequencies, where the turbulent pressure field tends to be more strongly coupled to the pipe vibration modes than the acoustic excitation, to values of $\simeq 10^{-3}$ at frequencies above the ring frequency: X generally varies as $\nu^{-1.5}$, with fluctuations associated with groups of circumferential modes of various n, and with the occurrence of higher-order acoustic cross modes, as shown in Fig. 4.18. At $\nu = 0.11$, the acoustic excitation is strongly

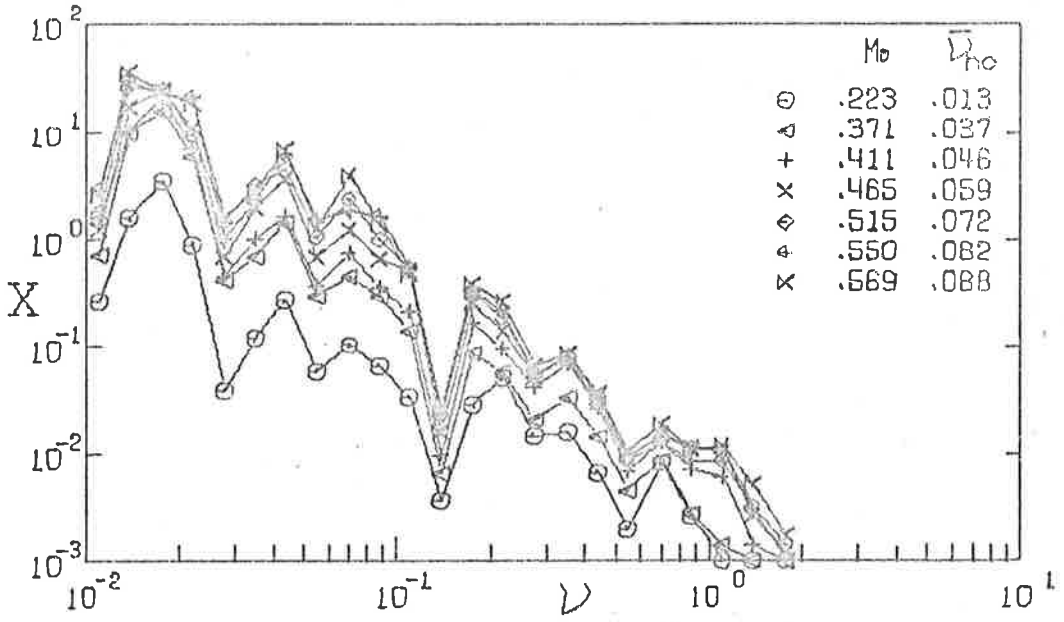

FIG. 4.18(a) X FØR STEEL PIPE NØ 1. $\beta = .00591$

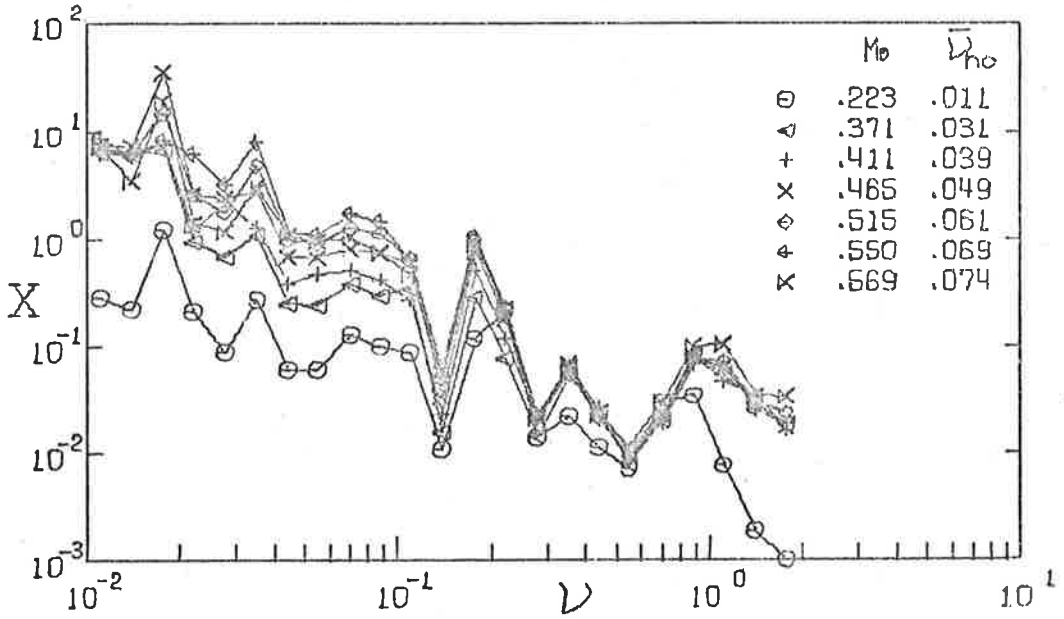

FIG. 4.18(b) X FØR STEEL PIPE NØ 2. $\beta = .0070$

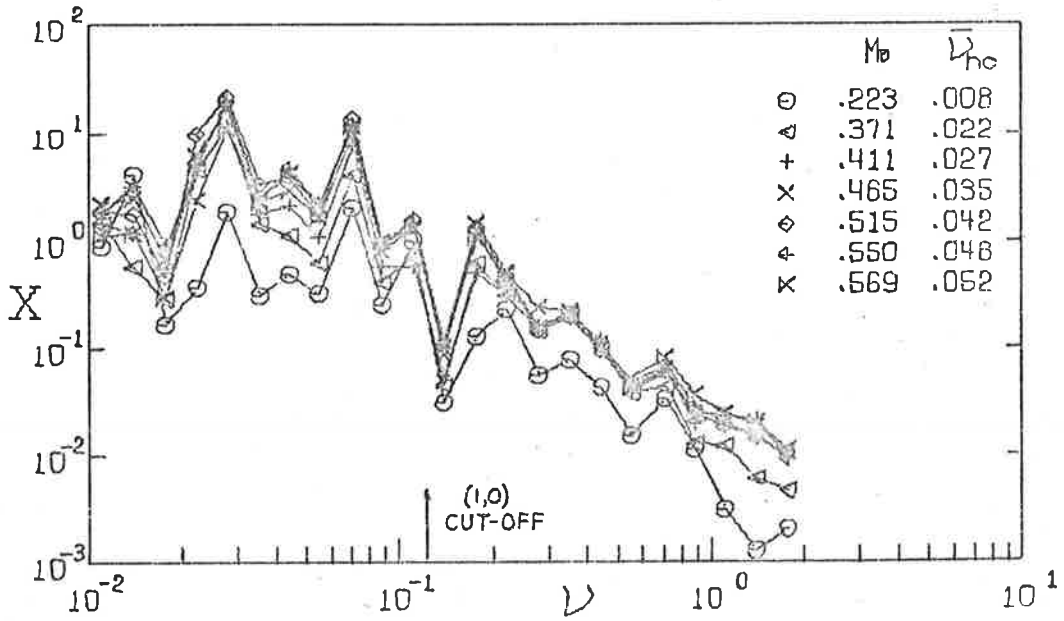

FIG. 4.18(c) X FØR STEEL PIPE NØ 3. $\beta = .0100$

coupled through the (1,0) acoustic mode to the n = 1 structural modes for the various pipes: these are supersonic and will be excited close to acoustic coincidence.

From these results, we see that, at higher frequencies, an acoustic excitation of low intensity relative to the flow excitation may in fact dominate the acoustic power radiation for low $\bar{\nu}_{hc}$. For $K_a >> 2$, the acoustic energy will tend to be equally distributed over many propagating acoustic modes, some of which will be strongly coupled to pipe modes with high radiation ratios (Fahy (1970)). This strong coupling is far greater than that produced by turbulent pressure fields for the same modes for $\bar{\nu}_{hc} << 1$. In such cases ($\chi << 1$), the presence of the acoustic excitation will be difficult to detect from measurements of the cross-spectral density of the wall-pressure field, as discussed in section 4.6. It is likely that, in the present experiments at the lowest flow speed, the measured levels of Φ_{yy}/Φ_p and Φ_{π}/Φ_p contain contributions from low level acoustic excitation.

4.9 SUMMARY

This chapter reported the details of experiments carried out to investigate the vibrational response of and acoustic radiation from steel pipes excited by fully-developed turbulent flow, for conditions such that $\bar{\nu}_{hc} << 2$ and $\bar{\nu}_{ac} < 2$. Measurements of the pipes' modal densities, modal and average quality factors, and vibrational response and acoustic radiation for various flow speeds have been documented, to provide a substantial data base with which theoretical analyses may be compared.

Measurements in one-third octave bands of the modal densities of the three steel test sections have agreed closely over the measurement range ($\nu < 0.2$) with the theoretical modal density curve (equation [2.10]), which is fundamental to the statistical analysis of the response and radiation. The effect of variations in pipe end conditions and of a static pressure differential across the pipe wall on the modal density were

found to be small.

The modal quality factors of the essentially lightly-damped steel pipes were dependent on the type of pipe end condition used and on the modal radiation ratios. For free-free end conditions, the modal quality factors were found to be approximately independent of frequency when acoustic radiation damping was small: when the modal radiation ratios approached unity value, the radiation damping increased and the modal quality factors decreased in close agreement with predicted values. For pipes with rigid end conditions, for all but low axial-order n = 1 modes, the pipe end conditions contributed little additional modal damping over that which existed for the free-free end conditions. On the other hand, with the push-fit joints used in all flow experiments, considerable increases in modal damping occurred, associated probably with the phenomenon of gas pumping in the joints, resulting in curves of modal quality factor possessing a remarkable order: for constant circumferential mode order n, the modal quality factor decreased with increasing frequency, the rate of decrease increasing with n. Measurements in one-third octave bands of average quality factors agreed closely with the arithmetic means of the modal quality factors in the appropriate bands. The measurements for test sections in-situ were used in theoretical preditions.

The measured vibrational response was not only effectively circunferentially homogeneous but also spatially uniform over the pipe surface. Experimental data indicated that the non-dimensional space-averaged spectral density of the wall acceleration Φ_w was proportional to the non-dimensional spectral density of the turbulence wall-pressure field Φ_p; to the average pipe quality factor Q; to the fifth or higher power of the internal flow speed M_o; and to the inverse cube of the pipe wall thickness parameter β. These findings are in substantial agreement with the theoretical predictions of section 2.2.6. Additionally, qualified agreement between experimental and theoretical frequency dependence (the latter based on approximate equations) was found: however, errors varying from 10dB to 20dB between

the detailed statistical predictions and experimental results were found for the present conditions, where $\bar{\nu}_{hc} << 2$ and the Corcos model is used as the model for the cross-spectral density of the wall-pressure field.

Calculations, based on the wavenumber-frequency spectrum of the modal joint acceptance, demonstrated that, for the present condition ($\bar{\nu}_{hc} << 2$), the large theoretical overestimates which occur for the vibrational response of steel pipes to turbulent flow excitation may well result from overestimates in the low-wavenumber domain of the spectral density of the pressure field predicted by using the Corcos model. Considerable experimental evidence exists to show that the Corcos model is not valid for use in conditions far removed from hydrodynamic coincidence. The dependence of the differences between theoretical predictions and the measurements, on frequency and flow speed and β, concur qualitatively and, to some extent, quantitatively with this argument.

Measurements of the acoustic power radiation showed that the radiation field could be considered essentially cylindrically symmetric about the pipe axis. Subsonic vibration modes tended to dominate the power radiation for $\nu < \nu_{ac}$, although the contribution from supersonic modes served as a useful lower bound estimate over the frequencies where such modes existed. Comparisons of the experimental and theoretical radiation ratios clearly illustrated the relative contributions of subsonic and supersonic modes. Measurements of the acoustic power radiation suggested that the non-dimensional radiated power was proportional to $\Phi_p Q_s M_o^5/\beta^n$, where $n \simeq 2$ or 3. Again overestimates of up to 20dB existed between the exact theoretical and measured results, although the frequency dependence was fairly well predicted. These radiation overestimates were proposed to result also from the use of the Corcos model of the cross-spectral density of the excitation.

The application of light-weight damping treatments to the pipe surface produced large reductions in both response and acoustic radiation over a broad frequency range: larger reductions are expected for rigid

end conditions. By comparing the acoustic radiation spectral densities from the steel pipes for unit flow- and unit acoustic-excitation spectral densities, the wall-pressure field associated with turbulent pipe flow was seen to be more efficient in generating acoustic radiation at frequencies below the first acoustic cross mode inside the pipe than acoustic pressure fields, for the range of $\bar{\nu}_{hc}$ tested: for higher frequencies, however, acoustic pressure fields were progressively more strongly coupled than turbulence pressure fields.

CHAPTER 5

EXPERIMENTS WITH A BRASS PIPE

5.1 INTRODUCTION

In the present chapter, an experimental examination of the effects of hydrodynamic coincidence on the vibrational response and the acoustic power radiation from a thin-walled pipe is described. For hydrodynamic coincidence to occur at all requires $\bar{\nu}_{hc} \geq 2$. As M_o is always subsonic over the test section length of the induced-flow rig, it is necessary that $\bar{\nu}_{ac} \geq 2$ to achieve coincidence; consequently case 3, but not case 4, of section 2.2.8 may be achieved with the present experimental arrangement.

A brass tube with $\beta = 0.00044$ was constructed, so that, for the available range of flow speeds at the downstream end of the rig, $0.35 \leq \bar{\nu}_{hc} \leq 2.63$: i.e. hydrodynamic coincidence will occur, although only for the higher flow speeds. Also $\bar{\nu}_{ac} = 19.80$: thus, $\bar{\nu}_B$ and $\bar{\nu}_A$ are real and equal to 1.001 and 19.78 respectively. Accordingly, there will be no supersonic modes within the frequency range, $0.93 < \nu < 18.37$. Since no supersonic modes exist below $K_a \simeq 1$ and $\nu = 18.37$ lies well above the measurment range, the statistical analysis predicts that acoustic radiation will occur only for $0.091 < \nu < 0.93$. Since hydrodynamic coincidence can occur for subsonic (nonradiating) modes only, Φ_π/Φ_p should depend on the fifth power of the flow speed, in contrast to $\Phi_{\ddot{w}}/\Phi_p$ which may depend on some higher power of the flow speed.

5.2 EXPERIMENTAL APPARATUS

The test section was constructed from two sheets of brass shim material of thickness, $h = 0.056$ mm. Brass was chosen since it has consistent material properties with lower M_{Lp} than steel, is lightly damped (in contrast

to P.V.C.), and may be readily worked to form a joint. The thin-walled tube was formed over a cylindrical mould to produce the desired internal diameter. Each joint was butt-soldered, lapped with a 6 mm brass shim strip, and then polished to reduce the surface inhomogeneity. The tube was glued with araldite into two end flanges, and locked into a rigid supporting brace which fitted into the test rig, as shown in Fig. 5.1. All internal surface imperfections at the glued and soldered joints were carefully removed, although flexing of the experimental rig and laboratory temperature variations produced 'wrinkles' in the pipe surface.

The supporting brace was enclosed within a small airtight box, whose interior walls were lined with fibreglass (100 mm thick) to provide a free-field environment around the pipe. A vacuum pump and manometer were connected to the box to provide for partially evacuating the volume surrounding the pipe, in order to pre-tension the brass pipe as a precaution against collapse during experiments. Prior to starting an experimental run, the box pressure was sufficiently reduced to maintain a static pressure differential acting to tension the pipe wall under the flow conditions. Microphones, attached to the brace in the manner shown in Fig. 5.1, allowed measurements of the intensity of both near- and far-pressure fields to be made. These measurements were recorded using the Real Time Analyser as described in section 3.3.4.

5.3 MODAL DENSITY AND QUALITY FACTORS

An investigation of the modal density of the brass pipe was attempted. An electromagnet was used to drive the pipe, while the wall response was monitored with a B & K 4133 12.7 mm microphone mounted 1 mm from the pipe wall. A Beat Frequency Oscillator and Level Recorder were used to sweep the electromagnetic excitation slowly through frequency to produce a response-frequency plot: resonance frequencies were detected aurally and by sharp variations in the response plot. Experimental problems, associated with high modal overlap and large drifts in resonance frequency

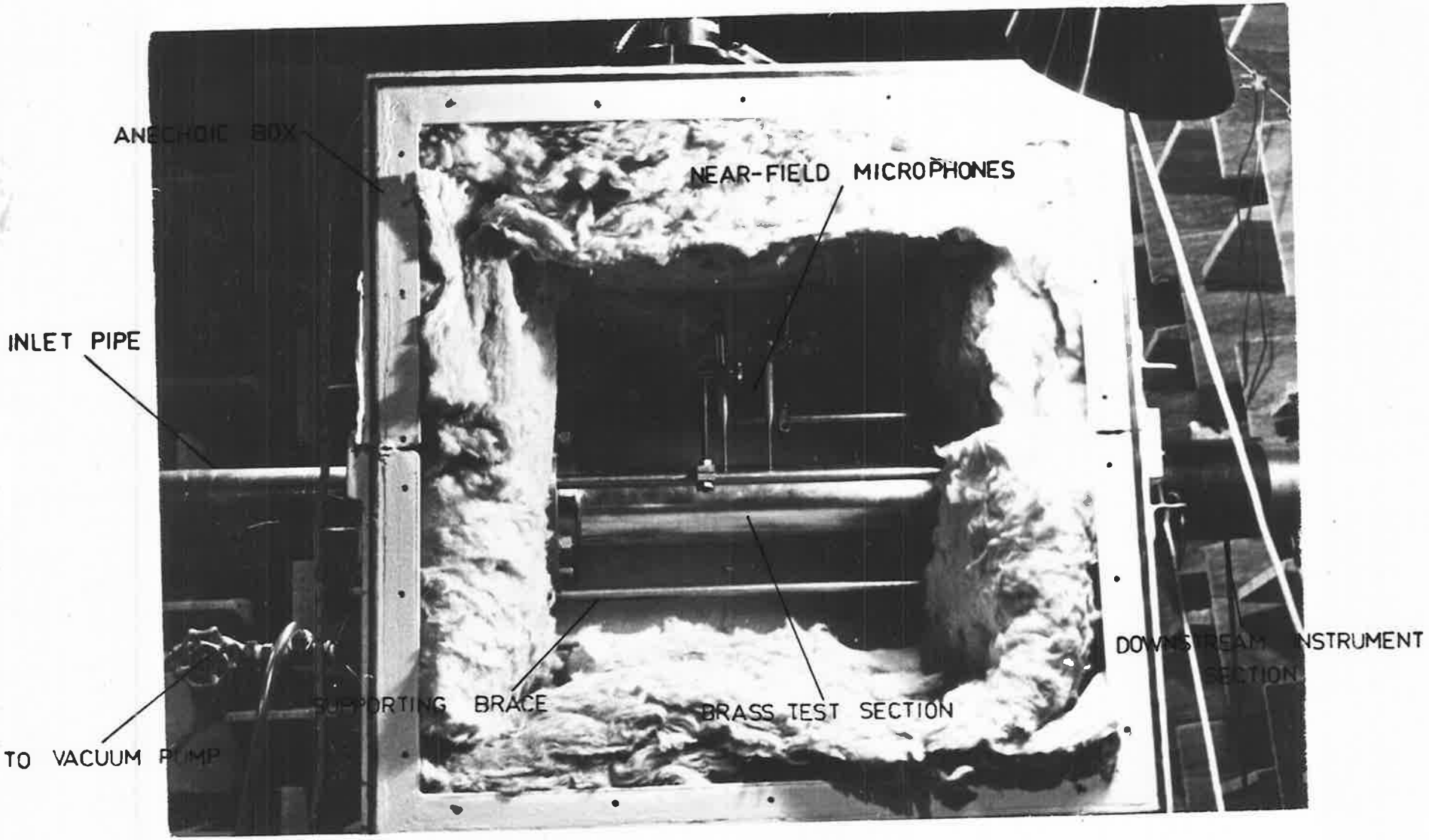

FIG. 5.1 BRASS TEST PIPE MOUNTED IN FLOW RIG

during the measurement process, prevented the determination of the order of most of the resonant modes even at relatively low frequencies. Measurements, made of the resonance frequencies of the more isolated resonant modes, agreed closely with predictions from Arnold and Warburton (1953). The low frequency modal density was established by counting the number of resonance frequencies occurring in one-third octave bands: non-dimensionalised results are shown in Fig. 4.1. Close agreement exists between the data and the theoretical curve, and the frequency variation is much smoother than for the steel pipes, although the experimental data tend to exceed the theoretical estimate by approximately 10%. The effect of a static pressure differential Δp on the modal density could not be determined experimentally, since it was not possible to maintain Δp with sufficient stability. However, calculations, based on the work of Fung, Sechler and Kaplan (1957) of the changes in modal resonance frequencies produced by the experimental Δp's, predict little variation in the density of supersonic modes for the range of experimental conditions encountered.

Measurements of one-third octave band averaged and, where possible, modal quality factors were made using the response-decay method, where a near-field microphone was used to sense the wall vibration. The effect of small Δp's on the average quality factors is presented in Fig. 5.2. At low frequencies, Q increases with increasing Δp in a manner which appears to be associated with the shift in resonance frequencies of lightly-damped modes of high circumferential order. For $\nu > 0.3$, Q becomes independent of the applied Δp. The quality factors of the identifiable modes are consistent with the average values.

Values of Q and Q_s, as used for theoretical calculations, are shown in Fig. 5.2: Q represents the mean of the experimental data for low Δp, while values of Q_s, the quality factors of supersonic modes, have been calculated from equation [2.37].

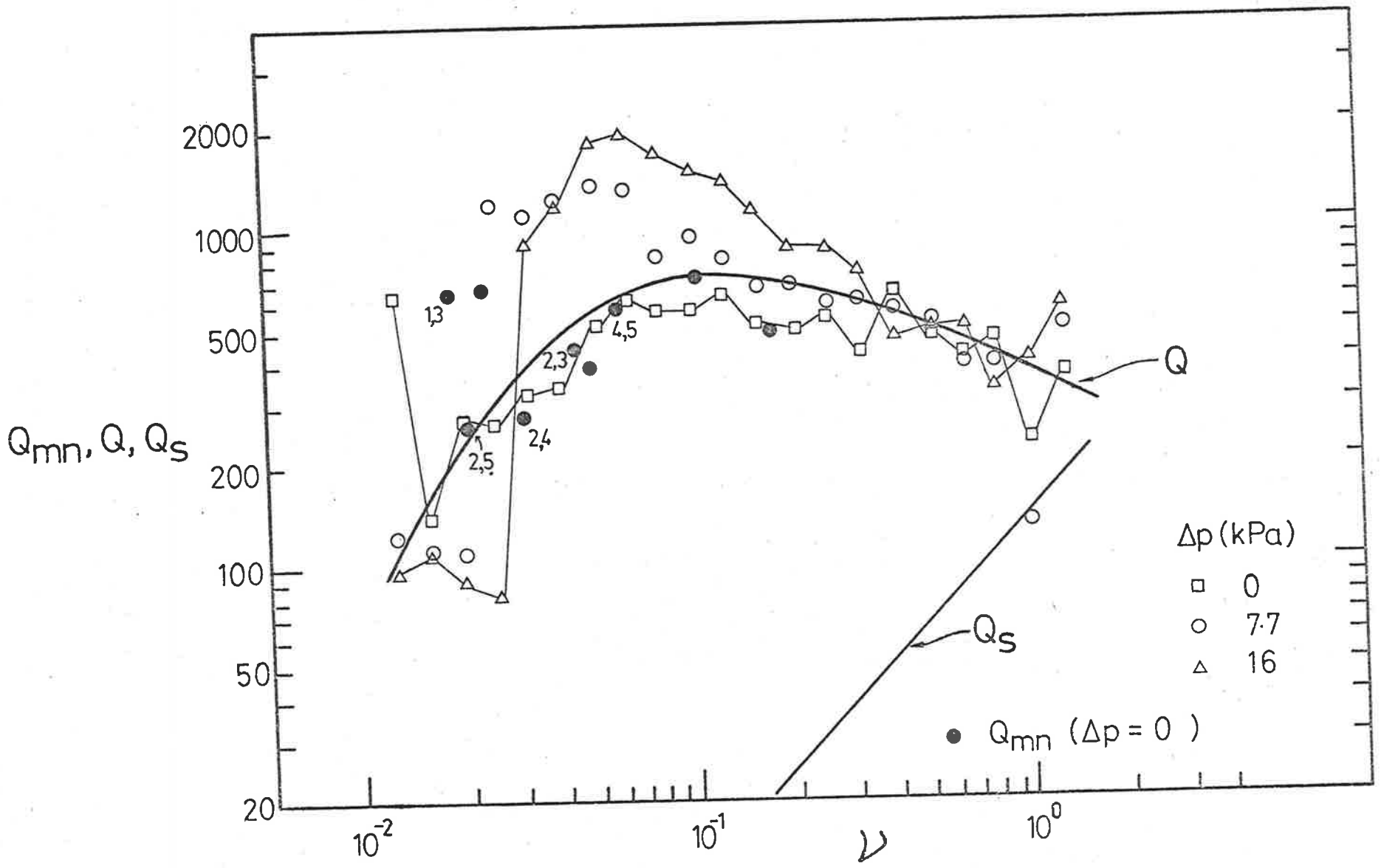

FIG. 5.2 QUALITY FACTORS OF BRASS PIPE No. 5 β =0·00045

5.4 ACCELERATION RESPONSE

5.4.1 Introduction

For the present pipe flow configuration, hydrodynamic coincidence is predicted to occur for the higher flow speeds. Coincident modes, which will exist for all $\bar{v} < \bar{v}_{hc}$ for $\bar{v}_{hc} > 2$, respond both as forced running waves, travelling downstream, and as standing waves. At coincidence, an amplification in vibrational response is expected. This is predicted from the joint acceptance expressions and is therefore included in the statistical analysis (equation [2.20]). The assumptions made in deriving the approximate expression (equation [2.29]) consider that coincidence may not occur: consequently, for the present case, the dependence of the vibrational response on flow speed is expected to be stronger than M_o^5 as predicted by the equation [2.29].

Measurement of the vibrational response of the brass pipe was performed with non-contacting transducers, to avoid the mass-loading problems associated with the use of accelerometers on light-weight structures. An available capacitance-type displacement probe was too bulky for use inside the small anechoic box. However, measurements of the near-field pressures with a 12.7 mm microphone were found to be proportional to the brass pipe wall accelerations, providing the distance between the pipe surface and the microphone diaphragm was much less than an acoustic wavelength. A microphone, placed close to the pipe wall, was used for wall acceleration measurements.

5.4.2 Near-field Pressure Measurements

The practicality of using a microphone located in the near pressure field of the brass pipe to measure the wall accelerations was examined by comparing the output of a capacitance-type displacement probe, located a constant distance from the pipe wall, with that of a near-field microphone. The calibrated displacement probe, which gave an output proportional to the displacement of a vibrating object, was placed at

the calibration distance (0.375 mm) from the pipe wall, and a B & K 4133 12.7 mm microphone was positioned a fixed distance h'(=1 mm) from the pipe wall, axially adjacent to the displacement probe. (It had been found that the pipe response was spatially uniform.) The brass pipe was excited both electromagnetically and acoustically (by the efflux from an air valve inside the pipe), for different static pressure differentials existing across the pipe wall. The near-field pressure measurements made with the microphone were found to be directly proportional to the pipe accelerations and independent of the excitation method or the static pressure differential used, at least for $\nu < 0.4$, for $h' = 1$ mm. As h' increased, so the frequency range over which the pressure was proportional to the wall acceleration decreased, as did the sensitivity of the method. The errors were controlled by the accuracy with which the microphone could be re-positioned relative to the brass pipe wall during the flow experiments: the resulting measurements are believed accurate to within $\pm$ 3dB for $0.05 < \nu < 0.8$.

Microphones of different diameter (B & K 4133 12.7 mm, B & K 4136 6.35 mm, and B & K 4138 3.25 mm) were found to yield essentially the same near-field pressure spectra for the same h' in each case, except for $\nu > 1$ when the measured spectra decreased as the diaphragm diameter increased, the result of differing phase variations in acoustic pressure across the microphones' diaphragms. It is concluded that fair estimates of the pipe wall accelerations over the whole frequency range of interest can be made using a near-field microphone as a transducer.

The effects of a static pressure differential Δp across the pipe wall were investigated by monitoring the changes in near-field intensity produced by variations in Δp for acoustic excitation from inside the pipe, where the internal excitation SPL was used as the reference level. The near-field intensity was proportional to the wall acceleration level, at least for low ν, and reflected the behaviour of all resonant modes, rather than solely the radiating modes as with far-field measurements. The applied Δp's produced significant increases in the resonance frequencies

of non-radiating modes, so that a well ordered dependence on Δp was not always found, as was the case for the far-field pressures (see section 5.5). In general, reliable estimates of the effect of Δp on the pipe wall accelerations have been possible using this method: the required corrections were found to be less than 2dB for $\nu > 0.4$.

5.4.3 Spectral Characteristics - comparisons between theoretical predictions and experimental data

The experimental non-dimensional acceleration spectral densities of the brass test section, non-dimensionalised by values of Φp from Fig. 3.6, are presented in Fig. 5.3 for the flow speeds tested in the present experiment. The experimental data have been corrected for the effects of the various Δp's, as described previously.

At low frequencies $\nu < 0.15$, several prominent peaks in $\Phi_{\ddot{w}}/\Phi_p$ occur, even though the curves of experimental modal density and Q are smooth functions of ν. These measured variations are probably associated with the differing effects of Δp on modal quality factors and resonance frequencies for different circumferential order modes. For $\nu > 0.1$ and for the higher flow speeds, the curves of $\Phi_{\ddot{w}}/\Phi_p$ increase with ν, and a broad but pronounced peak in $\Phi_{\ddot{w}}/\Phi_p$ exists near the ring frequency for each M_o, reflecting the theoretical modal density maximum and response amplification which are predicted to occur at $\bar{\nu} = 1$. The spectral levels increase with M_o, although some intersection between different curves is found for $\nu < 0.3$.

For $M_o < 0.52$, coincidence will not occur. The measured acceleration spectral densities for the three lower values of M_o may reasonably be expected to depend on the fifth power of the flow speed, as suggested by equation [2.29], while the data for $M_o > 0.52$ should depart somewhat from this. The experimental dependence of $\Phi_{\ddot{w}}/\Phi_p$ on M_o is examined by replotting the data for all M_o in the form suggested by equation [4.1]. This is shown in Fig. 5.4(a), where values of Q have been taken from Fig. 5.2: the curve of the approximate analysis is included for comparison. While a certain

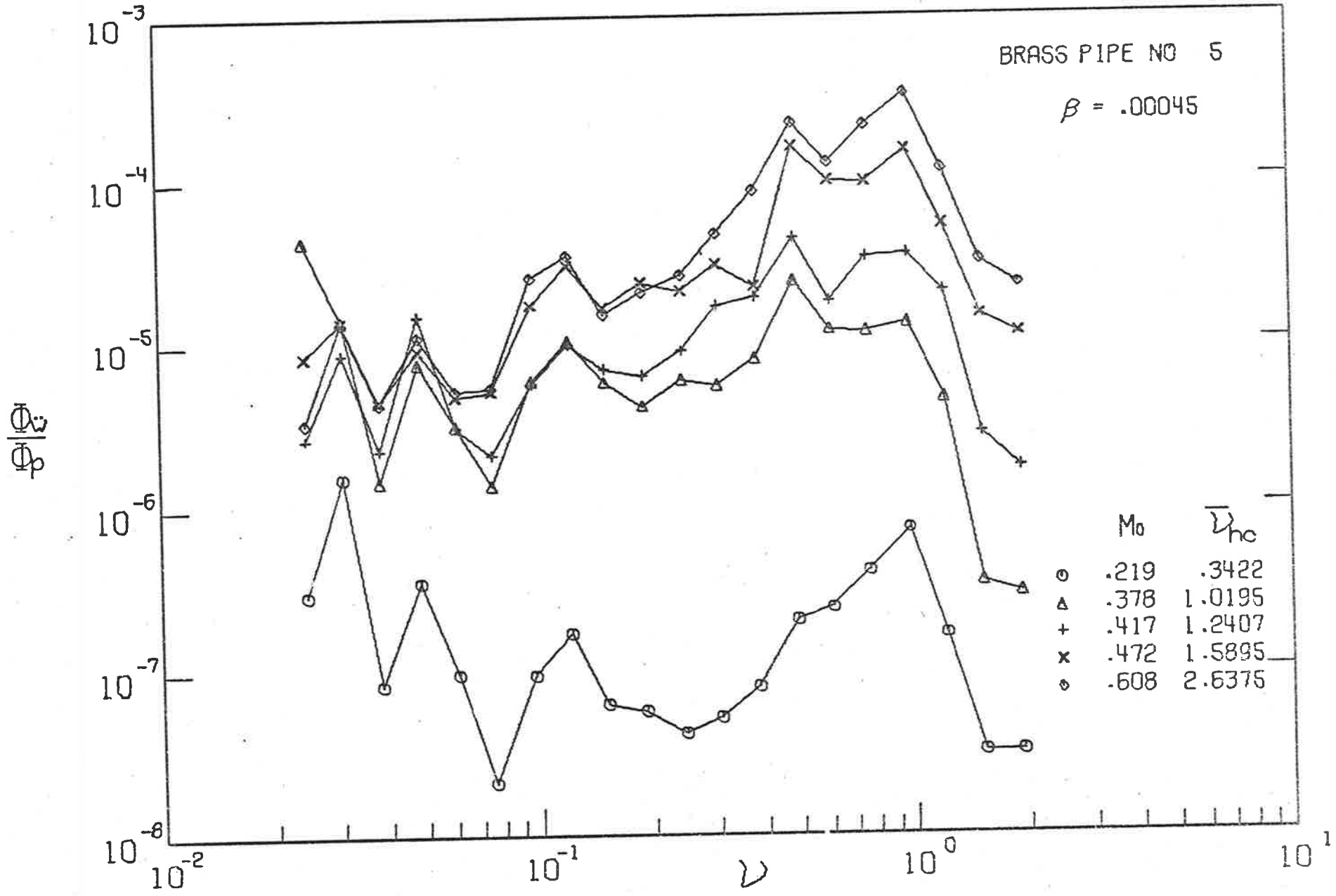

FIG. 5.3 $\Phi\ddot{w}/\Phi_p$ FOR VARIOUS M_o. BRASS PIPE β=.00045

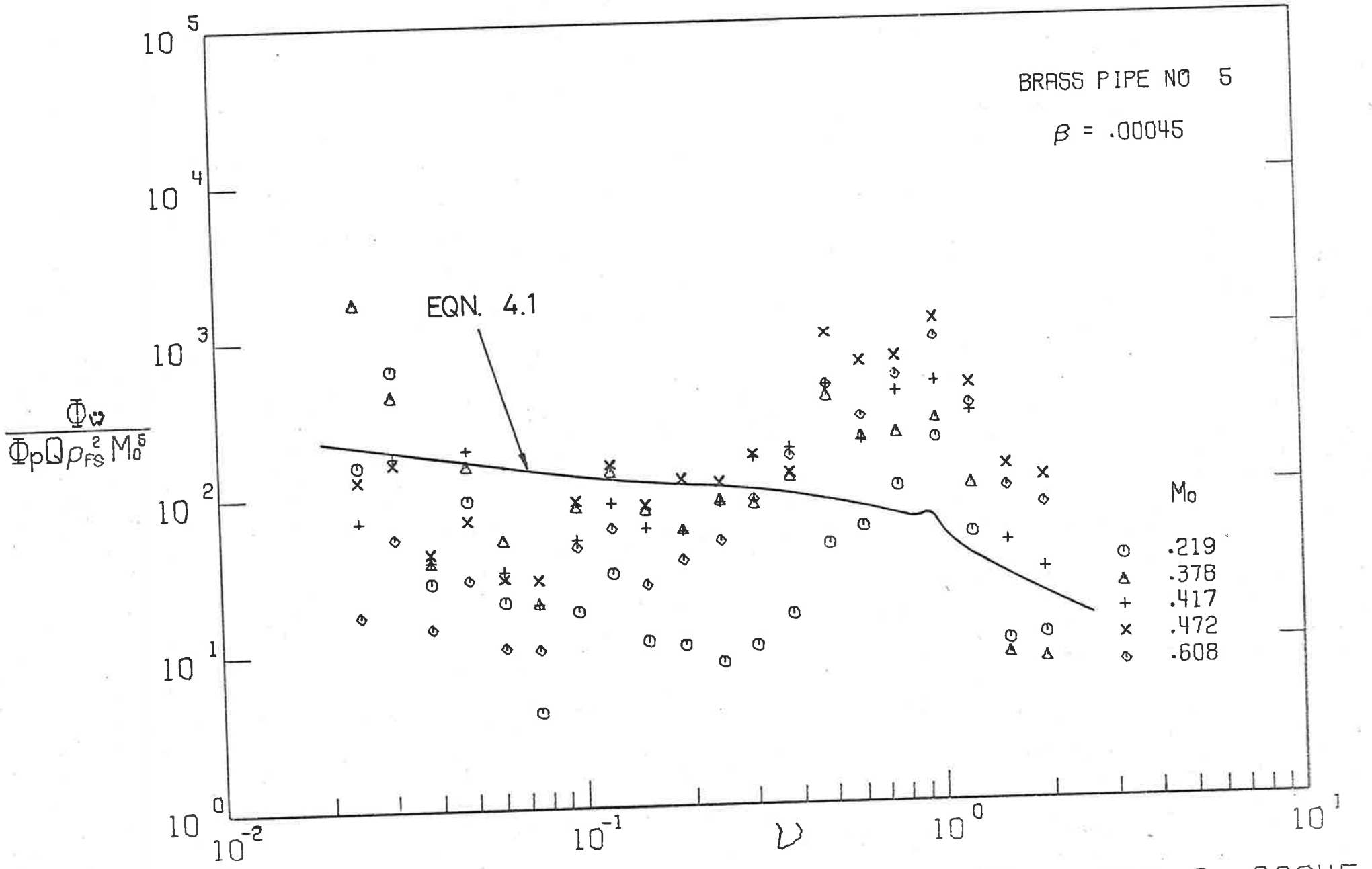

FIG. 5.4(a) EFFECT OF FLOW SPEED ON Φ_w/Φ_p. BRASS PIPE β=.00045

scatter exists, the agreement with the approximate theoretical expression is fair over the whole frequency range. A better collapse may be produced for $\nu > 0.1$, however, by re-plotting the data in the form $\Phi_{\ddot{w}}/(\Phi_p Q \rho_{fs}^2 M_o^7)$, as shown in Fig. 5.4(b): an approach to hydrodynamic coincidence raises the dependence on $\Phi_{\ddot{w}}/\Phi_p$ on M_o above M_o^5, although the exact dependence is not clear from this work.

A more detailed comparison is presented in Fig. 5.5, where calculations from the statistical analysis (equation [2.20]) are given for three flow speeds; values of Q from Fig. 5.2 have been used. Generally, the experimental data agree well with theoretical predictions. This is especially true for $\nu \simeq 1$ where Δp corrections are minimal, and for $\nu \lesssim 0.4$ where the measurements are most accurate. For $M_o = 0.219$ for $0.08 < \nu < 0.4$, the experimental data are $\simeq$ 10dB less than the theoretical estimate, while for $M_o = 0.371$ and 0.472, close agreement occurs for all frequencies. The discrepancies result in part from errors in the model of the turbulence pressure field, which are important for $\bar{\nu}_{hc} << 2$ (see section 4.6). Computations of $\Phi_{\ddot{w}}/\Phi_p$ using the exact analysis (equation [2.30]) agree closely with those using the statistical approach, which are shown in Fig. 5.5. It is concluded that for situations involving an approach to coincident conditions, close estimates of the structural response may be made using the statistical analysis presented in Chapter 2.

5.5 ACOUSTIC RADIATION

The brass pipe is lightly damped and its response to turbulent flow excitation was expected to be controlled by its standing wave response. Considering the absorptive properties of the box liner, the resulting acoustic radiation was assumed to have a cylindrical radiation pattern, especially for frequencies where supersonic modes exist. No examination of the directivity was undertaken since each re-positioning of the microphone required dismantling the anechoic box. For acoustic power measurements, the microphone was mounted at the mid-span position and 135mm from the pipe axis; this point was considered

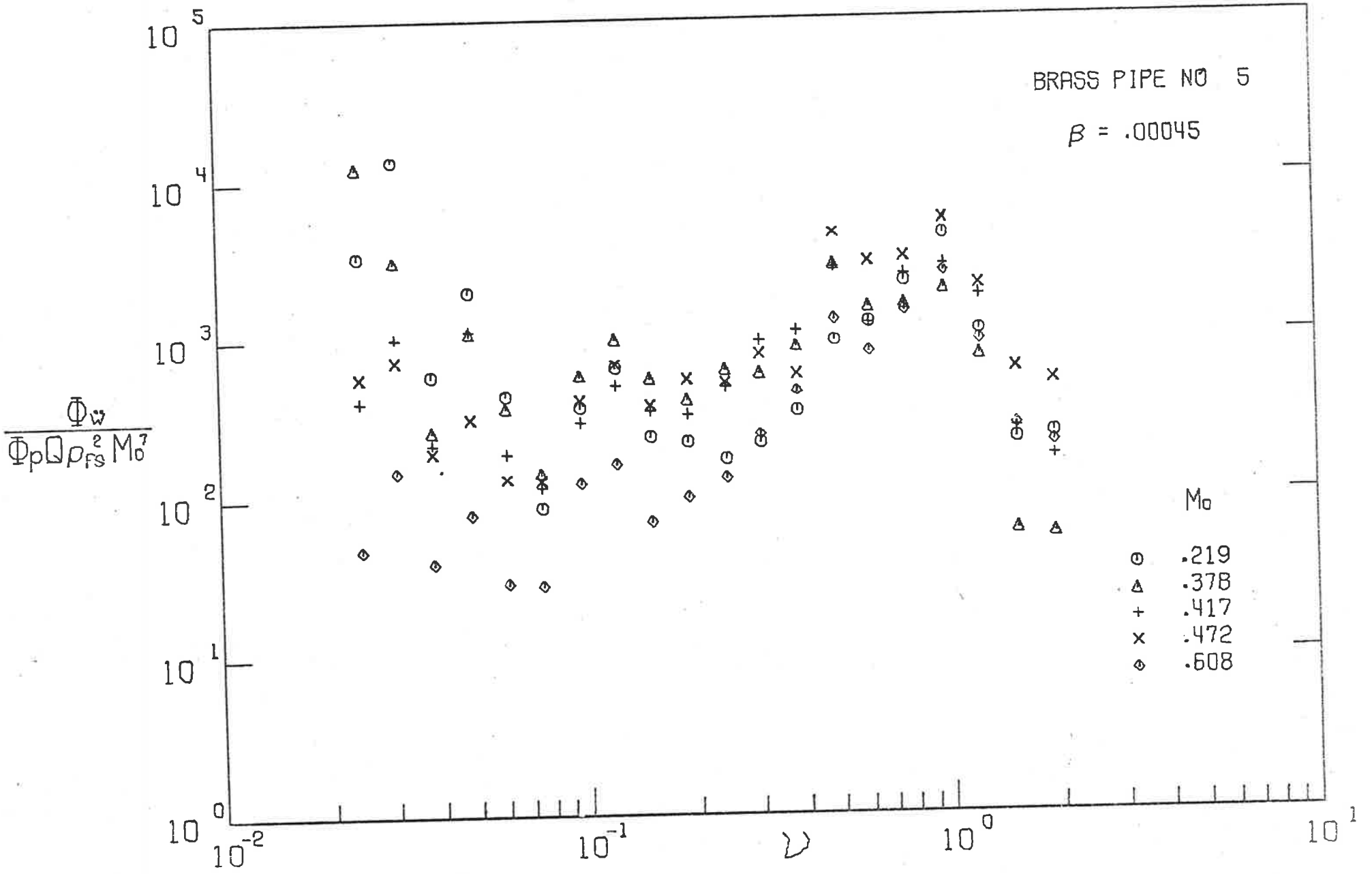

FIG. 5.4(b) EFFECT OF FLOW SPEED ON Φ_w/Φ_p. BRASS PIPE β=.00045

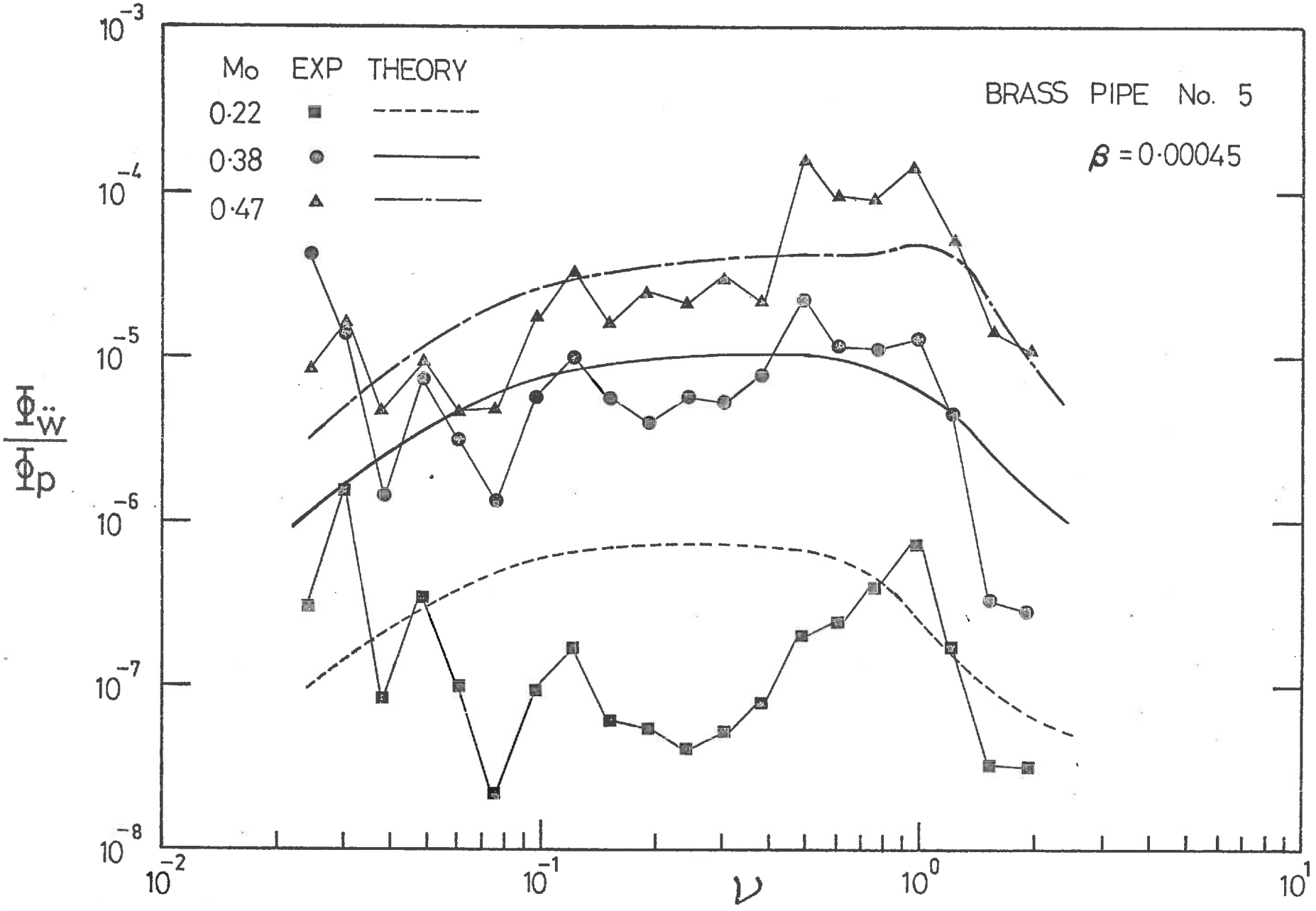

FIG. 5.5 $\Phi_{\ddot{w}}/\Phi_p$ — COMARISON OF EXPERIMENT & THEORY — BRASS PIPE

to lie in the radiation far-field for $\nu > 0.05$. Two pipes of the same dimensions and construction were tested. After a series of successful tests at different flow speeds, the first collapsed during flow excitation while the effect on the acoustic radiation of reducing the pressure differential Δp across the pipe wall was still being examined. The second test pipe produced essentially the same radiated power levels, but only the results for this latter pipe are presented.

The effect on the acoustic power radiation of variations in Δp is shown in Fig. 5.6 for two flow speeds. Φ_π/Φ_p decreases as Δp increases, although the reductions are greatest at low frequencies. This behaviour suggests that the pipe damping increases with increasing Δp for flow excitation. This interpretation agrees with the observations of Davies (1971), (who used similar flow speeds and panel thicknesses) but is contrary to the Q variations described in section 5.3. The results of Fig. 5.6 have been extrapolated to zero pressure differential to determine the corrections to the measurements of Φ_π/Φ_p which are required to remove the effect of Δp. The corrected experimental data are shown in Fig. 5.7 for the range of flow speeds tested. The spectral densities Φ_π/Φ_p exhibit the high-frequency cut-off in acoustic radiation for $\nu > 1$, discussed in the introduction; in contrast, considerable radiation is produced by subsonic modes ($n = 2$) at low frequencies (compare with steel pipes). The range of supersonic modes is shown, together with the predicted location of the more efficient, low-frequency subsonic modes.

It has been proposed that, for subsonic flow speeds, the acoustic radiation from pipes will depend on the fifth power of the flow speed. For the two higher flow speeds, $M_o = 0.472$ and 0.608, hydrodynamic coincidence will occur but only for subsonic modes. The data are re-plotted as $\Phi_\pi/(\Phi_p Q_s \rho_{fs}^2 M_o^5)$ (equation [4.5]) in Fig. 5.8 to examine the experimental dependence on flow speed where values of Q_s are calculated from equation [2.37] The resulting collapse is fair, but indicates that subsonic modes contribute

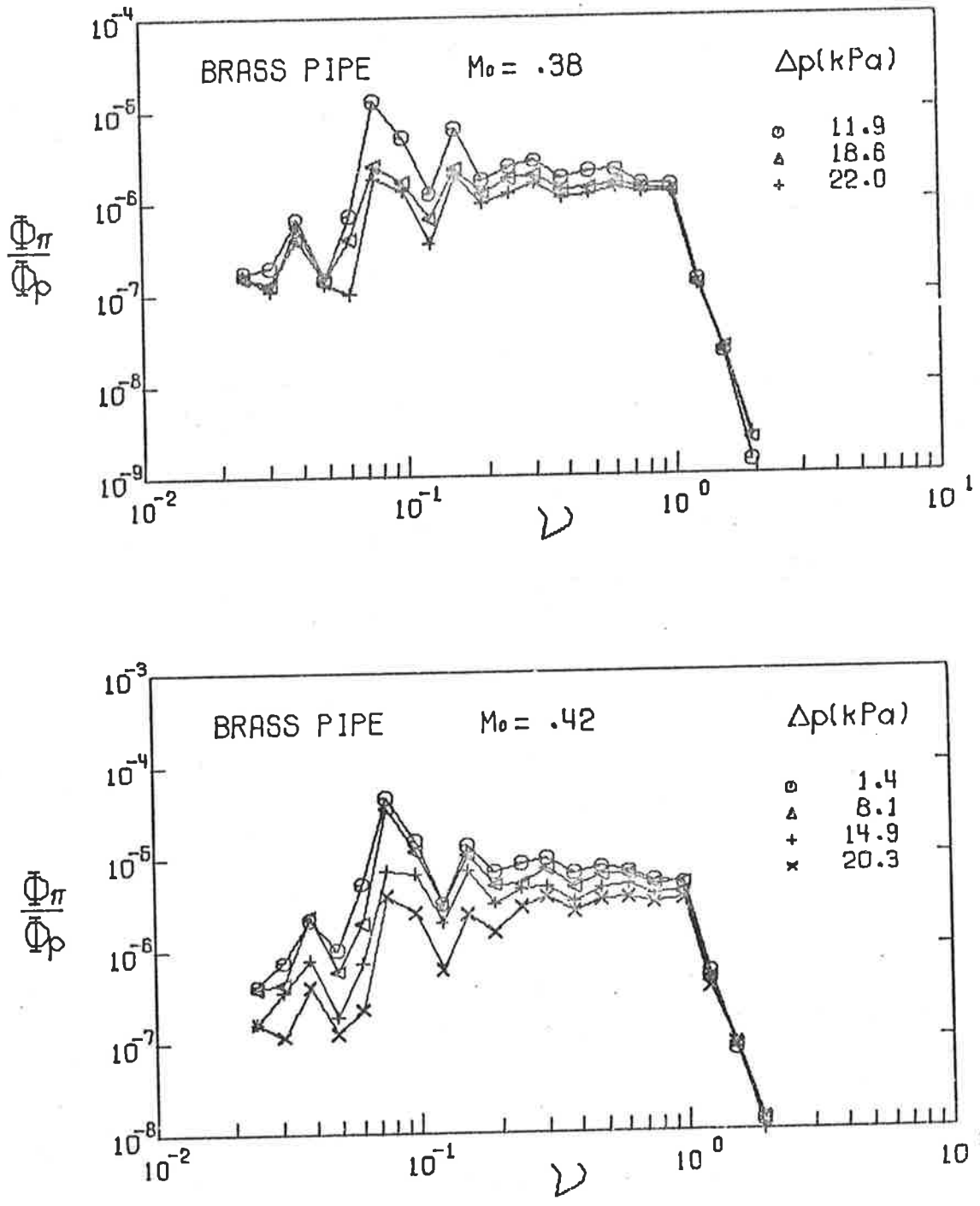

FIG.5.6 EFFECT OF PRESSURE DIFFERENCE ON Φ_π

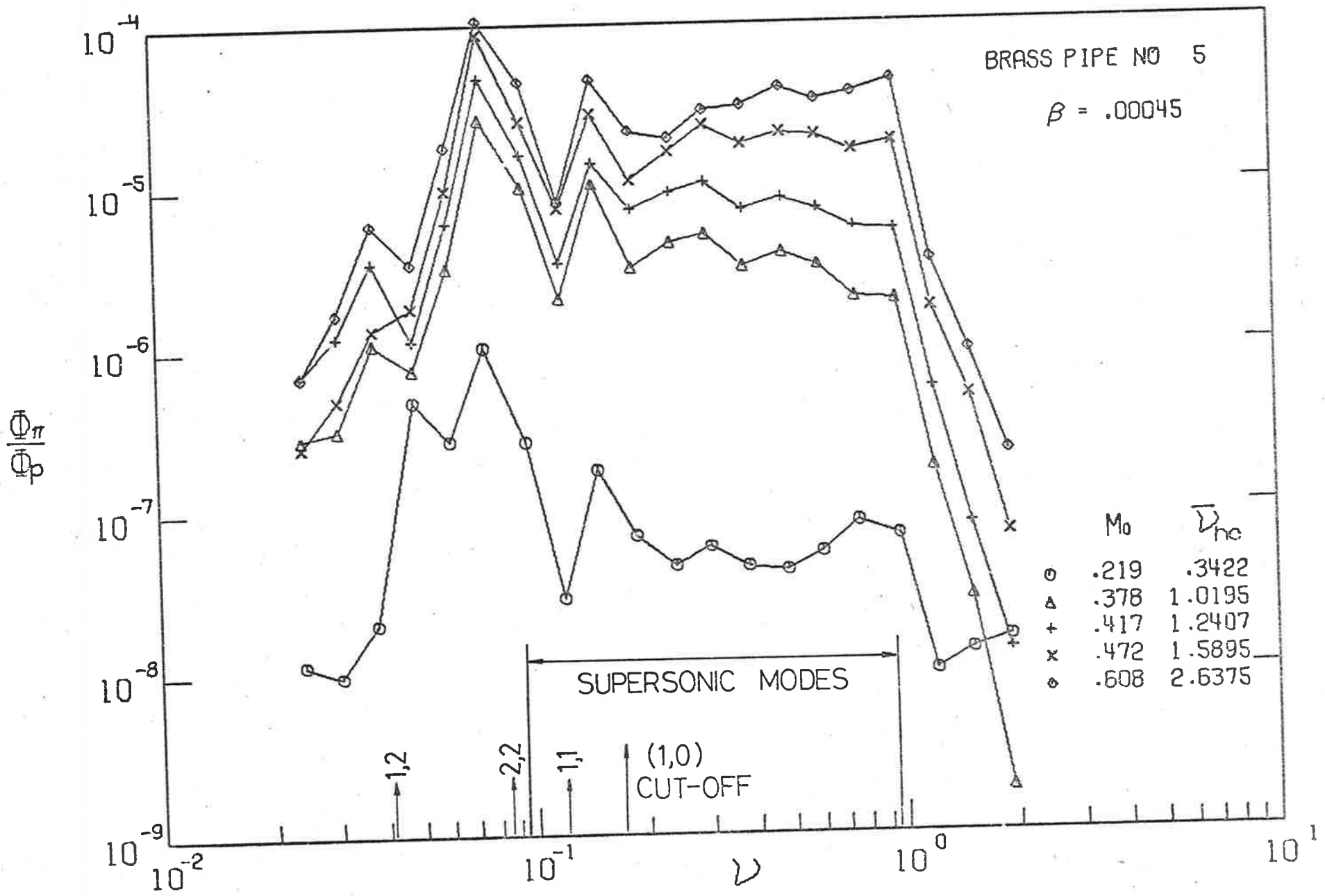

FIG. 5.7 Φ_π/Φ_p FOR VARIOUS M_0 . BRASS PIPE β= .00045

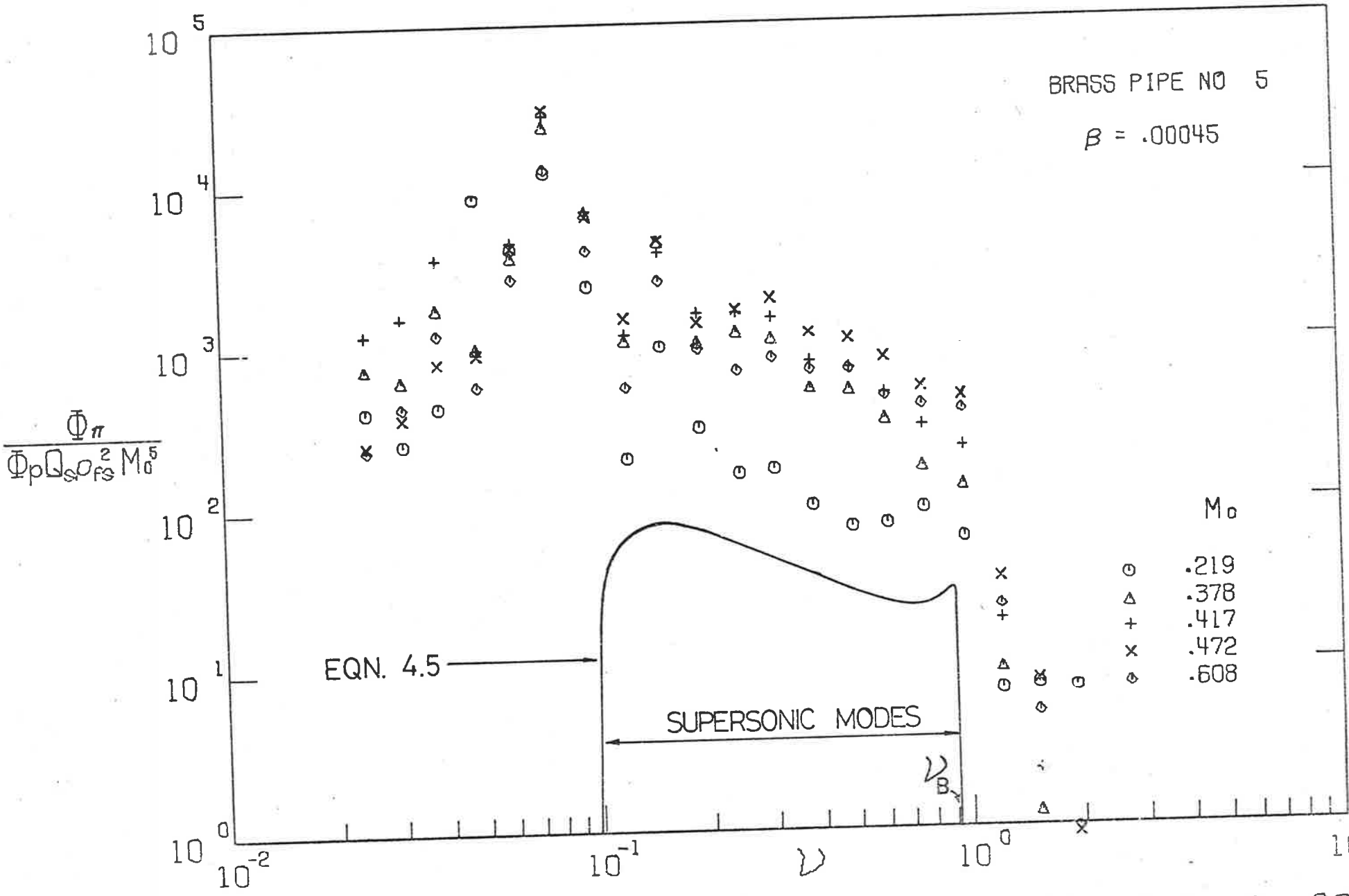

FIG. 5.8 EFFECT OF FLOW SPEED ON Φ_π/Φ_p. BRASS PIPE $\beta = .00045$

significantly to the acoustic power radiation; the data for $M_o = 0.22$ are inconsistent with those for other flow speeds. The theoretical approximation (equation [4.5]) is also shown. Over the range of supersonic modes, the theory underestimates the experimental results by from 10 to 15dB. These differences result both from approximations made for the joint acceptance and from acoustic radiation from subsonic modes. For frequencies below the first supersonic mode, subsonic modes radiate high levels of acoustic power: on the other hand, the radiation cut-off at $\nu \simeq \nu_B$ is well predicted.

Comparisons of the experimental results with the statistical calculations from equation [2.22] (which contains no approximation for the joint acceptance) are shown in Fig. 5.9 for several flow speeds spanning the experimental range. Values of Q_s from Fig. 5.2 have been used in these theoretical calculations. Over the frequency range of supersonic modes, where the statistical theory applies, generally poor agreement is found. While the theoretical cut-off in acoustic radiation at high-frequency ν_B is well-predicted, considerable radiation seems to be produced by subsonic modes over the whole frequency range. This contribution can be predicted with the exact analysis from equation [2.34]. This is shown in Fig. 5.10 for $M_o = 0.378$, where the exact and statistical analyses are compared. The experimental variation of Φ_π/Φ_p with ν in Fig. 5.9 is closely predicted by the exact analysis in Fig. 5.10. Generally, the exact summation need only be carried out over the more efficient (lower n) modes, but must certainly not be restricted to only those modes which are supersonic, as in the statistical approach. The subsonic modes are seen to be responsible for the majority of the acoustic radiation at all frequencies, even though their radiation ratios are low; i.e. $10^{-3} < \sigma < 10^{-1}$.

Comparisons of the experimental radiation ratios for the brass pipes with the theoretical predictions are made in Fig. 5.11. The various experimental curves are seen to be independent of M_o, which is consistent with the finding that subsonic modes control the radiation, but contrary to the exact statistical predictions. The average values of σ are usually less

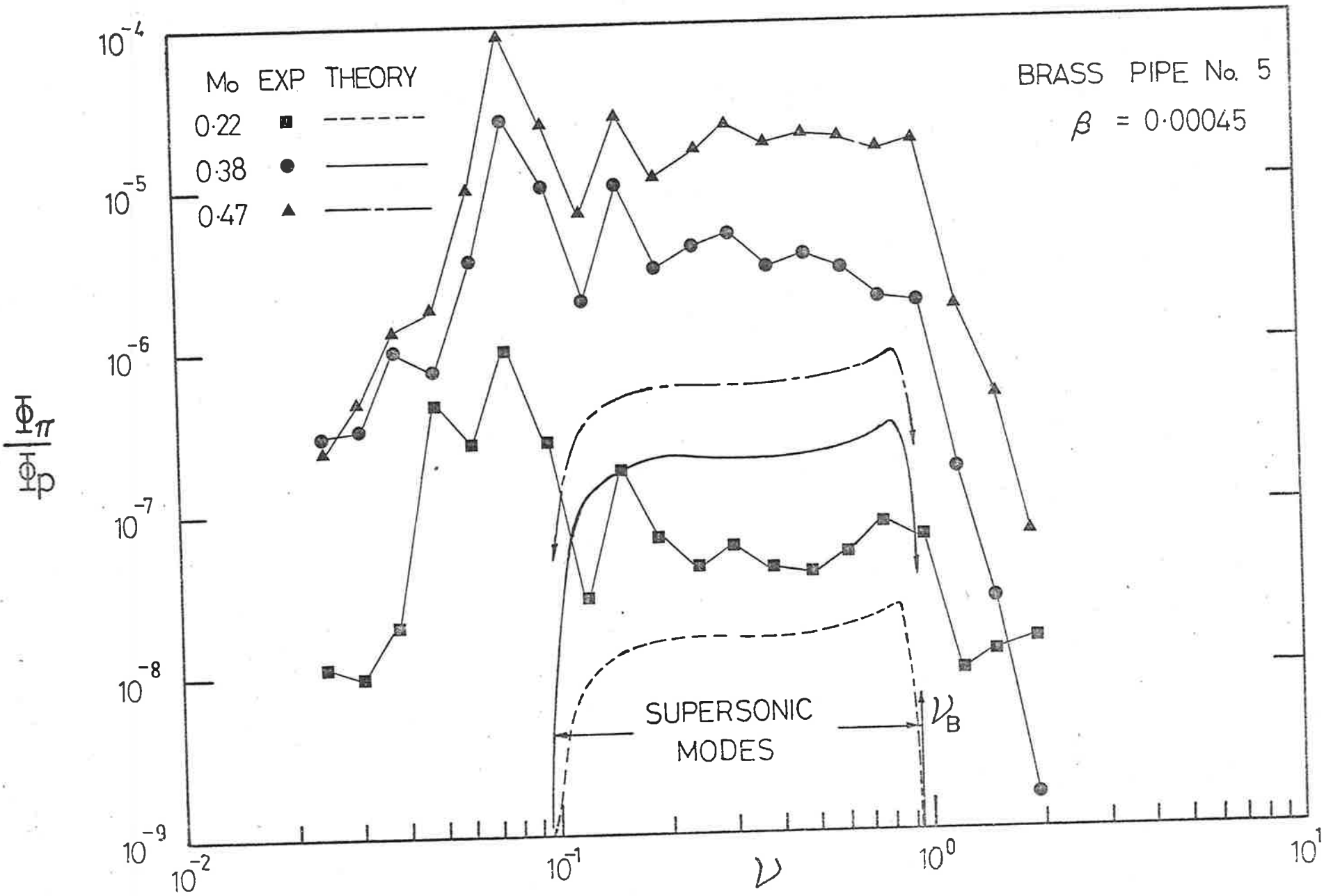

FIG. 5.9 Φ_π/Φ_p — COMPARISON OF EXPERIMENT & THEORY — BRASS PIPE

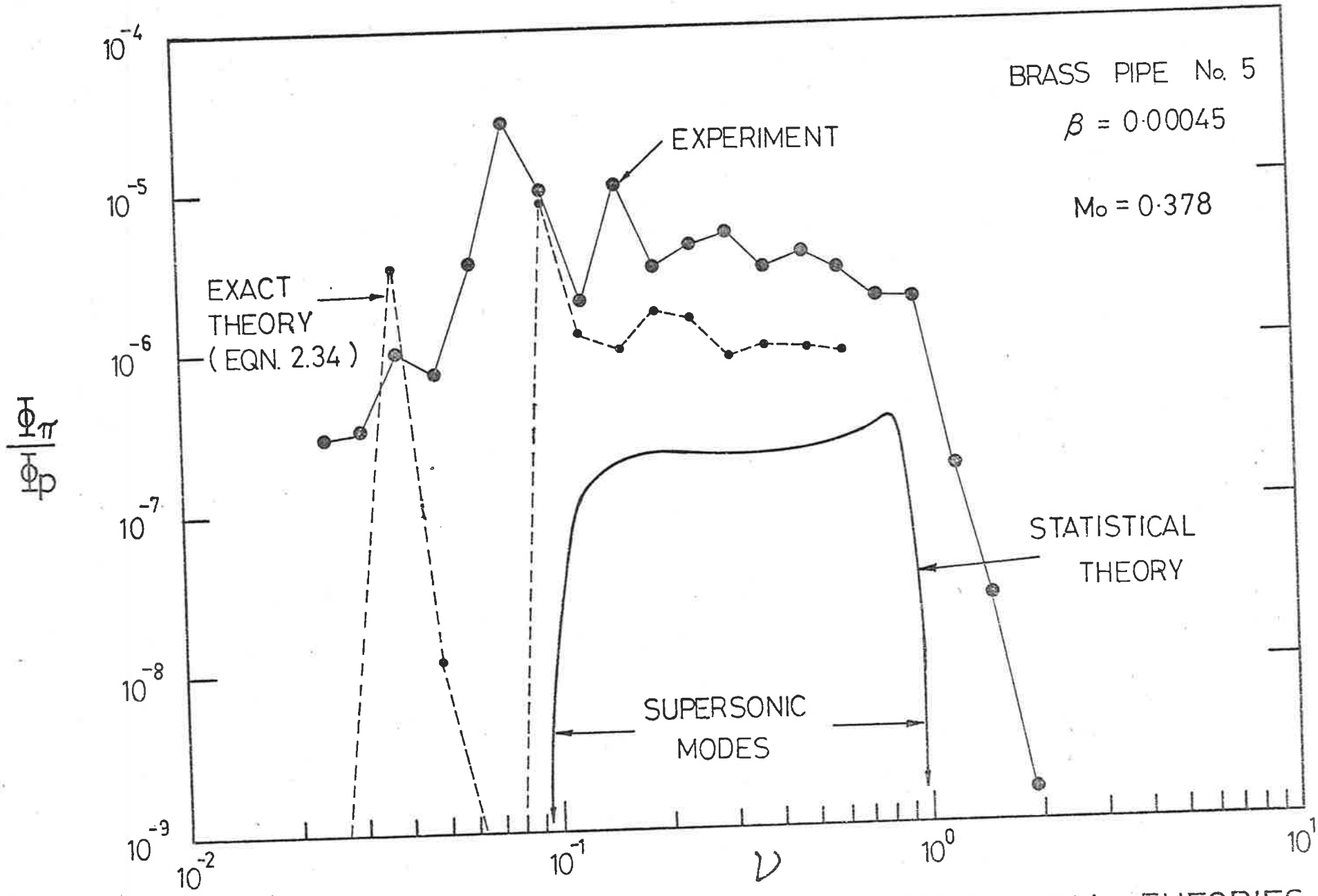

FIG. 5.10 Φ_π/Φ_p — COMPARISON OF EXACT & STATISTICAL THEORIES

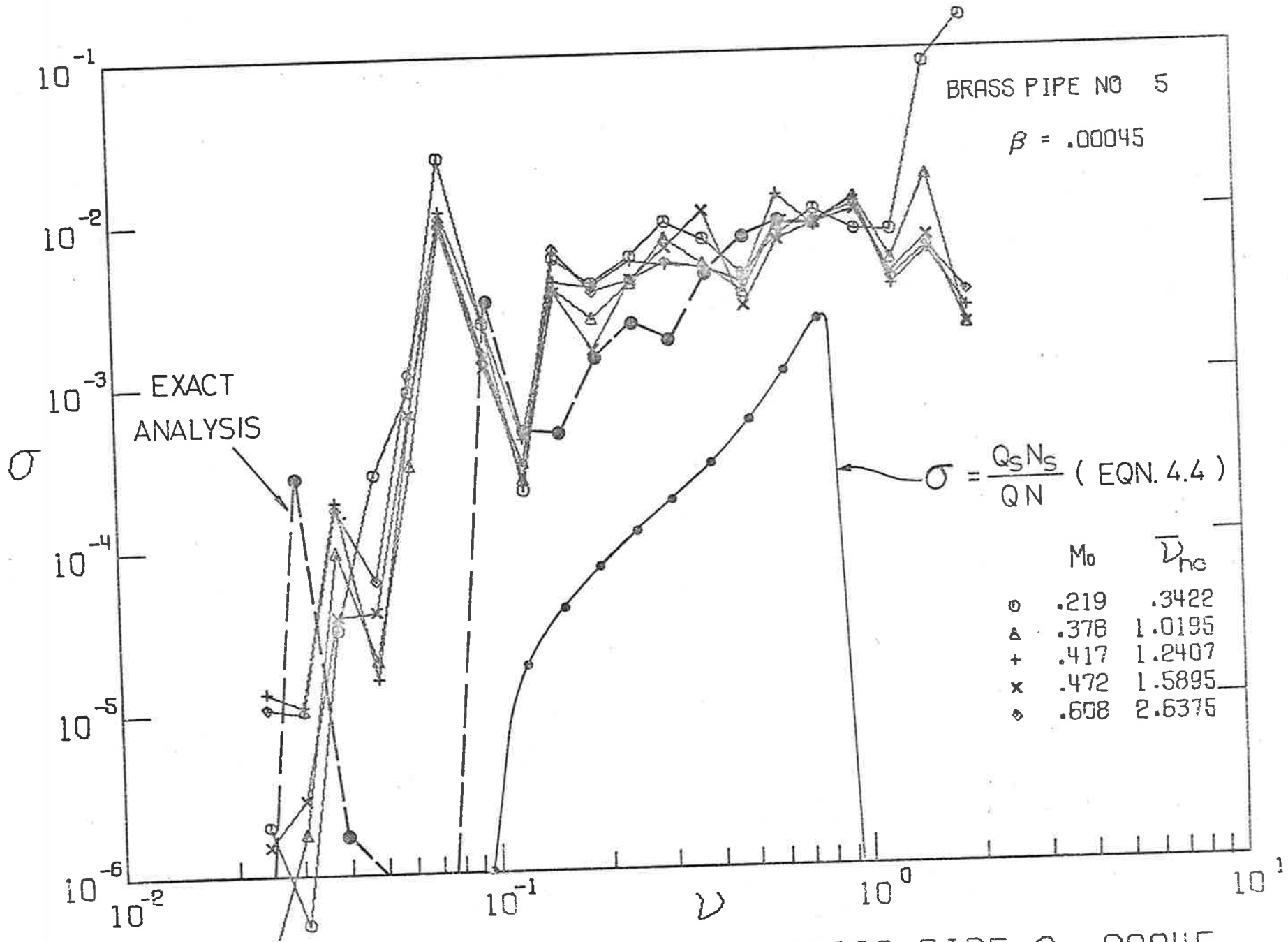

FIG. 5.11 σ FOR VARIOUS M_o . BRASS PIPE β=.00045

than 10^{-2}, in contrast with the previous case of steel pipes, where $\nu_{ac} < 1$. Calculations based on equation [4.4], which predicts an M_o^5 dependence of $\Phi_{\ddot{w}}/\Phi_p$ and Φ_π/Φ_p, include realistic values of Q_s and Q, and are found to lie at least 10dB below the experimental data; the differences result from the acoustic radiation produced by the subsonic modes. Calculation of the average radiation ratios using the exact analysis further support the suggestion that subsonic modes control the acoustic radiation at all frequencies for this pipe, as shown in Fig. 5.11.

5.6 COMPARISON WITH FAR-FIELD ACOUSTIC EXCITATION

The relative joint acceptance of flow and acoustic excitations was investigated using the same approach as followed with steel pipes. The additional effects on the acoustic power radiation caused by a static pressure differential were examined for comparison with those observed during turbulent flow excitation, as presented in Fig. 5.6.

The experimental details have been described in section 4.8, although for the present case, measurements of the acoustic radiation were performed inside the anechoic box. The same microphone position was used for both excitations. Initially, the effect on the acoustic radiation of tensioning the brass pipe with a static pressure differential was examined. The results are presented dimensionally in the form ϕ_π/ϕ_p in Fig. 5.12 for pressure differentials of 0, 7.8, and 16.3kPa. It is seen that the principal effect of tensioning the pipe in this manner is to reduce the acoustic radiation, presumably because the damping of the various structural modes has increased. This is the same kind of behaviour that was found when the static pressure differential was varied for flow excitation (Fig. 5.6); the changes in ϕ_π/ϕ_p for the various Δp's are of similar, though slightly greater, magnitude than those produced in Φ_π/Φ_p for similar Δp's for flow excitation. For zero Δp, acoustic excitation produced a 'crackling' of small wrinkles in the brass tube; this crackling inflated the levels of low-frequency acoustic radiation in a manner not found for flow excitation when the wrinkles were suppressed by the flow and any small Δp. It therefore appears that the

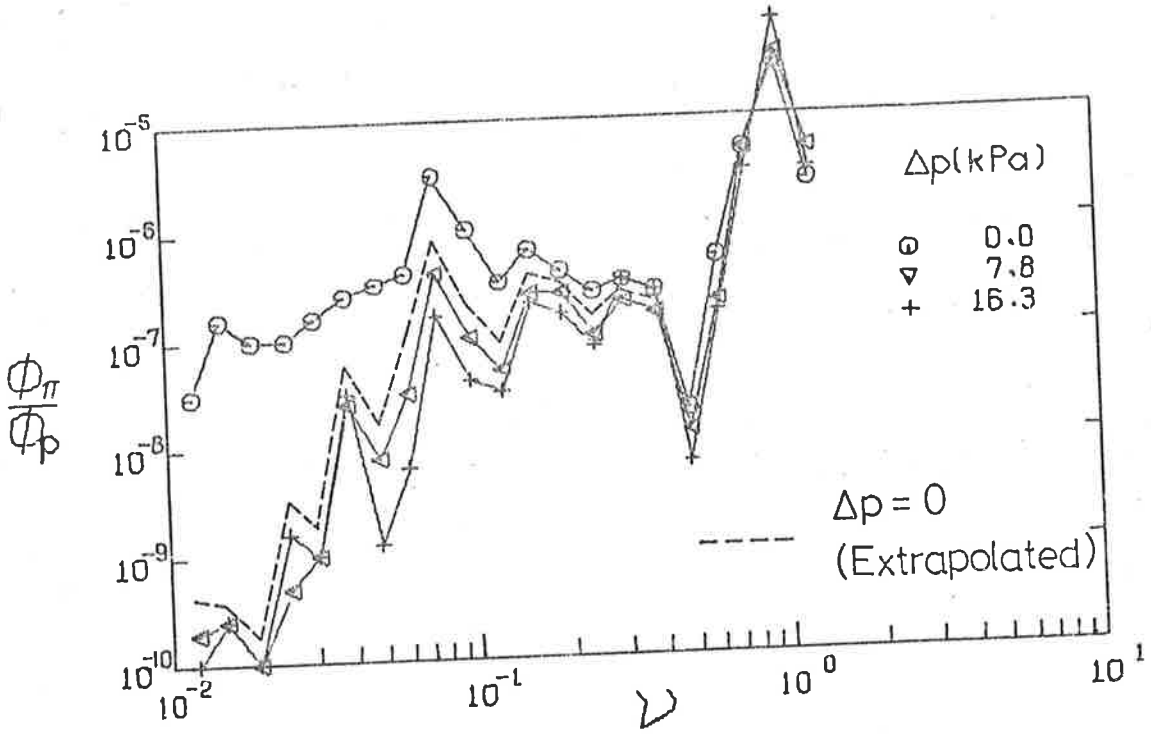

FIG.5.12 EFFECT OF PRESSURE DIFFERENCE ON ϕ_π/ϕ_p FOR ACOUSTIC EXCITATION OF BRASS PIPE

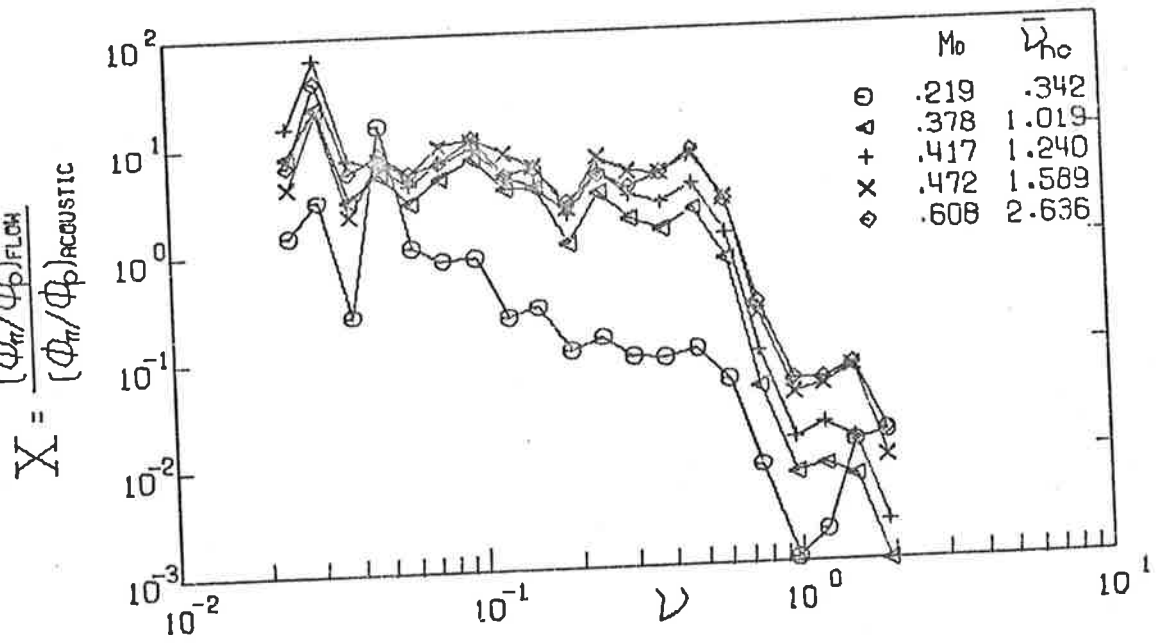

FIG.5.13 X FOR BRASS PIPE β=0.00045

additional damping is produced mainly by structural mechanisms with a smaller proportion occurring as a result of the presence of the flow.

The relative effectiveness of the turbulent flow and far-field acoustic excitations is examined, as previously described, by dividing the spectral density of the acoustic power radiation for unit turbulent flow pressure field spectral density by the acoustic radiation spectral density for unit acoustic excitation spectral density, for zero Δp in both cases; i.e. as $X = [\phi_\pi/\phi_p]F/[\phi_\pi/\phi_p]A$, as shown in Fig. 5.13. The data in Fig. 5.12 for Δp = 7.8 and 16.3kPa has been used in a similar manner to that for the flow excitation in Fig. 5.6 to extrapolate to the correct acoustic radiation for zero Δp (so removing the influence of the crackling which occurred for zero Δp).

For $\nu < 0.65$ and $M_o \geq 0.37$, $X > 1$, so that for this range of $\bar{\nu}_{hc}$ and ν, the radiating structural modes are coupled more strongly to a turbulent pressure field excitation than to an acoustic field of the same intensity. The influence of the (1,0) acoustic cross mode is far weaker than in the case of steel pipes, which is expected since the values of $\bar{\nu}_{hc}$ are an order of magnitude higher in the present case than with the steel pipes.

5.7 CONCLUSIONS AND SUMMARY

The vibrational response and acoustic radiation from a thin-walled brass pipe, excited by fully-developed turbulent flow at conditions where hydrodynamic coincidence can occur, have been reported. In the experiments, the maximum value of $\bar{\nu}_{hc}$ was 2.63, and $\bar{\nu}_{ac}$ = 19.80, thus satisfying case 3 of section 2.2.8. Experiments were performed in a small anechoic box which enclosed the test section as a precaution against test section collapse during the operation of the flow rig.

At low frequencies ($\nu < 0.1$), the experimental modal density of the brass pipe was found to agree closely with the approximate theoretical prediction on which the statistical analysis of the response and radiation are based. Measurements of modal and average quality factors, using a near-field microphone,

gave consistent results at low ν, although the application of a static pressure differential across the pipe wall increased the average Q's at low frequencies in a manner which suggested strong increases in modal resonance frequencies. Values of the quality factors of the supersonic modes were calculated assuming unit radiation ratios.

The vibrational response was measured with a near-field microphone, calibrated by comparison with a capacitance probe to indicate the acceleration response of the pipe. The experimental response data were corrected empirically for the effect of the static pressure differences which existed during the flow. Spectra were obtained for five flow speeds. From these, it was seen that the non-dimensional spectral density of the wall acceleration $\Phi_{\ddot{w}}$ was proportional to the non-dimensional spectral density of the turbulence wall-pressure field Φ_p; to the average pipe quality factors Q; and to approximately the seventh power of the internal flow speed $M_o^7 . \Phi_{\ddot{w}}/\Phi_p$ generally peaked in the region of the ring frequency where the collapse on M_o was compact and where the effects of hydrodynamic coincidence were most strongly produced. Close agreement of the experimental results with the statistical and exact analyses occurred for the higher flow speeds as $\bar{\nu}_{hc}$ approached 2, which provides considerable support for the conclusions of the previous chapter concerning the use of the Corcos model for the turbulence wall-pressure field.

Measurements of the acoustic power radiation were corrected for the effect of the static pressure differential maintained across the pipe wall during the flow. One effect of increasing the pressure differential due to the flow was to reduce the acoustic power radiation, suggesting that in fact the flow provides some additional damping. The predicted high-frequency cut-off in radiation at $\bar{\nu} = \bar{\nu}_B$ occurred, but, for $\nu < \nu_B$, subsonic modes dominated the power radiation similar to the situation for the steel pipes.

The dependence of the non-dimensional spectral density of the acoustic radiation Φ_π on flow speed and pipe quality factors was not clearly established since subsonic modes controlled the radiated power, as demonstrated by comparisons of exact calculations (based on contributions from all resonant

modes) and the statistical analysis (which included only supersonic modes). The statistical analysis was seen to lead to large underestimates of the radiation ratios, due to the neglect of subsonic modes. It appears that Φ_π also depends on M_o^7. For values of $\bar{\nu}_{hc} > 1$, fully-developed flow was clearly shown to be coupled more strongly to the radiating modes for $\nu < 0.6$ than was a propagating acoustic excitation (in the absence of flow) of the same intensity on the pipe wall.

CHAPTER 6

EXPERIMENTS WITH A P.V.C. PIPE

6.1 INTRODUCTION

In this chapter, the vibrational response of and the acoustic radiation from a rigid P.V.C. pipe (test section 4), under conditions which satisfy case 2 of section 2.2.8 ($\bar{\nu}_{hc} < 2$ and $\bar{\nu}_{ac} > 2$) are examined.

For this pipe, the available range of flow speeds gives $0.038 \leq \bar{\nu}_{hc} \leq 0.25$, so that the resulting conditions are always well removed from hydrodynamic coincidence. The approximations developed in Chapter 2, which predict the dependence of the response and acoustic radiation on flow speed, are expected to apply to this case. Also, $\bar{\nu}_{ac} = 2.14$, with $\bar{\nu}_B = 1.21$ and $\bar{\nu}_A = 1.76$: consequently, from the assumptions made in the statistical analysis in the frequency range $1.11 < \nu < 1.61$, there will be no supersonic vibration modes and no acoustic radiation.

In Chapters 4 and 5, however, subsonic modes were found to control the acoustic radiation, a situation resulting partially from their relatively high quality factors and modal density compared with the supersonic modes: furthermore, the assumption of zero radiation ratio was grossly in error for low circumferential-order subsonic modes. For the present case, the P.V.C. pipe has high internal damping, so that the relative contribution to the acoustic power radiation from subsonic modes is expected to be less, making the statistical analysis more accurate.

6.2 VIBRATION CHARACTERISTICS AND GENERAL OBSERVATIONS

In the investigation of the resonance characteristics of the P.V.C. pipe, a small square of steel shim was cemented to the pipe wall to enable electromagnetic excitation to be used to vibrate the pipe. At any but the lowest frequencies of interest, the high modal overlap of the P.V.C. pipe prevented the isolation of many individual resonant modes. Therefore the

modal density could not be determined.

Quality factors of those identifiable modes were measured using the response-decay method described in Chapter 4; these are presented in Fig. 6.1, together with one-third octave band average Q measurements. In general, $Q \simeq 25$ for all ν: the pipe is heavily damped. This value has been used in all theoretical calculations.

Introductory experiments on the homogeneity of the vibration response and the directivity of the acoustic radiation to turbulent flow excitation revealed certain differences between the characteristics of the present P.V.C. pipe and those of the steel pipes of Chapter 4. The acceleration response was found to be circumferentially homogeneous (within $\pm$ 1dB) for all ν. On the other hand, the acceleration response increased in the flow direction: for $\nu < 0.35$, a maximum increase in mean circumferential level of 2dB over the pipe length was observed, while for $\nu > 0.35$, the increases in mean circumferential level were up to 5dB. In addition, the axial increases were found to decrease as the flow speed increased. The acoustic radiation was axially symmetric for all ν, but, like the acceleration response, the radiated levels increased over the pipe length in the flow direction. In particular, for $0.3 \leq \nu \leq 1$, increases of up to 5dB in SPL over the pipe length in the flow direction occurred, the most prominent increases being at frequencies corresponding to the (1,0) and (2,0) acoustic cross modes (i.e. at $\nu = 0.30$ and $\nu = 0.51$ respectively for $M_o = 0.22$). For certain frequencies within the latter range, particularly for low M_o, the decreases in SPL as the distance from the pipe axis increased were greater than expected from a cylindrical source.

It was concluded that a weak acoustic field, whose intensity was well below that of the turbulence wall-pressures, was present inside the pipe, and it will be called the turbulence-generated acoustic field. At frequencies below the (1,0) acoustic cut-off frequency, essentially only acoustic plane waves propagate inside the pipe for low M_o. These couple poorly to pipe structural modes, as shown in Fig. 4.18 for steel pipes.

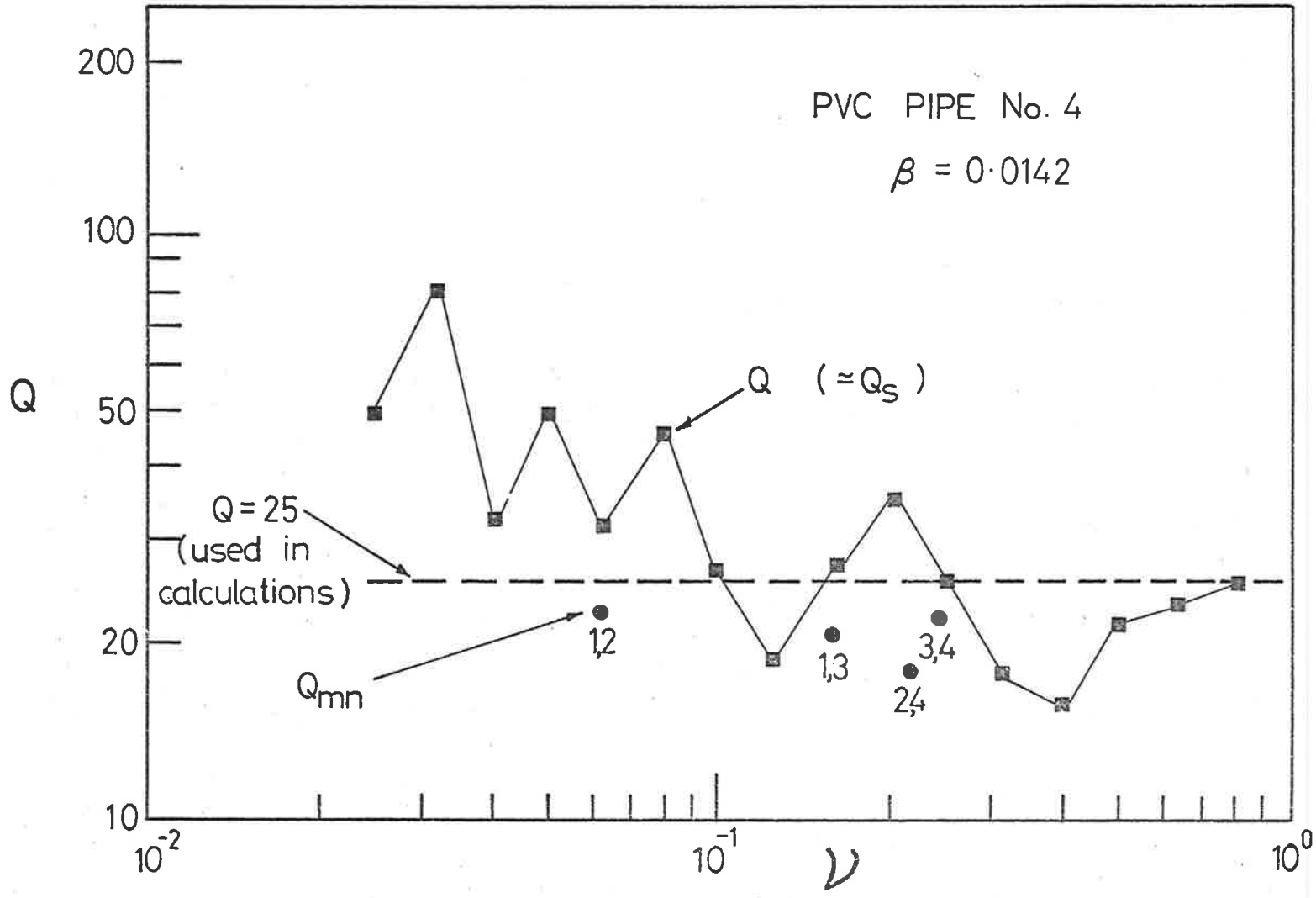

FIG. 6.1 QUALITY FACTORS OF P.V.C. PIPE No. 4

If acoustic plane waves are the dominant excitation, a forced axi-symmetric wall response and an acoustic radiation field, propagating along the pipe axis in the flow direction, are to be expected, as were, in fact, observed for acoustic excitation without flow. They were not found for flow excitation. Moreover, driving the pipe with an internal acoustic field of higher intensity than existed during operation of the flow produced negligible changes in both the vibration response and the acoustic radiation at these low frequencies. It is concluded that below the (1,0) cut-off frequency in the present experiments the turbulence-generated acoustic field is not a significant source of pipe vibration or acoustic radiation.

On the other hand, for higher frequencies, higher-order acoustic modes may be excited. These couple strongly to pipe vibration modes of the same circumferential order (supersonic for $\bar{\nu} < 1$) but poorly to all other modes. Thus, at or above the cut-off frequency of the (n,p) acoustic mode, vibration modes of circumferential order n may tend to control the pipe response and acoustic radiation, for sufficiently strong acoustic fields. As commented on before, acoustic radiation from subsonic modes ($K_n > K_a$) of the P.V.C. pipe will be less significant than from those of steel (or brass) pipes since the P.V.C. modes are heavily damped, while the steel pipe modes are not: however, the application of damping treatments to steel pipes (section 4.7) may cause the small acoustic excitation to become more significant for $\nu \simeq 0.12$, since the n = 1 modes retain their initial Q values and are coupled most strongly to the (1,p) modes.

Estimates of the contribution made by the turbulence-generated acoustic field to the total response and acoustic radiation of this P.V.C. pipe were attempted. It was assumed that increases from $I_1(\omega)$ to $I_2(\omega)$ in in the acoustic intensity acting on the pipe wall were indicated closely by increases from $S_1(\omega)$ to $S_2(\omega)$ in the flow inlet acoustic intensity (measured in the reverberation chamber), although this is only strictly true for $M_o << 1$ and for frequencies below the (1,0) acoustic mode cut-off. Increases in $I(\omega)$ will cause increases in the pipe output response from $R_1(\omega)$ to $R_2(\omega)$:

R_1 is the response spectral density to the undisturbed flow excitation, which contains an intrinsic level of turbulence-generated acoustic excitation $Y(\omega)$ in addition to the turbulence pressure field excitation $\phi_p(\omega)$; and R_2 is the response to a disturbed excitation containing $\phi_p(\omega)$ and a higher-level acoustic component $nY(\omega)$. Then

$$R_1(\omega) = \kappa(\omega).[\phi_p(\omega) + Y(\omega)] \qquad [6.1]$$

and $$R_2(\omega) = \kappa(\omega).[\phi_p(\omega) + nY(\omega)] \qquad [6.2]$$

where $\kappa(\omega)$ is the pipe transfer function between input and output and is considered to be independent of the excitation, (a reasonable assumption, which is necessary to make correction estimates); n is the ratio of acoustic wall-pressure input excitations I_2/I_1, and is assumed given closely by S_2/S_1. The required response is $\kappa\phi_p$, so that the correction to be subtracted from $10\log_{10}(R_1)$ to remove the contribution due to $Y(\omega)$ is $10\log_{10}(R_1/\kappa\phi_p)$, where, from equations [6.1] and [6.2],

$$\left(\frac{R_1}{\kappa\phi_p}\right) = \frac{(R_1/R_2)\ (n-1)}{n(R_1/R_2) - 1} \qquad [6.3]$$

Thus, by superimposing a strong acoustic signal on the flow field, while monitoring both the changes in wall response (R_2/R_1) and the changes in acoustic excitation $(S_2/S_1 = n)$, the required corrections to the observed levels R_1 (either pipe response or radiation) can be made.

To verify the original assumption that $n = S_2/S_1$ was equal to I_1/I_2, a horn driver was mounted at the upstream instrumentation section and driven to produce an acoustic intensity at the pipe wall greater than that of the turbulence pressure field. By monitoring the changes in the acoustic intensity at the pipe wall I_2/I_1 and in the inlet intensity S_2/S_1 when the flow was turned on, it was found that the errors in this assumption were less than 3dB for $M_o = 0.22$, so that at least at low M_o, the assumption appears valid. In general, the horn driver was not an effective source at higher M_o, and so a flow spoiler (20mm long x 5mm diameter) protruding from the wall

of the upstream instrumentation section was used to generate higher acoustic levels.

The corrected experimental data are presented in the following sections, but some comments on their magnitude are given here. No corrections to the acceleration response were necessary for $\nu < 0.3$ and otherwise were usually less than 2dB for all flow speeds. One exception is for $0.5 < \nu < 1$ for $M_o = 0.22$ where adequate corrections were not possible as $(R_2/R_1) \simeq (S_2/S_1)$. The acoustic radiation data required no corrections for $\nu < 0.25$. For $M_o = 0.22$ and 0.37, corrections of up to 6dB were made at higher frequencies, and it is believed, from considerations of the strong variations in the dependence of Φ_π/Φ_p on M_o about the (1,0) acoustic cross mode cut-off frequency, that these are too small. However, for $M_o = 0.57$ and, to a lesser extent, $M_o = 0.47$, the required corrections in Φ_π/Φ_p were generally less than 2dB.

6.3 ACCELERATION RESPONSE

The corrected experimental data are presented in Fig. 6.2, in non-dimensional form $\Phi_{\ddot{w}}/\Phi_p$ for the four flow speeds tested. As described in the previous section, the acceleration response was circumferentially homogenous, but varied for $0.3 < \nu < 1$ by up to 5dB over the test section length, although this variation decreased as M_o increased. The data were measured at the mid-span position, where the acceleration levels represented the mean of the pipe response. For $\nu < 0.3$, no corrections for the presence of an acoustic field were required, while it is believed the measurements have been undercorrected to some extent for $0.5 < \nu < 1$, especially for $M_o = 0.22$ and 0.37. Except for $M_o = 0.22$ and for $\nu > 0.5$, the curves of $\Phi_{\ddot{w}}/\Phi_p$ vary smoothly with ν, as expected from the Q variation in Fig. 6.1. The sudden level change at $\nu \simeq 0.6$ in $M_o = 0.22$ data is presumably the result of the turbulence-generated acoustic field; likewise the peak at $\nu \simeq 1$ for $M_o = 0.47$. In general $\Phi_{\ddot{w}}/\Phi_p$ increases with flow speed.

The dependence of $\Phi_{\ddot{w}}/\Phi_p$ on M_o was investigated by re-plotting the

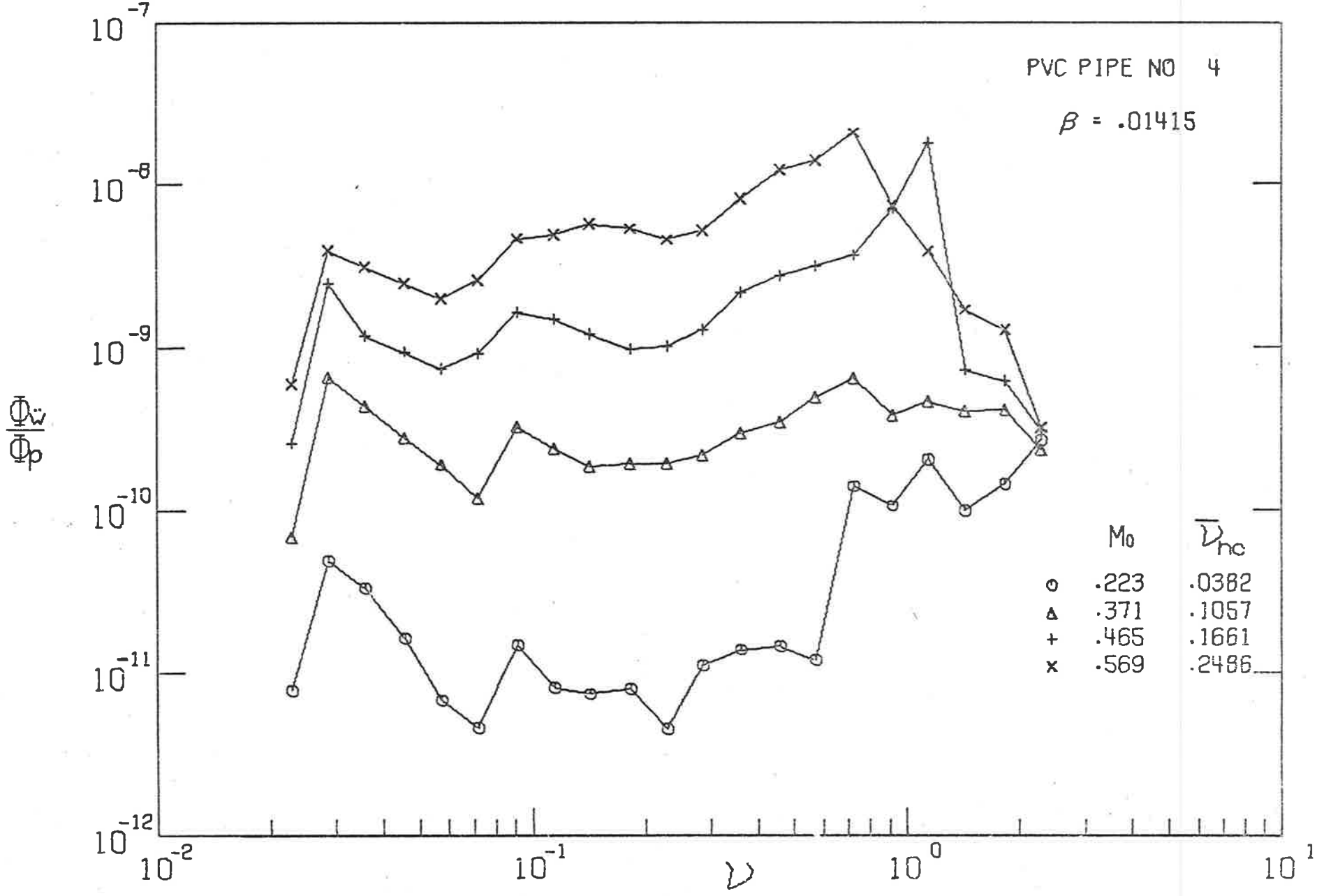

FIG. 6.2 $\Phi\ddot{w}/\Phi_p$ FOR VARIOUS M_0. PVC PIPE β=.01415

results in the form $\Phi_{\ddot{w}}/(\Phi_p Q\rho_{fs}^2 M_o^5)$ as suggested by equation [4.1], which is valid for $\bar{\nu}_{hc} << 2$. However, the collapse of data was poor and the mean experimental data lay below the curve from equation [4.1] by values which varied from approximately 17dB at low ν to 3dB at $\nu = 1$. Fig. 6.3 shows the data re-plotted in the form $\Phi_{\ddot{w}}/(\Phi_p Q\rho_{fs}^2 M_o^7)$, where a close collapse occurs for the most frequencies. For $M_o = 0.57$, $\bar{\nu}_{hc} = 0.25$ for this pipe, and so this dependence on M_o^7 results from an approach to coincident conditions. A further comparison between the experimental results and theoretical predictions is given in Fig. 6.4, where the statistical analysis (equation [2.20]), involving no approximations, has been used ($Q = 25$). The theoretical prediction overestimates the experimental data by about 5dB for all $\nu < 1$ for $M_o = 0.57$, while for $M_o = 0.22$, the overestimate varies between 15 and 20dB.* The closer agreement at $\nu \simeq 1$ for $M_o = 0.22$ results from the presence of acoustic excitation. Errors in the form of the model of the turbulence wall-pressure field are again believed to be the cause of the differences in agreement between $M_o = 0.22$ and 0.57, as has been discussed in Chapter 4. It is noted that the frequency dependence of the experimental data is well predicted for $\nu < 0.6$.

6.4 ACOUSTIC POWER RADIATION

The experimental data of the acoustic power radiation, corrected for the influence of the turbulence-generated acoustic field, is presented in non-dimensional form Φ_π/Φ_p in Fig. 6.5 for the four flow speeds tested. As previously discussed, Φ_π/Φ_p was axially symmetric for all ν, but increased by up to 5dB over the test section length in the flow direction for $0.3 \leq \nu \leq 1$. For $\nu < 0.25$, no corrections to the radiation data were made, while for $0.3 < \nu < 1$, large corrections were required for $M_o = 0.22$ and 0.37; small corrections only were made to the data for $M_o = 0.57$.

In Fig. 6.5, it is seen that for $\nu < 0.25$, the Φ_π/Φ_p data increase with M_o as did the $\Phi_{\ddot{w}}/\Phi_p$ data at low ν. For $M_o = 0.57$, Φ_π/Φ_p is essentially independent of ν up to $\nu \simeq 1$, above which it drops sharply. Φ_π/Φ_p for

* The closer agreement between theory and experiment for the P.V.C. pipe than for the steel pipes reflects the much closer approach to hydrodynamic coincidence occurring for the P.V.C. pipe.

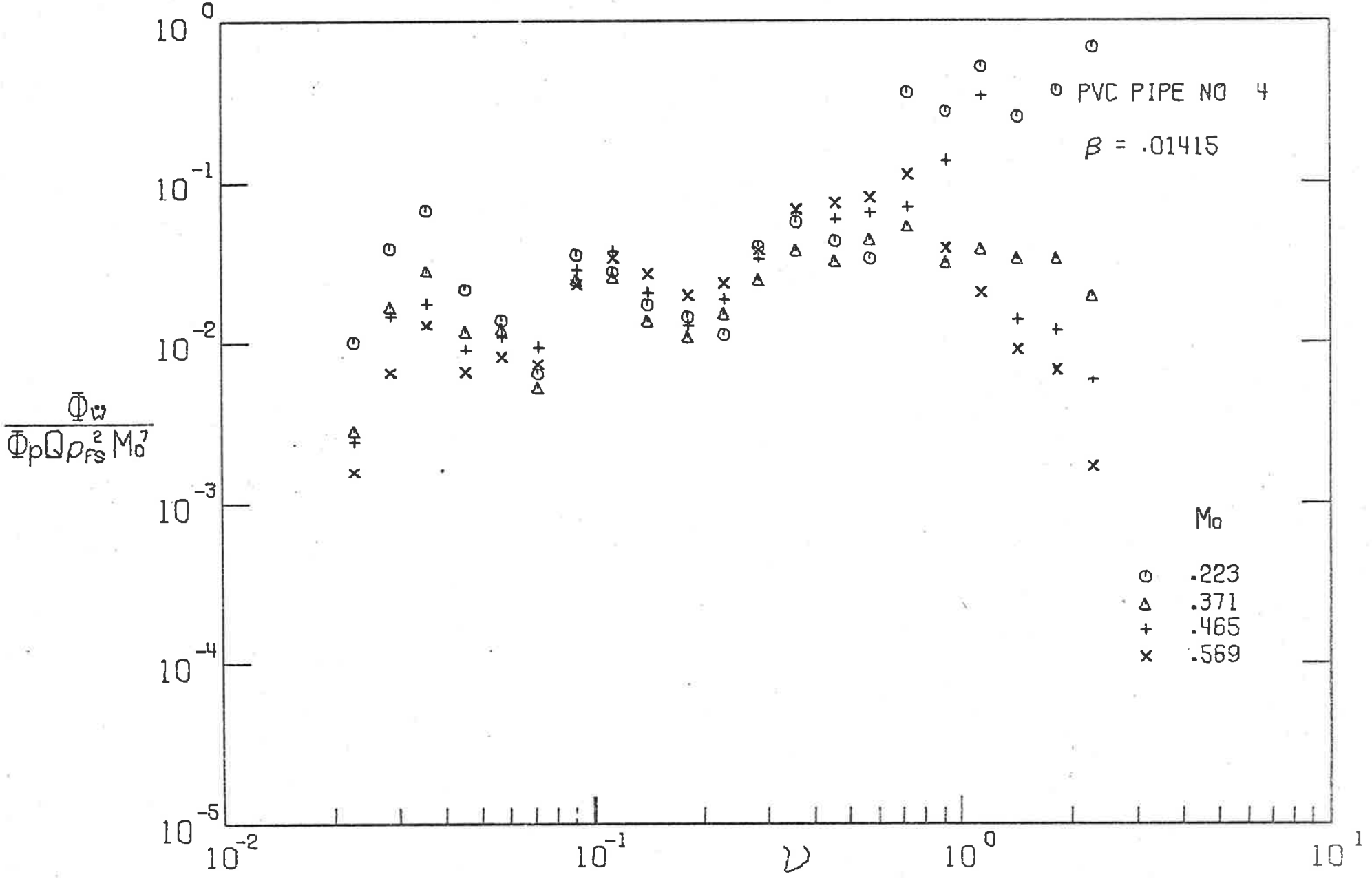

FIG. 6.3 EFFECT OF FLOW SPEED ON Φ_w/Φ_p. PVC PIPE β=.01415

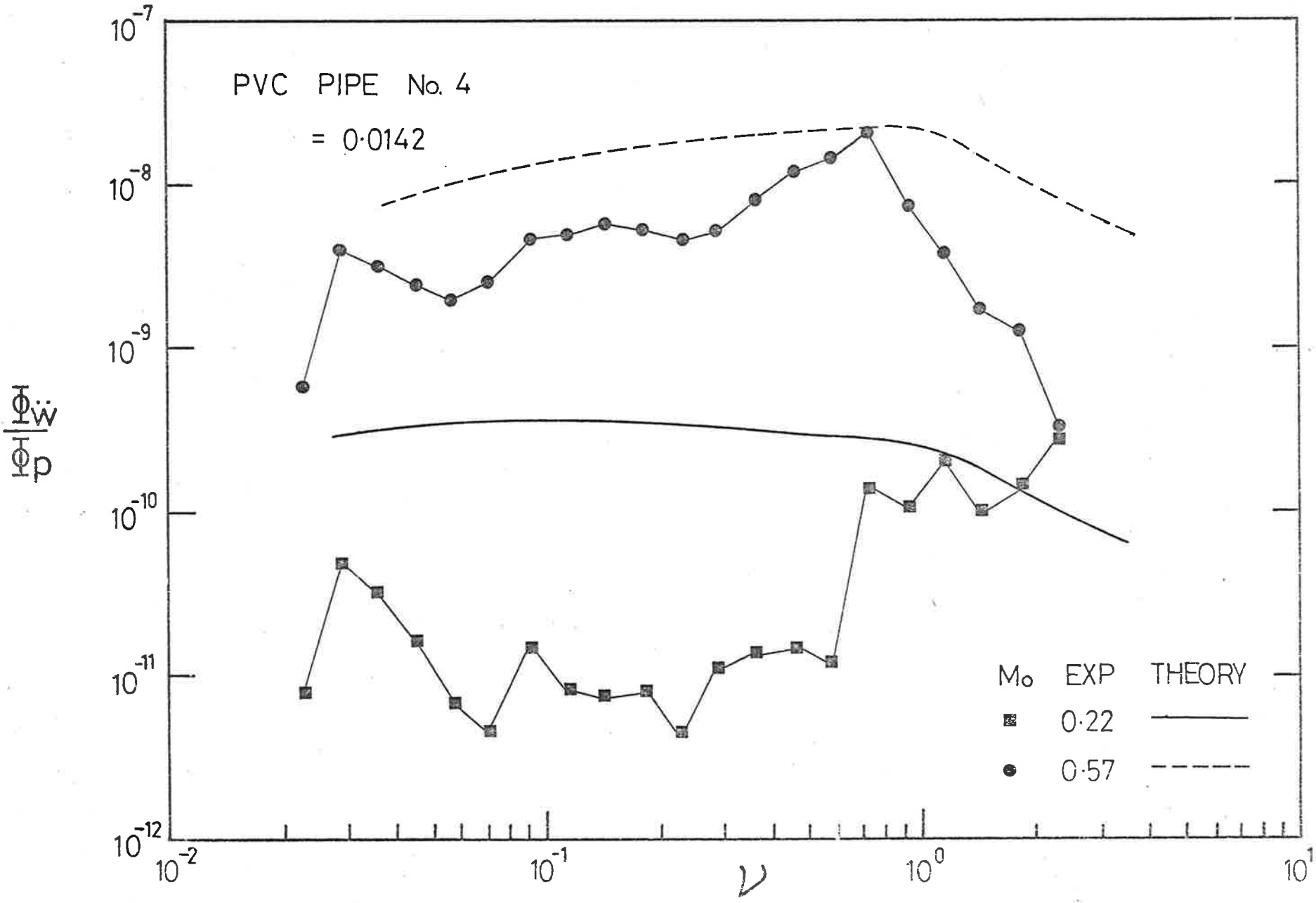

FIG. 6.4 $\Phi\ddot{w}/\Phi p$ — COMPARISON OF EXPERIMENT & THEORY — PVC PIPE

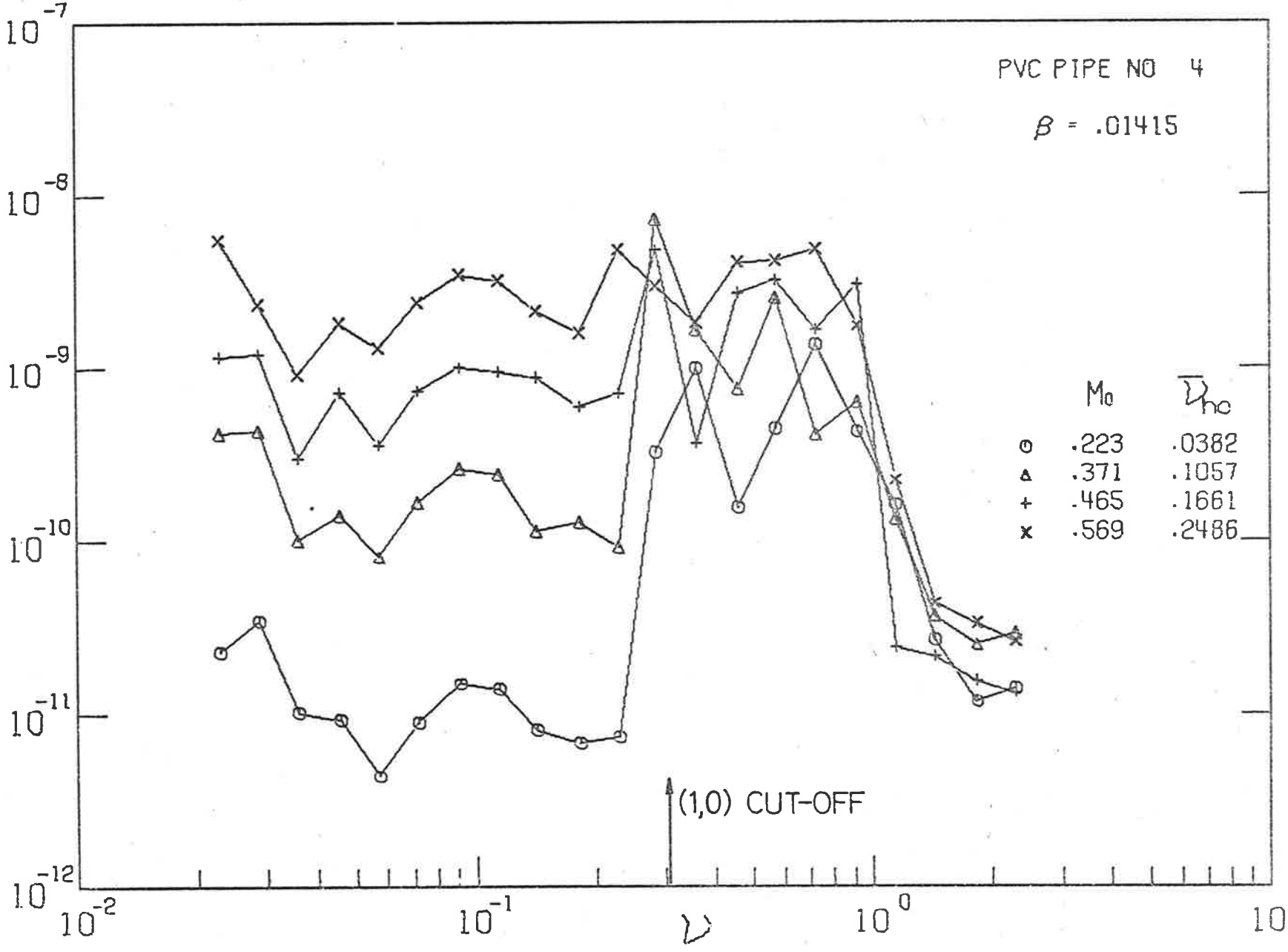

FIG. 6.5 Φ_π/Φ_p FOR VARIOUS M_0. PVC PIPE $\beta = .01415$

M_o = 0.47 shows similar behaviour, except at $\nu \simeq 0.25$. Φ_π/Φ_p data for M_o = 0.22 and 0.37 diverge sharply from this behaviour for $0.3 < \nu < 1$, the result of the turbulence-generated acoustic excitation which has not been removed successfully by the correction procedure.

With this in mind, the dependence of the acoustic radiation of the flow speed is examined in Fig. 6.6 by plotting the data in the form $\Phi_\pi/(\Phi_p Q_s \rho_{fs}^2 M_o^5)$, as suggested by equation [4.5]. Equation [4.5] is also shown; the range of frequency for which supersonic modes are predicted to exist, is indicated. For $\nu \lesssim 0.2$, the collapse of data is quite close, although the M_o dependence is more closely M_o^6 than M_o^5. The data for M_o = 0.47 and 0.57 lie some 8 to 12dB below the approximate theoretical estimate, while the lower M_o data lie closer to the prediction. The statistical analysis predicts no acoustic radiation from supersonic modes for $\bar{\nu}_B < \bar{\nu} < \bar{\nu}_A$ i.e. $1.11 < \nu < 1.61$. A sharp cut-off in acoustic radiation exists for all M_o at $\nu \simeq 1$, but the predicted rise in Φ_π/Φ_p at ν_A is not obvious, although there are few data points for $\nu > \nu_A$. At frequencies below the first supersonic mode, the level of the radiation does not decrease significantly below that in the region of supersonic modes ($0.2 \lesssim \nu < \nu_B$), implying that again subsonic modes have higher radiation ratios than assumed.

Comparisons of the experimental radiation ratios for the P.V.C. pipe with the theoretical prediction (equation [4.4]) are made in Fig. 6.7. For $\nu \lesssim 0.25$, the curves of σ are effectively independent of M_o, while for $\nu > 0.25$, the levels of σ decrease with increasing M_o, as Φ_π/Φ_p becomes influenced less by the turbulence-generated acoustic excitation. The experimental data for M_o = 0.47 and 0.57 lie from 3 to 10dB below the theoretical prediction. This could result from the choice of a constant quality factor for all modes, when perhaps $Q_s << Q$ as is the case for steel pipes; alternatively, the correction method may introduce errors for higher M_o. It is interesting to note that, between ν_B and ν_A, a drop in σ occurs for all M_o, and for $\nu > \nu_A$, σ tends to increase as predicted.

Additional comparisons between the experimental data Φ_π/Φ_p and

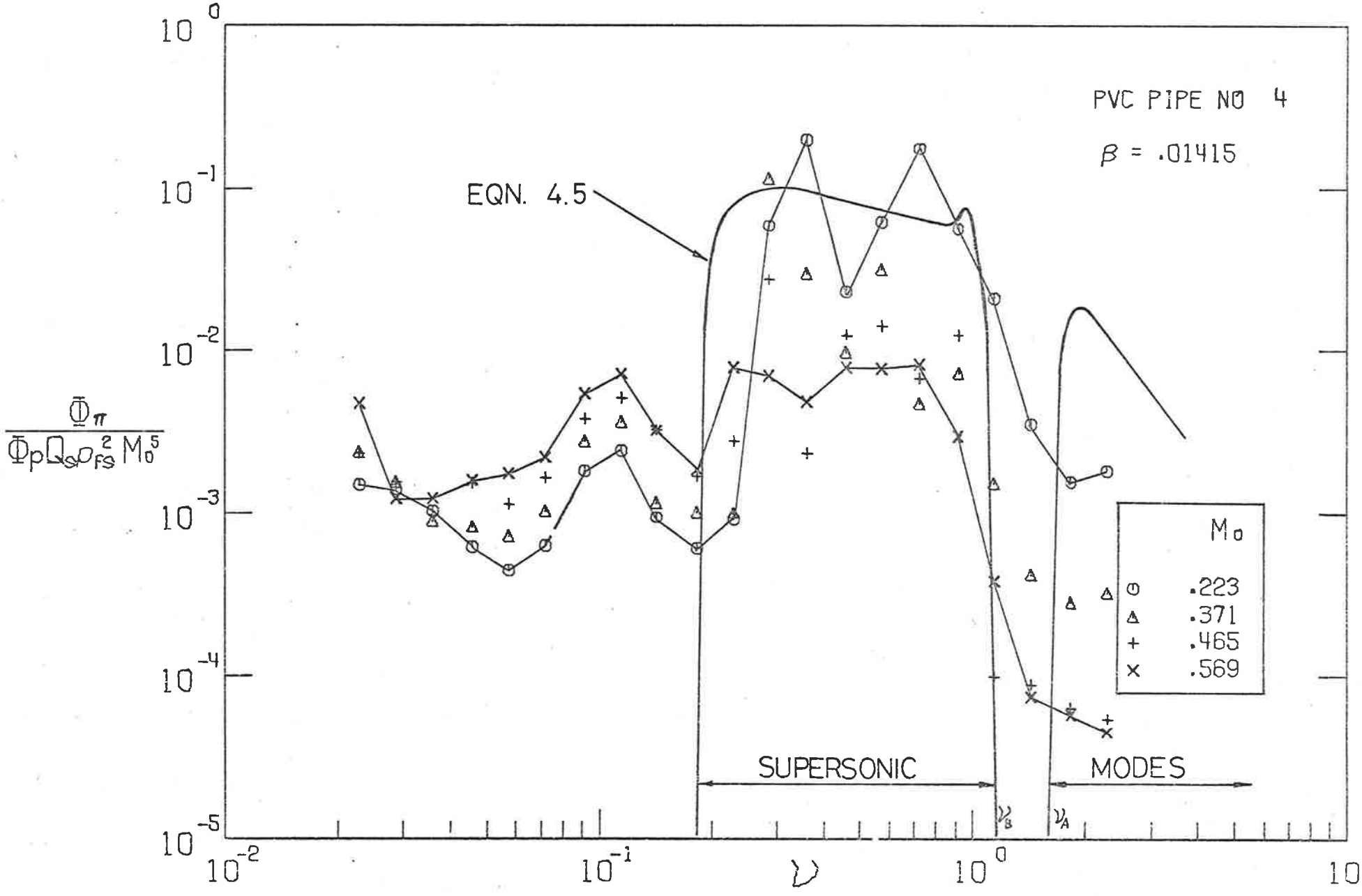

FIG. 6.6 EFFECT OF FLOW SPEED ON Φ_π/Φ_p. PVC PIPE β=.01415

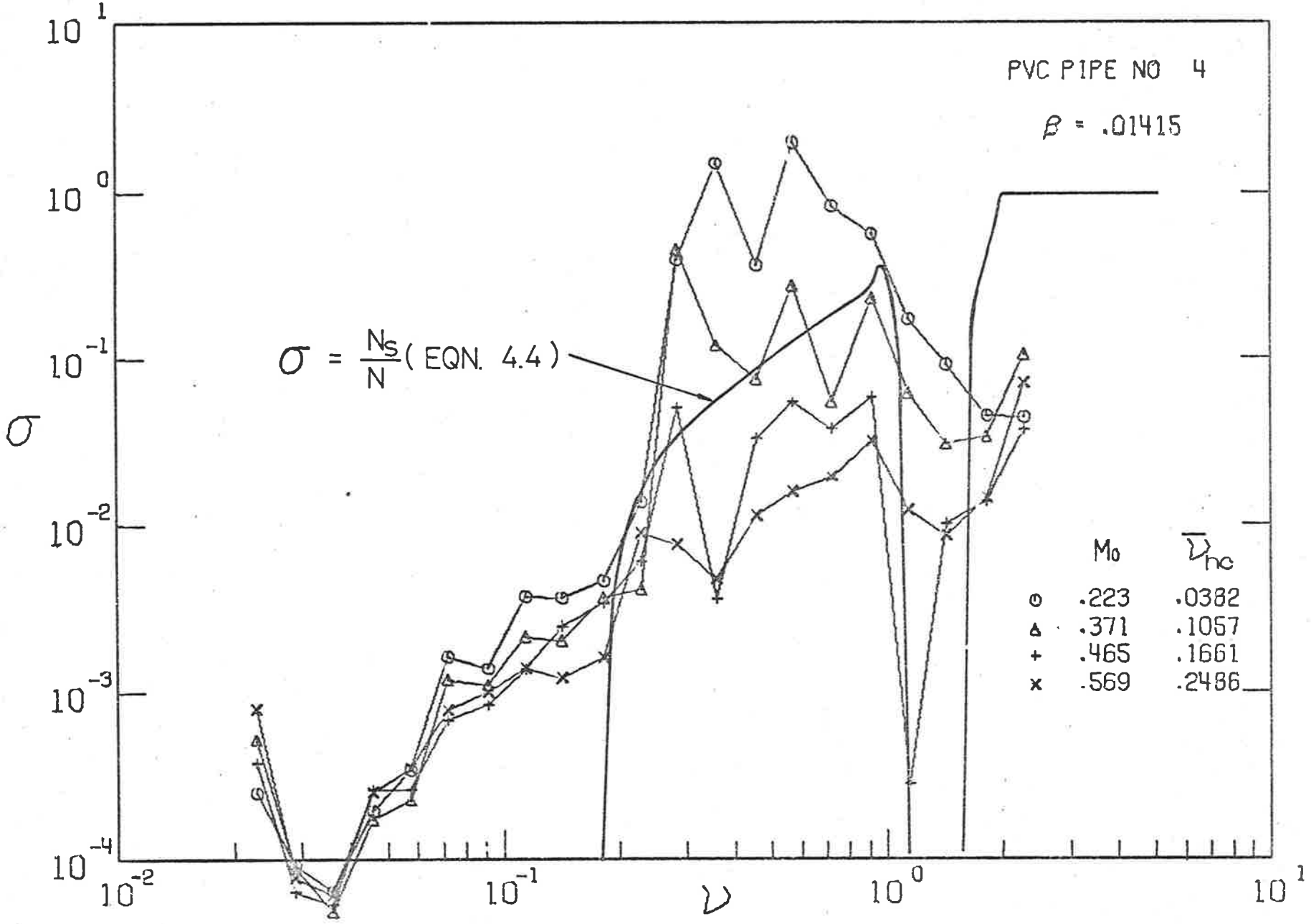

FIG. 6.7 σ FOR VARIOUS M_0. PVC PIPE β=.01415

the statistical theoretical approach (equation [2.22]) are presented in Fig. 6.8 for the highest and lowest flow speeds. For $M_o = 0.57$, the theoretical approach overestimates the experimental data by about 11dB in the region of supersonic modes for $\nu < \nu_B$, while, for $\nu > \nu_A$, the overestimate increases to 24dB. The experimental data for $M_o = 0.22$ agree closely with the appropriate theoretical curve for all ν. This is due to the presence of the turbulence-generated acoustic field inside the pipe, which, for $\nu > 0.25$, increases the acoustic radiation above the levels produced by the turbulent flow alone - the agreement is fortuitous and should not be misinterpreted as an example of good agreement between theory and experiment.

6.5 SUMMARY

The pipe/flow configuration examined in this chapter has been for $\bar{\nu}_{hc} < 2$ and $\bar{\nu}_{ac} > 2$. As well, the P.V.C. pipe used possessed high material damping. Thus the situation is quite different from those involving steel or brass pipes.

The low Q's for the P.V.C. pipe prevented any exact determination of the modal response of the pipe even though the theoretical modal density was lower than for the steel test sections. As a consequence of the low Q's, the effects of a turbulence-generated acoustic field inside the pipe were more noticeable; at higher frequencies especially, the acceleration response and the power radiation increased over the pipe length in the flow direction, probably in proportion to the intensity of the turbulence-generated acoustic field inside the pipe. Corrections to these measurements were made at those frequencies where significant internal acoustic excitation existed.

Analysis of these corrected data indicated that the non-dimensional spectral density of the acceleration response $\Phi_{\ddot{w}}$ was proportional to the non-dimensional power spectral density of the turbulence wall-pressure field Φ_p and to the average pipe quality factors Q, but depended on M_o^7 rather than M_o^5 as predicted by the approximate equation. Similar differences between

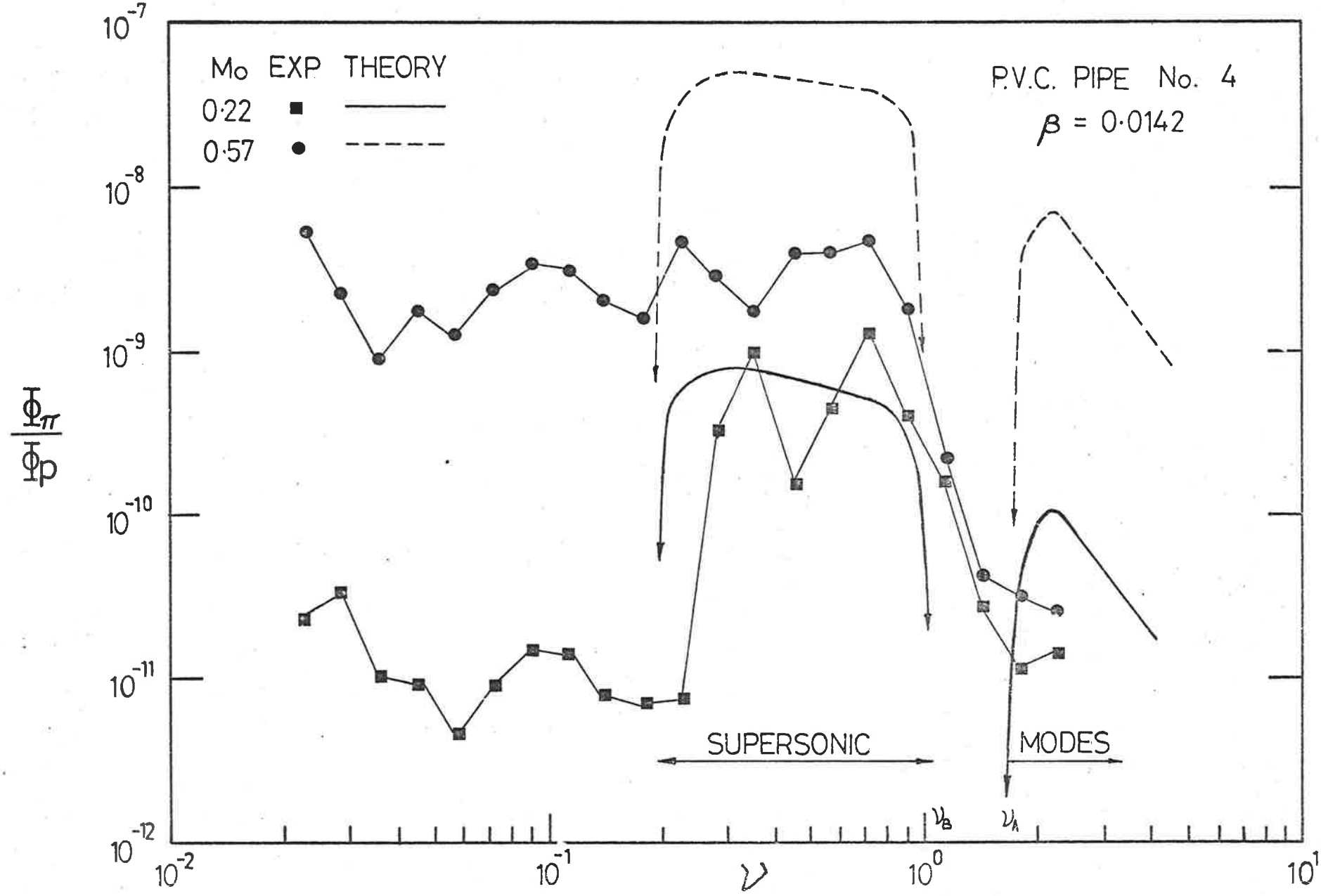

FIG. 6.8 Φ_π/Φ_p — COMPARISON OF EXPERIMENT & THEORY — P.V.C PIPE

the statistical predictions and the measured results, as occurred with the steel pipes, were found, in that the absolute values of the differences decreased quite strongly as $\bar{\nu}_{hc}$ increased. The non-dimensional spectral density of the power radiation Φ_{π} was found to be proportional to $\Phi_p Q$ and to depend on the fifth or sixth power of M_o. For the valid sets of data, the statistical theory overestimated the measurements by from 8 to 12dB over the frequency range of supersonic modes. Some evidence was found to support the existence of the region $\bar{\nu}_B < \bar{\nu} < \bar{\nu}_A$ in which little radiation occurs due to a lack of supersonic modes.

CHAPTER 7

GENERAL DISCUSSION

The results of a detailed experimental investigation of the vibrational response of and the acoustic radiation from thin-walled pipes, excited by fully-developed turbulent pipe flow, have been presented in the previous three chapters for a wide range of flow and structural parameters. In particular, the dependence of the response and radiation on flow speed, frequency, pipe wall thickness and quality factors has been measured. Specific conclusions, reached from comparisons of these results with the exact, statistical and approximate theoretical analyses of Chapter 2, have been given in the relevant earlier chapters. This chapter summarises the more important of these conclusions and makes some additional and more general comments about the problem.

(i) For the range of $\bar{\nu}_{hc}$ tested in these experiments, calculations of the vibrational response of flow-excited pipes, using the statistical analysis and measured average quality factors, agree closely with those made using the exact formulation which is based on measured values of modal quality factors and resonance frequencies. The statistical analysis provides an accurate representation of the theoretical vibrational response with considerable savings in computing time. Likewise, calculations of the acoustic power radiated from supersonic vibrational modes (for which the radiation ratios are unity) from the two analyses agree closely.

(ii) The assumption that supersonic modes control the radiated acoustic power from pipes is not valid for pipes in general: comparisons of the acoustic power radiation using both the exact analysis, which includes the contribution from subsonic modes, and the statistical analysis, which is based on supersonic modes only, show that subsonic modes in fact produce from

10 to 20 dB more power than supersonic modes for all frequencies up to the acoustic coincidence frequency, especially when significant acoustic radiation damping occurs. Simple approximations for the radiation ratios of the more efficient subsonic modes must be developed before the statistical analysis can be extended to give reliable predictions of the radiation from subsonic modes.

On the other hand, the statistical analysis allows the dependence of the response and radiation on flow and structural variables in practical situations to be investigated analytically.

(iii) The degree of agreement between theoretical predictions of the vibrational response and acoustic radiation and the data measured during the experimental programme depends on the closeness of conditions to hydrodynamic coincidence ($\bar{\nu}_{hc} \geq 2$). For the brass pipe ($0.34 < \bar{\nu}_{hc} < 2.64$), hydrodynamic coincidence occurred and close agreement existed. For the steel pipes ($0.008 < \bar{\nu}_{hc} < 0.09$), and, to a lesser extent, for the P.V.C. pipe ($0.04 < \bar{\nu}_{hc} < 0.25$), conditions were far removed from hydrodynamic coincidence and theoretical overestimates of the response and radiation of from 10 to 25 dB were found. These discrepancies between experiment and predictions can be attributed to the inappropriate use of the Corcos model for the cross-spectral density of the turbulence wall-pressure field, which leads to overestimates of up to 30 dB for values of $\bar{\nu}_{hc}$ representative of the practical piping systems.

(iv) The modal density function for pipes, which is derived from a simplified resonance-frequency equation, closely predicts the mean curve of the experimental data.

(v) The quality factors of the lightly-damped pipes (steel and brass) are generally high. For rigid end conditions which allow no relative motion between the pipe and the end flanges, acoustic radiation damping reduces the Q's of the modes with high radiation ratios: then, the variation of the Q's of modes of constant circumferential order with varying axial order can be predicted with fair accuracy.

If relative motion occurs between the pipe ends and flanges, large

reductions in the modal Q's can occur, associated probably with the pumping of gas around the joint.

In each frequency band, the measured average Q is well approximated by the arithmetic mean of the Q's of the individual modes in the same band.

(vi) The non-dimensional spectral densities of the acceleration response of the various test sections $\Phi_{\ddot{w}}$ are proportional to the non-dimensional spectral density of the turbulence wall-pressure field Φ_p; to the average quality factors of the particular test section; and to the fifth or higher power of the non-dimensional flow speed M_o. The dependence on M_o increases with $\bar{\nu}_{hc}$: for steel pipes, $\Phi_{\ddot{w}}$ was found to be proportional to M_o^5 or M_o^6, for the P.V.C. pipe M_o^7, and for the brass pipe M_o^7, in contrast to the theoretical M_o^5 dependence which is only valid for $\bar{\nu}_{hc} << 1$.

For steel pipes, $\Phi_{\ddot{w}}$ depends essentially on the cube of the pipe wall-thickness parameter β.

(vii) The non-dimensional spectral densities of the acoustic power radiation of the various test sections Φ_π are found to be proportional to Φ_p; to the fifth or higher power of M_o, and to an average quality factor, which is not Q_s or Q but an average of Q_{mn} weighted by the radiation ratios of the individual modes. For all frequencies below the acoustic coincidence frequency, the radiation is controlled by low circumferential-order subsonic modes, which are usually more lightly-damped than supersonic modes at the same frequency. The assumption of equal modal energy, normal in statistical energy analysis, is not valid for predictions of the acoustic radiation from pipes, at low frequencies at least.

For steel pipes, Φ_π depends on the square or cube of the pipe wall-thickness parameter β.

(viii) As seen from equation [2.29] and [2.30], variations in pipe wall material affect $\Phi_{\ddot{w}}$ and Φ_π through parameters ρ_{fs} and M_{Lp}, and ρ_{fs}, M_{Lp} and N_s respectively. The dependence of $\Phi_{\ddot{w}}$ and Φ_π on these can be estimated from the statistical analysis by using appropriate approximations. For

example, for $\bar{\nu}_{hc} << 1$, $\Phi_{\ddot{w}}$ is proportional to $\rho_{fs}^2 \ M_{Lp}^5$ and Φ_π is proportional to $\rho_{fs}^2 \ M_{Lp}^4 / N_s$.

Comparison of mean values of $\Phi_{\ddot{w}} \beta^3 M_{Lp}^5 f(\nu)/(\Phi_p Q \rho_{fs}^2 M_o^5 \nu)$ for each different test section shows a considerable spread between the reduced data for different materials. This results mainly from the errors introduced by the Corcos pressure field model which are dependent on $\bar{\nu}_{hc}$. However, the steel and P.V.C. data for approximately the same values of $\bar{\nu}_{hc}$ show close agreement with each other, are independent of frequency as expected, but lie some 15 dB below the approximate theoretical prediction. On the other hand, mean values for the brass pipe agree closely with the theoretical prediction, except for $\nu > 0.4$ where hydrodynamic coincidence increases the dependence of $\Phi_{\ddot{w}}/\Phi_p$ on M_o to M_o^7 as $\bar{\nu}_{hc}$ approaches 2.

The discrepancies which exist between the experimental data for the steel and P.V.C. test sections and the theoretical predictions are reasonably well explained in terms of the probable errors in the model of the cross-spectral density of the turbulence wall-pressure field. Furthermore, good agreement is found for the brass pipe data. Thus the dependence on the material of the pipe wall (ρ_{fs} and M_{Lp}) appears to be represented correctly in the statistical analysis.

(ix) Large broad-band reductions in the vibrational response of lightly-damped steel pipes can be produced by the application of simple damping treatments to the pipe surface. These reductions correspond to reductions in the average Q's of the resonant vibration modes. While the Q's of modes of circumferential order $n \geq 2$ can be reduced by factors in excess of 20 by such treatments, the Q's of $n = 1$ modes, which have a strong influence on the radiation at low frequencies but little influence on the response of the undamped pipe, cannot be damped effectively. Consequently, while the reductions in Φ_π are generally similar to the reductions in $\Phi_{\ddot{w}}$, at those low frequencies where $n = 1$ modes influence the radiation from the undamped pipe, much smaller reductions in Φ_π occur.

(x) For the range of $\bar{\nu}_{hc}$ tested, the joint acceptance due to excitation by fully-developed turbulent pipe flow is greater than the joint acceptance for propagating acoustic plane waves acting in the absence of flow. This difference increases with $\bar{\nu}_{hc}$. However, above the lowest cut-off frequency for higher order acoustic modes, propagating acoustic waves generally have a higher joint acceptance than the joint acceptance for excitation by turbulent pipe flow: only when $\bar{\nu}_{hc} \gtrsim 1$ will the flow be coupled more strongly to pipe vibration modes, as occurred for the brass test section for $\nu < 1$.

Since $\bar{\nu}_{hc} << 1$ in most practical situations, it appears that acoustic excitation from sources immersed in the flow will generally tend to control the response and radiation from pipes, even for high internal flow speeds and especially at frequencies at and above the onset of propagation of higher-order acoustic modes inside the pipe.

The influence on the vibrational response of and acoustic radiation from pipes excited by fully-developed turbulent flow of variations in pipe material and structural dimensions and in flow speed and gas density have been investigated theoretically and experimentally in considerable detail: a large degree of agreement has been found between theory and experiment in various areas, demonstrating a good comprehension of the phenomena involved.

Certain aspects of the general pipe radiation problem, which require further research, can now be raised.

(i) It has been suggested that the Corcos model seriously overestimates the contribution of the low-wavenumber components of the spectral density of the turbulence wall-pressure field. No valid measurements at these wavenumbers, which include the contribution of the turbulence-generated acoustic field, have been made for pipe flows: it would be of some interest to establish the correct levels of the wavenumber-frequency spectral densities of the wall-pressure field for a series of representative pipe flows.

(ii) Of considerable practical importance is the description

of the characteristics of the wall-pressure field generated by other flow control components, such as orifice plates, bends and valves. In such cases, it is usually assumed that the acoustic field radiated inside the pipe from such sources will be coupled more strongly than other excitations present to the vibration modes of the pipe and so will determine the acoustic power radiation: however this has not been verified experimentally. Investigation of the relative contributions to the total acoustic radiation produced by these intense pressure fields local to such sources is warranted to determine, at least, under what conditions the acoustic field radiated by various standard piping components is the controlling excitation.

PART II: EXCITATION WITH ACOUSTIC PLANE WAVES

CHAPTER 8

8.1 INTRODUCTION

In practical piping systems, the important sources of high noise levels are the very intense, incompressible pressure fields generated in regions of high static pressure drop which occur at flow control devices, such as valves and sharp angle bends. These complex pressure fields will feed energy into the surrounding pipe in various ways.

Firstly, there is the localised action of the incompressible pressure fluctuations themselves: these are of high intensity close to the control device but decay quickly with distance away from the device. Such a localised excitation will contribute to the generalised force on the pipe mode shapes in a similar manner to that described in Chapter 2, except that the excitation can be non-homogeneous over the internal surface of the pipe (both axially and circumferentially in the general case). Mechanical vibration of the components of the flow control device, resulting from the loading of these local pressure fields, can also feed energy directly to the pipe wall. There is also the acoustic field which is radiated from the incompressible flow region surrounding the source.

An ideal mechanical vibration filter placed several excitation wavelengths from the source region will remove the effects of the near-field and mechanical excitations from the response of the downstream pipe. The propagation of acoustic energy inside the pipe will be unaffected by such mechanical treatments, however, so that the radiated acoustic pressure field of the source can become distributed over considerable lengths of pipe. The transmission loss presented by the attached pipe to the propagating (and reflected) acoustic waves is therefore of considerable importance.

In contrast to previous approaches to this problem, this work

is restricted to the frequencies at which only plane-wave propagation can occur inside the pipe. It is this range of acoustic plane-wave propagation which often determines the peak levels of power radiation from small-diameter pipes or from pipes carrying liquids or hot gases and which also proves least amenable to noise control solutions. Interestingly, large and unexplained discrepancies between theoretical predictions and existing measurements of the pipe transmission loss are found to occur in this plane-wave region. The nature of the coupling between the axi-symmetric plane-wave pressure field and the wall response is apparently not understood even in this, the simplest experimental and analytical, case. Consequently, in the present investigation of the vibration response of and acoustic radiation from pipes excited acoustically, the region of plane-wave propagation inside pipes has been considered exclusively. The achievement of a thorough understanding of the important principles acting in this case seems a most desirable aim before proceeding to the more complex situation involving multi-modal acoustic propagation inside the pipe.

8.2 SURVEY OF PREVIOUS WORK

The original investigations of the transmission loss (TL) of pipes to internal acoustic excitation were made by Cremer(1955) and by Heckl (1958); both dealt primarily with the frequency range corresponding to the multi-modal acoustic propagation inside the pipe. Cremer derived an expression for the transmission impedance Z_τ of an infinitely long, thin-walled circular cylinder to a fluctuating pressure distribtuion inside the pipe. Only acoustic plane waves can propagate internally for frequencies such that $K_B < \simeq 2$ where $K_B = k_B a = \omega a/c_B$ and c_B is the acoustic wavespeed inside the pipe (see section 8.3): then Z_τ is controlled by the membrane-stiffness of the pipe and consequently increases as the pipe diameter decreases.

Using Cremer's expression for Z_τ, Heckl assumed that, as far as the acoustic radiation was concerned, the important pipe responses were

those components forced by the various internal acoustic modal pressure distributions, and that the radiation ratios of such wavemotions of the pipe wall were approximately unity: in addition, it was assumed that, at any frequency, the acoustic energy inside the pipe was equally divided between all possible propagating modes. Heckl's measurements of the TL of long pipes show minima at frequencies corresponding to the onset of propagation of individual acoustic modes of order higher than the plane wave. For frequencies where $K_B > 2$, he found good agreement between his theoretical predictions and experimental measurements when these were performed in octave bands. However, for frequencies when only plane waves could propagate, increases in the power radiation of up to 30dB were found above the theoretical prediction (based on the forced stiffness-controlled response): these were proposed to result from the coupling of non-propagating higher-order acoustic modes generated in the near field of the acoustic source with vibration modes of the pipe, which were resonant at the excitation frequencies. The measured values of the TL of the pipes tested were well below the theoretical predictions: these differences increased markedly as the asymmetry of the acoustic source increased, but decreased as Λ increased. No examination of the modal content of the structural response was reported, and the assumption regarding the equi-partition of acoustic energy between the higher-order modes was not investigated. The good agreement obtained for $K_B > 2$ was in spite of the fact that, in all frequency bands, supersonic resonant modes of the pipes would have been coincident with certain higher-order acoustic modes inside the pipe. One might expect that the TL of lightly-damped pipes would be quite strongly influenced by those resonant modes which are well coupled circumferentially and therefore excited at coincidence.

Kuhn (1974) has investigated certain aspects of these discrepancies for $K_B < 2$, using pipes with $\Lambda \simeq 300$, a = 15 mm, h = 0.81 and 2.31 mm (i.e. $\beta = 0.015$ and 0.046). For $K_B < 2$, the theoretical TL (based on a summary of existing work by Morfey (1971) but incorrectly plotted in Kuhn's Fig. 9) exceeded the measured data by from $\simeq$ 2dB at the cut-off frequency of the (1,0)

acoustic cross mode inside the pipe, by ≃ 15dB at K_B = 0.3, and by ≃ 30dB at K_B = 0.1 for β = 0.015. The vibrational response was resonant, rather than forced, and the n = 1 translational modes were responsible for the observed differences between theoretical and measured TL. The thicker pipe (β = 0.046) was found to radiate 5dB more acoustic power than the thinner pipe (β = 0.015), in contrast to an expected 9dB decrease in power radiation predicted on the basis of the increased membrane-stiffness of the thicker pipe. In his examination of the reasons for these discrepancies, Kuhn measured the maximum response of a length of pipe to internal acoustic excitation, with the source in different locations relative to the start of the test pipe. Most importantly, he found that, on de-coupling the mechanical and acoustic effects of the near field of the speaker source from the test pipe, reductions of up to 20dB in the vibration levels could be produced over a limited frequency range: these data were not presented relative to the theoretical forced-response level, and it was not stated whether the SPL in the far field of the source was maintained constant. Also, no actual measurements were made of the effect on the measured pipe TL of de-coupling the effects of the source near field from the test pipe, although he concluded that the non-propagating (1,0) acoustic mode was responsible for these discrepancies in TL at low K_B.

Karvellis (1975) has demonstrated that flow control devices do generate strong internal acoustic fields, which propagate both upstream and downstream away from the source. He found, for orifices and valves and for distances greater than 20a downstream from the source, that the acoustic field acting on the pipe wall was generally stronger than the wall-pressure field associated with fully-developed turbulent pipe flow. Depending on the axi-symmetry of the device, strong peaks in the acoustic wall-pressure field were produced at the cut-off frequencies of the various acoustic cross modes within the pipe. For example, for K_B < 2, only plane waves existed and the spectral density of the acoustic wall-pressure field was fairly smooth for all devices: then, for asymmetric sources (a globe valve and an eccentric orifice

plate), at distances greater than 20a , the strongest peaks in the wall-pressure spectral densities were produced at frequencies corresponding to the lower-order radial acoustic modes inside the pipe (the (1,0) or 2,0) modes) but not at the frequencies of the (0,1) or (0,2) modes (see section 3.3.1). For an axi-symmetric source (a conventional orifice plate mounted axially), the (0,1) symmetric mode was excited most strongly and the spectral density at the (1,0) mode frequency was smooth.

It appears that equi-partition of acoustic energy does not occur in general and that, in calculations of the TL of pipes, proper account must be taken of the actual energy levels carried by the acoustic modes which couple most strongly with the vibrational modes of the surrounding pipe. Even so, for axi-symmetric sources, planewave propagation may control the energy transmission inside the pipe for frequencies well in excess of the cut-off frequency of the (1,0) acoustic cross mode.

8.3 THEORETICAL CONSIDERATIONS

8.3.1 Propagation of Acoustic Modes Inside Circular Ducts

At a particular frequency, the acoustic power generated by a source inside a circular duct (assuming ro end reflections) may propagate away from the source in one or more modes. The acoustic pressure at a point inside the duct can be described, following Morse and Ingard (1968, p.509) but with different notation, by

$$p(x,r,\phi) = \sum_{np}\sum (A_{np} \text{ Cos } n\phi + B_{np} \text{ Sin } n\phi) \text{ Jn } (k_{np}r)e^{i(k_x x - \omega t)}$$

where (r,ϕ) are polar co-ordinates centred on the pipe axis, and x is the distance from the source. n is the number of diametral pressure node lines, and p is the number of axi-symmetric cylindrical pressure nodes. For a rigid wall pipe, the radial fluid velocity at the pipe wall is zero: then the natural modes of the duct are found from the boundary condition $\partial p/\partial r = 0$ at $r = a$. Table 3.1 shows the first eight roots of $K_{np}=(k_{np}a)$ and their associated modal patterns.

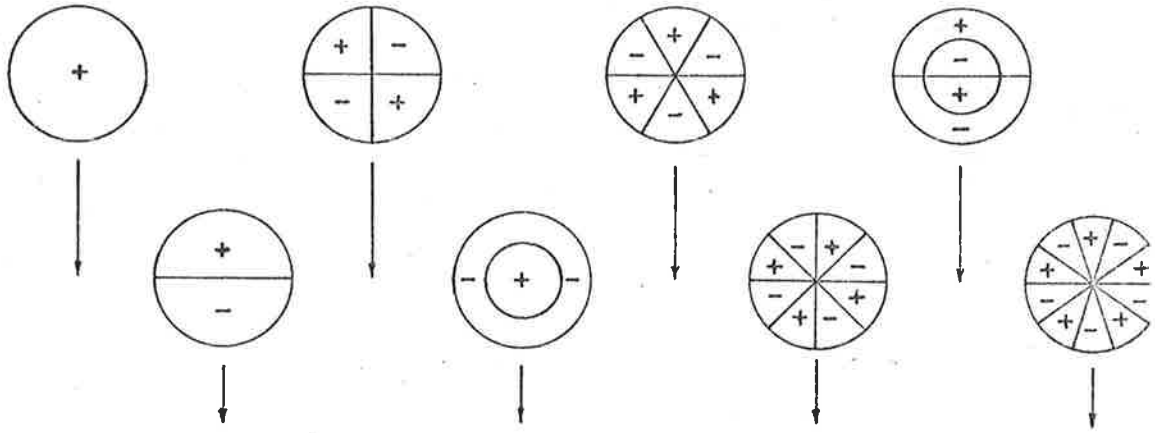

Mode n,p	0,0	1,0	2,0	0,1	3,0	4,0	1,1	5,0
K_{np}	0.000	1.841	3.054	3.833	4.200	5.319	5.331	6.415

Table 3.1 : Cut-off frequencies for acoustic modes in circular duct.

The axial wavenumber in the pipes is found from $K_x^2 = K_B^2 - K_{np}^2$ and the cut-off frequency of the (n,p)th mode ω_{np} is $K_{np}\ c_B/a$, below which the latter mode cannot propagate but decays rapidly with $|x|$. A_{np} and B_{np} are determined from the characteristics of the source and the duct termination.

At frequencies where $K_B < 1.84$, only plane waves can propagate inside the pipe, although, in the near-field of the source, the acoustic energy can be distributed in non-propagating modes as well. At high modal densities, equi-partition of the radiated energy amongst the possible modes tends to occur: then a 'random incidence' acoustic field will propagate down the pipe and statistical techniques can be used to estimate the coupling between the pipe mode shapes and the excitation. In this frequency range which corresponds to the existence of more than, say, 10 possible propagating modes or $K_B \geq 10$, the coupling of the acoustic source to any one acoustic mode is not likely to determine the overall response of the containing pipe. On the other hand, for $1 < K_B < 10$, the coupling of the source to the various acoustic modes will vary considerably between different low-order modes, as observed by Karvellis for flow control devices: then, the distribution of acoustic energy in the various propagating modes must be determined closely for each control device to enable any reasonable predictions of the vibrational

response to be made.

8.3.2 Pipe-wall response to internally-propagating (plane) acoustic waves

For an infinite pipe at low frequencies, the pressure field of an axi-symmetric acoustic mode propagating inside the pipe will force a response of the same wavenumber in the pipe wall : this wall response will therefore be axi-symmetric with an axial velocity equal to the axial propagation velocity of the acoustic mode (= ω/K_x). In general, we are concerned with acoustic plane waves i.e. the (0,0) mode rather than (0,1) mode.

Cremer (1955) has derived an expression for the transmission impedance of an infinite pipe z_τ, defined as $z_\tau = (p_1 - p_2)/j\omega w$, where p_1 is the acoustic pressure inside the pipe, p_2 is the external pressure, and w is the wall displacement: this can be written as

$$z_\tau = - \frac{jm'\omega}{\bar{\nu}^2} [1 - \bar{\nu}^2 + \beta^2 K_B^2] \qquad [8.1]$$

where $m' = \rho_s h$ is the pipe surface density. The terms in equation [8.1] represent, respectively, the reactance due to the pipe membrane stiffness, the mass reactance, and the reactance due to the pipe bending stiffness. For steel test section 3 ($\beta = 0.010$), $\nu < 1$ for much of the audible range, so that, for $K_B < 5$, $\beta^2 K_B^4 << 1$: thus the forced response of steel test sections 1 to 3 to plane-wave excitation will be membrane-stiffness controlled.

For pipes of finite length, however, in addition to this forced response, there will be a resonant response, due most likely to structural inhomogeneities in the pipe or to reflections of vibrational energy from the ends: such a coupling is not predicted by normal mode analysis (Powell (1958a)). In particular, for a finite pipe, the joint acceptance of the (m,n)th structural mode excited by a propagating acoustic mode can be found from equations (28), (31) and (32) of Bull and Rennison (1974a) (see Appendix A). The wall-pressure field of the (n,p)th propagating mode can be described by the cross-spectral density function

$$\phi_{np}(\underset{\sim}{\xi}, \omega) = \phi_{np}(\omega) e^{-a_x|\xi|} e^{ik_x\xi} \text{Cos } n\phi \qquad [8.2]$$

For a statistically homogeneous excitation over the internal surface of the pipe, $a_x = 0$. The separable narrow-band correlation coefficient then becomes

$$R_p(\xi, \eta, 0; \omega) = R_{px}(\xi, 0; \omega) \; R_{py}(0, \eta; \omega)$$

where

$$R_{px}(\xi, 0; \omega) = \text{Cos}\ (k_x \xi) \qquad [8.3]$$

$$R_{py}(0, \eta; \omega) = \text{Cos}\ (n \phi) \qquad [8.4]$$

Substitution of equation [8.3] into equation [31] of Appendix A leads to equation [37] of Appendix A, which with $K_m = k_m a$ reduces to

$$j^2_{mm}(\omega) = \frac{2K_m^2 \left[1 - (-1)^m \text{Cos}\ \Lambda K_x\right]}{\Lambda^2 (K_m^2 - K_x^2)^2} \qquad [8.5]$$

Putting equation [8.4] into equation [32] of Appendix A leads to

$$j^2_{nn}(\omega) = \tfrac{1}{4} \qquad [8.6]$$

when the circumferential order of the structural mode is equal to the circumferential order of the acoustic mode, and $j^2_{nn}(\omega) = 0$ otherwise.

From the simplified resonance frequency equation [2.8], only resonant structural modes of circumferential order $n \geq 1$ can be resonant below the ring frequency.* Thus, for $\nu < 1$, according to normal mode analysis, the coupling between an acoustic plane wave and any resonant structural mode is zero. By allowing for the circumferential variations in wall thickness which occur in practice, a finite coupling can be predicted between an acoustic plane wave and structural modes of circumferential order $n > 1$, and also between acoustic modes of order $n > 0$ and structural modes of different circumferential order. There are, however, considerable difficulties in establishing a relationship between the inhomogeneity distribution over the pipe surface and, say the changes in mode shapes produced: this is discussed in section 9.3.4.2.

* Kuhn & Morfey (1976), 47 (2) pages 147-161 have shown that $n = 0$ modes are resonant at $\nu_{mo} \simeq K_m$, although in this work their presence was never detected - see section 4.2.

In the near field of the acoustic source, the decaying higher-order modal pressure distributions will couple strongly to resonant modes of the same circumferential order. The joint acceptance of the driven structural mode can be estimated by assuming the near field of the higher-order mode to act over a length in the axial direction ℓ_x, which is approximately one-quarter of an acoustic wavelength at the excitation frequency,* but is correctly described by equation [8.4] in the circumferential direction: then $j^2_{mm}(\omega)$ will be reduced by a factor of $(\ell_x/\ell)^2 = (\lambda/4\ell)^2$ (Bozich and White(1970)). When higher-order modes can propagate inside the pipe, equations [8.5] and [8.6] can be used to estimate the coupling to structural modes of the same circumferential order.

The space-averaged spectral density of the acceleration response is found from equation [2.1] to be

$$\frac{[[\phi_{\ddot{w}}]]}{\phi_p} = \frac{8}{\rho_s^2 h^2} \sum_{\alpha} \frac{j^2_{\alpha\alpha}(\omega)}{[\{1 - (\frac{\omega_\alpha}{\omega})^2\}^2 + (\frac{\omega_\alpha}{\omega Q_\alpha})^2]}$$

For structural modes well separated in frequency, this reduces, at $\omega = \omega_\alpha$, to

$$\frac{[[\phi_{\ddot{w}}]]}{\phi_p} = \frac{8\ j^2_{\alpha\alpha}(\omega)\ Q^2_\alpha}{\rho_s^2 h^2} \qquad [8.7]$$

The magnitude of the resonant response will depend on the modal quality factors. For highly-damped pipe materials (low Q), the resonant response will be small and one expects that close agreement with the forced stiffness-controlled model for pipe response will be found. As the modal quality factors increase, the resonant response will increase relative to the forced component, leading, in turn, to increases in the power radiation.

* The characteristic axial extent of the near field is better approximated by a/K_{np} rather than $\lambda/4$.

8.3.3 Acoustic Power Radiation

An analysis of the acoustic radiation from a peristaltic wavemotion on a pipe of finite length ℓ and radius a, was presented in Brown and Rennison (1974), which is included as Appendix C. An expression for the velocity potential at a point in the radiation field of a small diameter pipe ($K_a << 1$)

was obtained by integrating the contribution from a distribution of point sources, which were arranged along the length of the pipe and used to model the peristaltic pipe velocity corresponding to a propagating surface wave. Then the far-field acoustic intensity generated by the propagating wave was found by time averaging the square of the instantaneous acoustic pressure ($=\rho\partial\phi/\partial t$) and dividing by ρc. The acoustic power followed by integrating this intensity over the surface of a far-field sphere, and was given by

$$\phi_\pi = \frac{S\rho c\, K_a\, \phi_{\dot{w}}}{2} \int_{K_B\Lambda(1-\frac{c_B}{c})}^{K_B\Lambda(1+\frac{c_B}{c})} \{ \frac{1 - \text{Cos}\ \zeta}{\zeta^2} \}\, d\zeta \qquad [8.8]$$

where S is the pipe area and $\phi_{\dot{w}}$ is the spectral density of the velocity response of the propagating axi-symmetric surface wave.

For the particular case of a long pipe ($K_a\Lambda > 10$) supporting a supersonic peristaltic wavemotion ($c_B > c$) for $K_a << 1$, such that $K_B\Lambda(1 - c_B/c) < -10$, the integral in equation [8.8] reduces to π, and the power radiation is closely given by

$$\phi_\pi(K_a \to 0) = S\rho c(\frac{K_a\pi}{2})\phi_{\dot{w}} \qquad [8.9]$$

The corresponding radiation ratio σ is $K_a\,\pi/2$. For sonic wavespeeds ($c_B = c$), the power radiated is found to be one-half that given by equation [8.9], while for subsonic wavespeeds ($c_B < c$), the power radiated goes to zero as $K_B\Lambda(1 - c_B/c)$ goes to infinity i.e. as the radiation occurs increasingly only from the pipe ends.

In general, $K_a \simeq 0(1)$ and the power radiation will be reduced by diffraction around the cylinder. This case will be important for supersonic wavespeeds: then, while $K_B < 2$ for plane-wave propagation, $K_a >> 2$ for $c_B >> c$. For supersonic wavespeeds on a long (infinite) cylinder, this effect can be estimated exactly, as discussed in Appendix C, where, in Fig. 4, $\phi_\pi(K_a)/\phi_\pi(0)$ is plotted againt K_a: for $K_a > 1$, $\phi_\pi(K_a)/\phi_\pi(0)$ tends to $2/(K_a\pi)$, or equivalently σ tends to unity, as expected for supersonic surface wave-motions. Fig. 4 has been used for all K_a corrections, independent of c_B/c.

When resonant modes contribute significantly to the power radiation, their radiation ratios can be estimated from equation [2.26]. When $K_a < K_n$, resonant modes of circumferential order n are subsonic and their σ's are correspondingly less than unity as discussed in Appendix B. The contribution to the total acoustic radiation made by these subsonic modes for plane-wave excitation is theoretically zero for perfectly homogeneous, circular pipes and therefore their influence has been neglected in previous work, especially as expressions for their radiation ratios have not been available until recently.

A lower bound to the acoustic power radiation from pipes excited by acoustic plane waves can then be proposed. In this, the radiation resulting from the forced axi-symmetric vibration response to a propagating acoustic plane wave is considered to represent the minimum level of acoustic radiation from the pipe. The contribution of resonant modes is assumed to be small, as they are theoretically uncoupled to the plane-wave excitation and generally have relatively low radiation ratios. The lower-bound model is a datum level with which actual power radiation measurements can be compared. For example, the modal content of the (response and) radiation can be examined relative to the lower-bound datum. Similarly, the effects of variations in the pipe end conditions or in the source/pipe configuration and the effectiveness of pipe damping treatments can be analysed in terms of an approach to the lower-bound prediction.

8.4 PRESENT WORK

Like Kuhn (1974), we are concerned to understand the discrepancies in TL found for steel pipes for plane-wave excitation.

As an introduction to this, a series of experiments were performed which established the validity of the lower-bound model for the power radiation from pipes excited by propagating plane waves: an experimental arrangement was used which closely satisfied the idealisations of the theoretical model i.e. $K_B\Lambda > 1$, $K_B < 2$, and low Q.

Now similar experiments have been carried out using lightly-damped steel pipes (high Q). In these, the dependence of the power radiation on variations in pipe length and wall thickness for constant radius, and on

the modal quality factors, was investigated: in addition the effects of strong asymmetries in the acoustic source and of the application of surface damping treatments and point masses to the pipe were examined.

The important results from these experiments are presented in the next chapter, together with conclusions concerning the magnitude of and reasons for the observed discrepancies.

CHAPTER 9

EXPERIMENTAL INVESTIGATIONS

9.1 INTRODUCTION

In view of the discrepancies observed between existing measurements and theoretical predictions in this plane-wave region, it was important to verify experimentally the concept of a lower bound to the acoustic radiation from a long pipe excited by acoustic plane waves propagating inside the pipe, before proceeding to more complex and practical situations not meeting the idealisations of the theoretical model.

The observed discrepancies appear to have resulted from departures in experiments from the assumed models, and so the present apparatus was constructed to avoid any significant experimental non-idealisations. For example, it was ensured that propagating acoustic plane waves were the only excitation, and the contribution to the acoustic power radiation made by resonant modes was effectively eliminated by using a pipe with high material damping to reduce the resonant response.

The end conditions, both acoustic and mechanical, were then relaxed to examine their effects on the lower-bound prediction in this case of a highly-damped pipe. Most of the details of these experiments have been presented in Brown and Rennison (1974) (Appendix C); those that are most important are summarised in section 9.2 , where additional and more comprehensive measurements are presented.

Subsequent experiments involved steel pipes representative of those used by Heckl (1958). Since light material damping existed, the resonant modes were expected to determine the vibrational response and, to a lesser extent, the acoustic power radiation. These increases above the lower-bound prediction were to be related to the actual modal resonances and quality factors present in the pipes, so that an estimation of the experimental joint

acceptances could be made. A range of pipes with different values of Λ and β have been used, and the orientation of the acoustic source has been varied to compare the results for a near-field excitation with those for an ideal far-field source. New conclusions are reached concerning the origin of the observed discrepancies between the experimental measurements and theoretical predictions of the vibrational response and acoustic power radiation.

9.2 EXPERIMENTS WITH HIGHLY-DAMPED PIPES ($Q \to 1$)

9.2.1 Experimental Design

The lower-bound model requires that the resonant component of the vibrational response of the pipe is small relative to the axi-symmetric forced level and that only acoustic plane-wave propagation occurs inside the test pipe.

To achieve the first condition, a pipe of high material damping and with a mechanical termination at the end of the pipe away from the acoustic source was used. In particular, a rigid P.V.C. pipe test section (ℓ = 3.5 m, a = 50 mm, h = 1.5 mm so that Λ = 70. and β = 0.0087) was selected. The average quality factors were low ($Q \simeq 25$) (measured as in section 6.2). The ends of the test pipe were clamped in solid concrete blocks and the mechanical termination, made of balsa-wood fingers, alternatively-layered with soft mastic, was attached to the outside of the pipe at the end opposite the source to reduce mechanical reflections.

As a far-field acoustic source, the source loudspeaker was contained in a high transmission loss (TL $\simeq$ 85dB) enclosure and connected via an isolation joint to one of the concrete blocks. The internal bore from the speaker to the test pipe was smooth to avoid the local generation of acoustic cross modes. An acoustic termination was mounted at the opposite end. For $0.2 < K_B < 2$, the absorption coefficient was greater the 0.98: that there was only plane-wave propagation for $K_B < 1.84$ was confirmed by noting that the pressure amplitude and phase remained constant across the source end of the pipe.

Different gases were used inside the pipe to vary the wavespeed of the forced response in an examination of the effects on the power radiation from finite pipes of subsonic, sonic, and supersonic structural wavespeeds: this also allowed the forced response to be monitored over a wider frequency range. For example, the plane-wave region extended to 2000 Hz for air inside the pipe and to 5000 Hz for Helium inside the pipe, but decreased to 1600 Hz using carbon dioxide inside the pipe.

The acceleration response was measured with B & K 4344 2g accelerometers attached to the pipe with double-sided adhesive tape, while the excitation pressure inside the pipe was measured with a B & K 4136 6.35 mm microphone mounted flush with the inside surface of the pipe-wall. Measurements of the sound power radiated were made in a reverberation chamber (equiped with a rotating diffuser) with a traversing microphone (B & K 4134 12.7 mm). The minimum value of $K_B\Lambda$ was 15; radiation end effects were therefore generally unimportant.

9.2.2 Vibration Response

At low frequencies (< 1500Hz or $\nu < 0.28$), a moderate resonant response was superimposed on the forced axi-symmetric response as in Fig. 6 of Appendix C for single-frequency excitation: but at 4000Hz, the variation in acceleration level was only $\pm$ 2dB over the whole pipe surface. When the ring frequency is approached (for helium inside the pipe), the pipe-wall mass acts to reduce the wall impedance: then equation [8.1] must be used in full for predictions of the forced response, and the mass loading by the accelerometers must be taken into account, as discussed in Appendix C.

For plane-wave propagation, the forced response is dependent only on the excitation pressure and not on the wavelength, so that the results for all gases (CO_2, air and helium/air mixture) can be presented together, as in Fig. 9.1. Good agreement exists between the experimental results and the theoretical predictions, both for single-frequency excitation and for excitation with one-third octave bands of random noise, although equation [8.1] becomes inaccurate for $\nu > 0.8$.

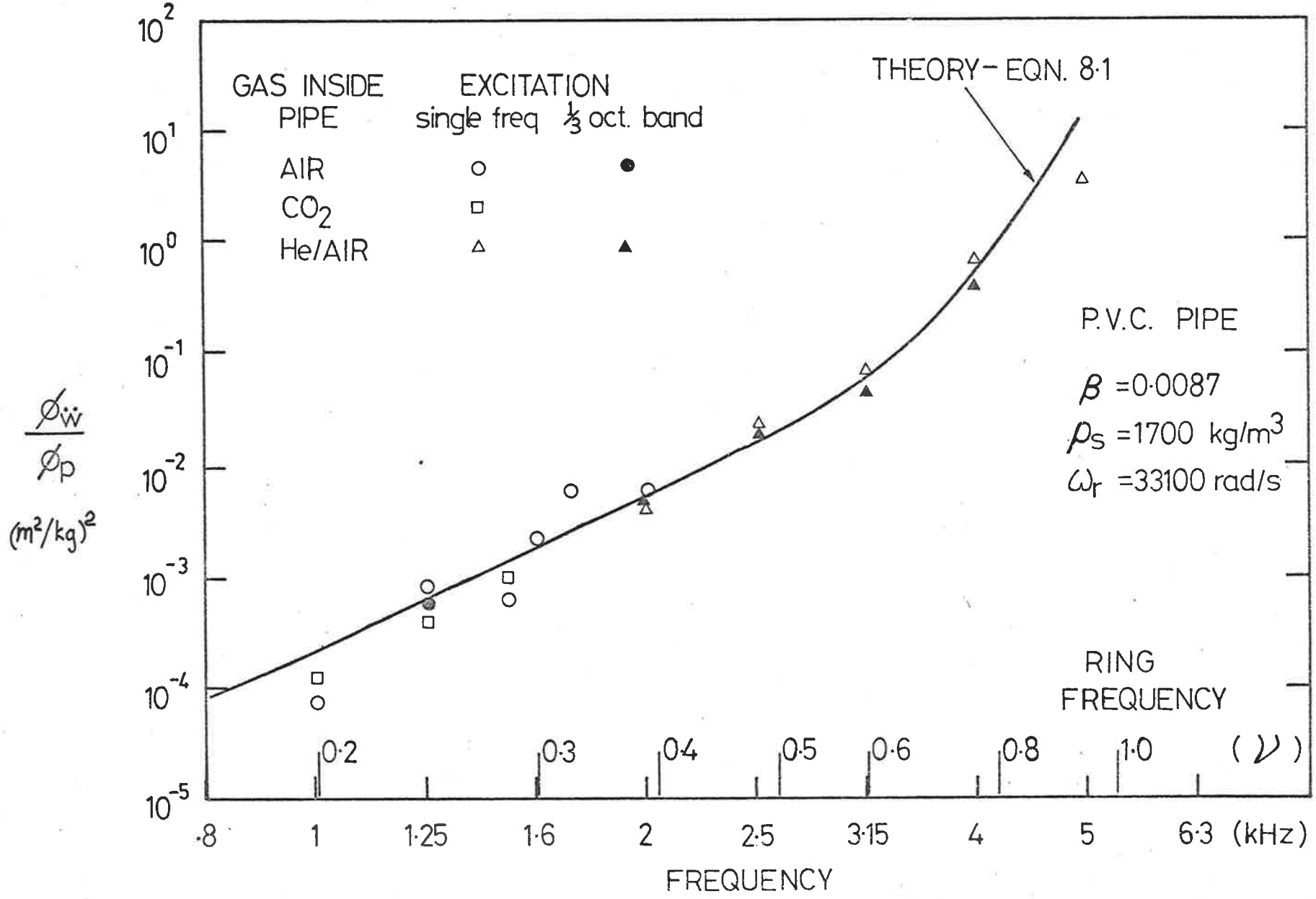

FIG. 9.1 AXI-SYMMETRIC RESPONSE OF P.V.C. PIPE TO INTERNALLY PROPAGATING PLANE WAVES

9.2.3 Acoustic Radiation

Measurements of the acoustic power radiation from the test pipe excited by acoustic plane waves propagating inside the pipe were made with excitation in single frequencies and with one-third octave bands of random noise. Different gases were used inside the pipe to examine the effect on the power radiation of varying the structural wavespeed. Theoretical considerations suggest that supersonic wavemotions are more efficient radiators than sonic wavemotions, which in turn are more efficient than subsonic wavemotions.

The directivity of the acoustic radiation showed qualitative agreement with general predictions. For a sonic wavespeed (air inside the pipe), the acoustic power was beamed along the pipe axis: the intensity, whether measured in an anechoic chamber or in the direct field of the pipe when in the reverberation chamber, was found to increase with distance along the pipe away from the source end, but to fall rapidly with radial distance from the pipe (6dB/doubling distance compared with 3dB/doubling distance for a line source).

In Fig. 9.2 measurements of the power radiated from the test pipe with different structural wavespeeds for the same excitation intensity are compared with the theoretical predicitons. Again, close agreement exists between theory and experiment The differences in radiation ratio are clearly demonstrated by the well-separated curves of power radiation for the three different wavespeeds.

The effects of varying the pipe end conditions were examined by removing first the mechanical and then the acoustic terminations. Though the pipe vibrational response became more resonant, only small changes in the power radiation occurred, as shown in Fig. 11 of Appendix C: this is expected, since the radiation ratio of peristaltic wavemotion is greater than the radiation ratios of the resonant modes of the pipe when the modes are subsonic, as they tend to be at low ν(see Appendix B). Local clamping of the pipe produced no significant changes in the power radiation, even though the wall

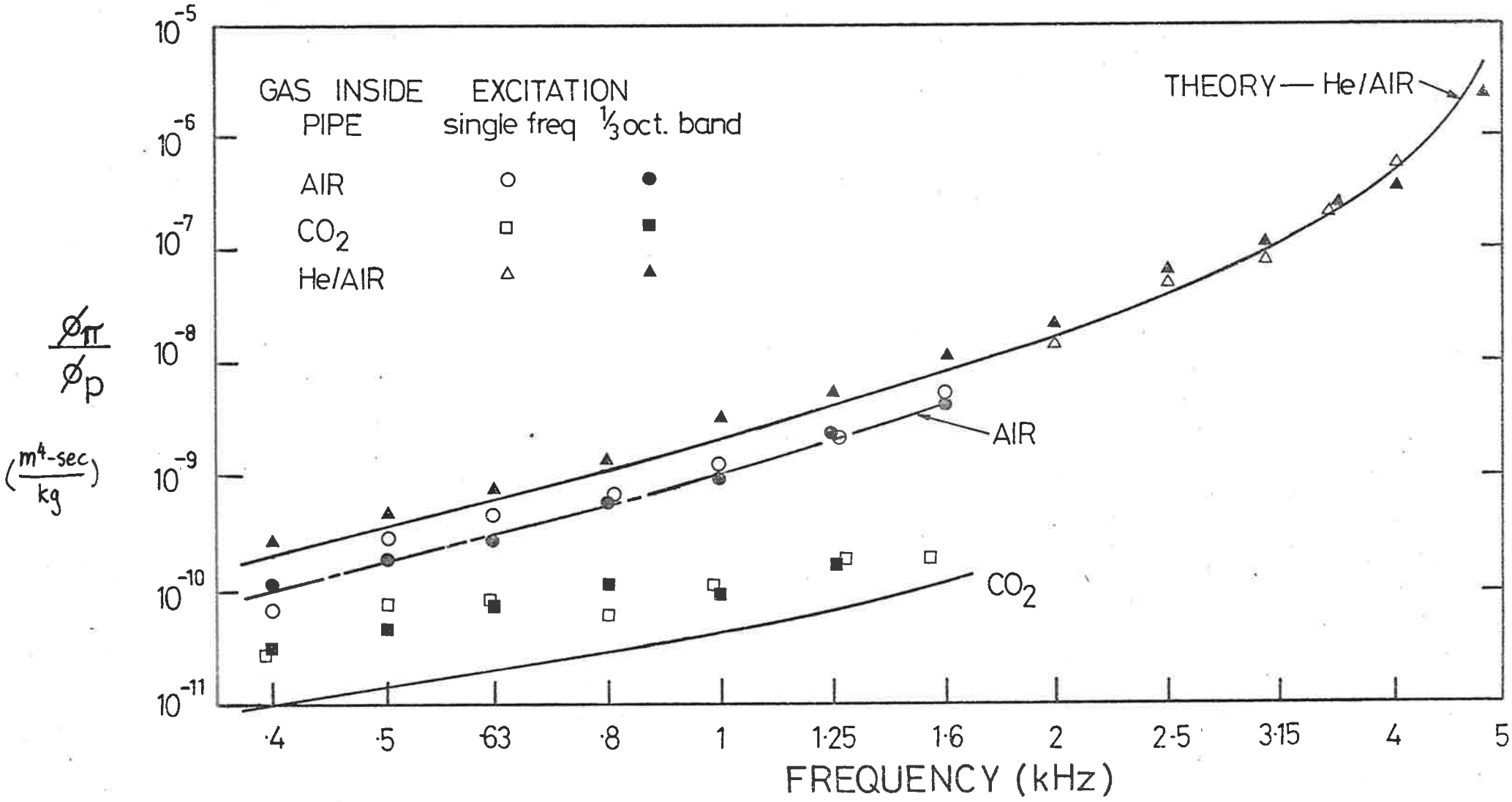

FIG. 9.2 ACOUSTIC POWER RADIATION FROM P.V.C. PIPE, EXCITED BY PROPAGATING ACOUSTIC PLANE WAVES

accelerations were reduced considerably near the clamp and a slightly greater resonant response occurred overall. Furthermore, the placement of an asymmetric source at the beginning of the P.V.C. test pipe produced no measureable increase in the radiated power above the level produced by the isolated far-field source excitation, for the same excitation level measured in the far field of the source: since the pipe is highly damped, the vibration response to any asymmetry in the pressure field will be localised and thus confined to the near field of the source (within a/K_{np}) and little additional power will be radiated.

9.2.4 Conclusions

Considerable care was taken to ensure that the experimental conditions closely represented those in the theoretical model. Although a mild resonant response was produced in the P.V.C. pipe by the acoustic plane-wave excitation, the forced axi-symmetric response was clearly distinguished at most frequencies and was well predicted by existing analysis. The amplitude of the resonant response relative to the forced response decreased as ν increased.

The acoustic power radiation from the P.V.C. pipe was predicted closely for supersonic, sonic and subsonic structural wavespeeds, by considering only the radiation produced by the forced axi-symmetric wavemotion. Even though a response in resonant modes existed, the radiation from these modes can be neglected when the resonant response is of similar amplitude to the forced response, since the modal radiation ratios are far lower than that of the peristaltic wavemotion. Experimental confirmation of the theoretical dependence of the radiation ratio of a forced axi-symmetric wavemotion travelling along a pipe on the structural wavespeed has been clearly demonstrated for a long, small diameter pipe. A relaxation of the pipe end conditions, allowing reflections of mechanical and acoustic energy to occur, produced no significant changes in the power radiation, although a small increase in the resonant response was found.

Thus, for this idealised experimental case of a highly-damped P.V.C. pipe ($Q \simeq 25$) excited by internally propagating, acoustic plane waves, the acoustic power radiation has been accurately represented by the lower-bound model.

9.3 EXPERIMENTS WITH LIGHTLY-DAMPED PIPES

9.3.1 Introduction

The differences between experimental measurements and theoretical predictions of the TL of pipes found by Heckl (1958) were proposed to arise mainly from the coupling of higher-order acoustic modes in the near field of the speaker source with resonant modes of the pipes and from reflections of the forced wavemotion from the ends of the pipe. In particular, Heckl found that an asymmetric source attached to the test pipe produced higher radiated power levels than one mounted axi-symmetrically and that the differences decreased as Λ increased. Similarly, Kuhn (1974) observed significant reductions in resonant response as the near field of his acoustic source was de-coupled from the test pipe, and he suggested that the measured differences in power radiation resulted purely from the influence of higher-order acoustic modes in the near field of the source. However, no experimental confirmation of this proposal has been presented.

The present experiments extend those described in section 9.2 and are necessary considering the differences discussed previously. These experiments were performed to examine the magnitude of the increase in power radiation relative to the lower-bound level, both for the idealised acoustic plane-wave excitation and for near-field excitation, for various pipe lengths and wall thicknesses. Modal characteristics of the test pipes were measured in detail to enable an estimation of the joint acceptance to be made. The effects on the response and power radiation of adding damping treatments to the pipe surface were examined to determine the required modal quality factors for the power radiation to approach the lower-bound prediciton.

9.3.2. Effects of Variation in Pipe Length and Wall Thickness

Experiments were carried out to consider the effects, on the vibrational response and on the power radiation from steel pipes, of variations in β for constant Λ (=80.) and of variations in Λ for constant β (=0.00591).

Rigid ends (glued with epoxy cement) were used in the experiments involving variations in Λ: the pipes were mounted in the reverberation chamber in massive ends. An anechoic termination was used inside the pipe to ensure plane-wave propagation. The acoustic source was placed outside the reverberation chamber and connected to the test section via a section of heavy-wall (h = 6mm) pipe of the same internal diameter. Two vibration isolators (see Fig. 3.3) were placed 2 m from the source between the source and the test sections to remove the effects of any mechanical and acoustic near-field excitation produced by the source. A smooth bore extended from source to termination. Thus acoustic plane waves propagating through the test section were the sole excitation.

The excitation pressure inside the pipe was measured with a B & K 4136 12.7 mm microphone mounted flush with the pipe wall. The wall acceleration response was measured with a B & K 8307 0.5g accelerometer and the radiated power measurements were made using standard reverberation chamber techniques. Measurements of average quality factors were taken using the response-decay method. Both air and a helium/air mixture were used inside the pipes, the latter to extend the plane-wave region of the experiment; the response measurements were found to be essentially independent of the gas used inside the pipe providing $K_B < 1.84$.

The results of the acoustic excitation experiments described in section 4.8 are used to demonstrate the effect of variations in β. In these experiments, the power radiation measurements were made in the anechoic chamber. Measurements of the TL (defined, for plane-wave propagation, by $TL = 10 \log_{10} (\phi_p \pi a^2 / \phi_\pi \rho c_B)$ of test pipe 1, excited by internal acoustic plane waves, conducted in both the anechoic and the reverberation chamber agreed with each other within $\pm$ 1 dB for frequencies greater than 1 kHz and within $\pm$ 3 dB for lower frequencies.

The measured results from these experiments, in which β was varied for constant Λ, are presented in Figs. 9.3(a) and (b). The increases in acceleration response above those predicted using the forced model (equation (8.1)) are shown in Fig. 9.3(a) for test sections 1, 2 and 3 (Table 3.1): the deviations from the forced prediction vary from 40 to 60dB at low frequencies to 20 to 30 dB at the cut-off frequency of the (1, 0) acoustic mode inside the pipe and are seen to be approximately inversely proportional to frequency. By referring to Figs. 4.4(a), (b) and (c), the peaks in these curves can be associated with the presence of groups of lightly-damped, low circumferential-order modes of low axial order. In Fig. 9.3(b), the corresponding data of the acoustic power radiation are presented as the ratio of the measured power radiated to that predicted from the lower-bound model. The measured discrepancies vary between 15 and 30 dB and the mean curves are fairly independent of frequency. At low frequencies, the smaller differences between the measured and theoretical power radiation (Fig. 9.3(b)) and the measured and theoretical acceleration response (Fig. 9.3(a)) reflect the large differences in radiation ratio between subsonic resonant modes and that of sonic axi-symmetric wavemotion. As frequency increases, these differences decrease as the average radiation ratio of resonant modes increases as ν approaches ν_{ac} (see Fig. 4.11(c)). There appears to be no clear dependence on β for either set of data, the differences between curves resulting from variations in average quality factors and modal densities between the pipes.

The effects on the pipe vibrational response and acoustic radiation of variations in Λ for constant β(=0.00591) are presented in Figs. 9.4(a) and (b). A helium/air mixture was used inside the pipes and measurements were made in the reverberation chamber. The frequencies, at which low axial-order modes of circumferential order $n \geq 2$ are resonant, are essentially independent of Λ for the pipes used and are shown in the figures. Again, the peaks in the response data can be associated with groups of lightly-damped low axial-order modes of $n \geq 2$: the ratios of the measured response to

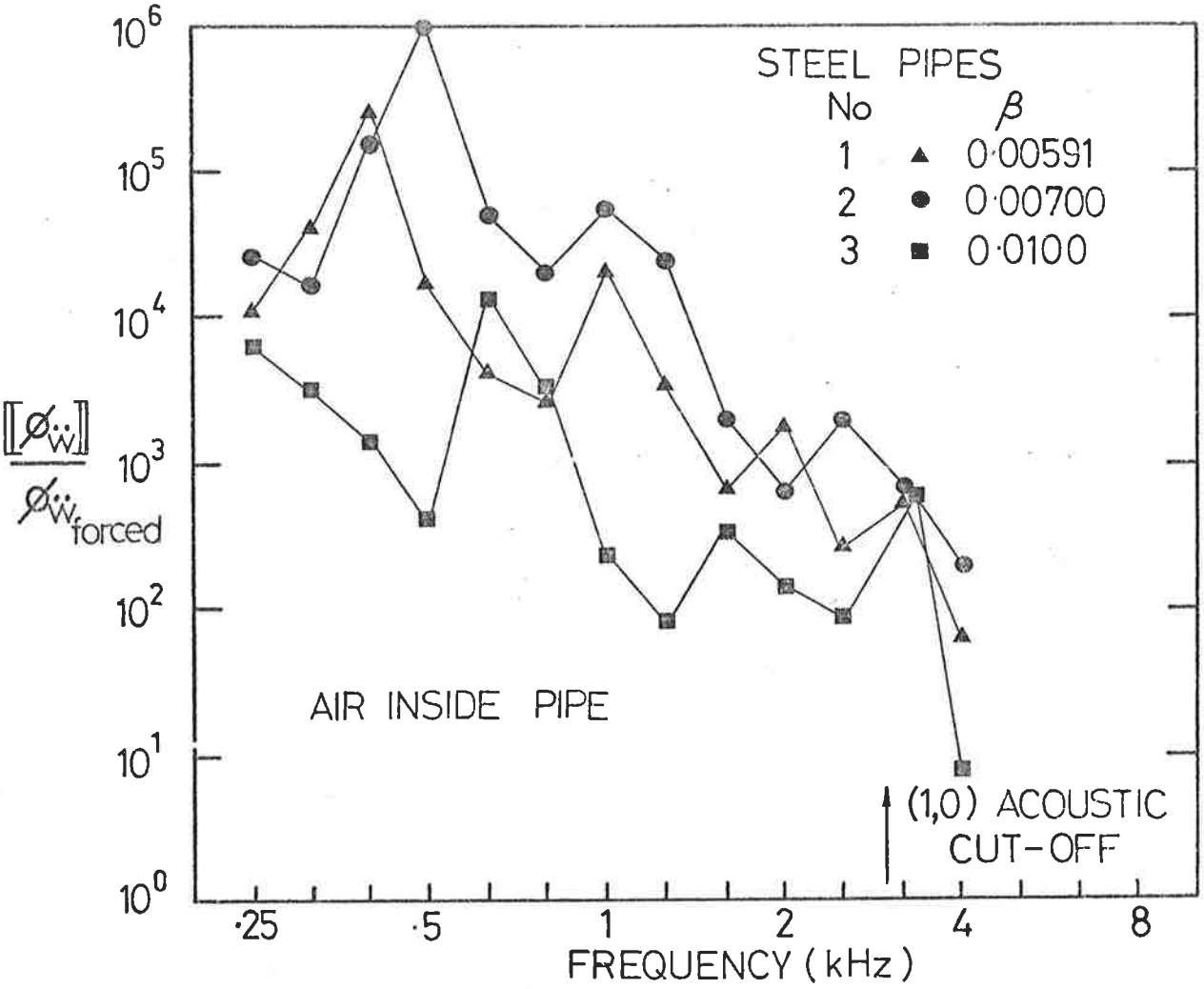

FIG. 9.3(a) EFFECT OF β ON RESPONSE - STEEL PIPES

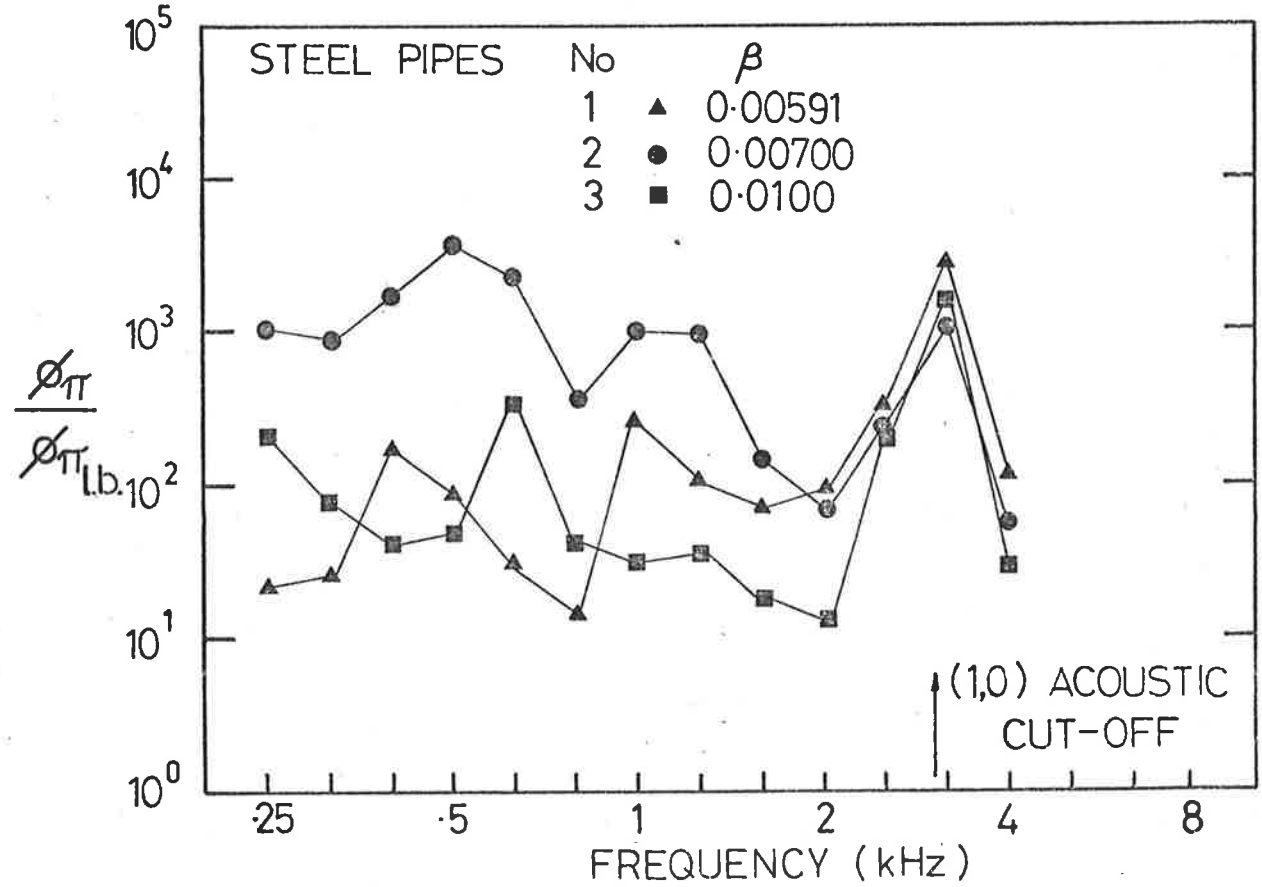

FIG. 9.3(b) EFFECT OF β ON POWER RADIATION

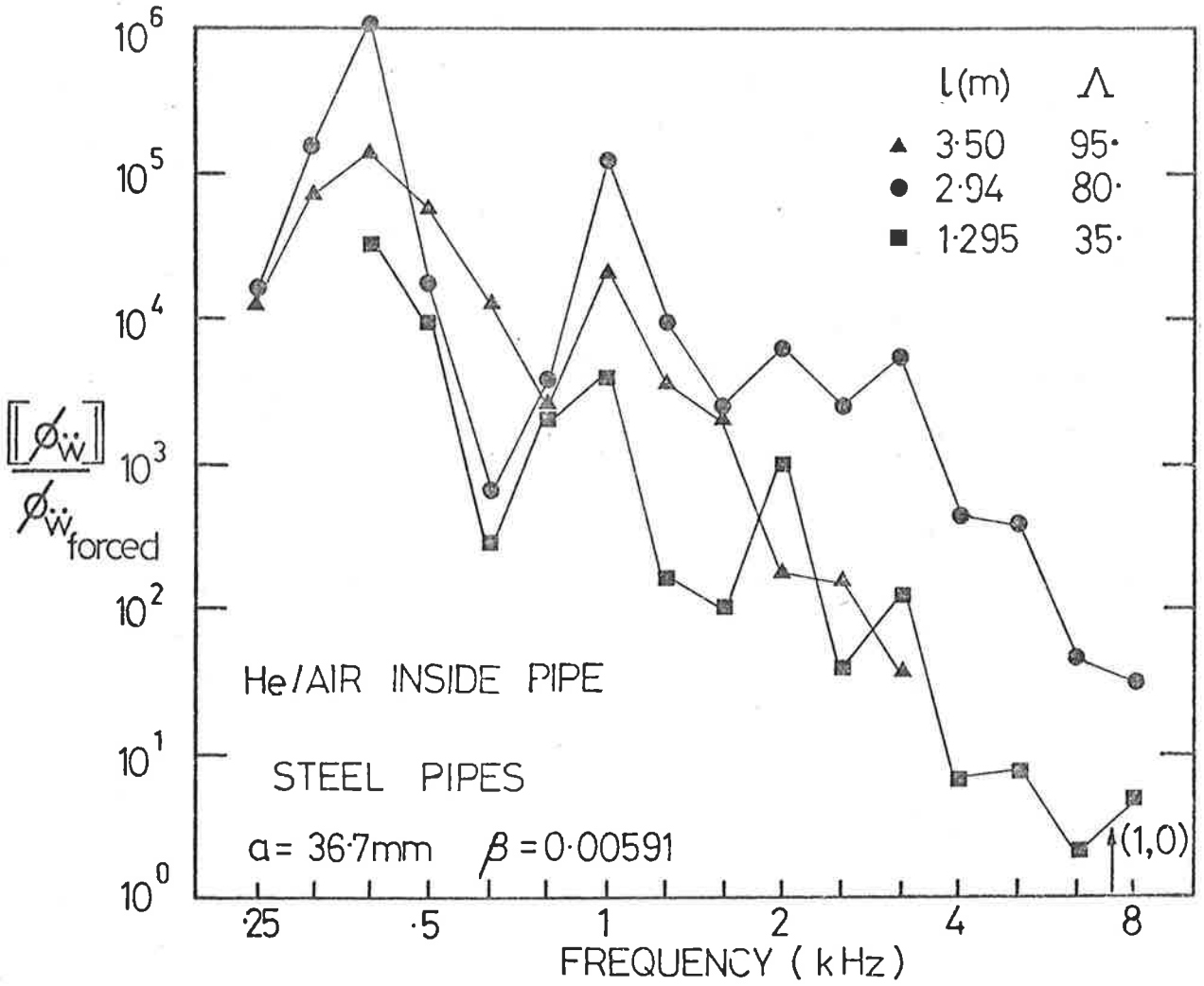

FIG. 9.4(a) EFFECT OF Λ ON VIBRATION RESPONSE

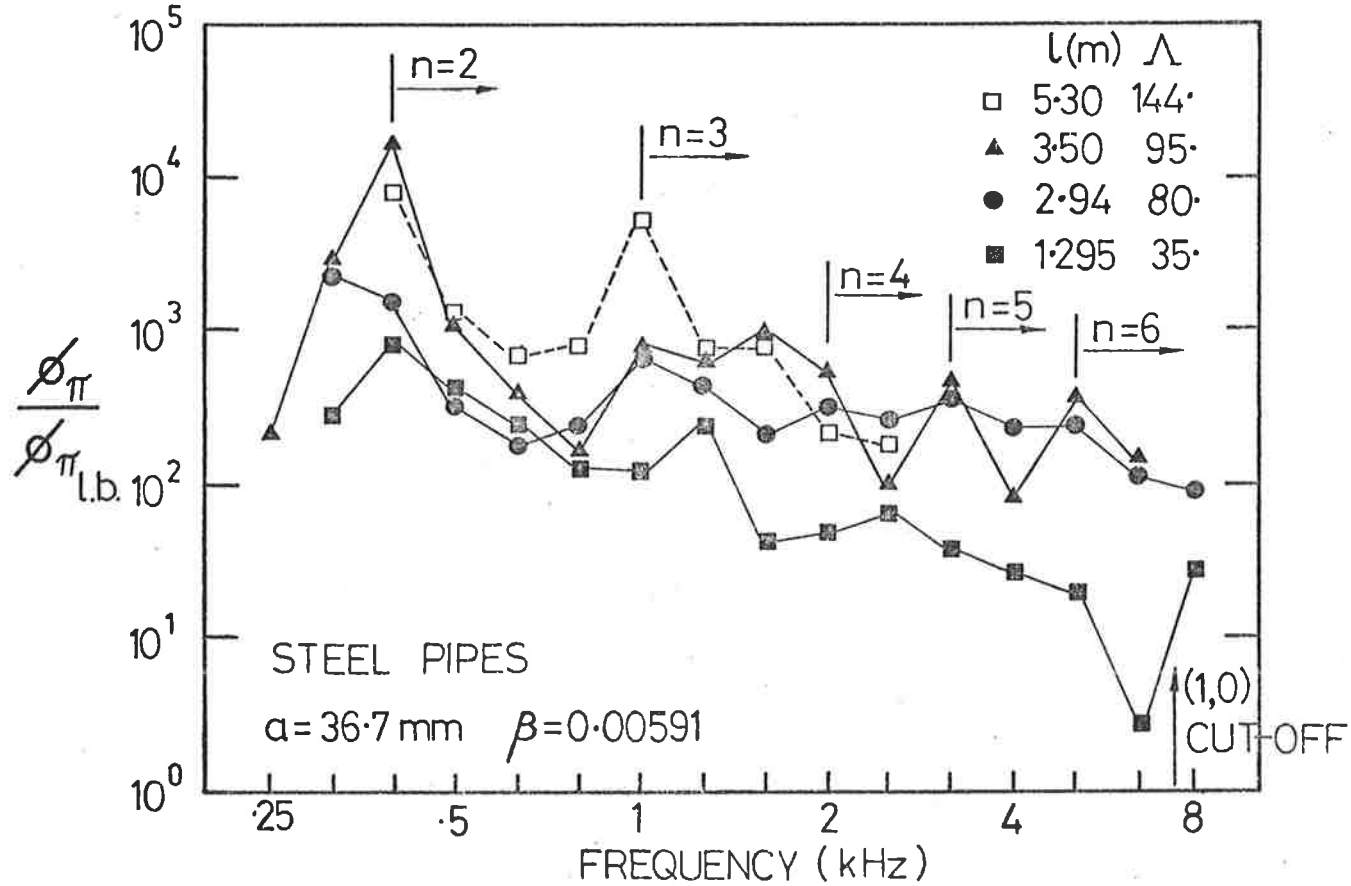

FIG. 9.4(b) EFFECT OF Λ ON POWER RADIATION

theoretical forced response decrease with increasing frequency but appear to increase slightly with increasing Λ. In Fig. 9.4(b), the ratios of the measured and theoretical power radiation have similar characteristics to those in Fig. 9.3(b): the mean curves are independent of frequency and tend to reflect the contribution of subsonic modes, even up to n = 6. Allowing for the variations in quality factors between pipes, it appears that the differences between measured results and theoretical predictions may increase slightly with increasing Λ: longer pipes (β constant) may radiate more power due to their higher modal densities ($N(\nu) \alpha \Lambda$). In fact the spread in data for the different pipes is of the same order as the change in pipe length, although, of course, differences in average quality factors between the pipes prevent definite conclusions being made.

It has been seen that large discrepancies between measured acoustic radiation levels and those predicted from the lower-bound model are produced for plane-wave excitation. These discrepancies are due to an unpredicted resonant response in all modes. In contrast to the experiments of Heckl and Kuhn, higher-order acoustic modes and mechanical vibrations generated at the source were isolated from the test section, so that the excitation was purely acoustic plane waves: this suggests that structural characteristics of the test section may be responsible for the observed coupling to resonant modes. However, the additional effects of the acoustic near field were also examined for comparison with the far-field plane-wave excitation.

9.3.3 Effect of the Source Near Field

The near field of an asymmetric source should be more strongly coupled to the resonant modes of the pipe than acoustic plane waves, even though the higher-order acoustic modes existing in the near field cannot propagate. This additional coupling, produced by the source near field for the same plane-wave intensity measured in the source far field, has been examined for test section 1 (β = 0.00591 and Λ = 80.3).

In Fig. 9.5, the measured power radiation from test section 1 for

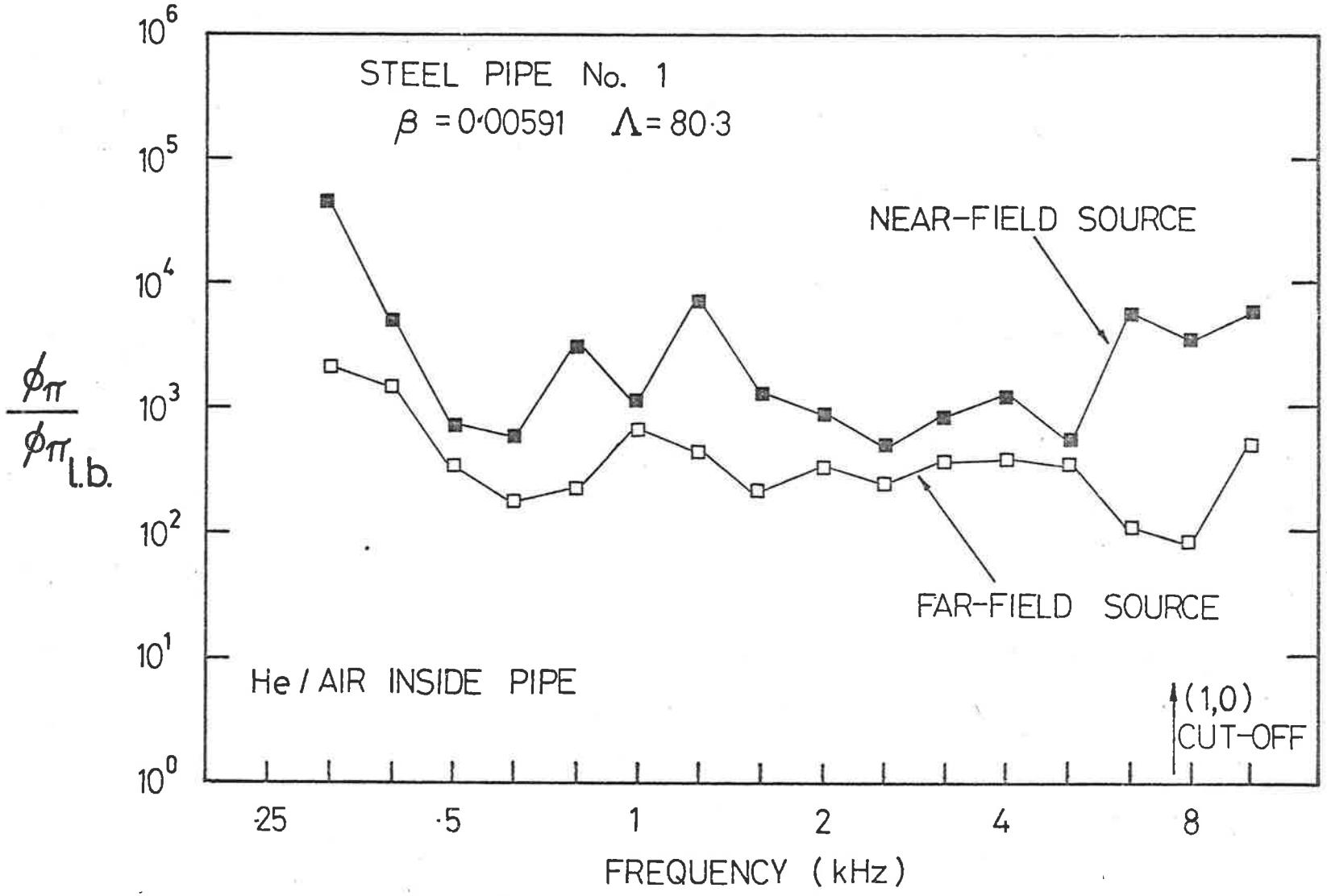

FIG. 9.5 COMPARISON OF POWER RADIATED FOR NEAR-FIELD AND FAR-FIELD EXCITATIONS

purely acoustic plane-wave excitation is compared with that with the source placed adjacent to the test section: the excitation intensity was measured in the far field of the source where only plane waves occurred. Additional increases of 5 to 10 dB in power radiation were produced over the whole frequency range: but these are small relative to the existing discrepancies for purely far-field excitation. Similar increases in acceleration response were produced by changing the source from the far-field to the near-field position.*

A more detailed examination of the coupling was made by monitoring the acceleration response of two individual resonant modes for different source configurations: the (4,1) and (9,1) modes of the steel pipe (Λ = 95.5) were used. With a similar experimental arrangement to that described above, the peak acceleration response of each mode was measured for single frequency excitation at its resonance frequency and for constant excitation intensity in the far field of the source (whose position could be varied). Dipole, asymmetric and axi-symmetric monopole, and far-field monopole sources were used. The results for the (4,1) mode are shown in Fig. 9.6, together with calculations for the dipole excitation which are based on equations (8.7), (8.4) and (8.5) and measured values of Q_{mn} and ω_{mn} and on the dipole pressure distribution measured adjacent to the source. Encouraging agreement is found.

For constant far-field plane-wave intensity, the source which excited the (1,0) acoustic mode most strongly, even when the (1,0) mode cannot propagate, produced the greatest response in the (4,1) vibration mode. These sources produced additional increases in the modal response of 15 to 30dB above the level due to far-field plane-wave excitation (of the same intensity away from the source): however, differences in excess of 40dB still exist between the measured response to acoustic plane-wave excitation and that predicted from the forced model. It is seen that the joint acceptance varies between 10^{-5} and 10^{-8}, depending on the excitation. For plane-wave excitation, $j_{mm}^2 \simeq 10^{-3}$ so that $j_{nn}^2 \simeq 10^{-5}$ for the (4,1) mode in Fig. 9.6: certainly, j_{nn}^2

* These measurements were conducted sequentially on the same day specifically to demonstrate the magnitude of the increases in acoustic power produced as the source was moved into the near field of the test pipe, all other parameters remaining the same.

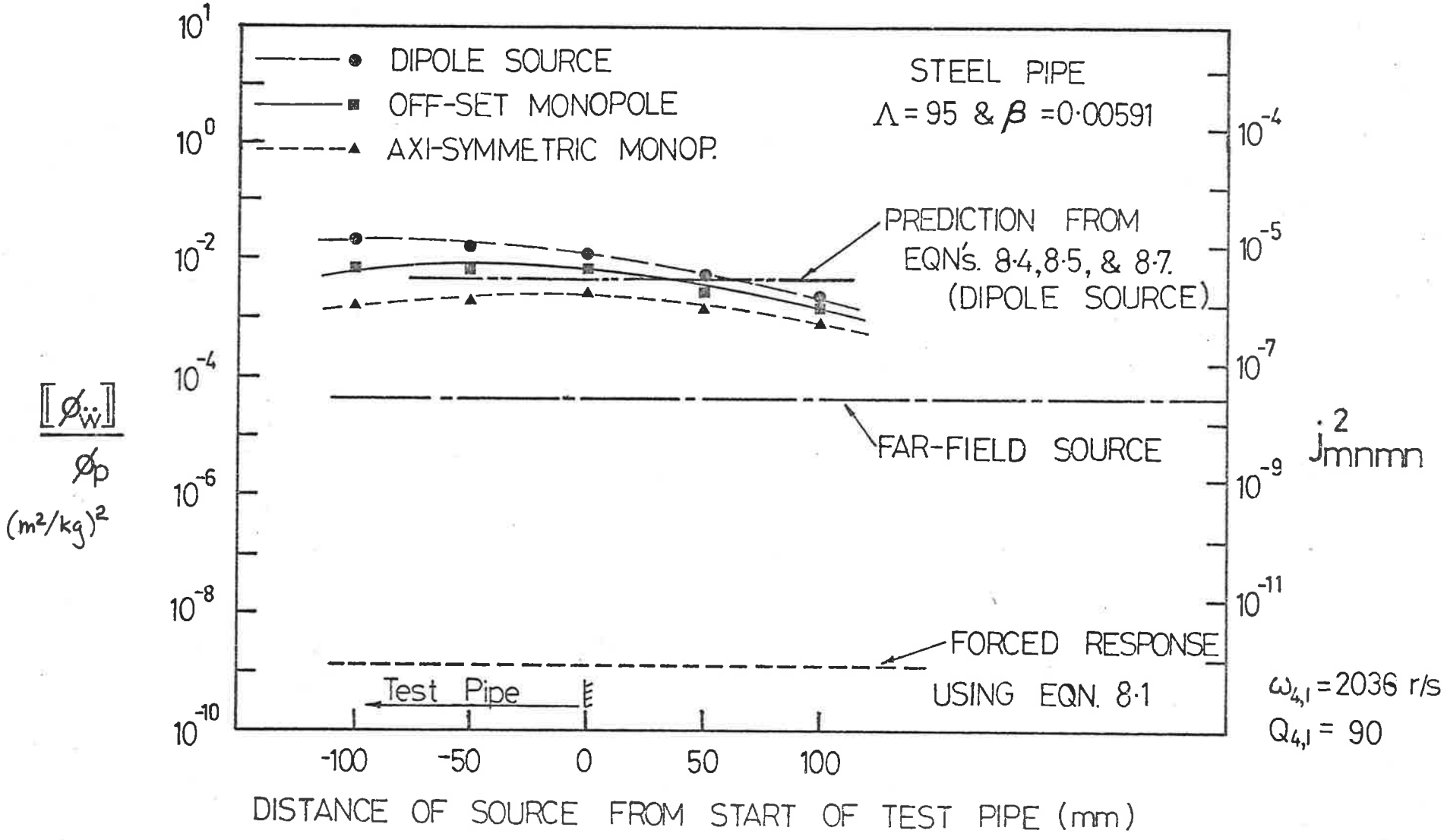

FIG. 9.6 VARIATION OF MODAL RESPONSE WITH SOURCE POSITION & TYPE

is not zero and, to some extent, approaches j_{mm}^2.

In the present case, strong differences between the measured results and theoretical predicitons result purely from the characteristics of the steel test sections. It has been shown that compared to purely plane-wave excitation, near-field source enhances the existing coupling by only small amounts above that produced by purely plane-wave excitation. It would seem that inhomogeneities in the pipe structure can cause fairly strong coupling between the axi-symmetric pressure field of the acoustic plane waves and resonant modes of $n > 0$, independent of any near-field effects: these inhomogeneities become important due to the higher pipe impedance to plane-wave excitation than found solely from considerations of the pipe mass. Experiments to examine the effects of such structural variations are discussed in section 9.3.4.

9.3.4 Considerations Concerning Pipe Structural Inhomogeneities

Variations in pipe wall thickness over the surface area of the pipe, such as result from normal manufacturing processes, will cause small deviations from the assumed mode shapes given by equation (2.6): these changes in mode shapes will allow a finite coupling to be produced circumferentially, resulting in a resonant response. Since all pipes will be imperfect to some extent, a resonant response will always occur in practical systems with plane-wave excitation. In the present section, experiments are reported which explore the effects on the coupling between the resonant modes and an acoustic plane-wave excitation of variations in the surface mass of an actual test pipe.

9.3.4.1 Effect of Changing the Surface Mass

Measurements of the wall thickness at different positions over the surface of the various test pipes revealed variations in h of from 5 to 15% around the circumference, and variations in the mean values of h of approximately 3% along the pipe lengths. For example, Fig. 9.7(a) plots the circumferential variation in h at several axial positions for the steel test section for which $\Lambda = 35.3$, $a = 36.7$ mm and $\beta = 0.00591$. It is proposed that these

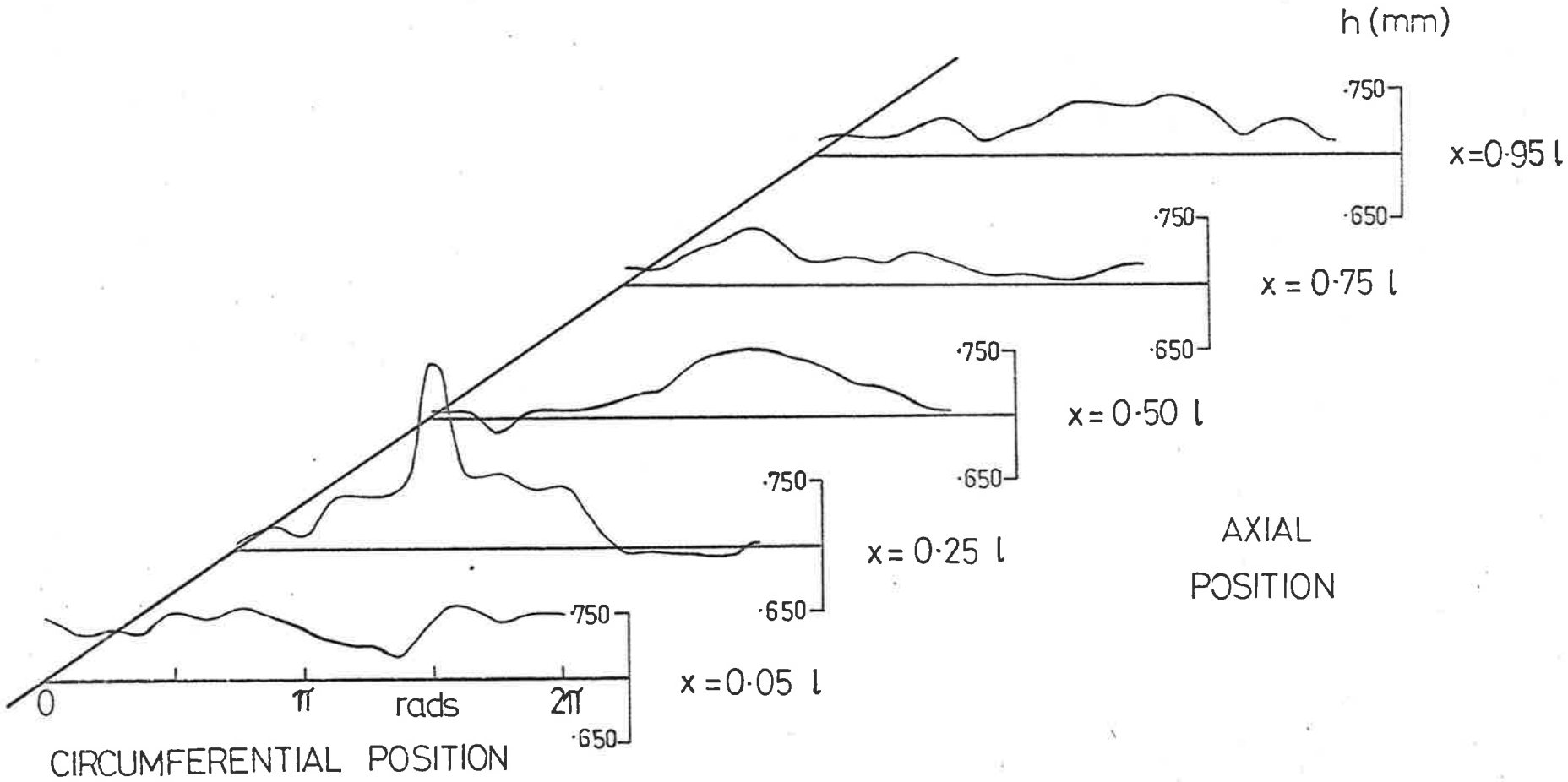

FIG. 9.7(a) VARIATION IN PIPE WALL THICKNESS WITH POSITION -STEEL PIPE $\Lambda = 35$ $\beta = 0{\cdot}00591$

random variations are responsible for small but important changes in the pipe mode shapes.

For plane-wave propagation inside the pipe, changes in the axial component of the mode shape will have a relatively small effect on $j^2_{mm}(\omega)$, at least at higher m. This is in contrast to the circumferential component, where even a small change from the theoretical mode shape will cause $j^2_{nn}(\omega)$, for plane-wave excitation, to increase from zero to some small but finite value. By further distorting the mode shapes of a real pipe in some random way, the circumferential coupling to plane-wave excitation should increase even more, provided that the modal resonance frequencies and masses are not significantly altered: then, if the modal quality factors and radiation ratios remain constant, the radiated power should increase over the level for the original pipe mode shape for the same excitation intensity.

Such an experiment was attempted: the power radiated from a bare steel pipe with $\Lambda = 35.3$ and $\beta = 0.00591$ was compared with the power radiated from the same pipe when five small point masses had been glued with epoxy cement at random positions to the pipe surface. The total added mass was 10% of the bare pipe. Measurements of the power radiation, internal excitation intensity inside the pipe and the quality factor for a single resonant mode were made in the reverberation chamber. The experiment was performed during a single evening so that all environmental conditions were stable. Measurements were accurate to within 0.5 dB using the long averaging times available on the B & K 2114 Spectrometer. Air was used inside the pipe. The only difference between the two parts of the experiment was the addition of the masses to the pipe.

The power radiated from a single mode of the unloaded pipe was measured at 12 frequencies spaced over the peaked portion of the modal response curve of the (2,2) pipe mode. The single-frequency acoustic excitation level and the modal resonance frequency were stable within 0.2 dB and 0.1 Hz, respectively, during the whole experiment. The power radiated was measured with the B & K 2114 Spectrometer (averaging time 300 secs) as

the microphone travelled across the chamber. The mode quality factor was determined from the response curve of the modal acoustic radiation and agreed within 13% of the value obtained from a response-decay curve measured in the normal way; this response curve is shown in Fig. 9.7(b) as curve (i). The five masses were glued to the pipe and the experiment repeated at the resonance frequency of the same mode, although this frequency was now slightly lower: the response curve is shown in Fig. 9.7(b) as curve (ii). The power radiated is shown to have increased by 3 dB while the modal quality factor has decreased by at least 15%, confirming that the coupling of the mode has increased by distorting the mode shape.

A similar experiment was performed using far-field excitation with one-third octave bands of random noise and also at single frequencies corresponding to the resonance frequencies of various vibration modes. For single frequency excitation, the order and approximate shape of each mode were determined by inspection with a moving near-field microphone. The addition of the masses caused the mode shape to distort locally at the load points although the overall shape and order of the mode remained the same: the resonance frequencies decreased slightly. The changes in mode shape were observed holographically in a later experiment. Reductions in modal quality factors also occurred, produced presumably by dissipation at the glued point-mass joints. The measured results are presented in Fig. 9.7(c). The acoustic radiation is seen to increase marginally at most frequencies throughout the plane-wave region, in spite of the occurrence of reductions in modal and average quality factors, which were, in some cases, quite large.

For single-frequency excitation at the resonance frequency of a single mode, equations [2.21] and [8.7] lead, for the αth mode, to

$$\frac{\phi_\pi}{\phi_p} = \rho c\, S \sigma_{rad}\, [[\phi_{\dot{w}}]]/\phi_p$$

$$= \frac{8\rho c\, S}{\rho_s^2 h^2}\, \sigma_{rad}\, \frac{j_{\alpha\alpha}^2\, Q_\alpha^2}{\omega^2} \qquad \text{at } \omega = \omega_\alpha \qquad [9.1]$$

From equation [9.1], it can be seen that if, on the addition of masses to the pipe surface, ϕ_π/ϕ_p increases for constant Q_α, or remains constant while

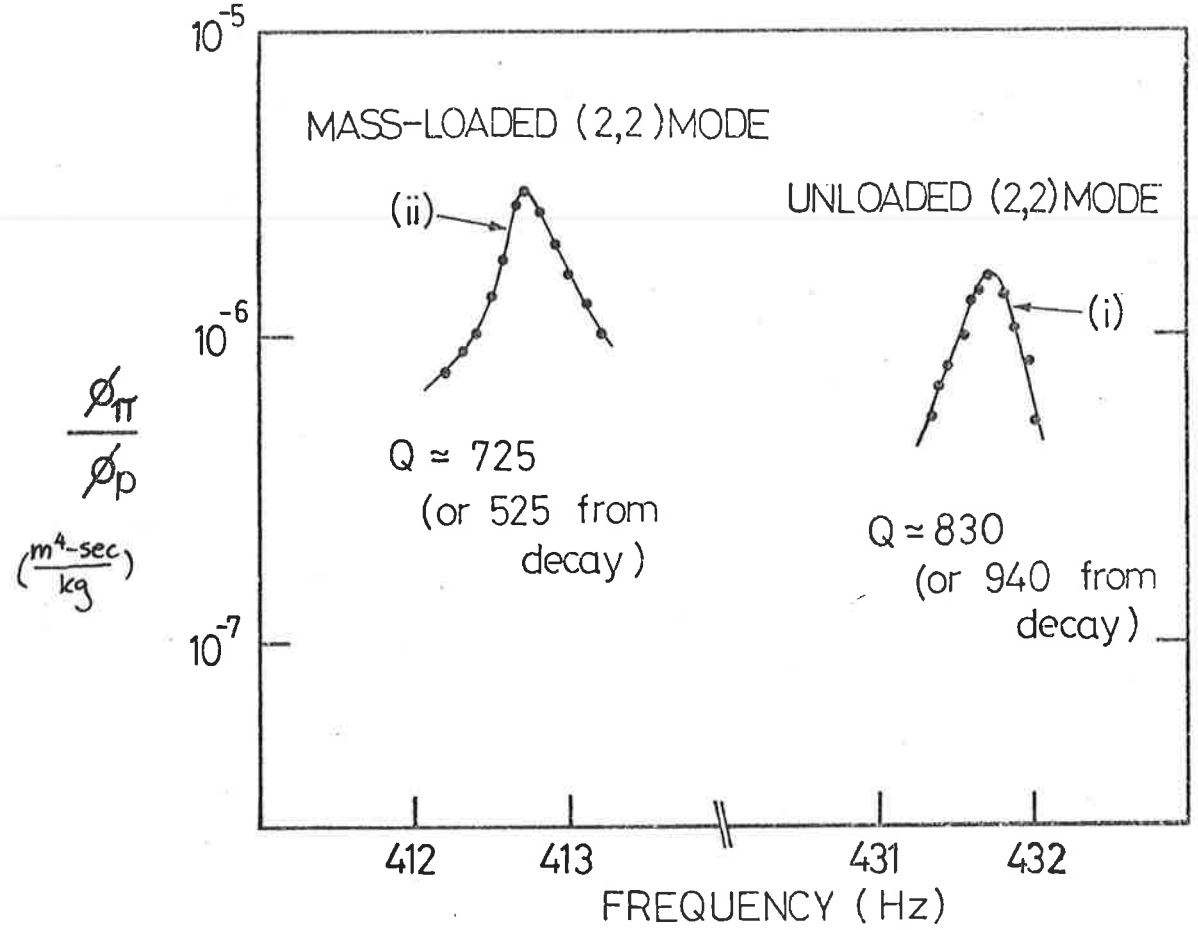

FIG. 9.7(b) EFFECT OF MASS LOADING ON POWER RADIATION FROM (2,2) MODE

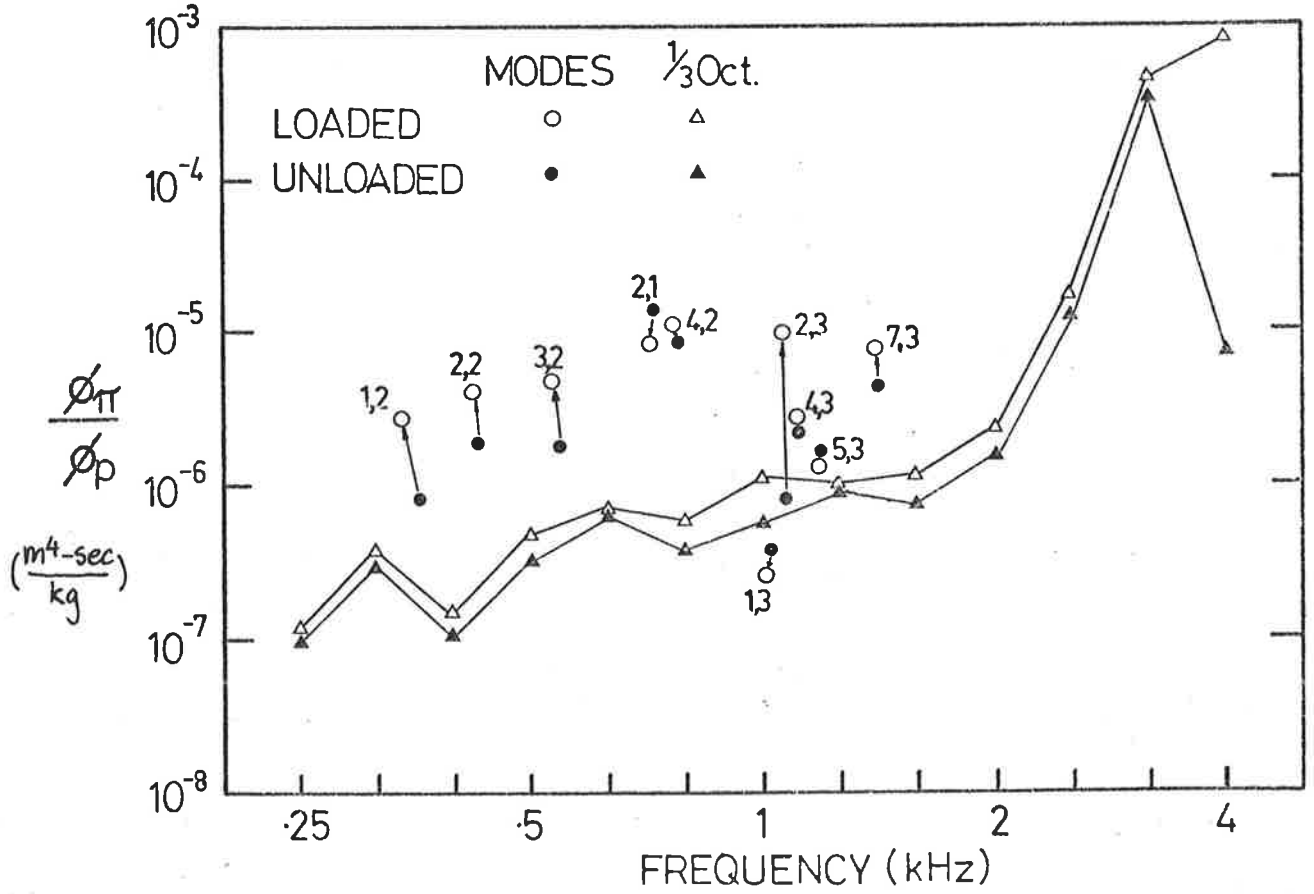

FIG. 9.7(c) EFFECT OF MASS LOADING ON ϕ_{π}/ϕ_p

Q_α decreases, $j^2_{\alpha\alpha}(\omega)$ will have increased (since σ_{rad} and ω will not vary significantly). Thus, variations in the parameter $\phi_\pi/(\phi_p Q_\alpha^2)$ will reflect the actual behaviour of $j^2_{\alpha\alpha}(\omega)$ more clearly.

Similarly, by analogy with the expressions developed for the power radiated from groups of modes in a narrow band of unit frequency when excited by fully-developed turbulent flow (as in equation (2.22)), the power radiated for internal acoustic plane-wave excitation can be expressed as

$$\frac{\phi_\pi}{\phi_p} = \frac{4\pi\rho c\ S\ N\ Q\ \overline{j}^2}{\rho^2{}_s\ h^2 \omega\omega_r} \qquad [9.2]$$

where N is the pipe modal density, Q is the effective quality factor averaged over all the modes in the band, and $\overline{j}^2$ is the averaged joint acceptance of all the modes in the unit-frequency bandwidth. Thus, if ϕ_π/ϕ_p increases or remains constant while Q remains constant or decreases, $\overline{j}^2$ will have increased: again, the behaviour of $\overline{j}^2$ is properly indicated by variations in the parameter $\phi_\pi/(\phi_p Q)$. The measured results have been re-plotted in these forms in Figs. 9.7(d) and (e).

In Fig. 9.7(d), the joint acceptance parameter for the individual modes is seen to increase strongly for most modes, while, in Fig. 9.7(e), the average joint acceptance parameter increases in all bands by amounts corresponding to the appropriate modal changes. These experiments were repeated with the same pipe but with a different arrangement of the same masses and yielded effectively the same results.

On the basis of these experiments, it appears that the distortions in the pipe mode shapes from their theoretically assumed forms are most important factors in determining the modal coupling in cases where a component of the mode shape is theoretically uncoupled to the excitation. In the next paragraph, it is argued that these increases in coupling result mainly from increases in the circumferential component of the joint acceptance.

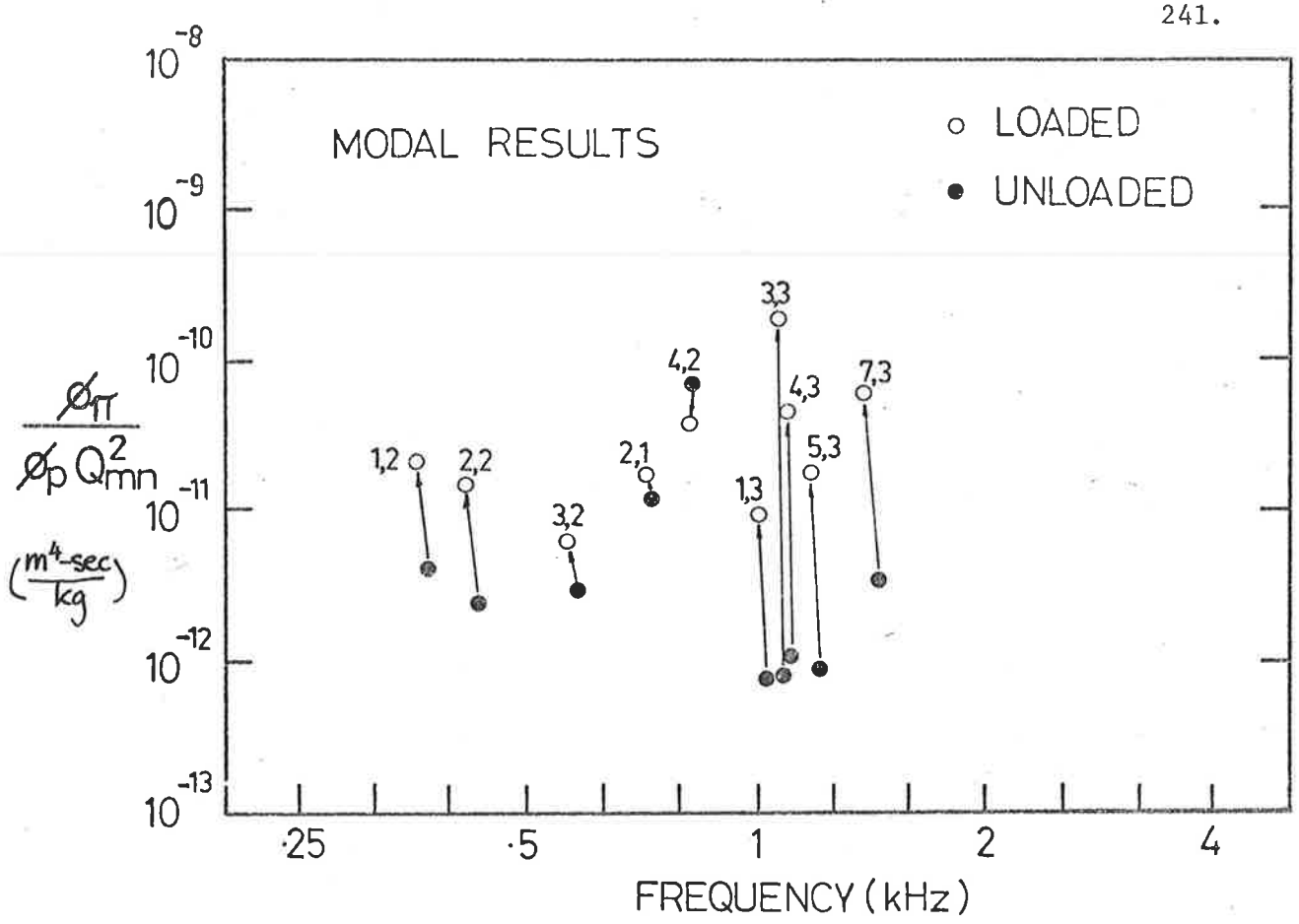

FIG. 9.7(d) EFFECT OF MASS LOADING ON j^2_{mnmn}

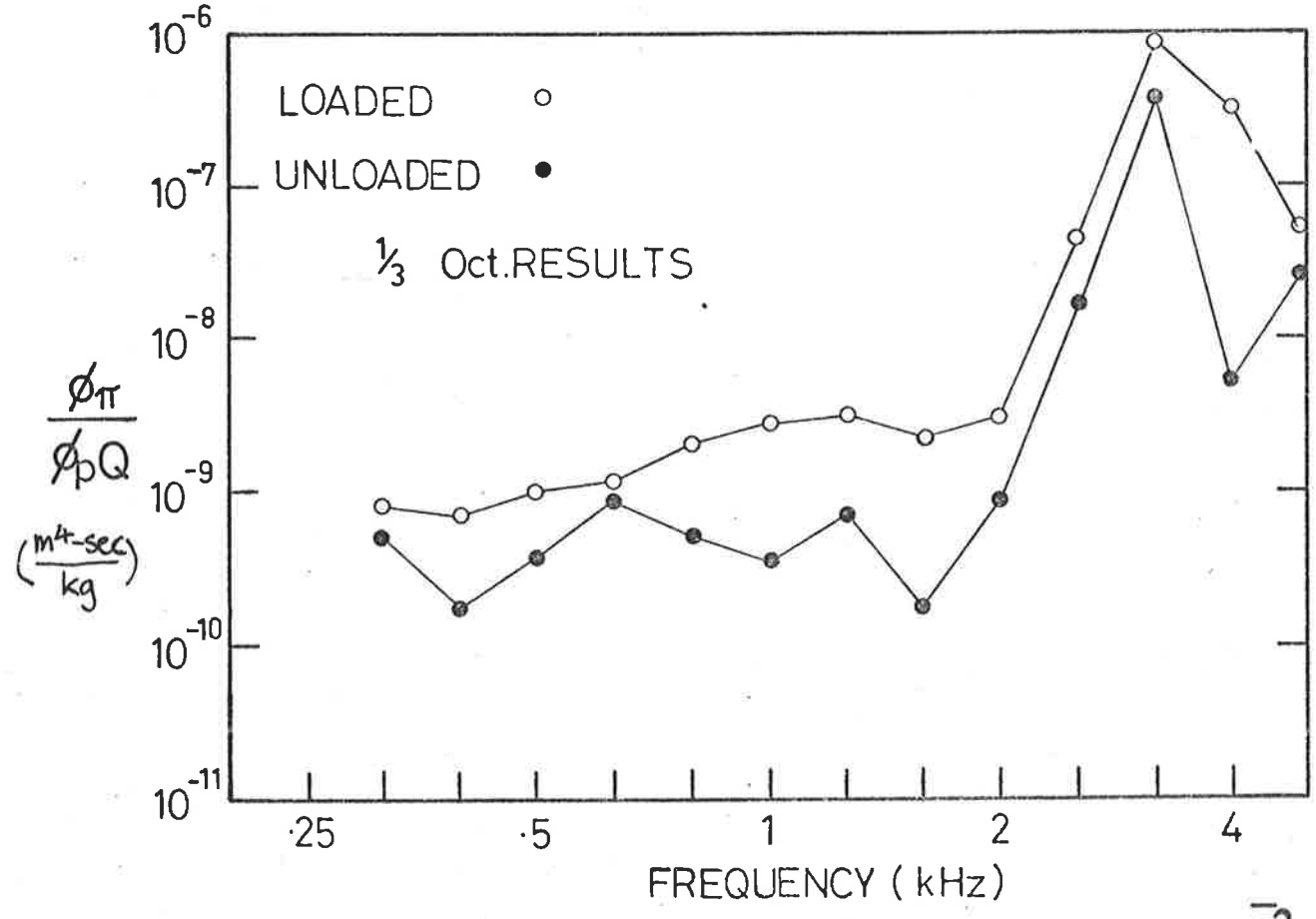

FIG. 9.7(e) EFFECT OF MASS LOADING ON $\bar{j}^2$

9.3.4.2 An Analysis of Effects of Mass Loading

The changes in axial and circumferential mode shapes and the associated variations in modal joint acceptance for plane-wave excitation are now examined analytically.

The changes in the circumferential and axial mode shapes and in their joint acceptance to plane-wave excitation, which are caused by variations in pipe wall thickness, are considered to be modelled, to a first approximation, by changes which will occur in uniform beams of length equal to the pipe circumference and the pipe length, respectively, as the result of similar thickness variations. For example, the resonance frequencies of (0,n) pipe vibration modes are closely predicted by the resonance frequencies of a beam of the same thickness as the pipe and of a length equal to the pipe circumference for $n > 2$.

The resonance frequencies and mode shapes of a beam of uniform thickness with simply-supported ends may be solved exactly, using, for example, Rayleigh's principle. The addition of a small mass to the beam will cause small reductions in the resonance frequencies and small distortions from the original mode shapes, while the overall mode orders will remain the same. These changes in shape may be expressed by a Fourier series over the normal modes of the original beam as

$$y(x) = \sum_{r=1}^{\infty} \phi_r \, \mathrm{Sin}\left(\frac{r\pi x}{\ell}\right) \quad , \qquad [9.3]$$

where $y(x)$ is the beam displacement of the loaded beam, $\mathrm{Sin}(r\pi x/\ell)$ is the shape of the rth mode of the original beam, and ϕ_r is the amplitude of the rth component mode. For the original beam vibrating in the mth order mode, $\phi_m = 1$ and $\phi_r = 0$ for $r \neq m$. The iterative method described by Jones and Mahalingam (1960) can be used to calculate the changes in resonance frequencies and mode shapes produced by small thickness variations in the original beam.

In particular, the changes in mode shape and joint acceptance of the (2,2) pipe mode, as tested in Fig. 9.7(b), are examined. The axial component

changes are assumed to be indicated by changes in shape and joint acceptance of the m = 2 mode of a beam of length 1.295m and thickness h = 0.75mm, when excited by a grazing-incidence acoustic plane wave propagating along the beam length, while the circumferential changes are assumed to be given by the changes in shape and joint acceptance of the m = 4 (equivalent to pipe n = 2) mode of a beam of length $2\pi a$ (where a = 36.6mm) and thickness h, when excited by an acoustic plane wave propagating across its width.

As an example, point loads of masses equal to 0,1,5,10 and 20% of original beam mass have been attached to the beams at an arbitrary position $x/\ell = 0.35$. The changes in mode shapes are shown in Fig. 9.8; these have been calculated from equation [9.3] using values from the iterative solution for ϕ_r given in Table (9.1). Then, the 'axial' joint acceptance can be calculated, using equation [29] of Appendix A for the mth mode, from

$$j_{mm}^2(\omega) = \frac{1}{\ell^2}\int_0^{\ell} dx \left(\sum_{r=1}^{\infty} \phi_r \operatorname{Sin} k_r x\right)\int_0^{\ell} dx' \left(\sum_{r=1}^{\infty} \phi_r \operatorname{Sin} k_r x'\right) R_{px}(x' - x)$$

where $R_{px}(x' - x) = \operatorname{Cos} k_B(x' - x)$. This leads to

$$j_{mm}^2(\omega) = \sum_{r=1}^{\infty} [\phi_r^2 j_{rr}^2(\omega)] + \frac{1}{\ell^2} \sum_{r=1}^{\infty} \frac{2\phi_r k_r [1-(-1)^r \operatorname{Cos} k_B \ell]}{(k_r^2 - k_B^2)} \sum_{s=1}^{\infty} \frac{\phi_s k_s}{(k_s^2 - k_B^2)}$$

$r \neq s$, and (r,s) both even or both odd.

[9.4]

$j_{rr}^2(\omega)$ is given by equation [8.5]. An upper bound to $j_{mm}^2(\omega)$ is given by the first summation only.

The 'circumferential' joint acceptance can be found from equation (30) of Appendix A, as

$$j_{mm}^2(\omega) = \frac{1}{(2\pi a)^2}\int_0^{2\pi a} dy \left(\sum_{r=1}^{\infty} \phi_r \operatorname{Sin} \frac{ry}{2a}\right)\int_0^{2\pi a} dy' \left(\sum_{r=1}^{\infty} \phi_r \operatorname{Sin} \frac{ry'}{2a}\right) R_{py}(y'-y,0;\omega)$$

where $R_{py}(y'-y,0;\omega) = 1$ for plane-wave excitation. Thus,

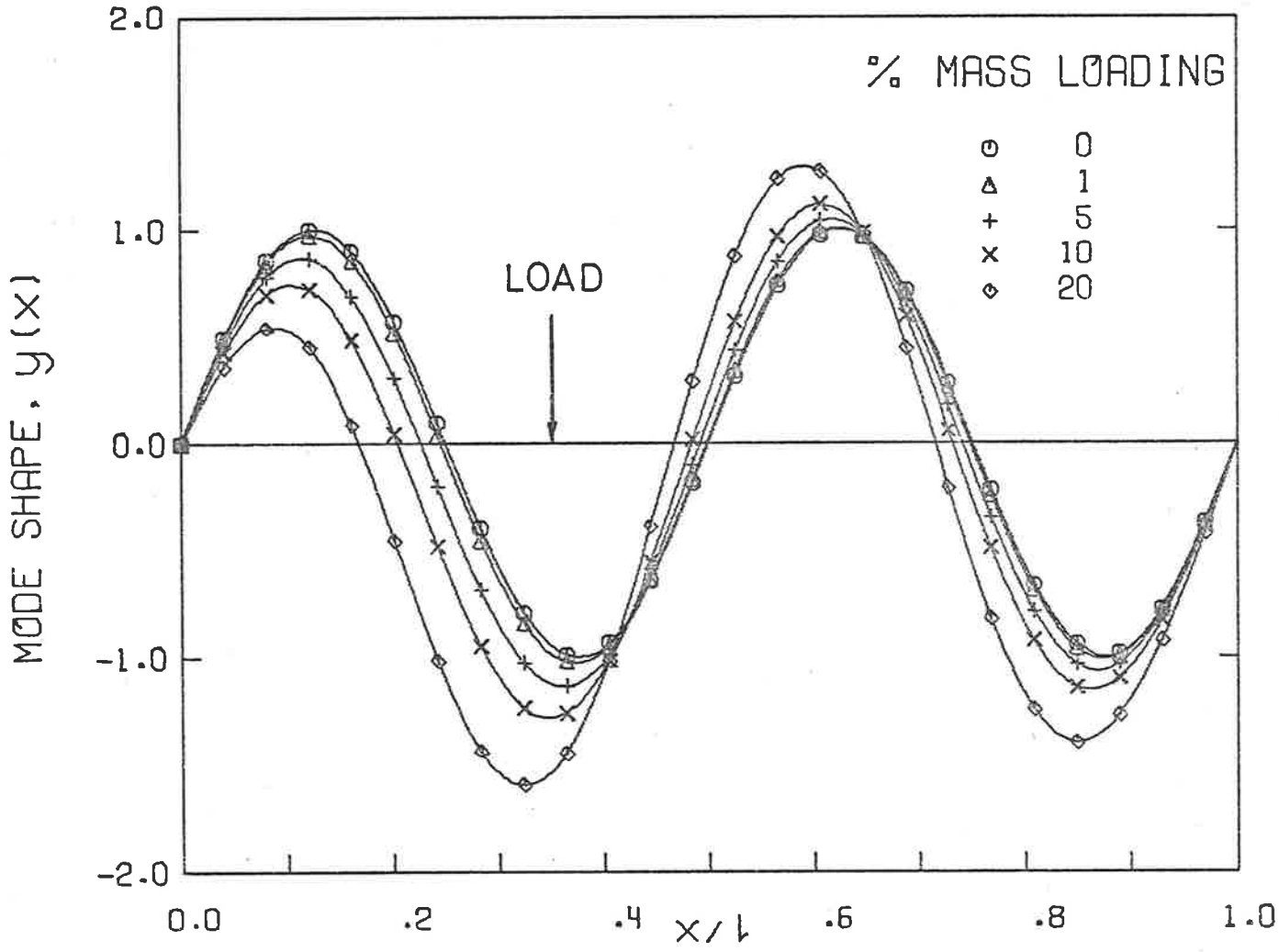

FIG. 9.8 EFFECT OF MASS LOADING ON BEAM MODE SHAPE

AXIAL MODE SHAPE

m = 2

Mass : % of unloaded beam	ϕ_1	ϕ_2	ϕ_3	ϕ_4	ϕ_5	$j^2_{mm}(\omega)$
0.0	-	1.00000	-	-	-	0.04776
1.0	-0.01186	1.00000	0.00319	0.00898	0.00035	0.04640
5.0	-0.06417	1.00000	0.01606	0.00444	0.00174	0.04703
10.0	-0.11855	1.00000	0.03195	0.00899	0.00349	0.04761
20.0	-0.20500	1.00000	0.06290	0.01820	0.00697	0.04540

CIRCUMFERENTIAL MODE SHAPE

m = 4 (equivalent to n = 2 circumferentially)

Mass : % of unloaded beam	ϕ_1	ϕ_2	ϕ_3	ϕ_4	ϕ_5	ϕ_6	ϕ_7	$j^2_{nn}(\omega)$
0.0	-	-	-	1.00000	-	-	-	0.00000
1.0	-0.02334	-0.02446	-0.03502	1.00000	0.01613	0.00569	0.00277	0.000399
5.0	-0.08679	-0.08776	-0.14082	1.00000	0.06056	0.02094	0.01031	0.005850
10.0	-0.16519	-0.16023	-0.29502	1.00000	0.11883	0.03991	0.01991	0.022749
20.0	-0.29622	-0.26906	-0.62472	1.00000	0.23357	0.07366	0.03745	0.082948

Table 9.1 : Variation of mode shapes and joint acceptances with added masses.

$$j_{nn}^2(\omega) = \frac{1}{(2\pi a)^2} \int_0^{2\pi a} dy \left(\sum_{r=1}^{\infty} \phi_r \sin \frac{ry}{2a} \right) \int_0^{2\pi a} dy' \left(\sum_{r=1}^{\infty} \phi_r \sin \frac{ry'}{2a} \right)$$

$$= \frac{1}{(2\pi a)^2} \left(\sum_{r=1}^{\infty} \frac{2a\phi_r}{r} [1-(-1)^r] \right)^2$$

$$= \frac{4}{\pi^2} \left(\sum_{r=1}^{\infty} \frac{\phi_r}{r} \right)^2 \quad , \qquad [9.5]$$

where the summation is taken over odd terms only.

Values of $j_{mm}^2(\omega)$ and $j_{nn}^2(\omega)$ for the above loadings are also given in Table (9.1). From the calculations, it is clear that the addition of small masses to the uniform beam will produce increases in $j_{nn}^2(\omega)$ from zero for the unloaded uniform beam to values approaching the theoretical value of $j_{mm}^2(\omega)$. For example, for a 1% mass addition, $j_{nn}^2(\omega) \simeq 0.0004$: it is unlikely that cylinders can be manufactured with the necessary precision to prevent circumferential inhomogeneities any less than 1 or 2%. Further mass additions cause larger increases in $j_{nn}^2(\omega)$ towards the value of $j_{mm}^2(\omega)$, which itself is relatively insensitive to changes in mass loading, varying by only 4% for a 20% mass addition. In particular, for a 10% mass addition from 10% load to 20% load, $j_{mm}^2(\omega)$ decreases by less than 1% of the unloaded beam value, while $j_{nn}^2(\omega)$ increases from 0.0059 to 0.0227 or by a factor of 3.85: this is rather close to the changes in power radiation measured for the (2,2) pipe mode for the addition of a mass of 10% of the bare pipe, as seen in Fig. 9.7(b). This suggests that, when the (2,2) mode was mass loaded, the most significant change was the change in circumferential mode shape, and that the increases in power radiation did result predominantly from an increase in circumferential coupling. Similar calculations have been made for several point masses at random positions over the beam lengths: essentially the same behaviour was found for all combinations of load positions.

It has been assumed that the changes in pipe mode shape in the circumferential direction can be modelled, to first order, by the changes in mode shape of a simply-supported beam of the appropriate dimensions: this is true

as far as the prediction of the resonance frequencies is concerned. However, the analogy is not complete since a difference in the slope of the mode shapes at the ends of the beams (Fig. 9.8) has been produced by the mass loading, and this is not possible for circumferential pipe modes. This inconsistency results from using sinusoidal functions for the mode shapes, and can only be eliminated by choosing a different set of orthogonal functions or polynomials to preserve the continuity of slope at the beam ends. Even so, the present analysis indicates, in a most believable manner, the nature of the variations in the joint acceptance which occur as the mode shapes distort from sinusoidal forms.

The conclusion reached from these experiments and the supporting analysis is that the strong resonant response observed for plane-wave excitation of the present steel pipes results mainly from the natural distortions from the assumed mode shapes in the circumferential direction, which lead to small but significant couplings to plane-wave excitation. It is the high membrane stiffness of the form of the cylindrical pipe which allows the second order effects of thickness variations to become important for plane-wave excitation.

9.3.5 Effects of Surface Damping Treatments

That the amplitude of the pipe resonant response can be reduced by the addition of damping treatments to the outside surface of the pipe has been demonstrated in section 4.7. In particular, it was found that, while large reductions in the Q's of those modes with $n \geq 2$ could be achieved relatively easily, the Q's of $n = 1$ modes were far less affected, being influenced more by the pipe end conditions and by acoustic radiation damping. A further investigation of the potential for the reduction of response and acoustic radiation levels by surface damping treatments has been carried out for acoustic excitation: the aim was to relate in detail the changes in acceleration response and power radiation to the changes in modal and average quality factors produced by damping treatments.

At the time these experiments were performed, it was not possible to mount the steel pipes in the reverberation chamber in a way which would ensure that direct radiation from the acoustic source did not influence the results, especially when damping treatments caused the radiated levels to approach the forced prediction: consequently, the pipes were mounted in the anechoic chamber pipe-flow rig, with the acoustic source placed at the choke and an acoustic termination placed at the flow inlet. The vibration isolators removed the effects of the mechanical and near-field excitations generated by the source so that the excitation was due to plane waves only.

Measurements of the acceleration response were made with a 0.5g accelerometer. The quality factors of individual modes and in one-third octave bands were measured using the far-field acoustic source as the excitation and using the response-decay method. The directivity of the pipe radiation was a function of the response of the modes which controlled the radiation. Axial, circumferential and radial traverses of the radiation field were made to enable the accurate prediction of the radiated power. When resonant modes controlled the radiation, for example, the pipe directivity was that of a line source as discussed in section 4.5, in contrast to the case described in section 9.2. Some difficulty was experienced in accurately assessing the directivity in marginal cases when the radiation was due to both forced and resonant pipe responses. Later measurements of the power radiation under the same conditions but made in the reverberation chamber showed that the errors involved in these anechoic chamber measurements are, as previosuly stated, within $\pm$ 1 dB for frequencies above 1 kHz and within $\pm$ 3 dB for lower frequencies.

Measurements with Steel Test Section 1 (h=0.75mm)

The modal resonance frequencies and quality factors of the pipe are presented in Fig. 4.4(a). The frequencies of low axial-order modes of fixed $n \geq 2$ are determined for this pipe by the bending stiffness of the

circumferential part of the modes: the modal density for $\nu < 0.5$ is a sharply-peaked function of frequency. The modal and average quality factors are determined mainly by the pipe end conditions for this experiment, as discussed in section 4.3. Except for the n = 1 modes, Q_{mn} in Fig. 4.4(a) decreases with m for fixed n from values of approximately 2000 to a constant value of approximately 400. The n = 1 modes, however, involve a translation of the pipe centre of mass and are consequently damped at low m by vibration of the end supports. The measured average Q's are represented closely by the arithmetic mean of the individual Q_{mn}'s in each band.

A mixture of helium and air was used inside the pipe to extend the frequency range for solely plane-wave propagation inside the pipe. The measured acceleration response relative to the forced prediciton (equation [8.1]) is presented in Fig. 9.9(a) for the bare pipe (upper curve). As observed previously, the differences vary from 40 to 50 dB at low frequencies to 30 dB at high frequencies and are associated with a response in resonant modes. The lower curve shows the effects on the resonant response of applying a mastic damping treatment (added mass < 20% pipe mass) in beads axially along the pipe exterior surface. Reductions of between 10 and 20 dB in the acceleration response over a broad frequency range are produced by the damping layer: these are greatest at the frequencies of low m, circumferential modes of $n \geq 2$, and are consistent with the changes in average Q's as shown in Fig. 9.9(c). Q's of 20 have been achieved in some bands.

The corresponding acoustic power radiation, presented as the ratio of the actual radiation to that predicted from the lower-bound model, is shown in Fig. 9.9(b). For the undamped pipe (upper curve), the peaks in power radiation correspond to radiation from groups of subsonic resonant modes as indicated. The smaller differences which exist between the measured and theoretical power radiation than between measured and theoretical acceleration response reflect the differences in radiation ratio between the inefficient subsonic modes (for $\nu << \nu_{ac}$) and the forced peristaltic

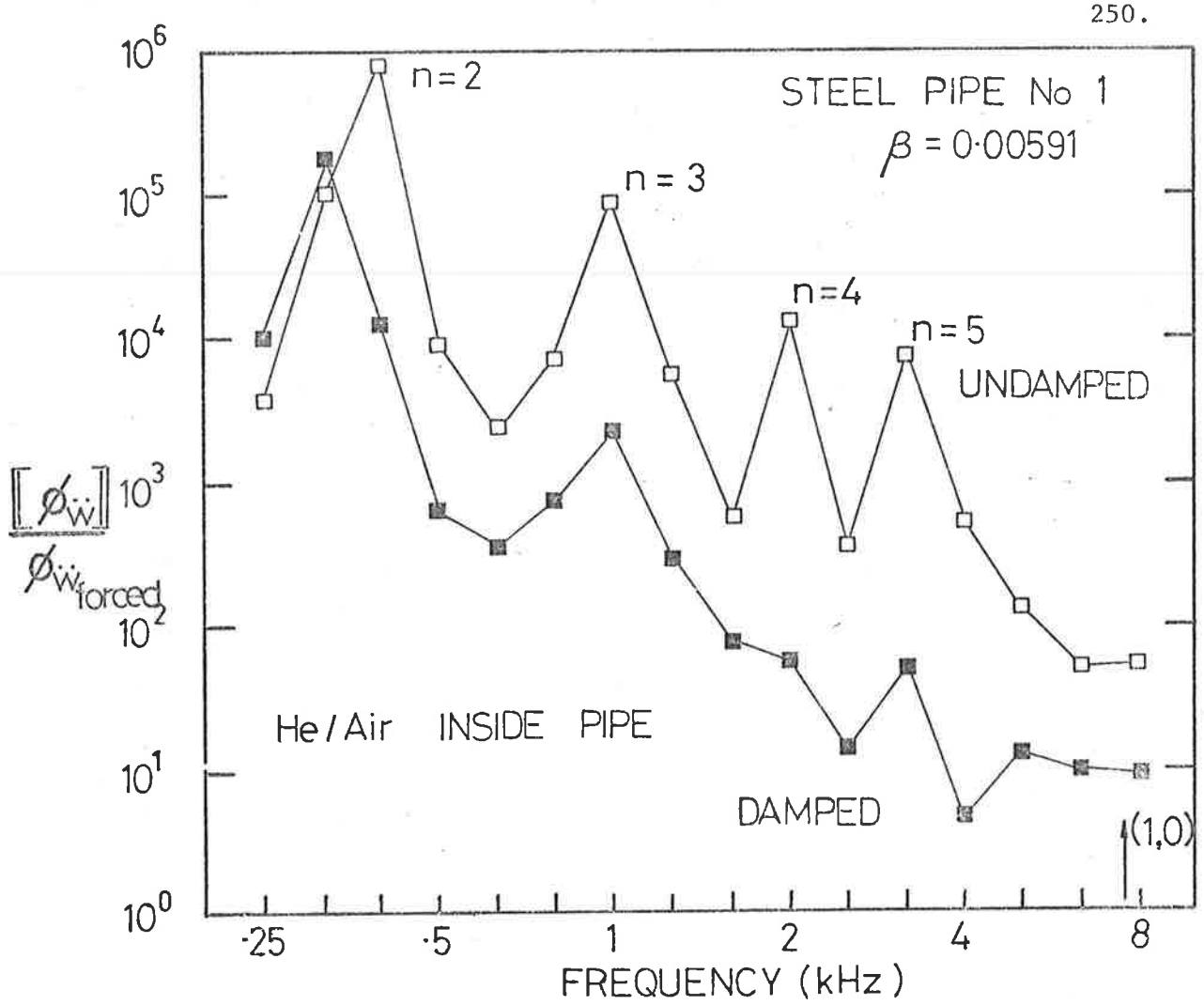

FIG. 9.9(a) EFFECT OF DAMPING ON RESPONSE

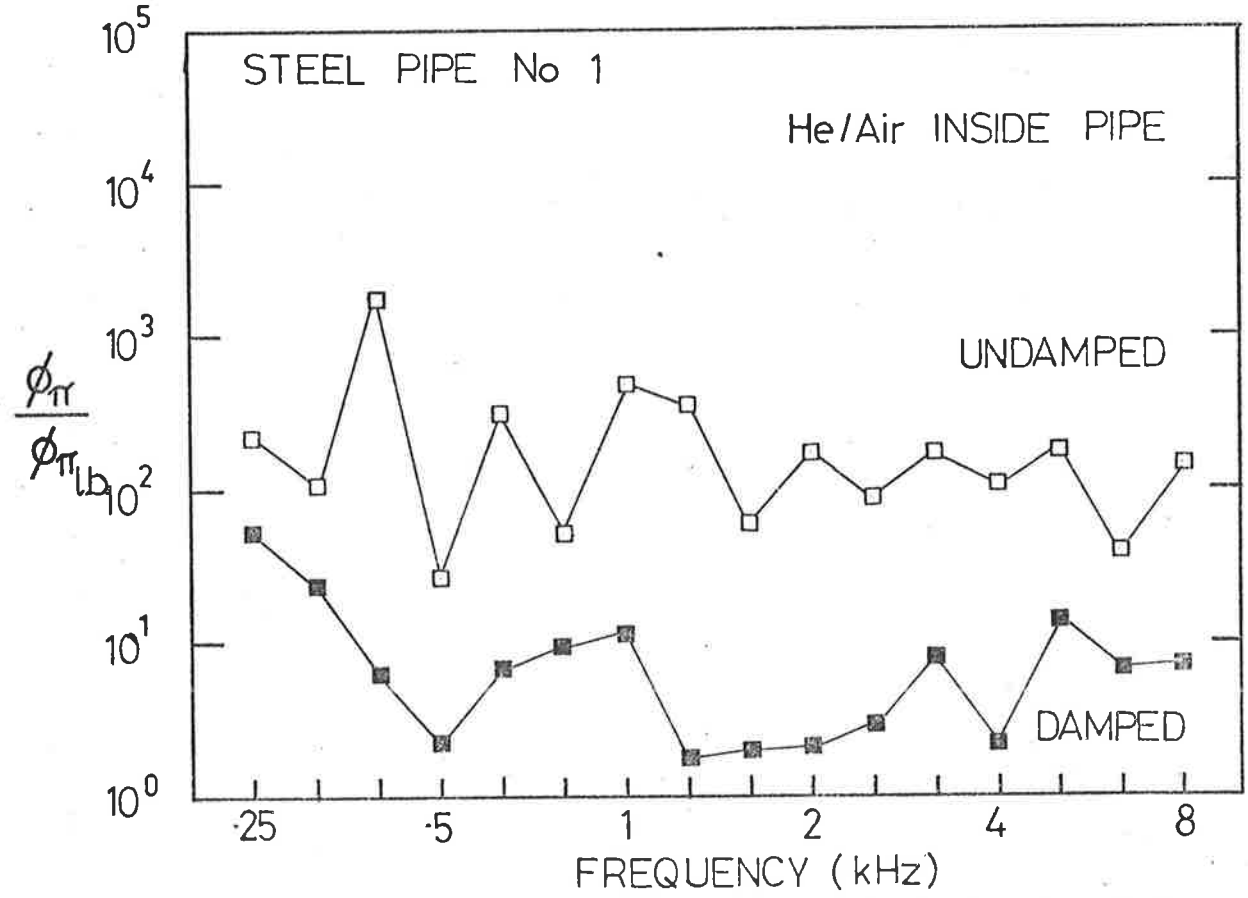

FIG. 9.9(b) EFFECT OF DAMPING ON RADIATION

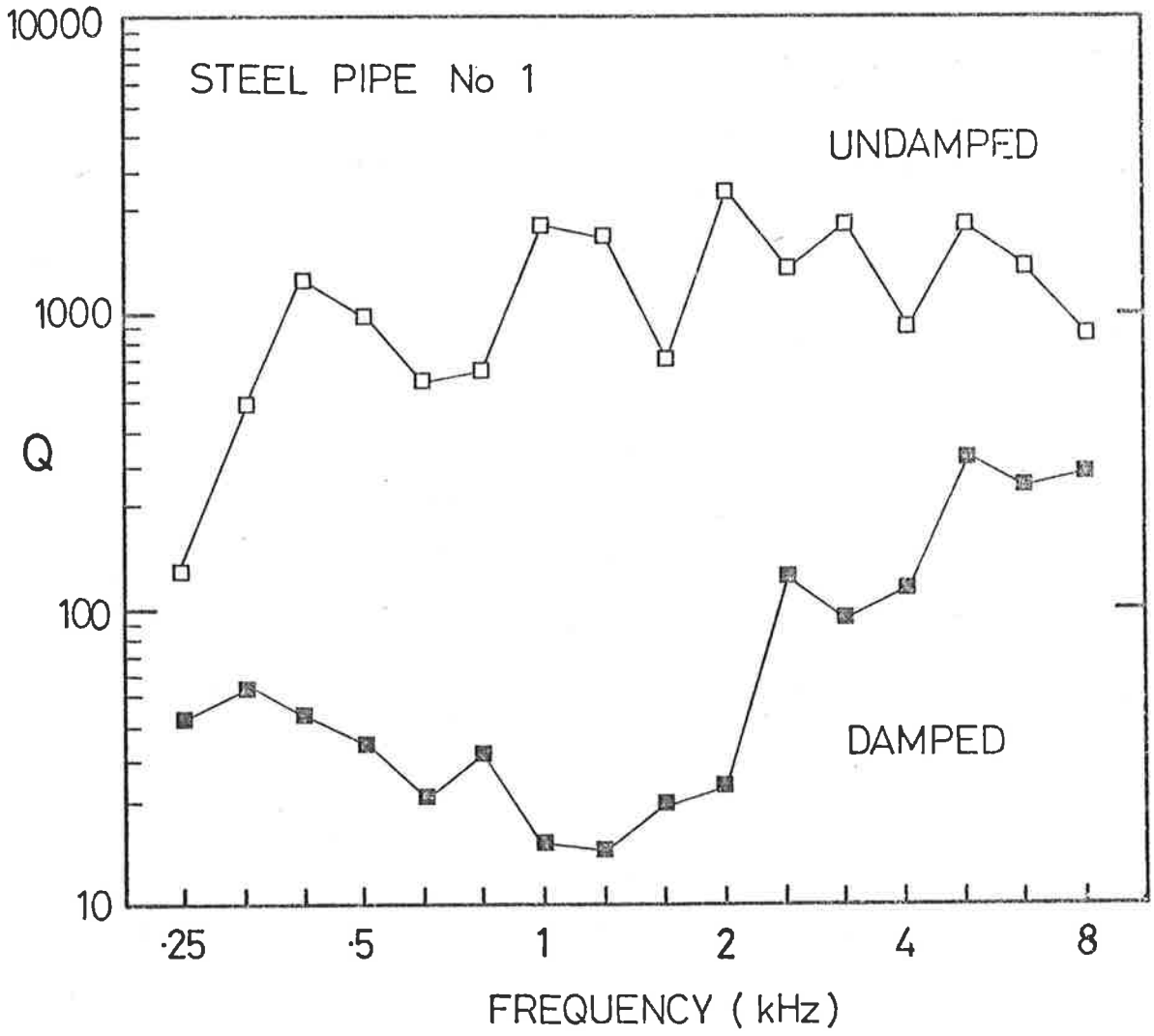

FIG. 9.9(c) EFFECT OF DAMPING ON Q's

wave motion. As K_a increases above unit value, the average radiation ratio of the subsonic modes increases and the differences in excess acceleration and excess power radiation become more equal. The application of damping treatment reduces the power radiated by between 10 and 20 dB, which is of the same order as the reduction in acceleration response. The resulting radiation in those frequency bands where the Q's were reduced to values of approximately 20 was usually quite directional in the direciton of propagation along the pipe. For these cases, the differences between theoretical and experimental power radiation were less than 5 dB. In general, however, differences of between 5 and 10dB occurred, corresponding to values of Q in the range 50 to 100.

Measurements with Steel Test Section 3 (h=1.28mm)

These same experiments were repeated using the thicker-walled test section 3 but with air inside the pipe. The measured acceleration response and power radiation are presented in Fig. 9.10(a) and (b). The (1,0) acoustic cross mode caused strong peaks in the response and radiation. The application of damping treatment produced reductions in acceleration response at all frequencies with the maximum reductions occurring in the lowest bands where n=2 and n=3 circumferential modes exist. In all bands, the acceleration reductions corresponded closely to the measured changes in average Q's; generally these could not be further reduced by additional damping treatment, being limited by the presence of n=1 translational modes, whose Q's for this thicker pipe were initially approximately 150 and could not be significantly reduced at all. This is in contrast to the case of test section 1, where the n=1 Q's were initially approximately 400 but were reduced to less than 50 in some bands. For the present pipe, the reductions in the acoustic power radiation were much smaller (from 2 to 5dB) than the corresponding acceleration reductions, and appear to have been limited by presence of the n=1 modes. The directivity of the radiation from this pipe was unchanged by damping treatment, in

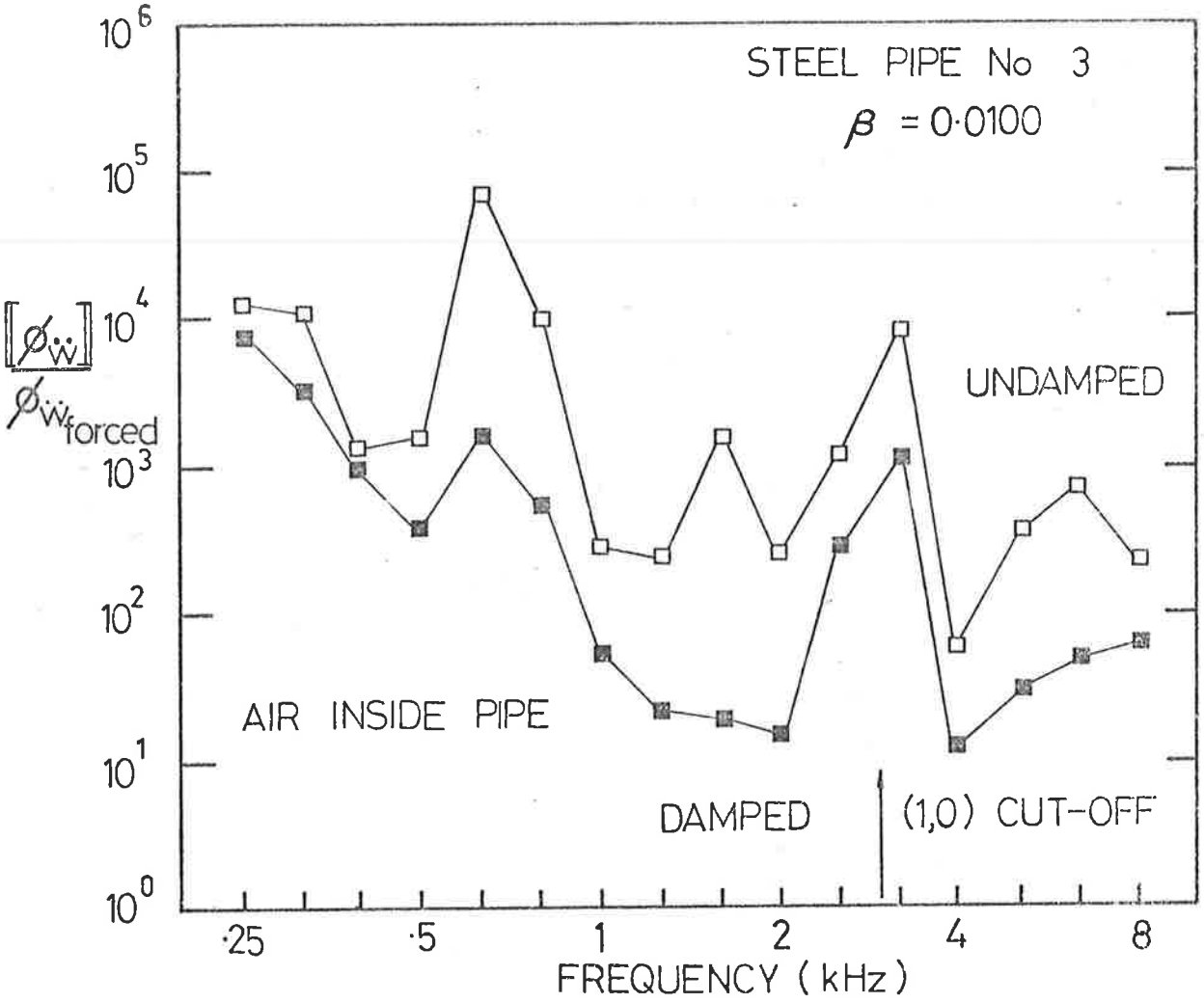

FIG. 9.10(a) EFFECT OF DAMPING ON RESPONSE

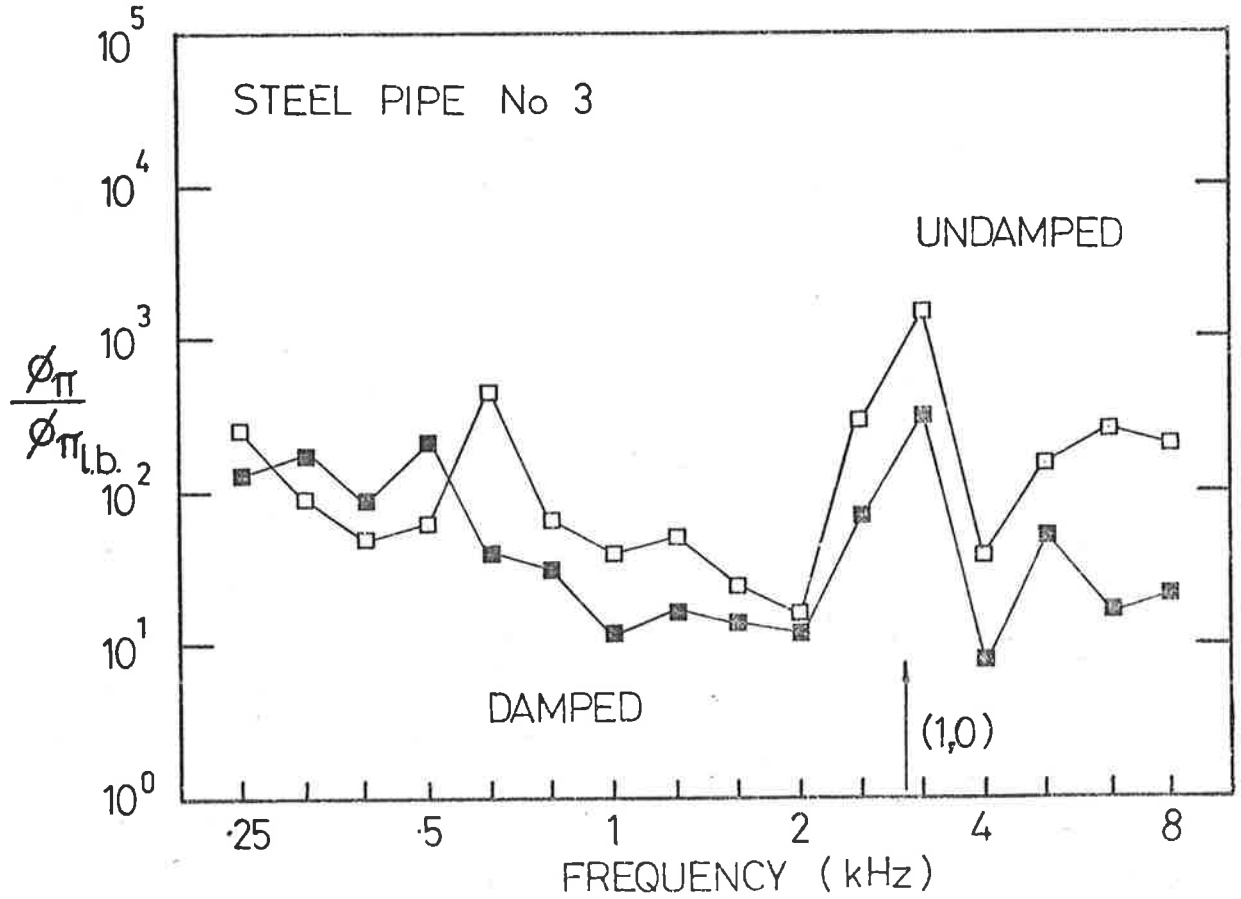

FIG. 9.10(b) EFFECT OF DAMPING ON RADIATION

contrast to the case for test section 1.

As discussed in section 4.7, vibration in n=1 translational modes involves essentially only axial bending, so that to damp these modes, any damping treatment should be spaced as far from the pipe neutral axis as possible, in order to amplify the axial straining of the damping treatment. This was attempted using three honeycomb strip spacers (10mm thick and milled to fit neatly onto the outside pipe surface) glued along the pipe axis. The damping treatment was applied liberally to a skin which was glued onto the honeycomb. No significant differences in average Q's resulted, and only small additional reductions (less than 3dB) in the acceleration response and power radiation were produced, compared with the mastic surface treatment.

From these results, it is seen that the application of damping treatments will cause significant reductions in the resonant vibrational response: this will lead, for thin-walled pipes, to substantial reductions in the power radiation, providing the modal quality factors of the n=1 modes can be reduced to values of approximately 20, in which case the lower-bound prediction for the power radiation will be approached. In general, however, it appears that the Q's of these translational modes cannot be significantly altered by light-weight damping treatments, in contrast to the Q's of circumferential modes of order $n \geq 2$. Since the n=1 modes have relatively high radiation ratios, they tend to control the acoustic radiation from damped pipes and, in the absence of effective damping treatments, would appear to prevent the lower-bound prediction being achieved.

9.4 SUMMARY

Experiments with a P.V.C. pipe of high internal damping have confirmed the existence of a lower bound to the acoustic power radiated from pipes excited by acoustic plane waves propagating internally. Accurate prediciton of the acoustic power radiation is possible, in this case, because the resonant response has been quite effectively damped by the low Q of the pipe, so that the vibrational response to the axi-symmetric

excitation has been predominantly forced. Also the radiation ratios of the resonant modes (usually subsonic) are much lower than that of the forced peristaltic wavemotion on which the lower-bound estimate depends. Additionally, experimental confirmation of the dependence of the radiation ratio of this forced peristaltic wavemotion on the speed of the structural wave, relative to the speed of sound in the surrounding acoustic medium, has been demonstrated for long, small-diameter pipes.

As the quality factors of the test pipes increased, the contribution of resonant modes to the total response was found to increase. Large differences of 20 to 30 dB between the measured power radiation and the lower-bound prediction were produced, even for purely plane-wave excitation, where the effects of the near field of the acoustic source were isolated from the test section. Measurements of the power radiated from lightly-damped (high Q) steel pipes, of fixed length and radius but of various wall thicknesses, demonstrated no clear dependence on wall thickness; although the power radiated per unit length from different lengths of constant radius and constant wall-thickness pipes seemed to increase slightly with pipe length. Moving the far-field source adjacent to the test section produced only small additional increases (5 to 10dB) in the radition above those measured for far-field excitation, suggesting that, in the present experiments at least, the observed departures from the lower-bound predictions result mainly from structural characteristics of the test section, such as the production variations in pipe wall thickness which were observed to be at least 5% of the mean thickness for all test sections.

The addition of point masses to the outside pipe surface, to distort the vibration mode shapes, was shown to lead to an increase in the experimental coupling, or joint acceptance, between the plane-wave excitation and various resonant modes of the pipe. Furthermore, an analysis of the effects of mass loading on the shapes and joint acceptance of a uniform beam with simply-supported ends, taken to first approximation to represent both the axial and circumferential components of the pipe structure, has been

used to predict, at least qualitatively, the nature of the circumferential coupling observed in the experiment with plane-wave excitation. It was concluded that, for plane-wave excitation in the present experiments, the coupling between the resonant modes and the axi-symmetric plane-wave excitation results from the intrinsic production variation in wall thickness which occurs around the circumference of the pipe.

The application of surface damping treatments to thin-walled pipes was found to be most effective in reducing the quality factors of, and thus the power radiated from, resonant modes of circumferential order $n \geq 2$. The n=1 translational modes are not generally susceptible to conventional damping treatments and remain relatively lightly damped: only when the Q's of these n=1 resonant modes are reduced to values of approximately 20 (as for the P.V.C. pipe) will the lower-bound prediction for the power radiation, as determined by the forced pipe response, be achieved.

CHAPTER 10

CONCLUSIONS

Detailed experimental and theoretical results on the vibrational response and the acoustic radiation from thin-walled pipes, excited by acoustic plane waves propagating inside the pipes, have been presented in Chapters 8 and 9.

General conclusions concerning the overall understanding of the problem can now be made.

(i) In the past, straightforward analysis of this problem has been found inadequate for the prediction of the acoustic radiation from pipes, even in tightly-controlled experimental situations. In the analysis, the radiation was assumed to result purely from that component of the vibration response which was forced by the propagating acoustic plane-wave excitation, whereas, in fact, the resonant response of the pipes determined the radiation.

(ii) When using pipes with high material damping to reduce the response of resonant modes relative to the forced response of the pipe wall, the measured forced response is well predicted from Cremer's theoretical expression for the pipe transmission impedance. At frequencies well below the ring and critical frequencies, the response is controlled by the pipe membrane stiffness, but, as frequency increases, the pipe mass causes the impedance to decrease more quickly as frequency approaches the ring frequency.

(iii) For long, small diameter pipes supporting a travelling peristaltic wavemotion, the acoustic radiation depends on the speed of the structural wavemotion relative to the speed of sound outside the pipe. For supersonic wavemotions, the radiation ratio tends to unit value for values of K_a greater than 1, while, for sonic wavemotion, the radiation ratio is

reduced to half that for supersonic wavemotion. For subsonic wavemotions, the radiation ratio decreases further below unity, as the radiation occurs increasingly only from the pipe ends, although in practice the radiation from resonant modes (even when materials with high material damping are used) will limit the minimum value of the radiated power for subsonic wavemotions.

(iv) The concept of a lower bound to the acoustic radiation from pipes excited by internally propagating acoustic plane waves is quite accurate for pipes of high material damping ($Q < 25$). Changes to the mechanical or acoustic end conditions have little effect on the accuracy of the prediction in such cases. The essential reasons for the good agreement between the lower bound and the measurements are the low amplitude of the response in resonant modes relative to the forced response and the large differences in radiation ratio between the efficiently radiating peristaltic wavemotions and the resonant modes of the pipes.

(v) The resonant contribution to both the vibrational response and the acoustic radiation increases as the structural damping decreases; for lightly-damped steel pipes ($Q \simeq 1000$), the resonant acceleration response exceeds the forced level by amounts varying from 30 to 60 dB, while the power radiated by this resonant response exceeds the lower-bound prediction by from 20 to 30 dB. The maximum increases in both acceleration response and power radiation occur at low frequencies and in those frequency bands where the modal quality factors and the density of resonant modes are highest.

(vi) Further increases in response and radiation relative to the forced and lower-bound predictions can be produced by using an acoustic source adjacent to the test pipe: then, depending on the orientation of this near-field source, higher-order acoustic modes, acting below cut-off and therefore existing only in the near field of the source, can drive the test pipe locally and more effectively than propagating plane-waves. However, these additional increases are small relative to existing differences between the measured levels produced by plane-wave excitation alone and the correspond-

ing forced predictions. Thus, while the near field of an acoustic source can be most important in determining the power radiation in practical systems where the source connects directly to the radiating pipe, it may not be responsible for the large discrepancies between the theoretical and measured power radiation results in the present experiments.

(vii) It appears, from experiments and supporting theoretical analysis, that the resonant response and the associated acoustic radiation result primarily from intrinsic inhomogeneities in the pipe, in particular, from variations in pipe wall thickness. Such variations cause distortions from the theoretical mode shapes, both circumferentially and axially: these lead, most importantly, to non-zero values of the circumferential joint acceptance to which the resonant vibration response and acoustic radiation are proportional. The joint acceptance is apparently never zero in practice, although it may be quite small.

(viii) For lightly-damped pipes, surface damping treatments will lead to large reductions in the Q's of modes of circumferential order $n \geq 2$, but will be relatively ineffective in reducing the Q's of $n = 1$ modes.

The response of thin-walled pipes, when determined by modes of order $n \geq 2$, can be reduced by significant amounts, varying from 10 to 15 dB, by using light-weight damping treatments. However, such treatments will have only qualified success in reducing the power radiation from the same pipes, since, at low frequencies, the power radiation is limited by the contributions from $n = 1$ modes. At higher frequencies, when modes of order $n \geq 2$ dominate the radiation, reductions of up to 15 dB can generally be achieved.

It appears that the power radiation from resonant modes can be reduced to the lower-bound prediction only when the Q's of the $n = 1$ modes are reduced to values of approximately 20. It is most difficult to damp these $n = 1$ modes and, therefore, the lower-bound prediction of the power radiation will be exceeded in the general case.

The present work has not examined the various effects of pipe flow on the excitation pressure field and on the vibrational response which is produced, as it is not expected that such effects will be very important for normal flow speeds. The most significant effect may be that higher-order modes will be able to propagate at frequencies below their cut-off frequencies for the no-flow case. Some of the remaining areas of importance in understanding the power radiation from pipes excited by internal acoustic pressure fields can be summarized now.

(i) In the present experiment with lightly-damped pipes for plane-wave excitation, the resonant radiation was found to greatly exceed the lower-bound prediction which is based on the forced response of the pipe. It is believed that similar discrepancies will be found at higher frequencies when propagation in higher-order acoustic modes can occur: then resonant pipe modes of the same circumferential order can be excited at acoustic coincidence and, in lightly-damped pipes, will establish the transmission loss of the pipe. The coupling between higher-order acoustic modes and resonant pipe modes needs investigation.

(ii) The total acoustic power inside pipes at frequencies where multi-modal propagation can occur is often assumed to be distributed equally between the various possible acoustic modes. However, this is not likely to be true for situations where only a few modes can propagate, as then the acoustic source appears to couple selectively to particular acoustic modes: the classification of such in-pipe sources in terms of their modal acoustic power distribution requires considerable work to be done.

(iii) An investigation of the maximum potential of damping treatment for the reduction of radiated acoustic power from thicker-walled pipes, more representative of industrial systems, seems quite justified on the basis of the present encouraging results.

REFERENCES

ARNOLD, R.N. & WARBURTON, G.B. (1953) — The flexural vibrations of thin cylinders. Proc. Inst. Mech. Engrs. (London) 167(1), 62-74.

AUPPERLE, F.A. & LAMBERT, R.F. (1973) — Acoustic radiation from plates excited by flow noise. J. Sound Vib. 26(2), 223-245.

BAILEY, J.R. & FAHY, F.J. (1972) — Radiation and response of cylindrical beams excited by sound. Trans. Amer. Soc. Mech. Engrs., J. Eng. Ind. 94, 139-147.

BAKEWELL, H.P. (1964) — Narrow-band investigations of the longitudinal space-time correlation function in turbulent flow. J. Acoust. Soc. Amer. 36(1), 146-148.

BLAKE, W.K. & CHASE, D.M. (1971) — Wavenumber-frequency spectra of turbulent-boundary-layer pressure measured by microphone arrays. J. Acoust. Soc. Amer. 49(3)Pt. 2, 862-877.

BOZICH, D.J. (1964) — Spatial correlation in acoustic-structural coupling. J. Acoust. Soc. Amer. 36(1), 52-58.

BOZICH, D.J. & WHITE, R.W. (1970) — A study of the vibration response of shells and plates to fluctuating pressure environments. NASA Contractor Report CR-1515.

BROWN, G.L. & RENNISON, D.C. (1974) — Sound radiation from pipes excited by plane acoustic waves. Noise, Shock & Vib. Conf., Monash Univ., Australia, 416-425.

BULL, M.K. (1967) — Wall-pressure fluctuations associated with subsonic turbulent boundary layer flow. J. Fluid Mech. 28, 719-754.

BULL, M.K. & RENNISON, D.C. (1974 a) — Acoustic radiation from pipes with internal gas flows. Proc. Noise, Shock & Vib. Conf., Monash Univ., Australia, 393-405.

BULL, M.K. & RENNISON, D.C. (1974 b) — Turbulent pipe flow as an acoustic noise source. Proc. 5th Australasian Conf. Hydrodynamics & Fluid Mech., Christchurch Univ., New Zealand, 583-590.

BULL, M.K. & RENNISON, D.C. (1974 c) — Noise generation by pipe flow: theory & experiment. Thermofluids Conf., Melbourne, Australia. IEA National Conference Publication 74/7.

CHANDIRAMANI, K.L. (1965) Interpretation of wall pressure measurements under a turbulent boundary layer. Bolt, Beranek & Newman Rept. 1310.

CHANDIRAMANI, K.L. & BLAKE, W.K. (1968) Low-wavenumber content of the spectrum of the wall pressure under a turbulent boundary layer. Bolt, Beranek & Newman Rept. 1557.

CHANDIRAMANI, K.L. *et al.* (1966) Structural response to inflight acoustic and aerodynamic environments. Bolt, Beranek & Newman Rept. 1417.

CHASE, D.M. (1969) Turbulent-boundary-layer pressure fluctuations and wavenumber filtering by non-uniform spatial averaging. J. Acoust. Soc. Amer. 46(5)Pt.2, 1350-1365.

CLAUSER, F.H. (1954) Turbulent boundary layers in adverse pressure gradients. J. Aero. Sciences 21, 91-108.

CLINCH, J.M. (1970) Prediction and measurement of the vibrations induced in thin-walled pipes by the passage of internal turbulent under flow. J. Sound Vib. 12, 429-451.

CORCOS, G.M. (1962) Pressure fluctuations in shear flows. Univ. of California, Inst. of Eng. Res. Rept., Series 183, No. 2.

CORCOS, G.M. (1963) The structure of the turbulent pressure field in boundary-layer flows. J. Fluid Mech. 18, 353-378.

CREMER, L. (1955) [Theory of the transmission loss of cyclindrical shells.] Acustica 5, 245-256.

CREMER, L., HECKL, M., & UNGAR, E.E. (1973) Structure-borne sound. (Springer-Verlag: New York.)

CROCKER, M.J. & PRICE, A.J. (1969) Damping in plates. (Letter to Editor) J. Sound Vib. 9(3), 501-508.

DAVIES, H.G. (1971) Sound from turbulent-boundary-layer-excited panels. J. Acoust. Soc. Amer. 49(3)Pt. 2, 878-889.

DAVIES, H.G. & FFOWES-WILLIAMS, J.E. (1968) Aerodynamic sound generation in a pipe. J. Fluid Mech. 32(4), 765-778.

DYER, I. (1959) Response of plates to a decaying and convecting random pressure field. J. Acoust. Soc. Amer. 31(7), 922-928.

FAHY, F.J. (1970) — Response of a cylinder to random sound in the contained fluid. J. Sound Vib. 13(2), 171-194.

FARABEE, T.M. & GIEB, F.E. (1975) — Measurement of boundary layer pressure fields with an array of pressure transducers in a subsonic flow. Proc. 6th International Congress on Instrumentation in Aerospace Facilities, Ottowa, Canada.

FORSBERG, K. (1966) — A review of analytical methods used to determine the modal characteristics of cylindrical shells. NASA Contractor Report CR-613.

FUNG, Y.C., SECHLER, E.E. & KAPLAN, A. (1957). — On the vibration of thin cylindrical shells under internal pressure. J. Aeronautical Sc., 24(9), 650-660.

HECKL, M. (1958) — [Experimental investigation of the transmission loss of cylinders.] Acustica 8, 259-265.

HECKL, M. (1962) — Vibrations of point-driven cylindrical shells. J. Acoust. Soc. Amer. 34(10), 1553-1557.

JONES, R.P.N. & MAHALINGAM, S. (1960) — The natural frequencies of free and constrained non-uniform beams. J. Royal Aero. Soc. 64, 697-699.

JUNGER, M.C. (1953) — The physical interpretation of the expression for an outgoing wave in cylindrical coordinates. J. Acoust. Soc. Amer. 25(1), 40-47.

JUNGER, M.C. & FEIT, D.M. (1972) — Sound, structures and their interaction. (MIT Press: Cambridge, Massachusetts.)

KARVELLIS, A.V. (1975) — An experimental investigation of the wall pressure fluctuations in piping containing simple control devices. Ph.D. Thesis, The Pennsylvania State University.

KINSLER, L.E. & FREY, A.R. (1962) — Fundamentals of Acoustics. (John Wiley & Sons: New York).

KUHN, G.F. (1974) — Sound transmission through ducts with and without flow. Inst. Sound Vib. Res. Tech. Rept. 65.

LYON, R.H. (1956) — Response of strings to random noise fields. J. Acoust. Soc. Amer. 28(3), 391-398.

LYON, R.H. & MAIDANIK, G. (1962) — Power flow between linearly coupled oscillator J. Acoust. Soc. Amer. 34(5), 623-639.

MAESTRELLO, L. (1965 a) — Measurement of noise radiated by boundary layer excited panels. J. Sound Vib. 2(2), 100-115.

MAESTRELLO, L. (1965 b) — Measurement and analysis of the response field of turbulent boundary layer excited panels. J. Sound Vib. 2(3), 270-292.

MAESTRELLO, L. (1967) — Use of turbulent model to calculate the vibration and radiation responses of a panel, with practical suggestions for reducing sound level. J. Sound Vib. 5(3), 407-448.

MAIDANIK, G. (1962) — Response of ribbed panels to reverberant acoustic fields. J. Acoust. Soc. Amer. 34(6), 809-826.

MAIDANIK, G. (1966) — Energy dissipation associated with gas-pumping in structural joints. J. Acoust. Soc. Amer. 40(5), 1064-1072.

MANNING, J.E. & MAIDANIK, G. (1964) — Radiations properties of cylindrical shells. J. Acoust. Soc. Amer. 36(9), 1691-1698.

MANNING, J.E., LYON, R.H. & SCHARTON, T.D. (1966) — Transmission of sound and vibration to a shroud-enclosed spacecraft. Bolt, Beranek & Newman Rept 1431.

*

MILLER, D.K. & HART, F.D. (1967) — Modal density of thin circular cylinders. NASA Contractor Report CR-897.

MORFEY, C.L. (1971) — Transmission through duct walls of internally-propagated sound. Proc. 7th I.C.A. Paper 24 A9, Budapest.

MORSE, R.M. & INGARD, U. (1968) — Theoretical Acoustics. (McGraw-Hill: New York.)

POWELL, A. (1958 a) — On the fatigue failure of structures to the vibrations excited by random pressure fields. J. Acoust. Soc. Amer. 30(12), 1130-1135.

POWELL, A. (1958 b) — On the approximation to the 'infinite' solutic by the method of normal modes from random vibrations. J. Acoust. Soc. Amer. 30(12), 1136-1139.

POWELL, A. (1964) — On the estimation of the generalised force due to random pressure and on necessary modes. J. Acoust. Soc. Amer. 36(4), 783-784.

RATTAYYA, J.V. & JUNGER, M.C. (1964) — Flow excitation of cylindrical shells and associated coincidence effects. J. Acoust. Soc. Amer. 36(5), 878-884.

RICHARDS, E.J. & MEAD, D.J. (1968) — Noise and acoustic fatigue in aeronautics. (John Wiley & Sons: London)

RIBNER, H. (1956) — Boundary-layer-induced noise in the interior of aircraft. University of Toronto, U.T.I.A.S. Report 37.

SCHLICHTING, H. (1968) Boundary-layer theory. (McGraw-Hill: New York).

SCHLOEMER, H.H. (1967) Effects of pressure gradients on turbulent-boundary-layer wall-pressure fluctuations. J. Acoust. Soc. Amer. 42(1), 93-113.

SMITH, P.W. (1955) Phase velocities and displacement characteristics of free waves in a thin cylindrical shell. J. Acoust. Soc. Amer. 27(6), 1065-1072.

SZECHENYI, E. (1971) Modal densities and radiation efficiencies of unstiffened cylinders using statistical methods. J. Sound Vib. 19(1), 65-81.

UNGAR, E.E. & CARBONELL, J.R. (1966) On panel vibration damping due to structural joints. AIAA Journal 4(8), 1385-1390.

WEYERS, P.F.R. (1960) Vibration and near-field sound of thin-walled cylinders, caused by internal turbulent flow. NASA Technical Note D-430.

WHITE, P.H. (1966) Transduction of boundary-layer noise by a rectangular panel. J. Acoust. Soc. Amer. 40(6), 1354-1362.

WILBY, J.F. (1967) The response of panels to turbulent boundary layer excitation. Ph.D. Thesis, Univ. of Southampton.

WILLMARTH, W.W. & WOOLDRIDGE, C.E. (1962) Measurements of the fluctuating pressure at the wall beneath a thick turbulent boundary layer. J. Fluid Mech. 14, 187-210.

YOURSI, S.N. & FAHY, F.J. (1973) Sound radiation from transversely vibrating unbaffled beams. J. Sound Vib. 26(3), 437-439.

*MARKS, L.S. (1967) Standard Handbook for Mechanical Engineers. 7th Edition (McGraw-Hill: New York)

Bull, M. K. & Rennison, D. C. (1974). Acoustic radiation from pipes with internal turbulent gas flows. In *Proceedings of Noise, Shock and Vibration Conference.* (p. 393-405). Organising Committee of the Noise, Shock and Vibration Conference, Clayton, Vic.

APPENDIX B

RADIATION RATIOS OF PIPE VIBRATION MODES

The acoustic power radiated from a structure vibrating in a single mode at frequency ω can be calculated from equation [2.21] as

$$\pi_\alpha = \mathrm{Rrad}_\alpha \, [[W_\alpha]]_t \qquad [B.1]$$

where π_α is the acoustic power radiated by the αth mode, $S = 2\pi a \ell$, Rrad_α $(=\rho c S \sigma_\alpha)$ is the radiation resistance of the αth mode, and $[[W_\alpha]]_t$ is the space and time-average modal displacement. For the (m,n)th mode of a finite cylinder and for mode shapes which are sinusoidal,

$$\pi_{mn} = \tfrac{1}{2}\rho c S \sigma_{mn} \frac{W_{mn}^2 \omega^2}{\varepsilon_m \varepsilon_n} \qquad [B.2]$$

where $\varepsilon_o = 1$ and $\varepsilon_i = 2$ for $i \geq 1$, and W_{mn} is the peak amplitude of the (m,n)th mode.

The radiation ratio σ_{mn} will be a function of K_a, m, n and Λ. Junger (1953) has argued in an exact analysis of the radiation impedance of infinite cylinders supporting periodic axial and circumferential displacement distributions, that, for wavemotions which are supersonic with respect to the surrounding acoustic medium (i.e. $K_a > K_b$), σ_{mn} tends to unity: however, for subsonic wavemotions (i.e. $K_a < K_b$), $\sigma_{mn} = 0$. He suggested that finite pipes will display similar radiation characteristics. These principles have been used by Manning and Maidanik (1964) to predict the average radiation ratios of thin-walled cylinders with $\Lambda \simeq 1$: as discussed in section 2.2.5, supersonic vibrational modes exist on pipes for all $\nu < \nu_{ac}$, so that a lower bound to the acoustic radiation can be estimated by considering only the supersonic modes (for which $\sigma = 1$). Similarly, with the assumption of equal modal energy, a lower bound to the radiation ratio may be estimated by dividing the modal density of supersonic modes by the total modal density (section

4.5.3). The experimental results of Manning and Maidanik (Λ = 1.33 and β = 0.002) were generally 3 dB less than their theoretical predictions for $\nu < 1$: the differences may have resulted from variations in Q between supersonic and subsonic modes. In general, the neglect of subsonic modes seems justified for these short cylinders: Szechenyi (1971) provides further supporting evidence in a similar experimental situation. In pipes ($\Lambda >> 1$), the vibrational response tends to be controlled by modes of low circumferential order in contrast to the situation involving short, thin-walled cylinders: the radiation ratios of these low n subsonic modes will not necessarily be negligible, so that these modes tend to have a strong influence on the radiation.

Junger and Feit (1972, p. 277) have developed a general analytical approximation to σ_{mn}, as a function of K_a, m, n and Λ. Following their analysis, an expression can be derived for the pressure generated at a far-field point by an acceleration distribution of fixed circumferential mode order but of arbitrary axial form. The method of stationary phase can be used to form an approximation to this pressure, which can then be specified to allow for a sinusoidal acceleration distribution. The acoustic power can be obtained by integrating the energy flux from the pipe over the surface of a large sphere centred on the origin of the pipe. Using equation [B.2], an expression for the modal radiation ratio may be formed as

$$\sigma_{mn} = \frac{16\Lambda}{\pi^4 m^2} \int_0^{\pi/2} \frac{\begin{matrix}\mathrm{Cos}^2 \\ \mathrm{Sin}^2\end{matrix} \left(\frac{K_a \Lambda}{2} \mathrm{Cos}\ \zeta\right) d\zeta}{\mathrm{Sin}\zeta \left| H_n' (K_a \mathrm{Sin}\zeta) \right|^2 \left(1 - \left\{\frac{K_a \Lambda \mathrm{Cos}\zeta}{m\pi}\right\}^2\right)^2} \qquad [B.3]$$

for m and n $\geq$ 1, where m is the number of axial half-wavelengths and n is the number of full circumferential waves. $\mathrm{Cos}^2(\ )$ is used when m is odd, and $\mathrm{Sin}^2(\ )$ is used for m even. This expression requires numerical evaluation, although approximations can be applied effectively in certain situations, such as when $K_a << 1$ and $K_a << K_m$ and when $K_a \Lambda >> 1$ as well (Junger

and Feit (1972, pp. 215-222)). For pipes, where $\Lambda >> 1$ and $K_m < K_a$, useful approximations are not generally possible.

In Fig. B.1, numerical calculations of σ_{mn} against K_a are presented for $\Lambda = 10$, $m = 1$, and various n from 1 to 4. When $K_a < K_b$ (i.e. subsonic modes), σ decreases as K_a decreases at a rate dependent on m, n and Λ, while for $K_a > K_b$ (i.e. supersonic modes), $\sigma \simeq 1$ (as suggested by Junger (1953)). Curves of σ_{mn} against K_a for $\Lambda = 100$ and $m = 10$ for the same range of n are also presented: the two sets of curves thus have the same value of K_m, but different values of Λ. The effect of increasing Λ is to further decrease σ_{mn} (for low order n) at values of $K_a < K_m$.

Alternatively, σ_{mn} can be plotted against K_a/K_b, as in Fig. B.2 for the same modes. $\sigma \simeq 1$ when $K_a > K_b$ for all modes, as assumed in the statistical analysis; however the sharp cut-off in σ predicted in the statistical analysis for $K_a < K_b$ does not occur, except for high n. For example, for $\Lambda = 10$, $\sigma_{11} = 0.1$ at $K_a/K_b \simeq 0.42$; $\sigma_{12} = 0.1$ at $K_a/K_b \simeq 0.50$; and $\sigma_{13} = 0.1$ at $K_a/K_b \simeq 0.58$. By neglecting the radiation from subsonic modes, large underestimates of the total acoustic radiation can occur at frequencies where the modal densities of subsonic modes is greater than the modal density of supersonic modes or when the supersonic modes are more heavily damped (by end losses or by acoustic radiation) than the subsonic modes .

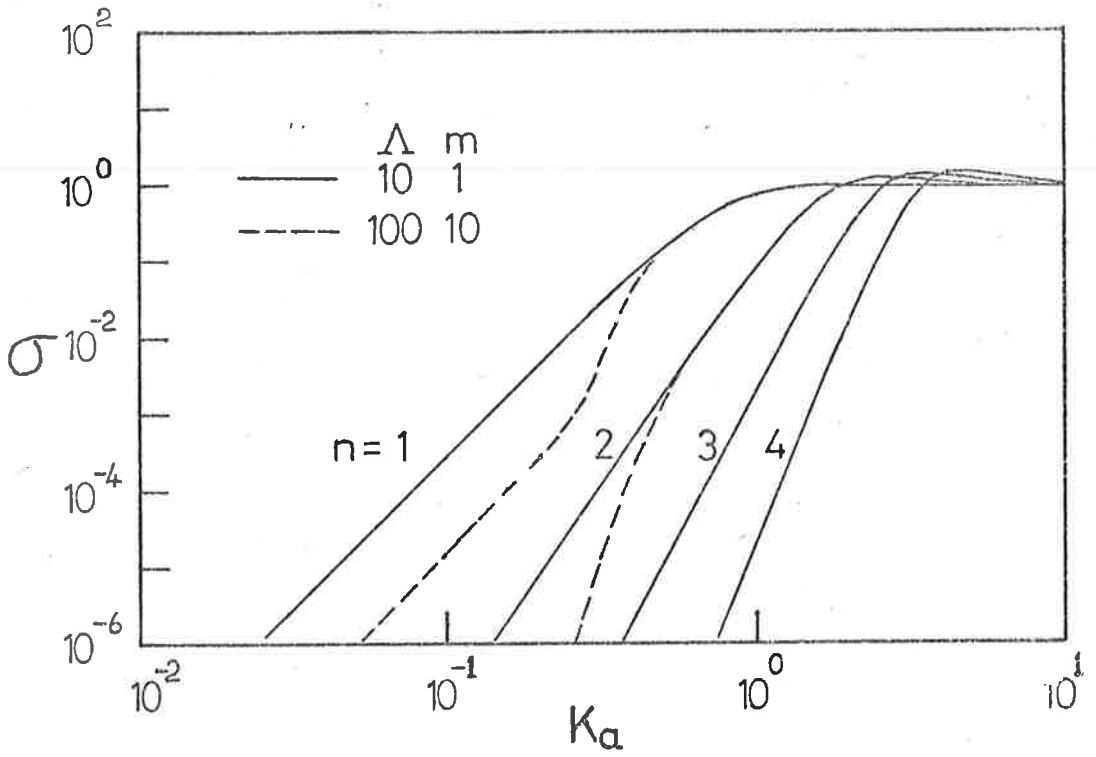

FIG. B1 EFFECT OF K_a ON σ FOR VARIOUS n

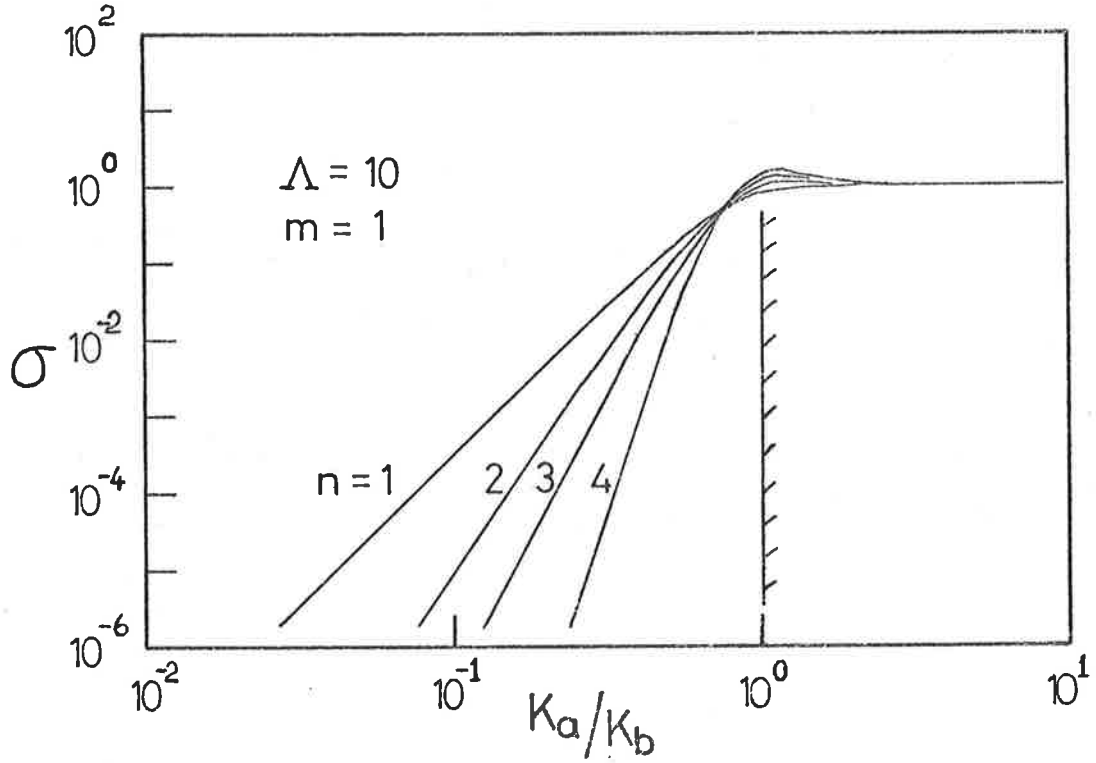

FIG. B2 EFFECT OF K_a/K_b ON σ

Brown, G. L. & Rennison, D. C. (1974). Sound radiation from pipes excited by plane acoustic waves. In *Proceedings of Noise, Shock and Vibration Conference.* (p. 416-425). Organising Committee of the Noise, Shock and Vibration Conference, Clayton, Vic.